Catalyseurs de nickel Supportés Préparés par la Méthode de l'Hydrazine Aqueuse. Propriétés Hydrogénantes et Stockage d'Hydrogène : Effet du Support. Effet de l'Ajout d'Argent

Robert Wojcieszak

U.F.R. STMP
Ecole Doctorale : SESAMES
Molecular and Theoretical Chemistry and Physico-Chemistry

Thesis

submitted in fulfillment of the requirements for the degree of

Doctor at Henri Poincaré University, Nancy-I

in Molecular Chemistry and Physico-Chemistry

by **Robert WOJCIESZAK**

Study of Supported Nickel Catalysts Prepared by Aqueous Hydrazine Method. Hydrogenating Properties and Hydrogen Storage. Support Effect. Silver Additive Effect.

Members of jury :

M. Jean-Pierre CANDY	Director of Research CNRS, Villeurbanne
M. François GARIN	Director of Research CNRS, Strasbourg
Mme Maria ZIÓŁEK	Professor, Adam Mickiewicz University, Poland
M. Jacques-Charles VEDRINE	Professor, ENSCP, Paris
M. Serge MONTEVERDI	Assistant Professor, U.H.P., Nancy-I
M. Mohammed M. BETTAHAR	Professor, U.H.P., Nancy-I (Thesis Director)

Laboratoire Structure et Réactivité des Structures Moléculaires Complexes
Catalyse Hétérogène (SOR)
Faculté des Sciences & Techniques-54500 Vandoeuvre-lès-Nancy

« Life does not deserve to be worried over… »

Maria Skłodowska-Curie

ACKNOWLEDGEMENTS

I am deeply indebted to my supervisor professor Mohammed M. Bettahar who gave me the opportunity to work with him in the Laboratory of Heterogeneous Catalysis at the Henri Poincaré University in Nancy. His help, stimulating suggestions and encouragement helped me in all the time of research and writing of this thesis. It was a great pleasure to conduct this thesis under his supervision.

I warmly thank Dr Serge Monteverdi for his excellent advice and friendly help. His extensive discussions around my work and constructive criticism have been very helpful for this study.

I am grateful to Michel Mercy who has helped me not to get lost during these three years. I want to thank him for all his help, support and valuable hints.

I would like to express my deep and sincere gratitude to Professor Maria Ziółek from Adam Mickiewicz University. Her great knowledge and her logical way of thinking have been of great value for me. Her understanding and personal guidance have provided a good basis for the present thesis.

My greetings go also to Directors of Research Jean-Pierre Candy and François Garin and to Professor Jacques-Charles Védrine who honored me by accepting to take part of the jury and to review my thesis.

During this work I have collaborated with many colleagues for whom I have great regard, and I wish to extend my warmest thanks to all those who have helped me with my work. Especially Dr Michał Zieliński, Dr Mariusz Pietrowski and Msc Agnieszka Jasik.

I would like to express my gratitude to Thierry Briot. Without his help, I would not have had the opportunity to study in France. Thanks for your encouragement, understanding and for supporting me all the time.

I thank my friends Gosia, Gosia, Klaudia, Kasia, Marta, Michał and Janusz, for encouraging and supporting me. Without you, and yours help it would have been impossible for me to finish this work.

I also wish to thank Madame Elisabeth Dumas for her sympathetic help in secretarial work.

My special gratitude is due to my family for the loving support and my loving thanks are due to Simonne and Georges Briot. They let me own a happy family in France.

And last but not least, I would like to thank the French Embassy in Poland for the financial support.

TABLE OF CONTENTS

INTRODUCTION

INTRODUCTION

Les catalyseurs supportés de nickel ont été largement étudiés à cause de leur très grande activité dans les réactions d'hydrogénation et d'hydrotraitement. Généralement, les catalyseurs de nickel sont obtenus par réduction de sels précurseurs par l'hydrogène à des températures relativement élevées. Très souvent, la réduction est précédée par le traitement thermique à hautes températures appelé calcination. Tous ces traitements provoquent des interactions fortes entre le support et le métal. Ils influencent donc la structure, la réductibilité et l'activité des catalyseurs supportés de nickel. Par conséquent, il est très difficile d'obtenir des catalyseurs au nickel bien dispersés, avec des particules métalliques de taille définie et de forme homogène.

Récemment, des méthodes nouvelles de préparation des catalyseurs de nickel ont été mises en oeuvre. L'une d'elles est la réduction chimique d'un sel de nickel par l'hydrazine en milieu aqueux. Des travaux récents ont montré l'intérêt de travailler en milieu aqueux comme solution pratique à l'avenir en catalyse homogène et hétérogène. Ceci nous a incités à entreprendre une étude des nanoparticules de nickel obtenues par la réduction de sels de nickel par l'hydrazine et stabilisés sur divers supports.

Il est bien connu que l'activité d'un catalyseur au nickel dépend de la nature du support qui peut modifier les propriétés de la phase active. Les propriétés physiques et chimiques du support, son acidité, la réductibilité et l'intensité de l'interaction avec la phase active jouent un rôle crucial dans la chimie complexe des catalyseurs supportés de nickel.

Les oxydes non réductibles tels que SiO_2 et Al_2O_3 ont été largement étudiés et ont été trouvés très actifs dans les réactions d'hydrogénation. Les oxydes réductibles tels que CeO_2 et Nb_2O_5 sont généralement reconnus pour être de bons candidats comme modèles dans l'étude des interactions fortes entre le support et le métal. Pour comparaison, le charbon actif a été également employé comme support de catalyseurs au nickel. L'utilisation du charbon actif comme support en catalyse s'accroît et cela est dû aux avantages qu'il offre par rapport aux oxydes traditionnels. Matériau bon marché et relativement inerte, le charbon actif montre une grande stabilité en milieu acide ou basique et possède une superficie élevée et des groupes fonctionnels riches en oxygène.

Dans le cas de catalyseurs bimétalliques, il été démontré que l'incorporation d'un second métal conduit à des performances nettement supérieures à celles du catalyseur monométallique. Nous avons utilisé l'argent comme additif pour modifier les

propriétés de surface et catalytiques du nickel supporté. Les nanoparticles Ni-Ag synthétiques n'ont, jusqu'à présent, suscité que peu d'intérêt dans la littérature.

L'activité des catalyseurs préparés a été étudiée dans la réaction d'hydrogénation du benzène en phase gazeuse. Cette réaction est employée couramment afin de caractériser divers systèmes catalytiques métalliques. C'est également une réaction très importante dans l'industrie chimique. En outre, les contraintes environnementale croissantes ont eu comme conséquence la nécessité d'éliminer le benzène, un carcinogène connu, dans les dissolvants et les carburants automobiles.

Ces dernières années, la production d' « énergie verte » est l'objet d'une très grande attention. C'est le cas de l'hydrogène, dont l'un des problèmes majeurs est le stockage. Du point de vue pratique, le stockage d'hydrogène dans les matériaux poreux semble être une solution idéale. Dans ce sens, il y a un intérêt expérimental et théorique considérable pour l'utilisation des matériaux carbonés nano-structurés synthétiques en tant que sorbants potentiels d'hydrogène. Malheureusement, ces matériaux contiennent des métaux (Fe, Co, Ni, Cu), utilisés dans le processus de leur synthèse et non éliminés pendant l'étape de purification. D'ailleurs, le traitement de purification lui-même mène à l'effondrement partiel de la nanostructure et à la formation de carbone amorphe.

Ces données nous ont incité à étudier des catalyseurs de nickel supporté sur un charbon actif commercial amorphe, comme matériaux pour le stockage de l'hydrogène. Le charbon actif est un matériau bon marché par rapport aux matériaux synthétiques nano-structurés du carbone. Le nickel est un métal employé couramment dans l'industrie.

Dans cette thèse nous avons exploré plusieurs facteurs déterminant les propriétés de surface et catalytiques des catalyseurs supportés de nickel non classiques, préparés en utilisant l'hydrazine comme réducteur. Ces facteurs sont : les conditions de la préparation des catalyseurs, la nature du support ou du précurseur métallique et la charge en métal. Les résultats obtenus sont comparés à ceux de catalyseurs conventionnels.

La présentation des résultats de ce travail est divisée en dix chapitres.

Une étude bibliographique est présentée dans le premier chapitre.

Toutes les méthodes et techniques utilisées dans la thèse sont rapportées dans le deuxième chapitre. Les catalyseurs préparés ont été caractérisés par différentes méthodes: Diffraction des Rayons X (DRX), Microscopie Electronique à Transmission

(MET) ou à Balayage (SEM), Cartographie X, Microanalyse X (EDS), Spectroscopie des Photons X (XPS), Spectroscopie Infra-rouge à Transformée de Fourier (FTIR), adsorption et désorption de N_2 à basse température, Réduction en Température Programmée sous hydrogène (H_2-TPR), Adsorption d'Hydrogène, Thermodésorption d'hydrogène en Température Programmée (H_2-TPD), Décomposition de l'Isopropanol.

Le troisième chapitre comporte la préparation et la caractérisation des catalyseurs de nickel supportés sur γ-Al_2O_3 et SiO_2 amorphe. Deux méthodes d'imprégnation ont été employées. La simple imprégnation (SIM) et la double (DIM) imprégnation par l'EDTA sont comparées. La méthode non classique de réduction par hydrazine est comparée à la méthode conventionnelle. Enfin, les catalyseurs préparés ont été étudiés dans la réaction d'hydrogénation de benzène en phase gazeuse.

Les quatrième et cinquième chapitres sont relatifs à la préparation et à la caractérisation des particules de nickel supportées sur les oxydes réductibles. Deux oxydes sont étudiés : Nb_2O_5 et CeO_2. Dans le cas des catalyseurs au niobium, les méthodes d'imprégnation SIM et DIM ont été employées. Les interactions fortes nickel-Nb_2O_5 ont été étudiées. Les catalyseurs non classiques réduits par l'hydrazine sont comparés aux catalyseurs préparés classiquement. Dans le cas des catalyseurs non classiques de nickel supportés sur la cérine, l'effet du pourcentage de nickel a été étudié. Les deux séries de catalyseurs ont été étudiées dans la réaction d'hydrogénation de benzène.

Le sixième chapitre est consacré aux catalyseurs bimétalliques nickel-argent. Les catalyseurs ont été préparés par réduction chimique avec l'hydrazine. Des catalyseurs avec différents rapports nickel-argent ont été étudiés. Deux silices différentes utilisées comme supports du nickel sont comparées. L'étude approfondie de l'effet d'addition de l'argent a été effectuée. Deux modes opératoires de réduction ont été comparés : réduction du nickel supporté et réduction/précipitation du nickel. L'activité des catalyseurs a été également examinée dans la réaction d'hydrogénation de benzène.

Le septième chapitre porte sur la préparation et la caractérisation de catalyseurs de nickel supportés sur charbon actif. Les effets du précurseur métallique et de la charge en nickel ont été étudiés. Différentes méthodes ont été utilisées pour la préparation des catalyseurs. Les catalyseurs classiques sont comparés à leurs contreparties non classiques préparés avec l'hydrazine. L'activité catalytique a été étudiée dans la réaction

de l'hydrogénation du benzène en phase gazeuse. L'effet « spillover » de l'hydrogène sur l'activité a été étudié par la dilution de catalyseur par le support.

La huitieme partie de cette thèse est consacrée à l'étude du stockage de l'hydrogène à température ambiante et haute pression. Les catalyseurs utilisés sont ceux décrits le Chapitre VII Nous avons étudié plusieurs facteurs qui déterminent le niveau de stockage : la méthode de préparation, la nature du précurseur métallique et le pourcentage de nickel ainsi que la dilution du catalyseurs par le support. Le mécanisme de stockage via le phénomène de spillover est proposé et discuté.

Finalement, tous les résultats sont rassemblés et discutés dans le Chapitre IX.

Par ailleurs, nous avons collaboré à l'étude de catalyseurs de nickel supportés sur CeO_2 et préparés par radiolyse γ par Sabah Chettibi (Université de Constantine). Nous avons examiné leur réactivité vis-à-vis de hydrogène et dans l'hydrogénation du benzène. Les résultats obtenus seront présentés dans la thèse de Sabah Chettibi en mai 2006. La publication commune est rapportée dans l'Annexe.

INTRODUCTION

Supported nickel catalysts have been widely studied due to their very high activity in the hydrogenation and hydrotreating reactions. Generally, the nickel catalysts are obtained by the reduction of impregnated solid under hydrogen flow at relatively high temperatures. Very often the reduction is preceded by the high temperature heat treatment called calcination. All these treatments influenced on the structure, reducibility and activity of the nickel supported catalysts. Therefore, it is very difficult to obtain well dispersed catalysts homogeneously shaped and sized nickel particles. Moreover the high temperature treatment gives rise to strong metal support interactions.

Recently the new methods of preparation of nickel catalysts have been established. One of them is the chemical reduction of nickel salt by hydrazine in aqueous media. Recent works have pointed out the interest of working in aqueous medium as a practical solution for the future in homogeneous and heterogeneous catalysis. This prompted us to undertake a study of nickel nanoparticles obtained by the reduction of nickel salts by hydrazine and stabilized on different supports.

As to the choice of the support, it is known that the activity of the nickel catalyst depends on the support nature which may modify the properties of the active phase. Both physical and chemical properties of the support, its acidity, reducibility and the extent of interaction with the active nickel phase play a crucial role in the complex chemistry of the supported nickel catalysts. Non reducible oxides such as SiO_2 and Al_2O_3 have been widely studied and they were found very active in the hydrogenation reactions. Reducible oxides such as CeO_2 and Nb_2O_5 are generally acknowledged are good candidates to exhibit strong metal support interaction. To compare with nickel–oxide support interaction, the activated carbon was also used as the nickel support. The use of activated carbon as a catalyst support is increasing due to the advantages it offers as compared to traditional oxides. Cheap and relatively inert material, activated carbon exhibits stability in acidic or basic media, a high surface area and oxygen-containing functional groups.

In case of the bimetallic catalysts it has been demonstrated that even with small particles bimetallic clusters are vastly superior to their monometallic counterparts. We used silver as an additive to modify the surface and catalytic properties of supported nickel. Ni-Ag synthetic nanoparticles have not still received much attention.

Activity of the prepared catalysts was studied in the gas phase hydrogenation of benzene reaction. This reaction is widely used in several studies in order to characterize various catalytic systems. It is also a very important reaction in chemical industry. In addition, increasing environmental awareness has resulted in the need to remove benzene, a known carcinogen, from solvents and transportation fuels.

In recent years the production of "green energy" has obtained much attention. From the practical point of view, the hydrogen storage in the porous materials seems to be an ideal solution. Also there has been considerable experimental and theoretical interest in the use of synthetic nano-structured carbon materials as potential hydrogen sorbents. Unfortunately, these materials contain metals (Fe, Co, Ni, Cu), used in the synthesis process and not removed during the purification step. Moreover, the purification treatment leads to the partial collapse of the nanostructure and formation of amorphous carbon. This prompted us to study nickel catalysts supported on an amorphous commercial activated carbon as materials for hydrogen storage. Activated carbon is a cheap material as compared to nano-structured synthetic carbon materials. Nickel is a metal widely used in the industry.

In this study we explored several factors determining the surface and catalytic properties of the supported nickel catalysts prepared by the hydrazine method. These factors are the conditions of catalyst preparation, the nature of the support or of the metal precursor and the metal loading. The results obtained are compared to that of conventional catalysts.

The presentation of the results of the work undertaken is divided into nine chapters.

A literature survey is presented in the first chapter.

All methods and techniques used in the thesis are reported in the second chapter. Prepared catalysts were characterized by different methods such as: XRD, XPS, low temperature adsorption and desorption of N_2, FTIR–pyridine adsorption, skeleton IR, TEM, SEM, X mapping, EDS, H_2-TPR, H_2-chemisorption, H_2-TPD, isopropanol decomposition

The third chapter comprises the preparation and characterization of the nickel catalysts supported on the commercial γ-Al_2O_3 and amorphous SiO_2 with high surface area. Two methods of impregnation were used. Simple impregnation method (SIM) and Double impregnation method (DIM) are compared. The comparison between classical method of reduction (in hydrogen flow) and non classical hydrazine reduction method is

made. Finally the prepared catalysts are studied in the gas phase benzene hydrogenation reaction.

The fourth and fifth chapters contain the preparation and characterization of the nickel particles supported on the reducible oxides. Two oxides are studied: CeO_2 and Nb_2O_5. In case of the niobia supported catalysts, the SIM and DIM methods of impregnation were used. The strong nickel-niobia interactions were studied. The non classical catalysts reduced by hydrazine are compared to the classically prepared catalysts. In case of the non classical nickel cerium catalysts, the effect of nickel content was studied. Prepared catalysts were studied in the benzene hydrogenation reaction.

The sixth chapter is consecrated to the bimetallic nickel–silver catalysts. The catalysts were prepared by the chemical reduction with hydrazine. The catalysts with different nickel–silver ratios were studied. Two different silicas used as nickel supports are compared. The deep study of silver effect was done. The comparison between impregnation and precipitation preparation methods is made. The activity of the catalysts was also examined in the benzene hydrogenation reaction.

The seventh part comprises the complete study of the nickel supported on activated carbon. The effects of nickel precursor and nickel loading have been studied. Moreover the different methods of preparation were used. The classical catalysts are compared to their non classical counterparts. The effect of the hydrogen spillover on catalysts activity was studied by the dilution of the nickel catalysts with the carbon support. The activity of the catalysts was studied in the benzene hydrogenation reaction.

The eighth part of this thesis is consecrated to the hydrogen storage study on the nickel supported on activated carbon catalysts. The study of hydrogen storage at room temperature was studied on the catalysts characterized in Chapter VII. We explored several factors determining the level of storage: method of catalyst preparation, nature of the metal precursor, metal loading and support catalyst dilution. The mechanism of hydrogen storage via spillover phenomenon is proposed and discussed.

Finally, all the results obtained are discussed and summarized in the ninth chapter.

We collaborated to the study of CeO_2 supported nickel catalysts prepared by γ-radiolysis by Sabah Chettibi (Contantine University). We examined the reactivity towards hydrogen and in benzene hydrogenation of these catalysts. The results obtained will be fully presented in the PhD Thesis of Sabah Chettibi. We report the common publication in Annex.

CHAPTER I
LITERATURE REVIEW

1. Nanoscale level

The recent definition of nanotechnology was done by National Nanotechnology Initiative (NNI) [1-2] in 2000. The essence of nanotechnology is the ability to work at the molecular level, atom by atom, to create large structures with fundamentally new molecular organization.

Nanoscale level is bridging the gap between molecular level system design and single crystal based solid state devices. In this Nanoscale regime, classical laws of physics which are valuable for bulk materials are no longer applicable by quantum mechanical rules [3]. Key to understanding the unique power and potential of nanotech is that, at the nanoscale (below about 100 nanometres), a material properties can change dramatically-these unexpected changes are called "quantum effects." With only a reduction in size and no change in substance, materials can exhibit new properties such as electrical conductivity, elasticity, greater strength, different colour and greater reactivity-characteristics that the very same substances do not exhibit at the micro or macro scales [3].

1.1. Nanomaterials

Nanostructured materials may be defined as those materials whose structural elements—clusters, crystallites or molecules—have dimensions in the 1 to 100 nm range [4-5]. The explosion in both academic and industrial interest in these materials over the past decade arises from the remarkable variations in fundamental electrical, optical and magnetic properties that occur as one progresses from an "infinitely extended" solid to a particle of material consisting of a countable number of atoms [4].
The recent interest in nanoscale properties of condensed matter is directly correlated to the appearance of surface effects when one or more dimensions are reduced below a critical length scale.
Two key factors controlling the properties of nanomaterials are the size and surface characteristics of nanoparticles [6-8]. These two factors are interrelated because the *surface to volume (S/V)* ratio increases as the size decreases [9]. Because surface atoms tend to be coordinatively unsaturated, there is a large energy associated with this surface. The smaller the nanocrystal, the larger the contribution made by the surface

energy to the overall energy of the system and, thus, the more dramatic the melting temperature depression [9].

Many names and labels have been used during the evolution of nanostructured materials. However the strict definitions have been presented [12]:

- ***Cluster*** – a collection of units (atoms or reactive molecules) of up to about 50 units. Cluster units are such moieties surrounded by a ligand shell that allows isolation of a molecular species (stable, isolable and soluble)
- ***Colloid*** – a stable liquid phase containing particles in the 1 – 1000 nm range
- ***Nanoparticle*** – a solid particle in the 1 – 1000 nm range that could be nanocrystalline, an aggregate of a crystallites or a single crystallite
- ***Nanocrystal*** – a solid particle that is a single crystal in the nanometer size range
- ***Nanostructured material*** – any solid material that has a nanometer dimension. Nanomaterials with three, two and one dimension are referring to as particles, thin films and thin wires, respectively
- ***Nanophase material*** – the same as nanostructured material
- ***Quantum dot*** – a particle that exhibits a size quantization effect in at least one dimension

According to Pomogailo [13], nanoparticles with regard to their size may be divided into three following types:

- ***Nanometric (ultradispersed)*** – particles with size ranging from 1 to 35-50 nm
- ***Highly dispersed*** – particles with size ranging from 30-50 to 100-500 nm
- ***Micrometric*** – this type of particles composed of individual particles and their aggregates with size ranging from 100-500 to 1000 nm

1.2. Metal nanoparticles

Metallic nanoparticles exhibit unusual optical, thermal, chemical and physical properties that are due to a combination of large proportion of high energy surface atoms compared to the bulk solid and to the nanometer scale mean free path of an electron in a metal [14]. Synthesis of metal nanoparticles has received considerable attention in the past two decades in view of the potential application for these new

materials. There are generally two routes for preparation of nanoscale particles: top-down and bottom-up. Top down methods reduce macroscopic particles to the nanosize scale, e.g. by the mechanical grinding of bulk materials, while bottom-up methods start with atoms that aggregate in solution or even in the gas phase to form particles of definite size under appropriate experimental conditions [12]. Top-down processes are hardly suited for preparing particles with uniform shape and particle size smaller than about 100 nm. However, bottom-up routes are much better for generating uniform particles with distinct size, shape and structure [12].

Nanoparticles have been synthesized by a variety of methods [11]. Common synthetic techniques for semiconductor nanoparticles employ the use of constrained environments, such as inverse micelles [15-18] ; capping agents, which arrest the growth of particles when they reach a certain size [19]; ionomers [20] and gels [19]; solid polymer environments [21-22]; or dendrimers [23]. For transition metal nanoclusters, however, some authors [24] points out that there are five general synthetic methods; the key requirement of each is that it results in the "facile deposition of metallic precipitates" [11]. These five methods are [11]:

- transition metal salt reduction,
- thermal decomposition and photochemical methods,
- ligand reduction and displacement from organometallics,
- metal vapor synthesis.
- γ-radiolysis

Especially the chemical reduction of metals salts from the solution or suspensions methods have been most extensively studied. The chemical precipitation from solutions is again probably the most versatile, economical and easy to perform procedure [25]. However, preparation techniques, especially of very small particles, involving the use of high concentrations of surfactants, such as precipitation in microemulsions, etc. The solution route to synthesize finely dispersed metal powders can be conducted in two distinct ways [26]: (i) direct precipitation of particles from homogeneous solutions using appropriate reducing agents, and (ii) preparation of finely dispersed particles of metal compounds, followed by subsequent conversion to metals of essentially the same shape through reduction in solution or gas phase, at ambient or elevated temperature and pressure [26].

The reduction of oxidized metallic species leading to neutral atoms, the building blocks of metal particles, is the result of redox reactions in which electrons from a

reducing agent are transferred to the metal according to the following schematic chemical equation (1) [26]:

$$mMe^{n+} + nRed \rightarrow mMe^{0} + nOx \qquad (1)$$

The driving force of the reaction is the difference between the redox potentials of the two half cell reactions, ΔE. The reduction reaction is thermodynamically possible only if ΔE is positive, which implies that the redox potential of the reducing agent must have a more negative value than that of the metallic species [26]. This difference should be larger than 0.3- 0.4 V; otherwise, the reaction may not proceed or proceed too slowly to be of any practical importance. Thus, strongly electropositive metals like Au, Pt, Pd, Ag, Rh will react even with mild reducing agents under ordinary conditions, while more electronegative metals like Ni, Co or Mo require very strong reducing agents and, frequently, extreme conditions of temperature and pressure [26].

Table I-1. Reducing agents and reaction conditions in the metal particle preparation [26].

Metal species	Reducing agent	Conditions	Reaction rate
Au^{3+}, Au^{+}, Pt^{4+}, Pt^{2+}, Pd^{2+}, Ag^{+}, Rh^{3+}, Hg^{2+}, Ir^{3+}	Organic acids, alcohols, polyols, sugars, aldehydes, N_2H_4, boranes, $NaBH_4$, H_2SO_3, H_3PO_2	298-343 K	Moderate or fast
Cu^{2+}, Re^{3+}, Ru^{3+}	Polyols, sugars, N_2H_4, aldehyds	343-393 K	Moderate or slow
Cd^{2+}, Co^{2+}, Ni^{2+}, Fe^{2+}, Mo^{3+}, In^{3+}, Sn^{2+}, W^{6+}	Polyols, N_2H_4, $NaBH_4$, boranes	298-433 K	Moderate or slow
Cr^{3+}, Mn^{2+}, Ta^{5+}, V^{2+}	$NaBH_4$, boranes	T,P » ambient	Slow

The selection of an appropriate reducing agent and working conditions listed in Table I-1 is applicable only for uncomplexed metal ions. If metallic species are involved in the formation of solute complexes or compounds, the standard redox potential, will be lower [26]. The decrease in the potential depends on the stability of these complexes or compounds, as reflected in the value of the stability constant, or the solubility product. The consequence of this effect is a drastic limitation in the choice of reducing agents capable of reducing a metal and the need for harsher conditions as the stability of its complex increases [26]. On the other hand, changing the value of ΔE through skillful manipulations of metal complex chemistry can be used to tailor the reactivity of the species in a given metal-reducing-agent system. The formation of different complexes is not the only tool available to alter the reactivity of a metal through ΔE manipulations [26]. The majority of redox systems in aqueous solutions involve H^+ and OH^- ions. As a result, the pH of the reaction medium can have a major impact upon the redox potential of the solutes, as predicted by the Nernst equation. Since metal species and reducing agents can be affected simultaneously by the pH, the overall effect upon ΔE and, consequently, the reduction process may be rather involved [26].

1.3. Nickel nanoparticles

Among the various kinds of metal nanoparticles, the preparation of some metal nanoparticles such as nickel are relatively difficult because they are easily oxidized [27]. Recently fine nickel powder has been studied extensively because of its potential applications such as conducting paints, rechargeable batteries, magnetic recording media and catalysts [28]. Several methods such as hydrogen arc plasma [29], borohydride reduction of metal salt [30-31], γ-ray irradiation [32-34], sonochemical [35] and thermal decomposition of organic nickel complexes [36-39] and chemical reduction with hydrazine in aqueous [40-44] and non-aqueous [27-28, 45-48] media have been used for preparation of nickel nanoparticles with nanometer size. As the need for desired properties of nickel powder and economical aspects of process, the chemical reduction method seems to be especially interesting. The soft reduction with hydrazine in aqueous media has been researched due to the good solubility of the nickel salt in water, low reaction temperature and simple procedure. In this method, the morphology of the nickel particles such as shape, size and size distribution of particles can be

relatively easy controlled by the reaction parameters, solvent composition, a nucleation agent and a surfactant [28, 49-50].

Degan and Macek [51] used hydrazine as a reducing agent to prepare nickel powders in the submicrometer size range from nonaqueous solutions of nickel salts. The rate and yield of the reaction were both enhanced at higher reaction temperatures but were limited by the relatively low boiling point of water. Nickel powders with mean particle sizes ranging from 0,1 to several μm and with up to 99,8% purity were obtained by this method. Chen [52] used a hydrazine for reducing nickel salt in water or n-hexanol solutions in the presence of cetyltrimethylammonium bromide (CTAB). The average diameter of nickel nanoparticles was found to decrease with the increase of hydrazine concentration and approached to a constant value when hydrazine concentration was above 0.5 M. Since a minimum number of atoms were required to form a stable nucleus, a collision between several atoms must occur for a nucleation. However, the probability was much lower than the probability for the collision between one atom and a nucleus already formed [53]. That is, once the nuclei were formed, the growth process would be superior to the nucleation. In addition, the resultant nanoparticles were essentially monodispersed. Therefore, it might be suggested that all of the nuclei were formed almost at the same time and grew at the same rate [53]. The number of the nuclei formed at the very beginning of the reduction determined the number and size of the resultant particles. At a low hydrazine concentration, the reduction rate of nickel chloride was slow and only few nuclei were formed at the early period of the reduction [53]. The atoms formed at the later period were used mainly to the collision with the nuclei already formed instead of the formation of new nuclei and therefore led to the formation of larger particles. With the increase of hydrazine concentration, the enhanced reduction rate favored the generation of much more nuclei and the formation of smaller nanoparticles [53]. When the concentration ratio of hydrazine to nickel was large enough (>10), the reduction rate of nickel chloride was much faster than the nucleation rate and almost all nickel ions were reduced to atoms before the formation of nuclei. The nucleation rate was not further raised, and the number of nuclei held constant with the increase of hydrazine concentration [53]. It was also found [52] that the average diameter of nickel nanoparticles was not effected by the increase of nickel chloride concentration when the nickel chloride was below 0.1 M. The results revealed that the size of nickel nanoparticles was not affected significantly by the nickel concentration when the hydrazine concentration was large enough.

Nagy [54] reported that the average diameter of both the nickel boride nanoparticles prepared in the water-CTAB-n-hexanol microemulsion system decreased first and then increased with the increase of their corresponding metal salt concentrations. They considered that the formation of the relatively large particles at low ion concentration was due to the fact that only few water pools contained the minimum number of ions required to form a nucleus, and hence only few nuclei were formed at the very beginning of the reduction. When the ion concentration increased, they found that the number of nuclei obtained by reduction increased faster than the total number of ions, and hence the particle size decreased [54].

1.4. Bimetallic nanoparticles.

Bimetallic nanoparticles, composed of two different metal elements, are of greater interest than monometallic ones, from both the scientific and technological views, for the improvement of the catalytic properties of metal particles [55]. This is because bimetallization can improve catalytic properties of the original single-metal catalysts and create a new property, which may not be achieved by monometallic catalysts. These effects of the added metal component can often be explained in terms of an ensemble and/or a ligand effect in catalysis [55].

As the name implies, bimetallic nanoparticles are metallic entities comprising atoms of two different metallic elements. Compared with monometallic nanoparticles, bimetallic nanoparticles are of special interest for several reasons. First, they may serve as models for studying the formation of different alloys. Second, these bimetallic particles may have more varied properties than monometallic particles as various combinations are possible. It is well established that the catalytic properties of the monometallic particles, including activity, selectivity or resistance to deactivation, can be altered by the addition of the second metal. Third, bimetallic particles could have particular structures not seen in bulk alloys, such as core-shell, cluster-in-cluster, separate, random structures, etc [12].

It is well known that the precipitation of a solid from a solution proceeds in two steps: nucleation and particle growth [56]. During the nucleation step nuclei are formed by a stepwise bimolecular addition of monomeric entities of the solute. In order to initiate the spontaneous growth of stable particles the small aggregates which form the nuclei have to reach a critical size. If these nuclei appear spontaneously without the

promoting effect of impurities the nucleation is called homogeneous [56]. In order to obtain monodisperse particles a first general condition must be fulfilled: nucleation and growth must be two completely separated steps. In case of the preparation of the bimetallic CoNi particles the heterogeneous nucleation can be achieved by forming *in situ* seed particles for example by adding, before the spontaneous nucleation takes place, a solution of silver nitrate which is readily reduced in the conditions of reduction of Co and Ni precursors and forms tiny metallic silver particles acting as foreign nuclei for the subsequent growth of Co and Ni particles. The addition of silver nitrate in the medium shortens the reaction time and makes easier the formation of monodisperse CoNi powders with a better reproducibility. Fievet et al. [56] showed that the bimetallic powders obtained from homogeneous nucleation exhibit a low degree of agglomeration, the particles are quasi spherical with a mean diameter in the micrometer size range (generally 1 μm – 2 μm) and a narrow size distribution. Bimetallic particles obtained from heterogeneous nucleation exhibit a very narrow size distribution and a mean size in submicrometer range. By varying the amount of the silver nitrate, the final particle size has been varied in the range 0,1 – 1 μm. From a simple model in which (i) silver nuclei are supposed to be independent of the amount of $AgNO_3$ introduced and (ii) no agglomeration is supposed to take place during the growth step (each metallic particle is issued from a single silver nucleus), it has been shown that the mean diameter of the final particles is expected to be proportional to $C^{-1/3}$ where C is the molar ratio Ag/[Co + Ni].

It is well known that Ag and Ni are insoluble in the liquid as well as a solid state [57]. However, there have been report of existence of a separate alloy phase with a fcc structure and a lattice parameter between that of silver and nickel [58-59]. Poondi et al. [60] have obtained metastable alloys of silver and nickel using a laser liquid-solid interaction technique. The shape of the particles was found to be dependent on laser parameters and the chemical composition of the precursor solution. The Ag/Ni alloy formation was also observed by Kumar et al. [57] in thermally evaporated stearic acid film. This formation occurred at the low temperature of 373 K. Authors proposed that the silver and nickel particles could grown simultaneously in the fatty acid matrix and a low temperature heat treatment of the nanoparticle film at 373 K resulted in the formation of a crystalline Ag-Ni alloy phase [57].

2. Supported nickel particles

The goal of a catalyst manufacturer is to produce and reproduce a commercial product which can be used as a stable, active and selective catalyst. To achieve this goal, the best preparative solution is sought which results in sufficiently high surface area, good porosity, and suitable mechanical strength [61]. The first of these, surface area, is an essential requirement in that reactants should be accessible to a maximum number of active sites. The properties of a good catalyst for industrial use may be divided, at least for the purpose of easy classification, into two categories [61]:

- properties which determine directly catalytic activity and selectivity, here such factors as bulk and surface chemical composition, local microstructure, and phase composition are important;
- properties which ensure their successful implementation in the catalytic process, such as thermal and mechanical stability, porosity, shape, and dimension of catalyst particles enter.

The requirements which are fundamental for catalyst performance generally require a compromise in order to produce a material which meets the contradictory demands imposed by industrial processes [61]. An acceptable solution is typically ascertained by a trial-and-error route. Catalytic materials become catalysts when they are used in industrial processes. A way this can be realized occurs when the variety of methods used to prepare catalytic materials are viewed in relation to their successful implementation in commercial applications [61].

2.1. Supports for nickel particles

Supported nickel catalysts have been widely studied in the heterogeneous catalysis. Supported catalysts consist of an active phase dispersed on a carrier [62-66]. The catalytic reaction takes place at the internal surface (i.e. in the pores) of the catalyst [67]. Good supports combine relatively high dispersion with a high degree of thermal stability of the catalytic component [62-63, 66]. Furthermore, the support should enable the production of a large shaped particle composed of very small easily sintered crystals of active phase which are prevented from coalescing by being separated by the support component [67]. The various supports have been already used as a nickel carrier. The supports the most widely utilized are the non reducible oxides such as SiO_2 [68-71],

Al_2O_3 [72-75], or the zeolites [76-77] and mesoporous materials e.g. MCM-41 and AlMCM-41 [78-81]. In case of the reducible oxides the TiO_2 [82-83], CeO_2 [84-85], and Nb_2O_5 [86-87] are the most popular. Moreover the non oxide carriers such as active carbon [88-89], were also studied. The supports used in this thesis are briefly described below.

2.1.1. Cerium (IV) oxide – CeO_2

Cerium (IV) oxide is a stable yellow oxide with a cubic fluorite structure (Figure I-1). It has been extensively studied because of its interesting redox and high dispersive properties. CeO_2 is able to change reversibly from Ce^{IV}, under oxidizing conditions to Ce^{III} (giving Ce_2O_3), under reducing conditions [90]. Oxygen atoms in CeO_2 units are very mobile and leave easily the ceria lattice, giving rise to a large variety of non-stoichiometric oxides with two limiting cases CeO_2 and Ce_2O_3 [90]. The oxygen vacancies are responsible for the ionic conductivity of the ceria. Ceria has an insulator behavior in the stoichiometric oxidized state CeO_2 and becomes conductor in the reduced state CeO_{2-x}, acquiring a great capacity to store and to carry oxygen. It was studied in particular in the aim to be used in the automobile emission control system [91].

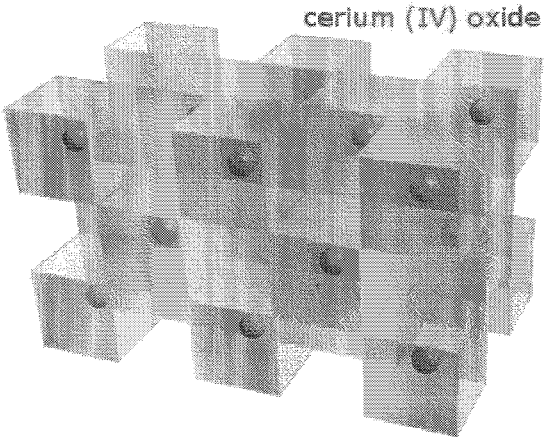

Figure I-1. Structure of the cerium (IV) oxide [92].

2.1.2. Niobium (V) oxide – Nb_2O_5

Hydrated niobium pentoxide (Nb_2O_5*nH_2O) which is usually called niobic acid has strong acidic properties on the surface and is used as solid acid catalyst. In particular, niobic acid containing large amounts of water exhibits high catalytic performances for acid-catalyzed reactions in which water molecules participate or are liberated [93]. Generally, hydrated niobium oxide crystallizes at 853 K, and its strong acid property disappears when it is heated to temperature higher than 800 K [94]. It possesses both Lewis acid sites and Brønsted acid sites on its surface.

Niobium (V) oxide is a white, air stable and water insoluble solid. It may be described as amphoteric but is more characteristicly inert. Its structure is extremely complicated and displays extensive polymorphism. Nb_2O_5 is probably comprised of NbO_6 octahedrons connected by edges and corners [94]. Figure I-2 shows a model of Nb_2O_5 structure.

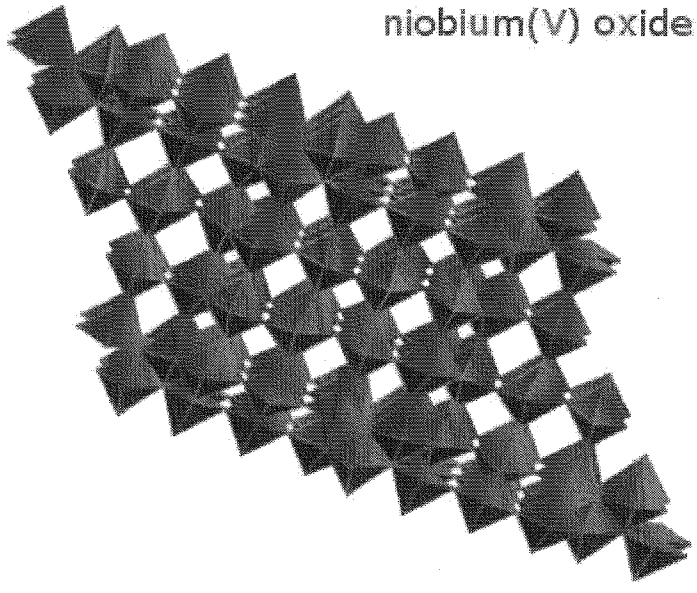

Figure I-2. Model of Nb_2O_5 structure [92].

High temperature reduction (1073-1573 K) of Nb_2O_5 with hydrogen gives the bluish black dioxide NbO_2 that has a distorted rutile structure and is diamagnetic. This

reduction is reversible. Further reduction of Nb_2O_5 (1573-1973 K) produces the gray monoxide NbO that has a cubic structure [94].

2.1.3. Silicon (IV) oxide – SiO_2

Silicon dioxide (silica) is one of the most commonly encountered substances in both daily life and in electronics manufacturing. Crystalline silicon dioxide (in several forms: quartz, cristobalite, tridymite) is an important constituent of a great many minerals and gemstones, both in pure form and mixed with related oxides. SiO2 is formed by strong, directional covalent bonds, and has a well-defined local structure: four oxygen atoms are arrayed at the corners of a tetrahedron around a central silicon atom. The structure of the crystallized SiO_2 is shown in Figure I-3. The oxygen atoms are electronegative, and some of the silicon valence electron density is transferred to the oxygen neighbors, but it is incorrect to regard the material as a salt of a Si[+4] ion with O[-2] ions: the directionality of the bonds is essential to the observed structures. The bond angles around O-Si-O are essentially the tetrahedral angle, 109 degrees; the Si-O distance is 1.61 A (0.16 nm) with very little variation. The result of this flexibility in the bridge bonds is that SiO2, while it has many different possible crystalline structures, can very easily form amorphous materials [95].

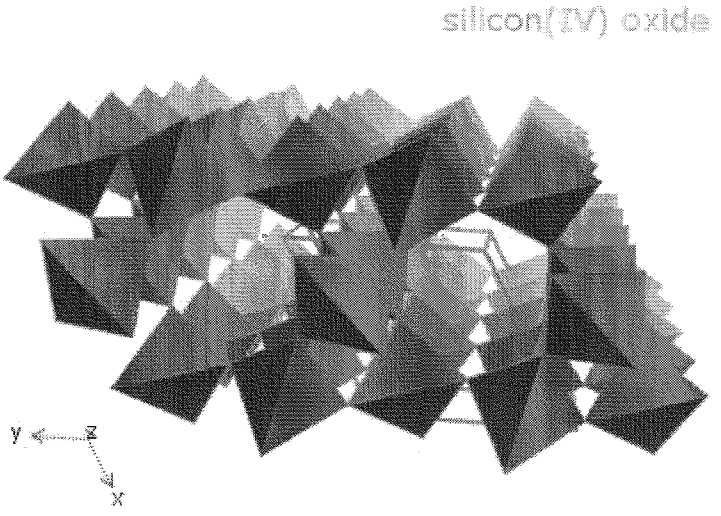

Figure I-3. Model of the quartz (SiO_2) structure [92].

Compared to the others oxides the surface of the SiO_2 is almost inert. The silanol groups present on the surface have a low acidity. The complete dehydroxylation of silica surface occurs at high temperature (973 K). Under this thermal treatment the chemical reaction between the silanol groups occurs provided the siloxane group (Si – O – Si) formation [98].

The amorphous silica (Fig I-4 and I-5) is usually obtained by the high temperature treatment of silica hydrogel to obtain an aerogels. Silica aerogels contain primary particles of 2-5 nm in diameter. Silica particles of such a small size have an extraordinarily large surface-to-volume ratio (~2 x 10^9 m^{-1}) and a corresponding high specific surface area (~900 m^2/g). The chemistry of the interior surface of an aerogel plays a dominant role in its chemical and physical behavior. It is this property that makes aerogels attractive materials for use as catalysts support [96].

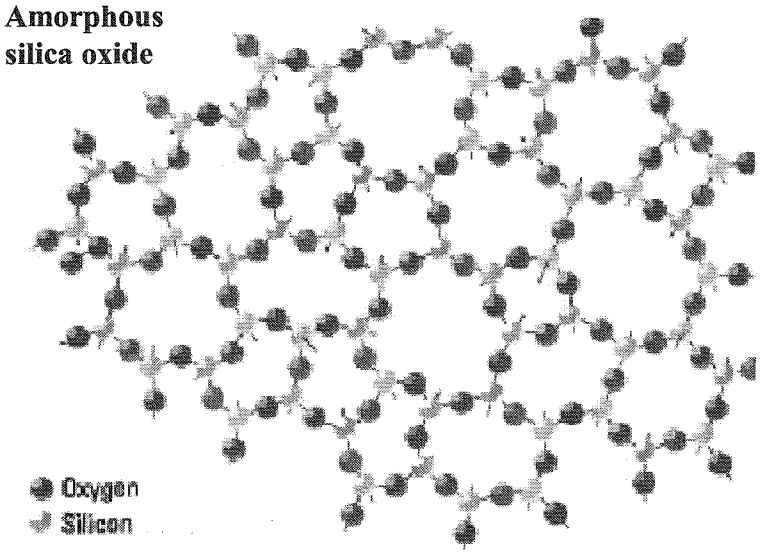

Figure I-4: Model of [SiO_4] tetrahedron arrangement in silica gel [97].

The nature of the surface groups of a silica aerogel is strongly dependent on the conditions used in its preparation. The extent of hydroxyl coverage is ~5 -OH/nm^2, a value consistent with other forms of silica. This value, combined with their high specific surface area, means that silica aerogels present an extremely large number of accessible hydroxyl groups. Silica aerogels are therefore a somewhat acidic material. A more striking effect of the hydroxyl surface is seen in the physical behavior of silica aerogels.

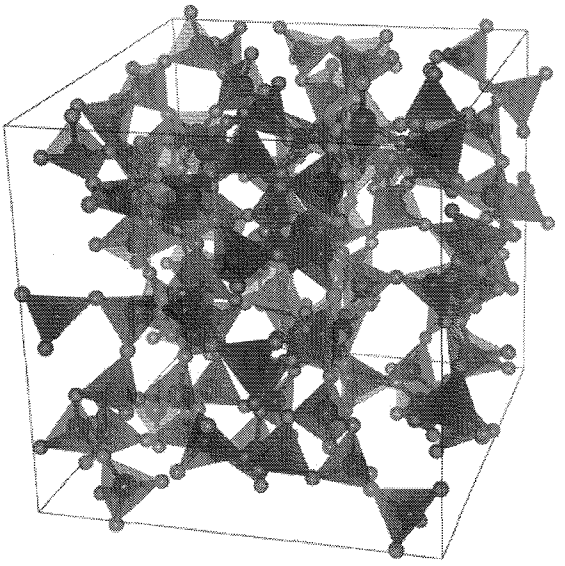

Figure I-5. Model of the amorphous (SiO_2) structure [92].

As with most hydroxyl surfaces, the surface of silica aerogels can show strong hydrogen-bonding effects. Because of this, silica aerogels with hydroxyl surface are extremely hygroscopic. Dry silica aerogels will absorb water directly from moist air, with mass increases of up to 20%. This absorption has no visible effect on the aerogel, and is completely reversible. While the adsorption of water vapor does not harm silica aerogels, contact with liquid water has disastrous results. The strong attractive force that the hydroxyl surface exerts on water vapor also attracts liquid water. However, when liquid water enters a nanometer-scale pore, the surface tension of water exerts capillary forces strong enough to fracture the solid silica backbone. The net effect is a complete collapse of the aerogel monolith. The material changes from a transparent solid with a definite shape to a fine white powder. The powder has the same mass and total surface area as the original aerogel, but has lost its solid integrity.

2.1.4. Aluminum (III) oxide Al_2O_3

Aluminum oxide, commonly referred to as alumina, possesses strong ionic interatomic bonding giving rise to its desirable material characteristics. It can exist in several crystalline phases which all revert to the most stable hexagonal alpha phase at elevated temperatures. This is the phase of particular interest for structural applications. Alpha phase alumina is the strongest and stiffest of the oxide ceramics. Its high hardness, excellent dielectric properties, refractoriness and good thermal properties make it the material of choice for a wide range of applications.

The aluminum oxides are commonly used as the supports for metal or oxides catalysts. Especially, the gamma γ-Al_2O_3 which is stable in both oxidizing and reducing atmospheres and at relatively high temperatures. Moreover, with an excellent combination of these properties and an attractive price, it finds a very wide range of applications.

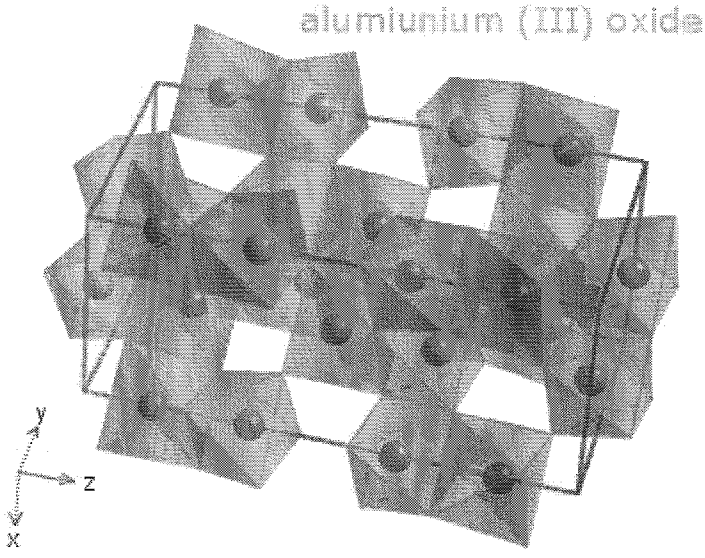

Figure I-6. Model of α-Al_2O_3 oxide crystallographic structure [92].

Figure I-6 shows a typical crystallographic structure of α-Al_2O_3 with the $[AlO_6]$ octahedral groups. γ-Al_2O_3 has a defected spinel structure with the layers of O^{2-} ions in the hexagonal packing and with the layers of Al^{3+} ions in the octahedral and tetrahedral coordination. Defected spinel structure means that the O^{2-} ions have a spinel structure but the cations deficit occurs [98].

2.1.5. Activated carbon (AC)

The chemical nature of amorphous carbon, combined with a high surface area and porosity, makes it an ideal medium for the adsorption and absorption of organic chemicals. Activated charcoal is a very mature technology that is designed to remove taste, smell and odor from gases and liquids through adsorption of the compounds that cause problems. Activated carbon is used primarily for purifying gases by adsorption, solvent recovery, or deodorization and as an antidote to certain poisons. Figure I-7 shows a model of graphite structure.

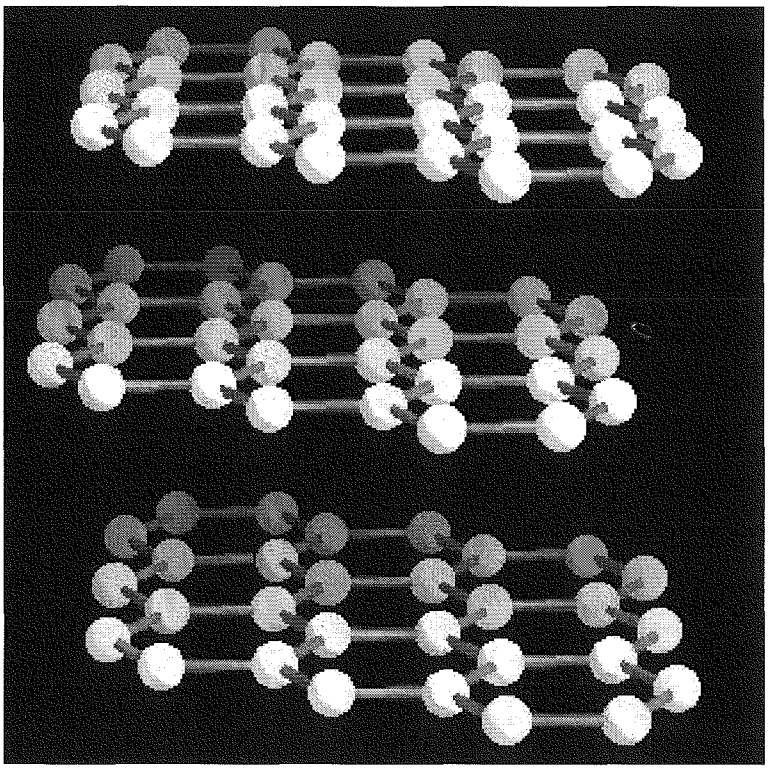

Figure I-7. Model of the graphite structure [92].

2.2. Methods of preparation of supported nickel catalysts

Methods of catalyst preparation are very diverse and each catalyst may be produced via different routes. Preparation usually involves several successive steps. Many supported metal and oxide catalysts are prepared by the succession of impregnation, drying, calcination and activation. The properties of heterogeneous catalysts depend on all their previous history. Three fundamental stages of catalyst preparation may be distinguished [99]:

- preparation of the primary solid (or first precursory solid) associating all the useful components (e.g., impregnation or coprecipitation);
- processing of that primary solid to obtain the catalyst precursor, for example by heat treatment;
- activation of the precursor to give the active catalyst: reduction to metal (hydrogenation catalysts), formation of sulfides (hydrodesulfurisation). Activation may take place spontaneously at the beginning of the catalytic reaction (selective oxidation catalysts).

2.2.1. Simple impregnation method (SIM)

Impregnation consists in contacting a solid with a liquid containing the components to be deposited on the surface. During impregnation many different processes take place with different rates [99].

- selective adsorption of species (charged or not) by coulomb force, van der Waals forces or H-bonds;
- ion exchange between the charged surface and the electrolyte;
- polymerisation/depolymerisation of the species (molecules, ions) attached to the surface;
- partial dissolution of the surface of the solid.

The type of product depends on (i) the nature of both reactants (the liquid and the solid surface), and (ii) the reaction conditions. The main parameters affecting the liquid are the pH, the nature of the solvent, the nature and concentrations of the dissolved substances. The first parameter affects ionisation and, in many cases, the nature of the ions containing the active elements. The second and third influence solvation. The main properties of the solid are the texture, the nature of functional groups (e.g., the number

and strength of the acidic and basic centres, the isoelectric point), the presence of exchangeable ions, and the reactivity (surface dissolution in acidic or basic solution, etc.). In the overall impregnation process the following important facts should be noted [99]:

- the properties of the liquid in the pores are different from those measured in the bulk;
- equilibrium between liquid and solid is slow to establish and even distribution of attached species inside the pores is not easy to attain;
- deposition involves many different types of interaction

2.2.2. Double impregnation method (DIM)

Two or several active components are introduced sequentially. Drying (and often calcination) takes place between the impregnations. For the second impregnation the properties of the surface to take into account are those of the solid obtained after the previous impregnation. In contrast to the simple impregnation method, in the DIM procedure preparation the support is preliminarily activated (modified) using the chelating agents such as EDTA, urea or citric acid [100-101]. This chelating compound allows to better dispersion of metal active phase. Moreover it could be decomposed at relatively low temperatures.

2.2.3. Precipitation method

In all precipitations it is essential to carefully control all the details of the process including [99]:

- the order and rate of addition of one solution into the other;
- the mixing procedure;
- the pH and variation of pH during the process
- the maturation process.

Precipitation involves two distinct processes, namely nucleation and growth. Nucleation requires that the system is far from equilibrium (high supersaturation, or, in the case of ionic species, a solubility product far exceeding the solubility constant of the solid to be precipitated) [99]. Growth of the new phase takes place in conditions which gradually approach the equilibrium state. In the co-precipitation of a phase associating two (or

several) elements, if one of them is contained in an anion and the second in a cation, the precipitate will have a fixed or at least very inflexible composition [99]. If both are cations (or both anions) the characteristics of the reactions with a common anion (or cation) of the solution, the solubility constants, and the supersaturation values will all be different, and the properties of the precipitate will change with time. Consequently, co-precipitation does not in general give homogeneous precipitates. Methods are available to produce homogeneous precipitates [99]. The dispersion of the precipitate changes with the degree of supersaturation and its evolution during precipitation. Low supersaturation leads to poorly dispersed solids. Highly dispersed solids are thermodynamically unstable and tend to lose dispersion (Ostwald ripening). This takes place during the process of precipitation itself. If the effect is desired, a special maturation (or ageing) step is carried out at the end of the precipitation [99].

2.2.4. Precipitation – deposition method

Precipitation-deposition method is a special technique in which an active element (e.g. Ni) is deposited onto a carrier (e.g. $Si0_2$) in suspension in the precipitating solution (e.g. $Ni(NO_3)_2$) by slow addition, or in situ formation, of a precipitating agent (e.g. NH_4^+). The technique takes advantage of the fact that precipitation onto the carrier needs a lower supersaturation than formation of the new phase directly from the liquid. It is essential to maintain supersaturation at a constant moderate level [99]. This is achieved, as in the homogeneous precipitation technique, by decomposition of a suitable substance (e.g. urea), which releases the precipitating agent continuously, or by controlled and progressive addition of the precipitating agent. The technique is excellent if the primary particles of the carrier are not porous (e.g. Aerosil). With a porous support deposition takes place preferentially in the external parts [99].

3. Hydrogen storage.

3.1. Methods and materials

Hydrogen is an ideal alternative to fossil fuels from an environmental point of view because its combustion does not generate pollutants such as particles, nitrogen oxides, sulphur oxides, hydrocarbons, and carbon monoxide. From an economic point of view, the use of hydrogen could revolutionize energy and transportation markets, which is what generates great interest toward this fuel [103].

Hydrogen is a perfect fuel in decreasing the emissions, since when reacted with oxygen it produces only water as a reaction product. One way to employ hydrogen is to use a fuel cell, which converts the chemical energy of hydrogen directly into water, electricity, and heat according to the reaction (2) [104]:

$$H_2 + \frac{1}{2}O_2 \rightarrow H_2O + electricity + heat \qquad (2)$$

However, hydrogen is not a primary source of energy since it does not exist in free forms on Earth. Hydrogen can be found in water and several other chemical compounds from which it has to be separated before it can be used. The energy needed for this has primarily to be produced with renewable energy sources in order to achieve the environmental benefits of hydrogen [104].

The concept of hydrogen economy is based on three important aspects of using hydrogen as the fuel for our energy needs, namely production, storage and distribution. However, today all the three aspects have not yet reached any mature status to be adopted and placed in position to be exploited by the society [105]. The available technologies for hydrogen production as well as for the hydrogen storage are not economical and the distribution infrastructure is yet to be built up [105].

Hydrogen storage basically implies the reduction of the enormous volume of the hydrogen gas. 1kg of hydrogen at ambient temperature and atmospheric pressure takes a volume of 11 m^3. In order to increase the hydrogen density in a storage system, work must either be applied to compress hydrogen, or the temperature has to be decreased below the critical temperature or, finally, the repulsion has to be reduced by the interaction of hydrogen with an other material [106]. The second important criterion of

a hydrogen storage system is the reversibility of the hydrogen uptake and release [106]. This criterion excludes all covalent hydrogen carbon compounds as hydrogen storage materials because the hydrogen is only released from carbon hydrogen compounds if they are heated to temperatures above 1073 K or if the carbon is oxidized. There are basically five methods in order to reversibly store hydrogen with a high volumetric and gravimetric density [106]:

3.1.1. High pressure gas cylinders

Compressed hydrogen seems to be the easiest method for hydrogen storage. The most common storage systems are high pressure gas cylinders with a maximum pressure of 20 MPa. New light weight composite cylinders have been developed which are able to withstand a pressure up to 80 MPa and so the hydrogen can reach a volumetric density of 36 $kg \cdot m^{-3}$ approximately half as much as in its liquid form at the normal boiling point [106]. The gravimetric hydrogen density decreases with increasing pressure due to the increasing thickness of the walls of the pressure cylinder. Most pressure cylinders today have used austenitic stainless steel, copper or aluminium alloys which are largely immune to hydrogen effects at ambient temperatures [106]. However, the current state of the art in compressed hydrogen cylinders is the carbon fiber wrap and a polymer liner. These tanks are light and robust.

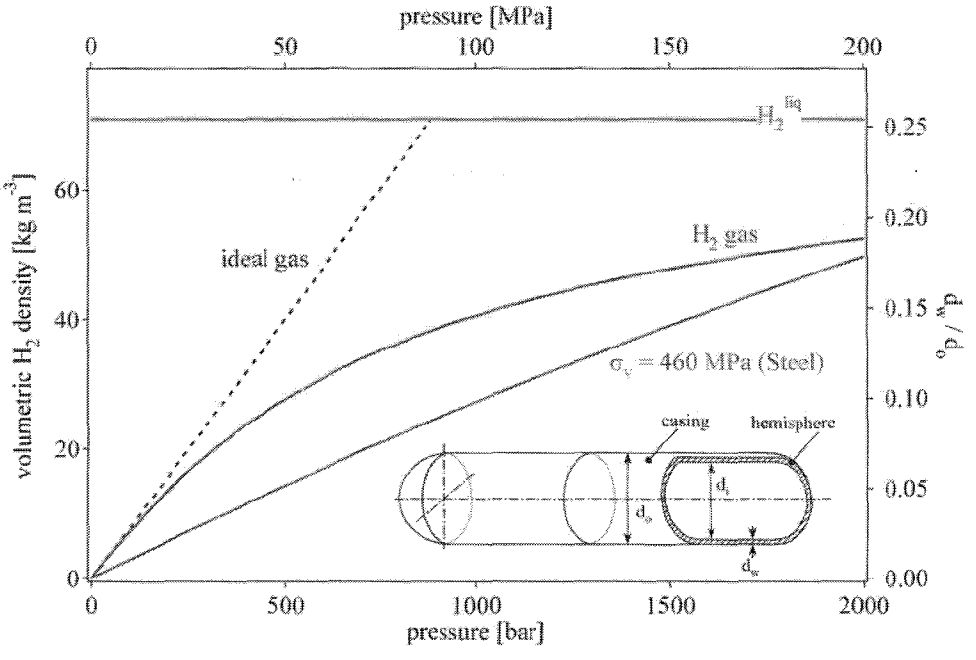

Figure I-8. Volumetric density of hydrogen inside the cylinder [106].

Figure I-8 shows the volumetric density of the hydrogen inside the cylinder. The volumetric density increases with pressure and reaches a maximum above 1000 bar, depending on the tensile strength of the material. However, the gravimetric density decreases with increasing pressure [106]. Non ideal gas behaviour of compressed hydrogen is showed.

3.1.2. Liquid hydrogen

Liquid hydrogen is stored in cryogenic tanks at 21.2 K at ambient pressure [106]. Due to the low critical temperature of hydrogen (33K) liquid hydrogen can only be stored in open systems, because there is no liquid phase existent above the critical temperature. The pressure in a closed storage system at room temperature could increase to about 104 bars. The volumetric density of liquid hydrogen is 70.8 $kg \cdot m^{-3}$ and slightly higher than that of solid hydrogen (70.6 $kg \cdot m^{-3}$) [106]. However, liquefaction consumes nearly 30% of the total energy contained in the hydrogen and in addition requires expensive equipment and energy to retain hydrogen in the liquid state. A relatively new way for researchers is the use of pressurized cryogenic tanks to enable use of both compressed hydrogen and/or liquid hydrogen, lessening the evaporation losses associated with the latter.

3.1.3. Metal hybrids

Chemical bonding of hydrogen in solid material is expected to offer the highest hydrogen density of the known storage methods. Various metals, intermetallic compounds and metallic alloys can react with hydrogen forming, mainly solid, metal hybrids. The reaction of hydrogen gas with a metal is called the absorption process and can be described in terms of a simplified one-dimensional potential energy curve (one-dimensional Lennard-Jones potential, Figure I-9) [106].

For the practical application, the metal hydrides can be distinguished in two groups depending on the temperature of hydrogen adsorption/desorption, below or above 423 K. Hydrogen reacts at elevated temperature with many transition metals and their alloys to form hydrides. The electropositive elements are the most reactive, i.e., scandium, yttrium, the lanthanides, the actinides, and the members of the titanium and

vanadium groups [106]. The binary hydrides of the transition metals are predominantly metallic in character and are usually referred to as metallic hydrides. They are good conductors of electricity, possess a metallic or graphite-like appearance, and can often be wetted by mercury [106]. Many of these compounds (MH_n) show large deviations from ideal stoichiometry (n = 1, 2, 3) and can exist as multi-phase systems [106].

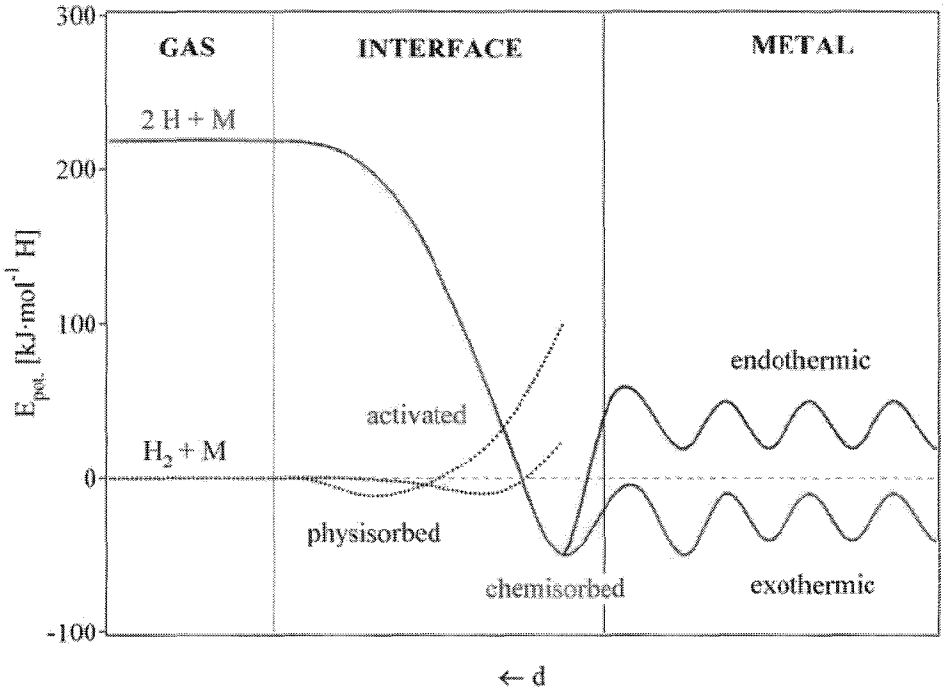

Figure I-9. Lennard-Jones potential of hydrogen approaching a metallic surface [106].

The lattice structure is that of a typical metal with atoms of hydrogen on the interstitial sites; for this reason they are also called interstitial hydrides. This type of structure has the limiting compositions MH, MH_2 and MH_3; the hydrogen atoms fit into octahedral or tetrahedral holes in the metal lattice, or a combination of the two types [106]. Only a small number of the transition metals are without known stable hydrides. A considerable "hydride gap" exists in the periodic table, beginning at group VI (Cr) up to group XI (Cu), in which the only hydrides are palladium hydride ($PdH_{0.7}$), the very unstable nickel hydride (NiH<1) and the poorly defined hydrides of chromium (CrH, CrH_2) and copper (CuH). In palladium hydride, the hydrogen has high mobility and probably a very low charge density. In the finely divided state, platinum and ruthenium are able to adsorb considerable quantities of hydrogen, which thereby becomes

activated [106]. The most important families of hybride are the ternary system AB_XH_N, where A is an element with a high affinity to hydrogen and B is an element with a low affinity to hydrogen [106]. The A element is usually a rare earth or an alkaline earth metal and tends to form a stable hydride. The B element is often a transition metal and forms only unstable hydrides such as nickel which is an excellent catalyst for the hydrogen dissociation. Some well defined ratios of B to A in the intermetallic compound: x = 0.5, 1, 2, 5 have been found to form hydrides with a hydrogen to metal ratio of up to two [106].

Some metal hydrides absorb and desorb hydrogen at ambient temperature and close to atmospheric pressure. One of the most interesting features of the metallic hydrides is the extremely high volumetric density of the hydrogen atoms present in the host lattice. The highest volumetric hydrogen density known today is 150 $kg \cdot m^{-3}$ found in Mg_2FeH_6 and $Al(BH_4)_3$ [106]. Metallic hydrides reach a volumetric hydrogen density of 115 $kg \cdot m^{-3}$ e.g. $LaNi_5$. Most metallic hydrides absorb hydrogen up to a hydrogen to metal ratio of H/M = 2. Greater ratios up to H/M = 4.5 e.g. $BaReH_9$, [107] have been found, however all hydrides with a hydrogen to metal ratio of more than 2 are ionic or covalent compounds and belong to the complex hydrides [106]. Metal hydrides are very effective to store large amounts of hydrogen in a safe and compact way. All the reversible hydrides working around ambient temperature and atmospheric pressure consist of transition metals; therefore the gravimetric hydrogen density is limited to less than 3 mass%. It is still a challenge to explore the properties of the light weight metal hydrides [106].

3.1.4. Storage via chemical reaction

Storage via chemical reaction is one of the methods where hydrogen is generated during the reaction of metals or chemical compounds with water. Metal such as sodium or lithium, reacts with water and produces the hydrogen. This reaction is not directly reversible but the metal hydroxide could be removing and next reducing to a metallic state using a solar furnace [106]. The major challenge with this storage method is the reversibility and the control of the thermal reduction process in order to produce the metal in a solar furnace.

3.1.5. Storage in carbon adsorbents

The adsorption of a gas on a surface is a consequence of the field force at the surface of the solid, called the adsorbent, which attracts the molecules of the gas or vapor, called adsorbate. The origin of the physisorption of gas molecules on the surface of a solid are resonant fluctuations of the charge distributions and are therefore called dispersive interactions or Van der Waals interactions. In the physisorption process a gas molecule interacts with several atoms at the surface of the solid.

It recent years the considerable hydrogen storage in nanostructured carbon materials has been reported over a temperature range from 77 K to ambient temperature. This storage is characterized as surface adsorption/condensation of hydrogen. The new carbon materials as nanofibres and nanotubes seem to be an ideal hydrogen adsorbent.

Carbon nanotubes can be divided essentially into two categories: single walled nanotubes (SWNT) and multi walled nanotubes (MWNT) as displayed in Fig. I-10.

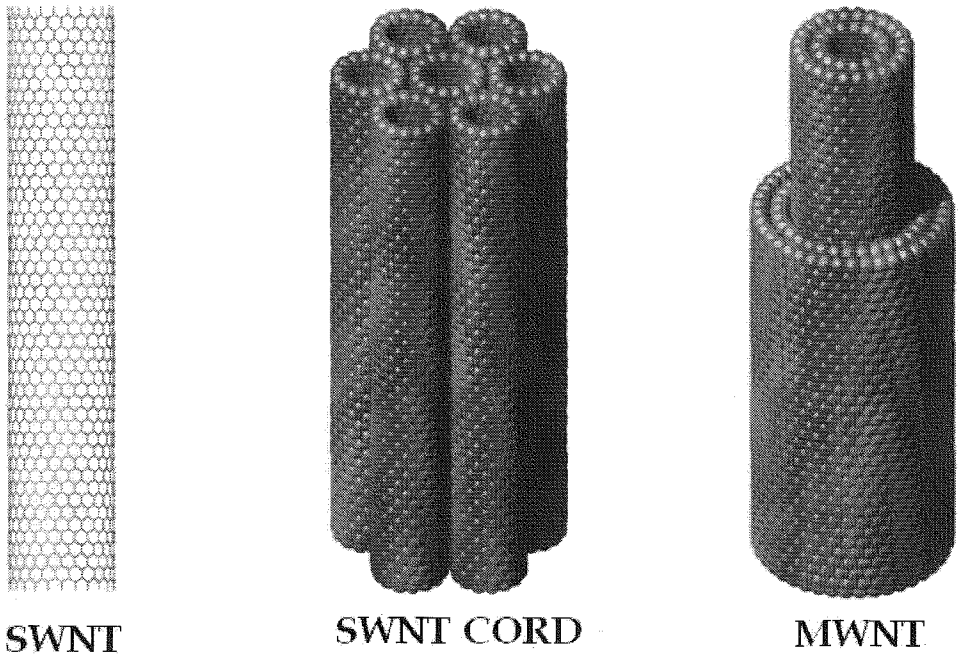

Figure I-10. Single (SWNT) and multi (MWNT) walled carbon nanotubes [108].

Ideally, single-wall carbon nanotube are made of a perfect graphene sheet, i.e. a polyaromatic mono-atomic layer made of an hexagonal display of sp^2 hybridized carbon atoms that genuine graphite is built up with, rolled up into a cylinder and closed by two caps (semi-fullerenes) [109]. The internal diameter of these structures can vary between 0.4 and 2.5 nm and the length ranges from few microns to several millimetres. MWNT can be considered as concentric SWNT with increasing diameter and coaxially disposed. The number of walls present can vary from two (double wall nanotubes) to several tens, so that the external diameter can reach 100 nm. The concentric walls are regularly spaced by 0.34 nm similar to the intergraphene distance evidenced in turbostratic graphite materials. It is worth to note that residual metallic particles coming from the production process can be found in the inner cavity of MWNT [109].

Graphitic nanofibres (GNF) consist of grapheme sheets aligned in a set direction. Three distinct structures may be existed: platelet (0°), ribbon (90°) and herringbone (45°) as shown in Figure I-11. The angle in the parentheses indicates the direction of the nanofiber axis relative to the vector normal to the graphene sheets [110].

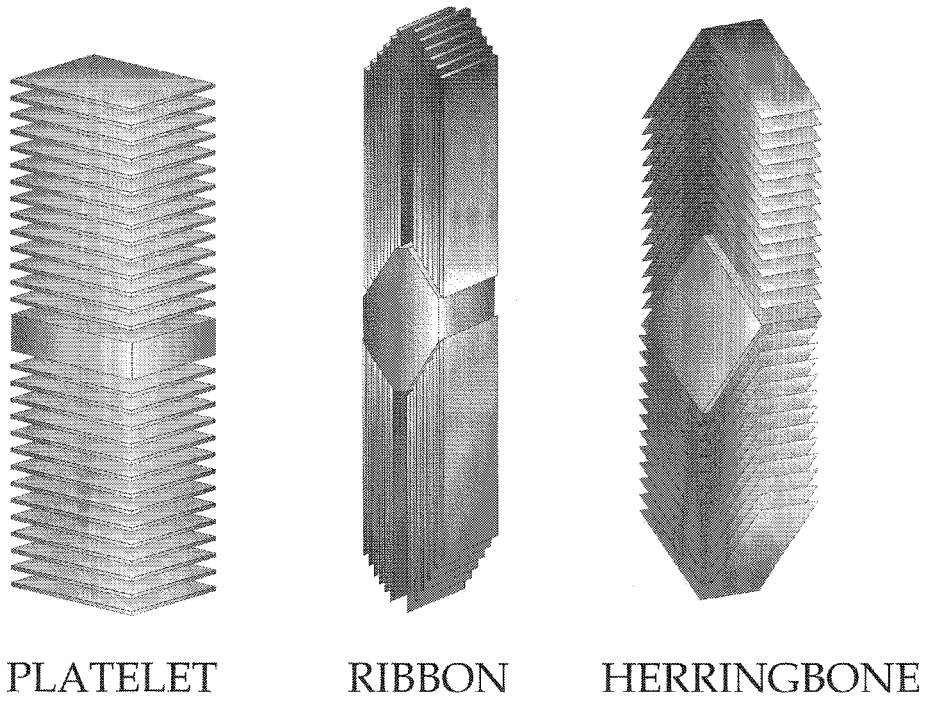

Figure I-11. Graphitic nanofibres (GNF) [108].

The spacing between graphite layers in each case is the same value found in conventional graphitic carbon, ~ 3.4 Å. The typically diameter of the nanofibres is the range of 5 – 500 nm [111].

Activated carbon can be manufactured from many different raw materials such as wood, peat and coal. Relatively high specific surface area ($\leq$ 2500 m^2*g^{-1}) and high total porous volume (~ 1 cm^3*g^{-1}) make the activated carbon as very good sorbent material. One might expect that the carbon performance as an adsorbent will depend on its source and structure [112]. Some adsorptive properties can be explained by differences in pore size distribution. Surface chemical functionalities, derived from the activation procedures, also influence adsorption, but their role depends on their accessibility, which in turn depends on the carbon microporosity.

3.2. Hydrogen storage on carbon materials

In order to obtain a suitable driving range for automotive application the United States Departament of Energy (DOE) target has been set to 6.5 wt.% of hydrogen which equals to 720 ml(STP)$*g^{-1}$.

Hydrogen, depending on the applied pressure and temperature, can be adsorbed and reversibly stored on solid surfaces as a result of physisorption (van der Waals forces) or chemisorption (as in metal hydrides). Materials with large specific area like nanostructured carbon and carbon nanotubes are possible substrates for physisorption. However, some authors argued that physisorption alone is not sufficient to reach the high capacity at ambient temperature [113]. In addition the mechanism of hydrogen storage is still disputed. Some authors proposed that the hydrogen storage capacity in metal containing catalysts is enhanced by the hydrogen spillover [114-115]. Chemisorption of hydrogen is due to the dissociation of hydrogen molecules. Hydrogen in this case is stored in atomic form. The breaking of the hydrogen bonding can be achieved by the incorporation of noble or transitions metals to the materials. However, it was shown that carbon surface has also the capability to dissociate the hydrogen molecules [116]. It is lower than for the platinum catalysts but it permits to hydrogenate the anthracene at 673 K. The authors postulated that the hydrogenation and adsorption occurred at the same active site [116].

Much debate has been held over the last few years on the hydrogen storage in carbon nanostructured is a viable option for hydrogen storage. Some researchers [117], claimed that high surface area activated carbons are not effective in storing hydrogen at room temperature because only a small fraction of the pore distribution interacts with hydrogen molecules and the interaction energy is small (Van der Waals interaction). Hydrogen adsorption characterized by this interaction is generally referred to the physisorption and hydrogen is adsorbed nondissociatively.

Looking into the research results that have been reported over the last years, there are conflicting data on the reversible storage of hydrogen in carbon nanotubes [118]. This is mainly caused by insufficient characterisation of the carbon material used [119]. Extraordinary hydrogen storage capacities of an order of a magnitude higher than anything known to date were reported in 1998 [120]. These capacity values could be questionable and may have to be seen with some scepticism since they are rather inconsistent and not reproducible. Hydrogen storage properties of nanotubes are not yet fully understood and explored. Nevertheless, there is still scientific interest particularly on Single Walled NanoTubes (SWNTs) that could be seen as a promising medium for the safe storage of hydrogen [118]. Most researchers agree that careful and systematic investigations should be undertaken concentrating on the development in order to improve the sorption behaviour and also on the adequate characterisation of these materials. Procedures such as ball milling and pre-treatment appear to increase the number of defects such as dangling carbon bonds and can result in highly defective structures where hydrogen is weekly chemisorbed and easily released [118]

As stated earlier, porous storage media and in particular carbon-based materials have attracted a lot of attention over the last years and triggered heated discussions on their potential. This is particularly due to the fact that no reproducible data exist to justify the really high, rather unrealistic, hydrogen storage capacities claimed in the past by several investigators [118]. The results obtained (Table I-2) so far on carbon nanotubes as hydrogen storage media seem conflicting and suffer from rather insufficient characterisation of the materials used [121]. Therefore, marketing of carbonaceous materials as hydrogen storage media should be seen as a long-term option. This is also confirmed by the fact that recent industrial and commercial efforts are at the moment concentrating on metal hydrides systems [119, 122]. Research for this class of materials is still at the laboratory stage targeting materials development with optimal hydrogen storage capacity, under low pressure-temperature [118].

Table I-2. Literature data of the hydrogen storage for different carbon materials.

material	Temperature [K]	Pression [MPa]	Max. wt.% of H_2 [%]	Reference
SWNT High purity	80	7	8.25	[123]
SWNT High purity	133	0.04	5-10	[124]
SWNT High purity	298	0.06	3.5-4.5	[125]
SWNT – Fe	298	0.08	0.005	[126]
SWNT – $TiAl_{0.1}V_{0.4}$	298	0.08	1.47	[126]
SWNT milled in Ar	298	0.08	0.1	[127]
SWNT milled in D_2	298	0.9	1.0	[127]
MWNT	298	0.1	0.25	[128]
MWNT - Li	298	0.1	0.7-4.2	[129]
GNF milled in D_2	298	0.9	0.5	[127]
GNF	298	12	65	[120]
GNF	298	18	0.01	[130]
GNF	77	8	0.01	[130]
GNF(Ribbon)	298	11.35	11.0	[120]
GNF(platelet)	298	11.35	54	[120]
GNF(herringbone)	298	11.35	67	[120]
GNF(K - dopped)	300	0.1	14	[131]
Activated carbon Surface 3000	298	10.5	0.3	[132]
Activated carbon Surface 1047	298	9.0	0.3	[133]
Activated carbon Surface 1040	77	0.1	2.6	[134]
Activated carbon Surface 2330	77	0.1	3.7	[134]
Activated carbon Surface 3000	77	0.1	4.5	[134]
Activated carbon Norit	77	0.1	2.6	[134]

Specific requirements in terms of cost, non-toxicity, recycling and re-use are also taken into consideration. A better understanding of the fundamentals of hydrogen adsorption/desorption processes and of the relationship between material properties and process parameters, may be required. Standardised characterisation procedures, validated materials data and qualified preparation processes are still lacking.

This is the reason that many researchers are claiming that at this point "round robin" and benchmarking exercises leading to the actual definition of standardised material production and characterisation procedures, are needed [118]. A number of papers and reviews recently published on the stage of the knowledge of the hydrogen uptake by carbon nanostructures [127, 135] agree on the most recommended methods. Nevertheless, there is still controversy [118] on the questions related to the sample purity. In any case, more coordinated and conjugated efforts may be essential for understanding the hydrogen sorption mechanism in carbon nanostructures [118]. Indeed it is known that carbon nanotubes are produced from metals catalysts and contain the some quantity of metals. These quantity may reached 10 wt.% of carbon material. Several groups have reported theoretical modelling results and simulations on hydrogen adsorption in carbon materials and are in most cases more favourable than experimental results. However, these simulations need refining to identify a "working combination": an adsorption mechanism compatible with the hydrogen storage requirements of 6.5wt.% and a volumetric density for adequate hydrogen storage capacity for practical applications (see transportation), at room temperature [118]. To ensure efficient hydrogen storage in carbon nanotubes, two issues still need to be resolved [136]. The first is whether hydrogen adsorption in Single Wall NanoTubes (SWNTs) is less or greater than in slit pores. If it is greater, then the "ideal" micropore volume fraction, size/shape and suitable pore diameter for reaching the targets set for mobile applications must be identified [137]. The other important issue is whether hydrogen adsorption occurs in the interstitial channels between adjacent nanotubes in a rope of SWNTs. As a next step, future efforts can focus on developing experimental procedures to provide carbon materials with tailored-made structures for maximum hydrogen storage capacity. Research work is already directed towards optimisation of the development and postproduction routes (purification, grinding, activation, conditioning, doping) for yielding, in a cost-effective way, reproducible materials [118]. In parallel, efforts are also concentrating on transferring these processes to mass production at a reasonable cost.

4. REFERENCES

[1] National Science & Technology Council. *National nanotechnology initiative.* Washington, DC: Committee on Technology, Subcommittee on Nanoscale Science, Engineering, & Technology. (2000).

[2] K.E. Drexler *Bull. of Sci. Techn. and Society* 24(1) (2004) 21

[3] E. Lucas, S. Decker, A. Khaleel, A. Seitz, S. Fultz, A. Pouce, W. Li, C. Carnes, K.J. Klabunde *Chem. Eur. J.* 7(12) (2001) 2505

[4] P. Moriarty *Rep. Prog. Phys.* 64 (2001) 297

[5] F. Rosei *J. Phys. Condens. Matter.* 16 (2004) S1373

[6] C.B. Murray, D.J. Norris, M.G. Bawendi *J. Am. Chem. Soc.* 115 (1993) 8706

[7] A.P. Alivisatos *J. Phys. Chem.* 100 (1996) 13226

[8] N. Nirmal, L. Brus *Acc. Chem. Res.* 32 (1999) 407

[9] C. Burda, X. Chen, R. Narayanan, M.A. El-Sayed *Chem. Rev.* 105 (2005) 1025

[10] G. Schmid *Metals.* In *Nanoscale materials ic Chemistry* K.J. KlabundeEd., Wiley-Interscience, New York, 2001, Chapter 2, p. 15

[11] J.D. Aiken III, R.G. Finke *J. Mol. Cat. A : Chemical* 145 (1999) 1

[12] Ch. Hwai Peng, Phd Thesis, Sains Malaysia University, 2003, *Synthesis and characterization of mono- and bi- metallic nanocolloids for selective hydrogenation of fatty acids*

[13] A.D. Pomogailo *Russ. Chem. Rev.* 66(8) (1997) 679

[14] S. Panigrahi, S. Kundu, S.K. Ghosh, S. Nath, T. Pal *J. Nanopart. Res.* 6 (2004) 411

[15] J.P. Wilcoxon, A. Martino, R.L. Baughmann, E. Klavetter, A.P. Sylwester, *Mater. Res. Soc. Symp. Proc.* 286 (1993) 131

[16] J.P. Wilcoxon, R.L. Williamson, R. Baughman, *J. Chem. Phys.* 98 (1993) 9933

[17] F. Parsapour, D.F. Kelley, S. Craft, J.P. Wilcoxon, *J. Phys. Chem.* 104 (1996) 4978

[18] J.P. Wilcoxon, P.P. Newcomer, G.A. Samara, *J. Appl. Phys.* 81 (1997) 7934

[19] M.L. Steigerwald, L.E. Brus, *Acc. Chem. Res.* 23 (1990) 183

[20] N.L. Pocard, D.C. Alsmeyer, R.L. McCreery, T.X. Neenan, M.R. Callstrom, *J. Am. Chem. Soc.* 114 (1992) 769

[21] Y. Ng Cheomg Chan, R.R. Schrock, R.E. Cohen, *Chem. Mater.* 4 (1992) 205

[22] Y. Ng Cheomg Chan, R.R. Schrock, R.E. Cohen, *J. Am. Chem. Soc.* 114 (1992) 7290

[23] M. Zhao, L. Sun, R.M. Crooks, *J. Am. Chem. Soc.* 120 (1998) 4877

[24] G. Schmid_Ed.., Clusters and Colloids: From Theory to Applications, Chap. 6, VCH Publishers, New York, 1994.

[25] E. Matijevic *Farad. Discuss. Chem. Soc.* 92 (1992) 229

[26] D.V. Goia, E. Matijevic *New J. Chem.* (1998) 1203

[27] D.H. Chen, C.H. Hsieh *J. Mater. Chem.* 12 (2002) 2412

[28] K.H. Kim, H.Ch. Park, S.D. Lee, W.J. Hwa, S.S. Hong, G.D. Lee, S.S. Park *Mater. Chem. Phys.* 92 (2005) 234

[29] Z.L. Cui, L.F. Dong, C.C. Hao, *Mater. Sci. Eng. A* 286 (2000) 205

[30] J.P. Chen, C.M. Sorensen, K.J. Klabunde *Phys. Rev. B* 17 (1995) 11527

[31] J.A. Creighton, C.G. Blatchford, M.G. Albrecht *J. Chem. Soc. Faraday Trans. 2 Mol. Chem. Phys.* 75(5) (1979) 790

[32] F. Wang, Z. Zhang, Z. Chang *Mater. Lett.* 55 (2002) 27

[33] J.L. Marignier, J. Belloni, M.-O. Delcourt, J.P. Chevalier, *Nature* 317 (1985) 344

[34] N. Keghouche, S. Chettibi, F. Latre`che, M.M. Bettahar, J. Belloni, J.L. Marignier, *Radiat. Phys. Chem.* 74 (2005) 185.

[35] Y. Mizukoshi, K. Okitsu, Y. Maeda, T.A. Yamamoto, R. Oshima, Y. Nagata, *J. Phys. Chem. B* 101 (1997) 7033

[36] K.S. Suslick, M. Fang, T. Hyeon *J. Am. Chem. Soc.* 118 (1996) 11960

[37] V.F. Puntes, K.M. Krishnan, A.P. Alivisatos *Science* 291 (2001) 2115

[38] J.S. Bradley, B. tesche, W. Busser, M. Maase, M.T. Reetz *J. Am. Chem. Soc.* 122 (2000) 4631

[39] N. Coydente, M. Respaud, F. Secocq, M.J. Casanove, C. Amiens, B. Chaudret *NanoLett.* 1 (2001) 565

[40] A.G. Boudjahem, S. Monteverdi, M. Mercy, M.M. Bettahar *J. Catal.* 221(2) (2004) 325

[41] A.G. Boudjahem, S. Monteverdi, M. Mercy, M.M. Bettahar *Appl. Catal. A General* 250(1) (2003) 49

[42] Y.D. Li, L.Q. Li, H.W. Liao, H.R. Wang *J. Mater. Chem.* 9 (1999) 2675

[43] J. Gao., F. Guan, Y. Zhao, W. Yang, Y. Ma, X. Lu, J. Hou, *J. Kang Mater. Chem. Phys.* 71 (2001) 215

[44] D.H. Im, S.Y. Park, S.H. Hyun, B.Y. Lee, Y.H. Kim *J. Mater. Sci.* 39 (2004) 3629

[45] Y. Duan, J. Li *Mater. Chem. Phys.* 87 (2004) 452

[46] Syukri, T. Ban, Y. Ohya, Y. Takahashi *Mater. Chem. Phys.* 78 (2003) 645

[47] S.H. Wu, D.H. Chen *J. Coll. Inter. Sci.* 259 (2003) 282

[48] X.M. Ni, X.B. Su, Z.p. Yang, H.G. Zheng *J. Cryst. Growth* 252 (2003) 612

[49] Y.T. Moon, H.K. Park, D.K. Kim, C.H. Kim, *J. Am. Ceram. Soc.* 78 (1995) 2690

[50] K.H. Kim, Y.B. Lee, E.Y. Choi, H.C. Park, S.S. Park *Mater. Chem. Phys.* 86 (2004) 420

[51] A. Degan, J. Macek *NanoStruct. Mater.* 12 (1999) 225

[52] D.H. Chen, S.H. Wu *Chem. Mater.* 12 (2000) 1354

[53] I. Capek *Adv. Coll. Inter. Sci.* 110 (2004) 49

[54] J.B. Nagy *Colloid Surf.* 35 (1989) 201

[55] N. Toshima, T. Yonezawa *New J. Chem.* (1998) 1179

[56] G. Viau, F. Fievet-Vincent, F. Fievet *Solid State Ionics* 84 (1996) 259

[57] A. Kumar, Ch. Damle, M. Sastry *Appl. Phys. Lett.* 79(20) (2001) 3314

[58] R.P. van Ingren, R.H.j. Fastenau, E.J. Mittenmeijer *J. Appl. Phys.* 76 (1994) 1871

[59] R.P. van Ingren, R.H.j. Fastenau, E.J. Mittenmeijer *J. Appl. Phys.* 72 (1994) 3116

[60] D. Poondi, J. Singh *J. Mater. Sci.* 35 (2000) 2467

[61] J.A. Schartz, C. Contescu, A. Contescu *Chem. Rev.* 95 (1995) 477

[62] P.T. Cardew, R.J. Davey, P. Ellitt, A.W. Nienow, J.P. Winterbottom, in: B. Delmon, P. Grange, P.A. Jacobs, G. Poncelet (Eds.), *Preparation of Catalysts IV, Studies in Surface Science and Catalysis*, vol. 31, Elsevier, Amsterdam, 1987, p. 15.

[63] C. Perego, P.L. Villa, *Catal. Today* 34 (1997) 281

[64] J.F. LePage, in: G. Ertl, H. Knözinger, J. Weitkamp (Eds.), *Handbook of Heterogeneous Catalysis*, vol. 1, Wiley/VCH, New York/Weinheim, 1997, p. 49.

[65] J.T. Richardson, *Principles of Catalyst Development*, Plenum Press, New York, 1989.

[66] M.V. Twigg (Ed.), *Catalyst Handbook*, 2nd ed., Wolfe, London, 1989.

[67] M. Campanati, G. Fornasari, A. Vaccari *Catal. Today* 77 (2003) 299

[68] P. Burattin, M. Che, C. Louis *J. Phys. Chem. B* 104 (2000) 10482

[69] R.Z.C. van Meerten, T.F.M. de Graaf, J.W.E. Coenen *J. Catal.* 46 (1977) 1

[70] S. Takenaka, H. Ogihara, K. Otsuka *J. Catal.* 208 (2002) 54

[71] C.H. Bartholomew, R.B. Pannell *J. Catal.* 65 (1980) 390

[72] J. Zielinski *J. Catal.* 76 (1982) 157

[73] R. Molina, G. Poncelet *J. Catal.* 173 (1998) 257

[74] B.W. Hoffer, A.D. van Langeveld, J.P. Janssens, R.L.C. Bonné, C.M. Lok, J.A. Moulijn *J. Catal.* 192 (2000) 432

[75] Yu.A. Ryndin, J.P. Candy, B. Didillon, L. Savary, J.M. Basset *J. Catal.* 198 (2001) 103

[76] N. Davidova, N. Peshev, D. Shopov *J. Catal.* 58 (1979) 198

[77] M. Ziolek, K. Nowinska, K. Leksowska *Zeolites* 12(6) (1992) 710

[78] A. Lewandowska, S. Monteverdi, M. Bettahar. M. Ziolek *J. Mol. Catal. A: Chemical* 188(1-2) (2002) 85

[79] R. Wojcieszak, S. Monteverdi, M. Mercy, I. Nowak, M. Ziolek, M.M. Bettahar *Appl. Catal. A: General* 268(1-2) (2004) 241

[80] J.S. Jung, W.S. Chae, R.A. McIntyre, C.T. Seip, J.B. Wiley, Ch.J. O'Connor *Meter. Res. Bull.* 34(9) (1999) 1353

[81] V. Parvulescu, B.L. Su Catal. *Today* 69 (2001) 315

[82] V.R. Choudhary, A.M. Rajput, B. Prabhakar, A.S. Mamman *Fuel* 77(15) (1998) 1803

[83] D.G. Mustard, C.H. Bartholomew *J. Catal.* 67 (1981) 186

[84] T. Zhu, M. Flytzani-Stephanopoulos *Appl. Catal. A: General* 208 (2001) 403

[85] W. Shan, M. Luo, P. Ying, W. Shen, C. Li *Appl. Catal. A: General* 246 (2003) 1

[86] M.M. Pereira, E.B. Pereira, L.Y. Lau, M. Schmal *Catal. Today* 57 (2000) 291

[87] L.T. Santos, E.B. Pereira, N. Homs, J. Llorca, P.R. de la Piscina, M.M. Pereira *Catal. Today* 78 (2003) 459

[88] Z.G. Zhang, K. Okada, M. Yamamoto. T. Yoshida Catal. *Today* 45(1-4) (1998) 361

[89] D. Mehandjiev, E. Bekyarova. M. Khristova *J. Coll. Inter. Sci.* 192(2) (1997) 440

[90] L. Filotti, A. Bensalem, F. Bozon-Verduraz, G.A. Shafeer, V.V. Voronov, *Appl. Surf. Sci.* 109–110 (1997) 249.

[91] A. Trovarelli, *Catal. Rev. Sci. Eng.* 38 (1996) 439

[92] www.webelemnts.com

[93] K. Tanabe *Catal. Today* 78 (2003) 65

[94] I. Nowak, M. Ziolek, *Chem. Rev.* 99 (1999) 3603

[95] D. Dobkin www.batnet.com

[96] Berkeley Lab on www.eande.lbl.gov

[97] R. Lexman, www.batnet.com

[98] M. Ziolek, I. Nowak *Kataliza Heterogeniczna-wybrane zagadnienia*, UAM 1999, Poznan, Poland

[99] J. Haber, J.H. Block, B. Delmon *Pure and Appl. Chem.* 67 (1995) 1257

[100] J. Ryczkowski, T. Borowiecki, D. Nazimek *Ads. Sci. and Tech.* 14(2) (1996) 128

[101] J. Ryczkowski, T. Borowiecki *React. Kinet. Catal. Lett.* 49(1) (1993) 127

[102] F. Schüth, K. Unger, in: G. Ertl, H. Knözinger, J. Weitkamp (Eds.), *Handbook of Heterogeneous Catalysis*, vol. 1, Wiley/VCH, New York/Weinheim, 1997, p. 72.

[103] M. A. de la Casa-Lillo, F. Lamari-Darkrim, D. Cazorla-Amoros, A. Linares-Solano *J. Phys. Chem. B* 106 (2002) 10930

[104] T. Hottinen Master Thesis, University of Helsinki 2001, *Technical Review and Economic Aspects of Hydrogen Storage Technologies*

[105] B.Viswanathan, M.Sankaran, M.Aulice Scibioh *Carbon* 2 (2003) 12

[106] A. Züttel *Materials Today* 9 (2003) 24

[107] K. Yvon *Chimia* 52(10) (1998) 613

[108] P. Guay, Master Thesis, INRS 2003, *Modélisation Monte Carlo de l'adsorption de l'hydrogène dans les nanostructures de carbone*

[109] P. Serp, M. Corrias, P. Kalck *Appl. Catal. A: General* 253 (2003) 337

[110] A.C. Dillon, M.J. Heben *Appl. Phys. A* 72 (2001) 133

[111] N.M. Rodriguez, A. Chambers, R.T.K. Baker *Langmuir* 11 (1995) 3862

[112] J.A. Schwarz, *Hydrogen storage on activated carbon*, New York State ERDA, 1994

[113] M. Rzepka, P. Lamp, M.A. Casa-Lillo, *J. Phys. Chem. B* 102 (1998) 10894

[114] A.D. Lueking, R.T. Yang *Appl. Catal. A* 265 (2004) 259

[115] D.J. Browning, M.J. Gerrard, J.B. Lakeman, M. Mellor, R.J. Mortimer, M.C. Turpin *NanoLetters* 2 (2002) 201

[116] H. Takagi, H. Hatori, Y. Yamada *Carbon* 43 (2005) 3002

[117] L.O. Valøen *Global Watch Electrochemistry* (2001) 1

[118] E. Tzimas, C. Filiou, S.D. Peteves, J.B. Veyret *European Comission Raport* 2003, Petten, The Netherlands

[119] L.Schlapbach, A. Züttel *Nature* 414 (2001) 353

[120] A. Chambers, C. Park, R.T.K. Baker, N. M. Rodriguez *Phys; Chem. B* 102 (1998) 4253

[121] A. Züttel, L. Schlapbach Project C4 under IEA Task 12: *Metal hydrides and carbon for Hydrogen Storage*, 2001, 108-113.

[122] A. Züttel, Schin-ichi Orimo, *MRS Bulletin*, 27(9) (2002) 705

[123] Y. Ye, C.C. Ahn, C. Witham, B. Fultz, J. Liu, A.G. Rinzler, D. Colbert, K.A. Smith, R.E. Smalley *Appl. Phys. Lett.* 74(16) (1999) 2307

[124] A.C. Dillon, K.M. Jones, T.A. Bekkedahl, C.H. Kiang, D.S. Bethune, M.J. Heben *Nature* 386 (1997) 377

[125] A.C. Dillon, T. Gennett, J.L. Alleman, K.M. Jones, P.A. Parilla, M.J. Heben *Carbon nanotube materials for hyfrogen storage*, Proceedings of the US DOE Hydrogen Program Review, Vol. II, 1999

[126] M. Hirscher, M. Becher, M. Haluska, U. Dettlaff-Weglikowska, A. Quintel, G.S. Duesberg, Y. -M. Choi,P. Downes, M. Hulman, S. Roth, I. Stepanek, P. Bernier, *Appl. Phys. A* 72 (2001) 129

[127] M. Hirscher, M. Becher, M. Haluska, A. Quintel, V. Skakalova, Y. -M. Choi, U. Dettlaff-Weglikowska, S. Roth, I. Stepanek, P. Bernier, A. Leonhardt, J. Fink, *J. Alloys Comp.* 330(332) (2002) 654

[128] X.B. Wu, P. Chen, J. Lin, K.L. Tan *Int. J. of Hydrogen Energy* 25(3) (2000) 261

[129] F.E. Pinkerton, B.G. Wicke, C.H. Olk, G.G. Tibbetts, G.P. Meisner, M.S. Meyer, J.F. Herbst *J. Phys. Chem. B* 104 (2000) 9460

[130] C.C. Ahn, Y. Ye, B.V. Ratnakumar, C. Witham, R.C. Bowman, B. Fultz *Appl. Phys. Lett.* 73 (1998) 3378

[131] P. Chen, X. Wu, J. Lin, K.L. Tan, *Phys. Rev. Lett.* 82 (1999) 2852

[132] E. Poirier, R. Chahine, T.K. Bose *J Hydrogen Energy* 26 (2001) 831

[133] K; Shindo, T. Kondo, Y; Sakurai *J of Alloys and Compounds* 379 (2004) 252

[134] N. Texier Mandoki, J. Dentzer, T. Piquero, S. Saadallah, P. David, C. Vix Guterl *Carbon* 42 (2004) 2735

[135] A. Züttel, P. Sudan, Ph. Mauron, T. Kiyobayashi, Ch. Emmenegger, L. Schlapbach *Int. J. H. Energy* 27(2) (2002) 203

[136] C. N. R. Rao, B. C. Satishkumar, A. Govindaraj, Manashi Nath, *Chemphyschem* 2 (2001) 78

[137] M.G. Nijkamp, J.E.M.J. Raaymakers, A.J. van Dillen, K.P. de Jong, *Appl. Phys. A* 72 (2001) 619

CHAPTER II
EXPERIMENTAL METHODS AND CALCULATIONS

1. Experimental methods

1.1. Materials

1.1.1. Supports

γ-Al_2O_3 – γ-aluminum (III) oxide

Purchased from ALFA and Johnson Matthey Company (high purity 99.7 %). Total surface area of 100 m^2g^{-1}.

CeO_2 – cerium (IV) oxide

Purchased from CHEMPUR (high purity 99.9 %). Well crystallized with a total surface area of 15 m^2g^{-1}.

Nb_2O_5 – niobia (V) oxide

Purchased from CBMM as hydrated niobia (V) oxide (high purity 99.97 %). Total surface area of 30 m^2g^{-1}.

SiO_2(C) – silicon (IV) oxide

Purchased from CHEMPUR (High purity 99.9 %). Well crystallized with a total surface area of 15 m^2g^{-1}.

SiO_2(D) – silicon (IV) oxide

Purchased from DEGUSSA (High purity 99.9 %). Amorphous silica with a total surface area of 200 m^2g^{-1}.

SiO_2(V) – silicon (IV) oxide

Purchased from VENTRON (high purity 99.8%). Specific surface area of 400 m^2g^{-1}.

AC – activated carbon

Purchased from MERCK. (High purity 99.5%). Specific surface area of 1071 m^2g^{-1}.

1.1.2. Reagents

Nickel (II) nitrate hexahydrate [$Ni(NO_3)_2*6H_2O$] – was purchased from ANALAR – Hopkin & Williams LTD. Pure for analysis ≥ 99.0 %. Used as the nickel precursor.

Silver nitrate [$AgNO_3$] – was purchased from PROLABO. Pure for analysis ≥ 99.5 %. Used as the silver precursor.

Nickel (II) acetate tetrahydrate [$Ni(CH_3COO)_2*4H_2O$] – was purchased from FLUKA. Pure for analysis ≥ 99.0 %. Used as the nickel precursor.

Sodium Salt of the ethylenediaminetetraacetic acid [H_2Na_2EDTA] was purchased from POCH. Pure for analysis ≥ 99.5 %. Density $d^{20} = 0.83\ cm^3g^{-1}$.

Hydrazine hydrate solution [$N_2H_4*H_2O$] – 25% water solution – was purchased from FLUKA. Pure for analysis. Density $d^{20} = 1.01\ cm^3g^{-1}$. Used as the reductant for nickel and nickel – silver catalysts.

Benzene (C_6H_6) was purchased from MERCK. Pure for analysis ≥ 99.5 %. Density $d^{20} = 0.88\ cm^3g^{-1}$. Used for the catalytic tests.

Isopropyl alcohol (i-C_3H_6OH) was purchased from CHEMPUR. Pure for analysis ≥ 99.5 %. Density $d^{20} = 0.78\ cm^3g^{-1}$. Used for the acidity determination.

Pyridine (C_5H_5N) was purchased from POCH. Pure for analysis ≥ 99.5 %. Density $d^{20} = 0.98\ cm^3g^{-1}$. Used as the probe molecule in FTIR measurements.

Potassium bromide (KBr) was purchased from FLUKA. Pure for analysis ≥ 99.5 %. Used for the IR spectroscopy.

1.1.3. Gases

Hydrogen (H_2) – Purchased from AIR LIQUIDE. Hydrogen U (99.995%)

H_2/Ar (100 ppm) – Purchased from AIR LIQUIDE. Alphagaz 1 (99.999%)

O_2/Ar (100 ppm) – Purchased from AIR LIQUIDE. Alphagaz 1 (99.999%)

Argon (Ar) – Purchased from AIR LIQUIDE. Argon 1 (99.995%)

Helium (He) – Purchased from AIR LIQUIDE. Helium 1 (99.999%)

Oxygen traces were eliminated from argon, hydrogen, helium and H_2/Ar gases using a manganese oxytrap (Engelhardt) whereas O_2/Ar was used as received.

For H_2 – TPR study the hydrogen was mixed with argon using a diffuser with a molecular membrane.

1.2. Catalyst preparation

1.2.1. Impregnation of catalysts

Simple impregnation method (SIM)

The wet impregnation of nickel catalysts was performed using a nickel acetate (or nickel nitrate) solution as a precursor. The appropriate quantity of nickel salt was dissolved in 20 cm^3 of distilled water. The nickel acetate or nickel nitrate concentrations in the solution were calculated to obtain the 1, 5 or 10 wt.% of nickel. 5 g of the support was putted in to a flask (110 cm^3) and outgased at room temperature for 0.5 h. Then the solution containing the nickel salt was added under stirring. The mixture was stirred at room temperature for 1h, then evaporated in a rotary evacuator at 353 K. Obtained catalyst was dried in air at 353 K for 16 h.

The wet impregnation of bimetallic catalysts was performed using a nickel acetate and silver nitrate solutions as nickel and silver sources respectively. The appropriate quantity of nickel and silver salts were dissolved in 20 cm^3 of distilled water. The nickel acetate and silver nitrate concentrations in the solution were calculated to obtain the following Ni-Ag ratios: 0.9%Ni-0.1%Ag (denoted as 90NiAg), 0.75%Ni-0.25%Ag (denoted as 75NiAg) and 0.5%Ni-0.5%Ag (denoted as 50NiAg). 5 g of the support was putted in to a flask (110 cm^3) and outgased at room temperature for 0.5 h. Then the solution containing nickel and silver ions was added under stirring. The mixture was stirred at room temperature for 1h. Than it was evaporated in a rotary evacuator at 353 K. Obtained catalyst was dried in air at 353 K for 16 h.

Double impregnation method (DIM)

For the DIM impregnation method the appropriate quantity of the support was poured over a solution of H_2Na_2EDTA with the appropriate concentration and stirred for 15 min at ambient temperature. After filtrating and drying at 383 K for 1 h (temperature ramp 3 K min^{-1}) the obtained solid was impregnated with $Ni(CH_3COO)_2$ and calcined as described above for the simple impregnation method.

1.2.2. Chemical reduction with hydrazine (N_2H_4)

Impregnated catalysts

The chemical reduction of the impregnated catalysts with hydrazine was performed under argon atmosphere (flow rate = 100 cm^3min^{-1}) in a 3 necked reaction flask of 110 cm^3 dipping in a thermostatic water bath as showed in Figure II-1. The reaction flask was fitted with a reflux condenser and a thermocouple for the control of the reaction temperature and connected to a gas microchromatograph (Agilent G2890A) for the analysis of the gases evolved during the reduction process. A suspension of the supported nickel precursor (5g of impregnated sample in 60 cm^3 of distilled water) was stirred for 0.5 h at room temperature. The reaction mixture was then slowly heated from room temperature up to 353 K. Then 10 ml of 24-26 % aqueous hydrazine in excess was added. The pH of the solution was 10-12 and remained almost constant. The green color of the solids changed to black due to the Ni^{2+} and/or Ag^{+} ions reduction. Reaction was finished after 4 hours. After reduction the solid was filtered, washed with distilled water and dried in air at 353 K for 16 h.

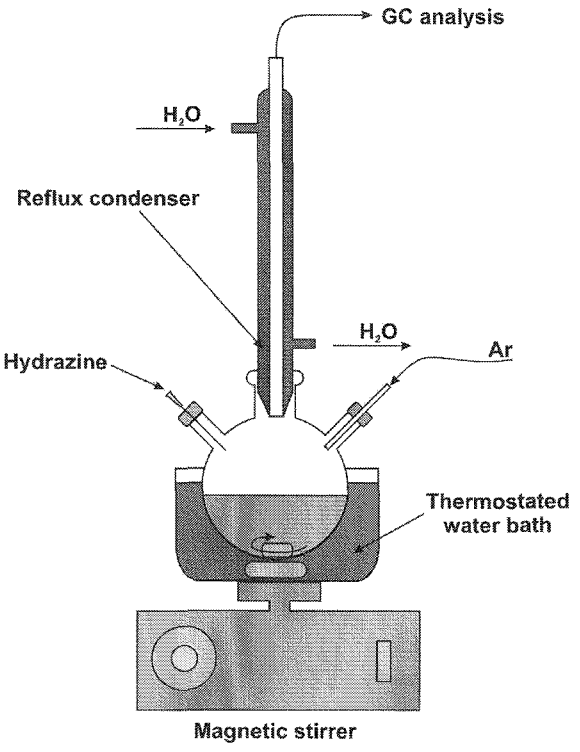

Figure II-1. Scheme of installation for catalysts reduction.

Precipitated catalysts

The reduction of non impregnated catalysts was performed under Ar flow (100 cm^3min^{-1}). The appropriate concentration of nickel acetate (or/and silver nitrate) and 5 g of required support was putted in 60 cm^3 of distilled water in a 3 necked reaction flask. Obtained suspension was stirred at room temperature for 0.5 h and then it was slowly heated to 353 K under argon. Then 10 ml of 24-26 % of aqueous solution of hydrazine in excess was added.

The pH of the solution was 10-12 and remained almost constant. The green color of the solids changed to black due to the Ni^{2+} and/or Ag^{+} ions reduction. Reaction was finished after 4 hours. After reduction the solid was filtered, washed with distilled water and dried in air at 353 K for 16 h.

1.3. Catalyst characterization

1.3.1. Physico-chemical and chemical characterization

Low temperature N_2 adsorption/desorption (BET method)

BET (Brunauer, Emmett, Teller) theory is a well-known rule for the physical adsorption of gas molecules on a solid surface. The concept of this theory is an extension of the Langmuir monolayer molecular adsorption to multilayer adsorption with the following hypotheses: (a) gas molecules physically adsorb on a solid in layers infinitely; (b) there is no interaction between each adsorption layer; and (c) the Langmuir theory can be applied to each layer. The BET method is widely used in surface science for the calculation of surface areas of solids by physical adsorption of gas molecules. Knowing the monolayer capacity of an adsorbent (i.e., the quantity of adsorbate which can be accommodated as a monolayer on the surface of a solid, the adsorbent) and the area of the adsorbate molecule, the surface area can, in principle, be calculated.

The textural parameters of the materials were determined by N_2 sorption at 77 K, using an automatic Thermoquest Sorptomatic 1990 apparatus. Specific surface area and specific pore volume were determined according to BET method. Dubinin-Radushkevich method was used to determine the micropore volume.

Hydrogen treatments

The activation of the catalysts was performed *in situ* before each test was carried out. It was performed in a flow of hydrogen pure (flow rate = 100 cm^3min^{-1}). 0.1 g of the catalyst were placed in a quartz reactor and heated at a rate of 10 K min^{-1} to 573 K. Then the sample was heated at 573 K for 2h. After the activation the sample was cooled to the desired temperature (catalytic tests) or treated in a flow of argon at 573 K for 1h and then cooled to the room temperature (H_2 adsorption study).

H_2–adsorption at room temperature

The hydrogen adsorption on the reduced catalysts was carried out using a mixture of H_2/Ar (100 ppm of H_2). 0.1 g of catalyst were placed in a quartz reactor and treated in a H_2 flow as described above. After activation the sample was purged in a flow of argon at the activation temperature for 1h. it was then cooled to room temperature in a flow of Ar. The hydrogen adsorption was carried out at room temperature in a flow (100 cm^3min^{-1}) of H_2/Ar (100 ppm of H_2 in Ar). The consumption of hydrogen was measured each 2 minutes with a thermal conductivity detector (TCD) in an Agilent G2890A series MicroGCs gas chromatograph (molecular sieves as chromatographic column, 8m), operated at 333 K. Scheme of installation is given in Figure II-2.

Hydrogen Temperature-Programmed Desorption (H_2–TPD)

The temperature-programmed desorption of adsorbed hydrogen (H_2 – TPD) was performed using an argon flow after the hydrogen adsorption (Fig. II-2). The catalyst was purged with argon at room temperature for 1h. The sample was then heated at a rate of 5 K min^{-1} to 1123 K under the argon flow (flow rate = 50 cm^3min^{-1}). The amount of the desorbed hydrogen was measured each 2 minutes with a thermal conductivity detector (TCD) in an Agilent G2890A series MicroGCs gas chromatograph (molecular sieves as chromatographic column, 8m), operated at 333 K.

Hydrogen Temperature-Programmed Reduction (H_2–TPR)

The temperature programmed reduction with H_2 (H_2 – TPR) of the samples was carried out using a H_2/Ar (1000 ppm of H_2) mixture as a reductant (flow rate = 82 cm^3min^{-1}). 0.1 g of the sample were placed in a quartz reactor and treated in a flow of argon at room temperature for 1h. It was then heated at a rate of 5 K min^{-1} to 1100 K

under the reductant mixture. Hydrogen consumption was measured each 2 minutes with a thermal conductivity detector (TCD) in an Agilent G2890A series MicroGCs gas chromatograph (molecular sieves as chromatographic column, 8m), operated at 333 K.

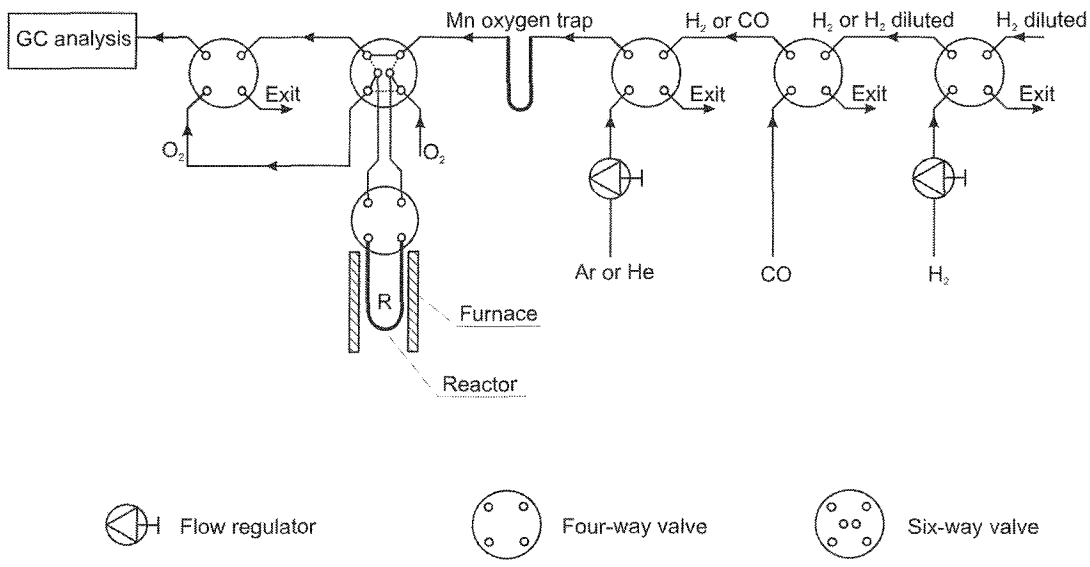

Figure II-2. Scheme of installation for H_2-TPD and H_2-TPR studies.

Determination of the degree of reduction

Controlled oxidation at high temperature was used as a method for determination of the degree of reduction. 0.1 g of the catalyst were placed in the quartz reactor and it was activated in a flow of hydrogen (100 cm^3min^{-1}) at 573 K for 2h. The catalyst was heated at a rate of 10 K min^{-1}. After activation the sample was purged in a flow of argon (100 cm^3min^{-1}) at the temperature of activation for 1h. Then the sample was heated to 623 K in a flow of argon at a rate of 10 K min^{-1}. The uptake of oxygen at 623 K was measured. A O_2/Ar mixture (100 ppm of O_2 in Ar) was used as a oxidant (flow rate = 100 cm^3min^{-1}). Oxygen consumption was measured each 2 minutes with a thermal conductivity detector (TCD) in an Agilent G2890A series MicroGCs gas chromatograph (molecular sieves as chromatographic column, 8m), operated at 333 K.

Isopropanol decomposition

Isopropanol decomposition was performed using a pulse micro-reactor and a helium flow of 40 cm^3 min^{-1}. The catalyst bed (0.05 g) was first activated at 673 K for 2 h under helium flow. The isopropanol conversion was studied at 523 K using 5µl pulses of isopropanol. The gases were analyzed by CHROM-5 GC (2 m column with Carbowax 400 (80-100 mesh) at 338 K in helium flow) on line with micro-reactor and detected by thermal conductivity detector (TCD).

1.3.2. Physical characterization

X-ray diffraction study (XRD)

Powder X-ray diffraction (PXRD) is the most widely used technique for characterizing solid materials. As the name suggests, the sample is in a powdery form, consisting of fine grains in the form of single crystallites. The positions and the intensities of the peaks can be used for identifying the underlying structure (or phase) of a solid material. If a monochromatic X-ray beam is directed at a single crystal, then only a few diffracted beams that are allowed by the Bragg's law may result: A sample of some hundreds of crystallites (i.e., a powder sample) show that the diffracted beams form continuous cones. A circle of film is used to record the diffraction pattern. Each cone intersects the film giving diffraction lines. The lines are seen as arcs on the film. For every set of crystal planes, one or more crystals will be in the correct orientation to give the correct angle to satisfy Bragg's equation. Every crystal plane is thus capable of diffraction. Each diffraction line is made up of a large number of small spots, each from a separate crystal. Each spot is so small as to give the appearance of a continuous line. If the crystal is not ground finely enough, the diffraction lines appear speckled.

XRD patterns were recorded using a Philips X'Pert Pro diffractometer of $\Theta/2\Theta$ with a Cu (αK_α = 1.54056 Å) radiation. The identification of the materials was made using a ICPDS diffraction data from International Center for Diffraction Data.

X-ray photoelectron spectroscopy (XPS)

X-ray photoelectron spectroscopy (XPS) is based on the analysis of the kinetic energy distribution of core level photoelectrons ejected as the result of irradiation with monochromatic or narrow band X-rays (Figure II-3). The best sensitivity is of the order

of a few percent of a monolayer and for most instruments spatial resolution is around 0.2 mm. With suitable calibration procedures elemental surface concentrations can be measured with accuracy of the order of 20%. It constitutes a major tool in catalyst characterization. The major interest is centered on observations of "chemical shift" effects which reflect the oxidation state, and the chemical environment of the emitter. Quantitative applications, especially to complex systems such as catalysts, can involve problems due to sample charging and to the choice of calibration procedures. They usually necessitate independent data concerning catalyst structure and texture. XPS has been widely used in catalyst research to provide general qualitative analyses, to investigate the depth profile distribution of active species, to obtain estimates of dispersion, clustering and other morphological variations, to study metal-metal and metal-support interactions and to examine the chemical states of additives, poisons and transition metal ions.

The XPS spectra were recorded at a residual pressure of 10^{-9} mbar on a KRATOS AxisULTRA electron energy spectrometer operating with a monochromatic Al - Kα radiation (1486.6 eV).

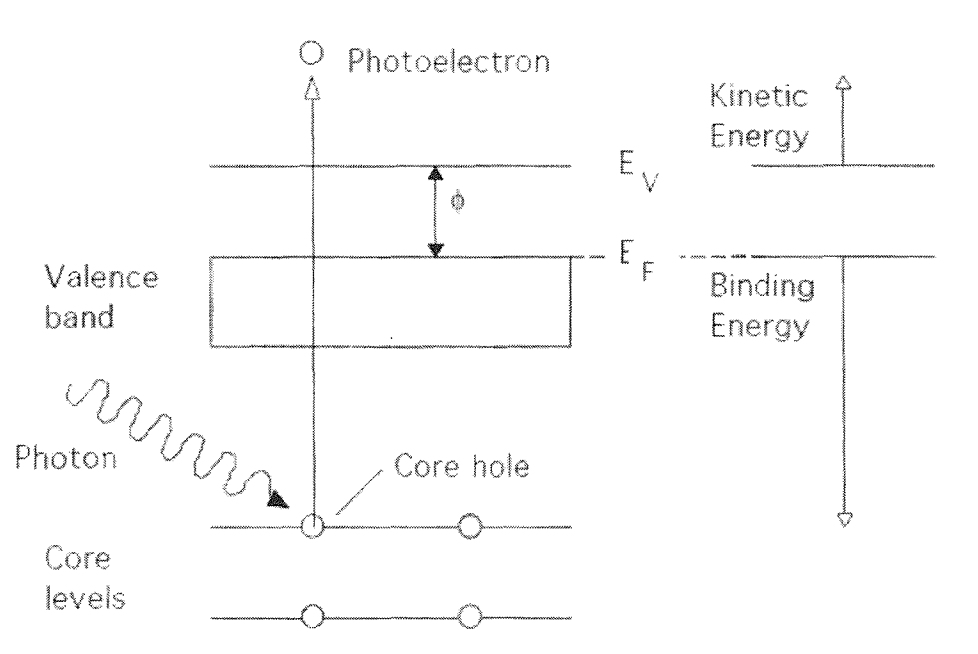

Figure II-3. Photoelectron effect.

Fourier transmission infrared spectroscopy (FTIR)

FTIR is most useful for identifying chemicals that are either organic or inorganic. It can be utilized to quantify some components of an unknown mixture. It can be applied to the analysis of solids, liquids, and gasses. The term Fourier Transform Infrared Spectroscopy (FTIR) refers to a development in the manner in which the data is collected and converted from an interference pattern to a spectrum. Today's FTIR instruments are computerized which makes them faster and more sensitive than the older dispersive instruments.

Molecular bonds vibrate at various frequencies depending on the elements and the type of bonds. For any given bond, there are several specific frequencies at which it can vibrate. According to quantum mechanics, these frequencies correspond to the ground state (lowest frequency) and several excited states (higher frequencies). One way to cause the frequency of a molecular vibration to increase is to excite the bond by having it absorb light energy. For any given transition between two states the light energy (determined by the wavelength) must exactly equal the difference in the energy between the two states [usually ground state (E_0) and the first excited state (E_1)].

A Bruker FTIR Vector spectrometer was used to detect infrared spectra of the samples. The resolution was selected to be 2 cm^{-1} and the number of scans – 64. The samples were dispersed in dry KBr pellet (0.001 g of the sample and 0.2 g of the KBr) with slight grinding for FTIR measurements at room temperature.

FTIR - Pyridine adsorption (FTIR-Py)

Pyridine adsorption coupled with IR measurements were used for determination of the supports acidity. All FTIR experiments were done using BIORAD FTS 3000MX instrument. The samples were prepared in the form of self-supporting discs (4 mg cm^2) and placed in IR cell equipped with KRS-5 windows. Catalysts were evacuated at 553 K at $<10^{-3}$ Pa for 1h. Pyridine was adsorbed at room temperature for 15 min and sample was evacuated for 15 min at 303 K and additional 5 min at 473 K to remove pyridine vapors.

Transmission electron microscopy (TEM)

Scanning transmission electron microscopy (STEM)

In electron microscopy as in any field of optics the overall contrast is due to differential absorption of photons or particles (amplitude contrast) or diffraction phenomena (phase contrast). The method provides identification of phases and structural information on crystals, direct images of surfaces and elemental composition and distribution. STEM represents a merger of the concepts of TEM and SEM. Modes of operation and mechanisms of contrast and of imaging are essentially the same as in TEM but the main advantage of STEM is the ability to carry out microanalysis at very high resolution (Energy Dispersive X-ray Spectroscopy and X-mapping analysis).

Energy dispersive X-ray spectroscopy (EDS) is the analysis of characteristic X-rays provides identification and quantification of elements with $Z > 10$; improvements in X-ray detectors should reduce this limit to $Z=6$. The original electron probe microanalysis (EPMA) was essentially a low SEM resolution with an X-ray detector but the SEM mode suffers from two disadvantages: X-ray spatial resolution is relatively poor and quantitative analysis involves corrections for various processes within the thick specimen. With specimens sufficiently thin for TEM or STEM use (~200 nm) the X-ray resolution is improved (40 nm) and a semi-quantitative analysis can be obtained without application of corrections; more rigorous treatment of the data gives relative concentrations to within about 5%, with a minimum detectable mass fraction of 0.3 wt%.

The TEM and STEM electron microscopy images were recorded placing a drop of the particles in THF onto a carbon film supported on a cooper grid. The samples were studied using a Philips CM20 STEM microscope with a LaB6 cathode operating at 200 kV.

1.4. Hydrogenation of benzene

1.4.1. Catalytic test

The benzene hydrogenation was performed in a quartz reactor equipped with a thermocouple. 0.1 g of the catalyst were placed in the reactor and it was activated in a flow of hydrogen pure (flow rate = 100 cm^3min^{-1}) as described above (1.3.1. Hydrogen treatment). After the activation, the sample was cooled to the desired temperature. A gas mixture containing benzene and hydrogen (1 vol.% of benzene) was prepared by

passage of a H_2 stream (10 cm^3min^{-1}) through benzene placed in a saturator maintained at 278.4 K. The reactant mixture was passed through the reactor with a total flow rate of 50 cm^3min^{-1}. The catalytic test was carried out at various temperatures (348 – 498 K temperature range) on the same catalyst. The sample was heated or cooled at a rate of 10 K min^{-1}. Benzene and the reaction products were analyzed each 6 min (5 injections at each temperature) using a 5730A Hewlett Packard gas chromatograph, operated at a programmed temperature and with a flame ionization (FID) detector. TCEP chromatographic column (2m column, Ø = 1,8 mm) has been used for separation the products of the hydrogenation reaction. It was prepared by impregnation of Chromosorb W HP with 1,2,3-tri(2-cyano-etoxy) propane (TCEP) (20 wt.%). Scheme of installation for benzene hydrogenation is given in Figure II-4.

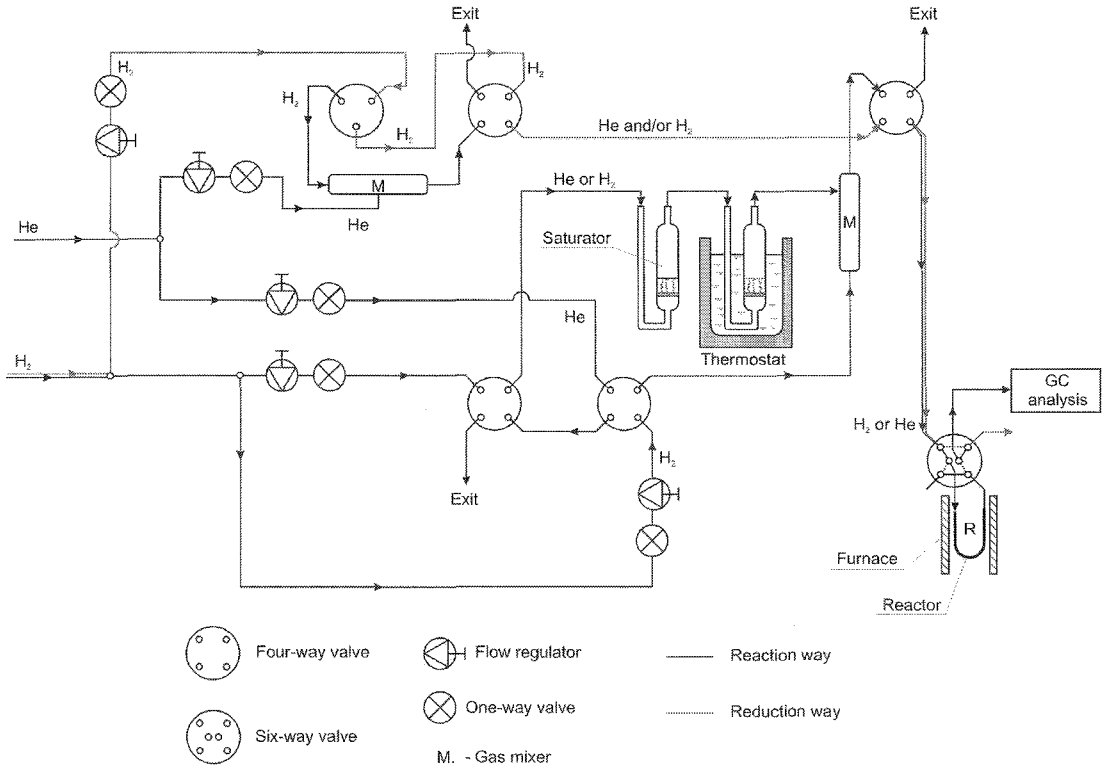

Figure II-4. Scheme of installation for benzene hydrogenation reaction.

1.4.2. Stability test

The stability test was performed in a quartz reactor equipped with a thermocouple. 0.05 g of the catalyst were placed in the reactor and activated in a flow of hydrogen according to the procedure described above (2.3. Hydrogen treatment). The stability tests were carried out using C_6H_6/He + H_2 as a reactant mixture (flow rate = 100 cm^3min^{-1}). The reactant mixture was prepared by passage of a He stream (10 cm^3min^{-1}) through benzene placed in a saturator maintained at 278.4 K. Then the reactant mixture was completed with He (40 cm^3min^{-1}) and H_2 (50 cm^3min^{-1}) to obtain the total flow rate of 100 cm^3min^{-1}. The stability test was carried out at 423 K for 16h. The reaction products were analyzed by GC in the same conditions as for the test of benzene hydrogenation.

1.4.3. Kinetic test

Determination of the activation energy for the catalysts was performed in a quartz reactor equipped with a thermocouple. 0.05 g of the catalyst were placed in the reactor and activated in hydrogen flow as ascribed above (2.3. Hydrogen treatment). After the activation the catalyst was cooled to 348 K. The catalytic test was carried out in the temperature range 348 – 403 K. The reactant mixture was prepared by passage of He stream (10 cm^3min^{-1}) through benzene placed in a saturator maintained at 278.4 K. Then the reactant mixture was completed with He (15 cm^3min^{-1}) and H_2 (25 cm^3min^{-1}) to obtain the total flow rate of 50 cm^3min^{-1}. The catalyst was cleaned in a hydrogen flow (100 cm^3min^{-1}) after each test. The reaction products were analyzed by GC in the same conditions as for the test of benzene hydrogenation.

1.5. Hydrogen storage at room temperature

High-pressure hydrogen uptakes were assessed with a specially designed volumetric adsorption/desorption system (Figure II-5). The unit consisted of a 4.13 cm^3 sample cell module connected to a reservoir; the standard reservoir volume used was 164 cm^3. Pressure was measured with a pressure gauge. Materials for construction of the sample cell module, including valves and fittings, were chosen such that the vessel could be heated to 773 K using an external source to outgas or activate the samples. The volume of the system, both with and without samples, was calibrated by attaching a reservoir with known volume to the sorption reservoir.

Room temperature desorption was measured by allowing the gas in the sample cell to expand into the desorption reservoir for a series of measurements. Desorption measurements from each separate pressure expansion were summed to determine the total amount of hydrogen released.

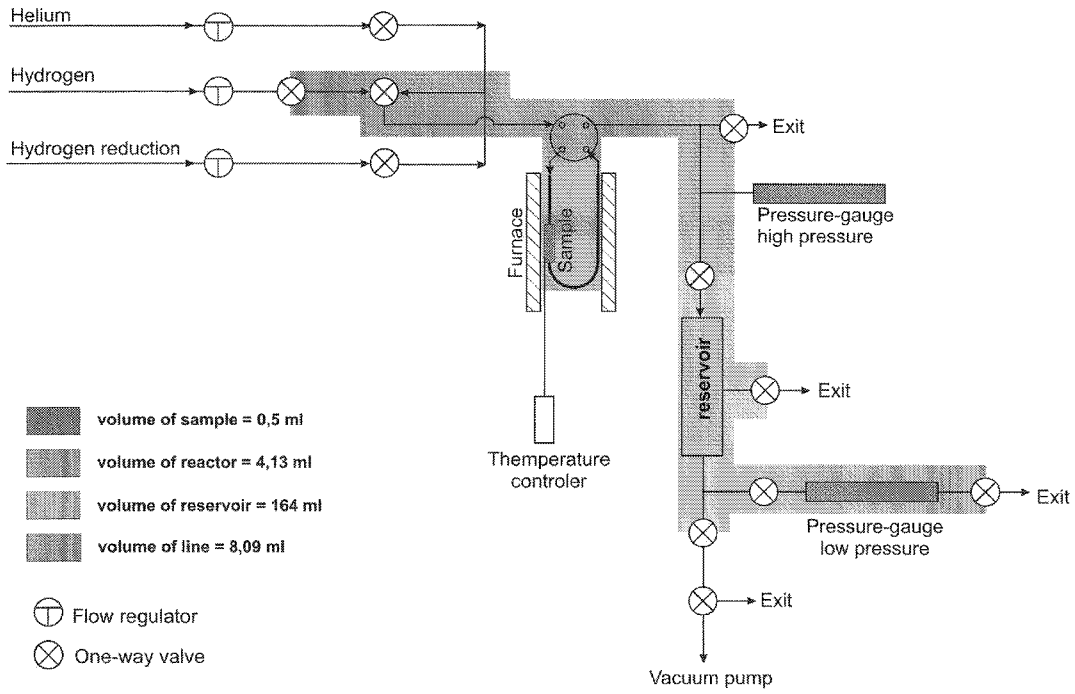

Figure II-5. Scheme of installation for hydrogen storage.

Initial sample mass for the high-pressure experiments was 400 mg. Before starting the sorption, the sample was purged in vacuum for 1 h at 473 K. It was then activated for 3 h at 623, 773 or 873 K in hydrogen with a flow rate of 100 cm^3 min^{-1}. After the hydrogen pretreatment, the sample was swept with a helium flow (100 cm^3 min^{-1}) for 2 h at 673 K, then cooled to room temperature under the helium flow. After the purging, the system was saturated in hydrogen for 16h at the desired pressure (20 or 30 bars). The sample was weighted after the desorption experiment in order to determine the weight loss due to the heat pre-treatment. This loss was less than 7%.

2. Calculations

2.1. Dispersion and particle size measurements by gas chemisorption

Selective chemisorption of different gases is the most frequently used technique for characterizing metallic catalysts. The measurement of the quantity of a gas adsorbed selectively on the metal at monolayer coverage, gives the metal surface area and the metal dispersion, if the stoichiometry of the chemisorption is known [1]. Measurements of the gas uptake has been carried out by various methods such as static (volumetry and gravimetry) and dynamic (continuous flow and pulse adsorption) methods. The flow technique seems to be most convenient than static methods since it is faster and does not require vacuum system [1].

The ideal, for a given catalyst, gas should be chosen to minimize adsorption on the support, to have an irreversible chemisorption on the metal and to know the true stoichiometry of chemisorption. The gases the most currently used are H_2, O_2 and CO.

Based on hydrogen chemisorption results nickel dispersion was calculated from [1] as follows (Ni/H stoichiometry was taken 1):

$$D = \frac{\frac{V \cdot n}{22414 \cdot m}}{\frac{wt}{100 \cdot M}} = \frac{100 \cdot V \cdot n \cdot M}{22414 \cdot m \cdot wt} \qquad (1)$$

where:

V	-	volume adsorbed	[cm^3 STP]
n	-	stoichiometric factor	(=2)
22414	-	molar gas volume (standard conditions)	[cm^3/mol]
m	-	sample weight	[g]
wt	-	nickel content	[wt%]
M	-	nickel atomic weight	(58.69 g/mol)

Where dispersion D is defined as a ratio of number of surface Ni atoms (N_s) to the total number of Ni atoms (N_T) (2):

$$D = \frac{N_S}{N_T} \tag{2}$$

The surface of active phase was determined based on the following [1](3):

$$S = a_m \cdot \frac{N_A}{M} \cdot D \tag{3}$$

where:

N_A is Avogadro number ($6.023*10^{23}$ mol)

a_m is the surface covered by one nickel atom (6.51 $Å^2$ [1]).

Assuming the spherical shape, average crystallite size (d) was calculated based on irreversible adsorption isotherm of hydrogen, according to the following:

$$d = \frac{6000}{S \cdot \rho} \tag{4}$$

where:

ρ is a metal density (8.90 g/cm^3 for Ni [1])

S is a surface area.

2.2. Particle size measurement by the XRD line broadening analysis

X-ray diffraction line broadening analysis (LBA) has been widely used for characterizing supported metal crystallites. A perfect crystal would extend in all directions to infinity so no crystal is perfect due to its limited sizes. Such a deviation from perfect crystallinity will lead to broadening of the diffraction peak. However, this type of peak broadening is negligible when the crystallite size is larger than 200 nm [1].

In 1918, Scherrer for a very first time observed that small crystallite size could give rise to peak broadening. He derived a well known equation for relating the crystallite size to the peak width, which is called the Scherrer formula [1]:

$$d = \frac{K\lambda}{\beta \cos\theta} \tag{5}$$

where:

K is the Scherrer constant (0.9 when $\beta_{1/2}$ is used)

λ is the wavelength of the X-radiation

β is the integral breadth of a reflection (in radians) located at 2Θ

Θ is the angular position of the peak maximum

2.3. Determination of specific surface area and pore volume by BET method

BET (Brunauer, Emmett, Teller) theory is a well-known rule for the physical adsorption of gas molecules on a solid surface. The concept of this theory is an extension of the Langmuir monolayer molecular adsorption, to multilayer adsorption with the following hypotheses: (a) gas molecules physically adsorb on a solid in layers infinitely; (b) there is no interaction between each adsorption layer; and (c) the Langmuir theory can be applied to each layer [2]. The resulting BET equation is expressed [3] by (6):

$$\frac{p}{V(p_0 - p)} = \frac{1}{VmC} + \frac{C-1}{VmC} * \frac{p}{p_0} \quad (6)$$

where:

Vm is the volume of the monolayer [cm^3g^{-1}]

V is the volume of gas adsorbed at p/p_0 [cm^3g^{-1}]

C is the BET constant

p is the equilibrium pressure at temperature of adsorption

p_0 is the saturation pressure at temperature of adsorption

Using the results of the above calculation the specific surface are can be calculated as follows (7):

$$S_{BET} = \frac{Vm^* N_A * \omega}{\nu} \quad (7)$$

where:

Vm is the monolayer adsorbed gas [cm^3g^{-1}]

N_A is the Avogadro number

ω is the adsorption cross section

υ is the molar volume of gas

2.4. Determination of the micropore surface area by Dubinin–Radushkevich method

The Micropore Volume Filling Theory was proposed by Dubinin-Radushkevich and co-workers for adsorption from gas phase. It is related to Eucken/Polany'i potential theory . The Dubinin–Radushkevich (DR) isotherm describes adsorption on a single type of uniform pores (in this respect the DR isotherm is an analogue of Langmuir-like local isotherms in adsorption on energetically heterogeneous solids) [2]. In the case of simple systems, experimental isotherms may be described by e.g. bi-DR isotherm -

corresponding to bimodal micropore system. This theory allows to describe a continuous distribution of pore sizes (or generally pore characteristics) [2].

The Dubinin–Radushkevich equation is as follows (8):

$$\log(V) = \log(Vo) - \frac{B*T^2}{\beta} * \left[\log\frac{Po}{P}\right]^2 \qquad (8)$$

where:

V is the volume adsorbed at equilibrium pressure [cm^3g^{-1} STP]

Vo is the micropore capacity [cm^3g^{-1} STP]

Po is the saturation vapor pressure of gas at temperature T [mm Hg]

P is the equilibrium pressure [mm Hg]

β is the affinity coefficient of analysis gas relative to Po gas

T is the analysis bath temperature [K]

B is the constant

For each point designated for Dubinin – Radushkevich calculations, the following calculation are done:

$$LV = \log(V) \text{ and } LP = \log\left(\frac{Po}{P}\right)^2 \qquad (9)$$

where:

LV is an independent variable

LP is the dependent variable

Assuming the adsorption of gas is restricted to a monolayer, the following can be calculated:

Monolayer capacity [cm^3g^{-1} STP]:

$$Vo = 10^{YI} \tag{10}$$

where:

YI is the Y-intercept [cm^3g^{-1} STP]

Micropore surface area [m^2g^{-1}]:

$$S\mu = \frac{\sigma * Vo * 6.023 * 10^{23}}{22414 * 10^{18}} \tag{11}$$

where:

σ is the molecular cross section area of gas [nm^2]

Vo is the monolayer capacity [cm^3g^{-1}]

2.5. Determination of the degree of reduction by O_2 reaction

The degree of reduction (D_R) was determined by the controlled oxidation of reduced nickel at high temperature [4]. The total quantity of oxygen used can give the degree of nickel reduction assuming that the follow reaction occurs:

$$Ni^0(s) + \frac{1}{2}O_2(g) \rightarrow NiO(s)$$

The degree of reduction (in %) of nickel could be calculated as follows (12):

$$D_R = \frac{2n_O}{n_{Ni}} * 100 \tag{12}$$

where:

n_O is the total number of moles of oxygen consumed [mol]

n_{Ni} is the total number of moles of nickel in the sample [mol]

2.6. Reaction rate and TOF in the benzene hydrogenation

Specific reaction rate (r) is the expression reserved to the reaction rates per unit mass of catalyst [5]. It is expressed in number of moles of the reactant per time unit and per mass unit of catalyst. It could be calculated from the equation (15):

$$r = \frac{[Bz] * d}{m_{cat}} \tag{15}$$

where:

[Bz] is the benzene concentration [$mol_{Bz}L^{-1}$]

d is the total flow rate [$Lmin^{-1}$]

m_{cat} is the mass of catalyst sample [g]

Turnover frequency (TOF) is defined as the number of revolutions of the catalytic cycle per unit time [5]. It is a chemical reaction rate, differential quantity depending on temperature, pressure and concentrations. The TOF present many advantages such as: i) possibility to compare to a value of TOF obtained on a different catalysts, ii) even if a value of TOF is approximate, it can immediately reveal whether the catalyst is truly a catalyst or is merely a reagent, iii) indicates the importance or not of crystalline anisotropy as reflected eventually in the size of clusters, and iiii) is useful in assessing the potential of new catalytic materials in relation to catalysts in current use [5].

The TOF [in s^{-1}] for nickel catalysts in hydrogenation of benzene reaction could be calculated from the following (16):

$$TOF = \frac{r}{S_{Ni}} \tag{16}$$

where:

r is the reaction rate [$molec_{Bz}*s^{-1}g^{-1}$]

S_{Ni} is a number of nickel surface active sites [$sites*g^{-1}$]

The reaction rate is expressed in molecules of benzene per second per gram and it can be determined as ascribed above (15). The number of nickel active sites can be determined by chemisorption of hydrogen at room temperature.

3. REFERENCES

[1] G. Bergeret, P. Gallezot in *Handbook of Heterogeneous Catalysis* 1997, vol. 2, p. 439

[2] A.W. Marczewski on *www.adsorption.org* , 2002

[3] M. Ziolek, I. Nowak in *Kataliza Heterogeniczna, wybrane zagadnienia.* AMU Edition Poznan, 1999

[4] C.H. Bartholomew, R.J. Farrauto, *J. Catal.* 45 (1976) 41

[5] M. Boudart, *Chem. Rev.* 95 (1995) 661

CHAPTER III
STUDY OF NICKEL CATALYSTS SUPPORTED ON Al_2O_3 AND SiO_2 OXIDES

INTRODUCTION

L'activité, la sélectivité et la durée de vie des catalyseurs métalliques supportés sont fortement influencées par la charge en métal, la taille des particules métalliques, la méthode de préparation et la nature du support. Plusieurs méthodes peuvent être appliquées pour obtenir les métaux fortement dispersés sur la surface du support. L'imprégnation est la méthode généralement utilisée. Si le support est microporeux, les étapes d'imprégnation, de séchage, de calcination et de réduction influeront sur la taille des particules métalliques dans le matériau final.

Dans ce contexte, des catalyseurs de nickel supportés sur les oxydes non réductibles Al_2O_3 et SiO_2 ont été préparés par simple (SIM) et double imprégnation (DIM). Les données de littérature montrent que la méthode DIM permet d'obtenir des catalyseurs supportés de nickel/alumina bien dispersés. Dans cette méthode, il y a deux étapes. La première est l'imprégnation de support inorganique par la solution de H_2Na_2EDTA et la seconde (après le séchage) est l'imprégnation par la solution contenant les ions actifs de métal. La phase métallique a été réduite par l'hydrazine aqueuse. Les matériaux obtenus ont été caractérisés et testés dans la réaction d'hydrogénation du benzène. Leurs performances ont été comparées à celles de catalyseurs conventionnels

1. INTRODUCTION

The activity and selectivity of supported metal catalysts are strongly influenced by the amount of metal, the size of dispersed metal particles, the preparation method and the support composition [1-3]. To improve the catalyst activity and its durability, it is necessary to obtain a well-dispersed active phase in the catalyst [4]. Several methods can be applied to obtain highly dispersed metals on the support surface [5]. Supported metal catalysts are commonly prepared by metal salt impregnation. If the support is microporous, it will imbibe a solution of a metal salt; drying, calcination (optional) and reduction will generate small metal particles. The classical method of the support impregnation results in obtaining small metal crystallites but only at very low metal contents in the catalyst [6]. It is also possible to obtain small metal crystallites by co-precipitation, but such catalysts are very difficult to reduce [7].

Supported nickel catalysts are most effectively prepared thought the optional combination of high dispersion and metal loading. Small metal particles may be formed on the surface of the support to which they are more or less firmly anchored, and on which they are effectively separated from each other. The average distance between the particles will depend on the metal content, the particle size and the surface area of the support [8].

Nickel catalysts were prepared by the double impregnation method (DIM) [9-10]. Previous findings and literature data allow to conclude that this preparation method is suitable for producing well dispersed nickel/alumina supported catalysts [9-12]. In DIM there are two stages, one by one. The first one is the impregnation of inorganic support by H_2Na_2EDTA solution and then (after drying) impregnation by solution containing active metal ions. In contrast to the classical simple impregnation method (SIM) [13], in DIM preparation procedure the carrier is preliminarily "activated" (modified) by EDTA introduced by impregnation and dried; the following preparation steps are the same as in SIM [14]. Modification of the support using impregnation by H_2Na_2EDTA has influence on the way of metal bonding, which is added in the next stage of preparation. It changes the concentration of metal in catalyst, decreases average nickel crystals size. Application of H_2Na_2EDTA on the stage of preparation favored high active phase dispersion. Presence of the EDTA adsorbed on the support surface assures homogenous distribution of the metal ions. The effect of the presence of EDTA is particularly visible in the low and average concentration of metal ions. As the

concentration of metal is increasing in impregnation solution, participation of favorable interaction EDTA–ion is gradually decreasing, what is caused by accelerated adsorption in support pores and the increase of the interactions between metal ions and hydroxyl surface groups [15].

Conventional supported metal catalysts are prepared by *in situ* reduction of a metal salt. The catalytic activity of the metal particles is strongly influences by their size and shape [1-2, 16-19]. However, it is often difficult to control the morphology of the final material, notably for impregnated catalysts [16-23]. An alternative method to obtain supported catalysts with well-defined metal particles is the preparation of supported catalysts from metal colloids.

Metal nanoparticles research has recently become the focus of intense work due to their unusual properties compared to bulk metal. The reason for such avid research arises from the drastic increase of the surface to volume ratio to such an extent that the material properties are determined much more by the surface atoms than by the framework atoms, with the result that the physical and chemical properties of the particles differ considerably from those of bulk solids [3-8]. They hold promise for use as advanced materials for electronic, magnetic, optical and thermal properties [9-10] and have also been applied in heterogeneous catalysis [7, 24-27]. The chemical route for the preparation of such materials is of particular interest since it allows a better control of the structure at the microscopic level [28-40]. The chemical methods have generally involved the reduction of the relevant metal salt in the presence of a stabilizer such as linear polymers [6, 41-44], ligands [44-45], surfactants [40, 46-48], tetraalkylammonium salts [49-50], or heterogeneous supports [51-53] which prevent the nanoparticles from agglomerating. Hydrazine is a good reducing agent for noble and transition metals ions, including in aqueous medium [53-56]. Recent works have pointed out the interest of working in aqueous medium as a practical solution for the future in homogeneous and heterogeneous catalysis [57].

In spite of the high number of studies published in the past decades, an increasing attention is paid to the hydrogenation of aromatics because of the stringent environmental regulations governing their concentration in diesel fuels [58-61]. Benzene hydrogenation has been chosen as the model aromatic feedstock [62-63]. This reaction has also been used as model reaction in heterogeneous catalysis by metals where metal-support interactions are involved [61-65].

In our laboratory, a systematic study of supported nickel nanoparticles, obtained by reduction of nickel salts in aqueous media, has been undertaken. Previous work showed that the size and shape of the metal particles, as well as their hydrogenating properties, strongly depended on the reduction conditions of the Ni^{2+} ions [26-27]. We now report the study of nickel nanoparticles supported on silica or alumina.

Supports

Aluminum oxide, commonly referred to as alumina, possesses strong ionic interatomic bonding giving rise to its desirable material characteristics. It can exist in several crystalline phases which all revert to the most stable hexagonal alpha phase at elevated temperatures. This is the phase of particular interest for structural applications. Alpha phase alumina is the strongest and stiffest of the oxide ceramics. Its high hardness, excellent dielectric properties, refractoriness and good thermal properties make it the material of choice for a wide range of applications. The aluminum oxides are commonly used as the supports for metal or metal oxides catalysts, especially, the γ-Al_2O_3 which is stable in both oxidizing and reducing atmospheres and at relatively high temperatures. In our study we used γ-Al_2O_3 with the specific surface area of 100 m^2*g^{-1}.

Silicon dioxide (silica) is one of the most commonly encountered substances in both daily life and in electronics manufacturing. Compared to the others oxides, the surface of the SiO_2 is almost inert. The silanol groups present on the surface have a low acidity. The complete dehydroxylation of silica surface occurs at high temperature (973 K). Under this thermal treatment the chemical reaction between the silanol groups occurs, providing the siloxane group (Si – O – Si) formation. The amorphous silica is usually obtained by the high temperature treatment of silica hydrogel to obtain an aerogels. The chemistry of the interior surface of an aerogel plays a dominant role in its chemical and physical behavior. It is this property that makes aerogels attractive materials for use as catalysts support. In our study we used silica from Ventron with the specific surface area of 400 m^2*g^{-1}. This support is denoted as SiO_2(V).

Catalysts

Two methods of impregnation were used, namely simple (SIM) and double (DIM) impregnation method. Two methods of preparation were used. In classical preparation, the impregnated precursor salt (nickel acetate) is calcined in air then reduced under a hydrogen flow. In non classical preparation, the impregnated precursor

salt is reduced in aqueous hydrazine media at 353 K then treated under same hydrogen flow. For more details, see Experimental section. Notation of prepared catalysts is listed in Table III-1.

Table III-1. Prepared catalysts.

catalyst	% wt. of Ni	Method of preparation
1NiSiO$_2$(V)	**1.0**	**SIM , classical**
1Ni/EDTA/SiO$_2$(V)	**1.0**	**DIM, classical**
1NiSiO$_2$(V)-H	**1.0**	**SIM, non classical**
1Ni/EDTA/SiO$_2$(V)-H	**1.0**	**DIM, non classical**
1NiAl$_2$O$_3$	**1.0**	**SIM, classical**
1Ni/EDTA/Al$_2$O$_3$	**1.0**	**DIM, classical**
1NiAl$_2$O$_3$-H	**1.0**	**SIM, non classical**
1Ni/EDTA/Al$_2$O$_3$-H	**1.0**	**DIM, non classical**
SiO$_2$(V)	**-**	**classical**
SiO$_2$(V)-H	**-**	**non classical**
Al$_2$O$_3$	**-**	**classical**
Al$_2$O$_3$-H	**-**	**non classical**

2. RESULTS AND DISCUSSION

2.1. Reduction of Ni^{2+} supported on SiO_2 and Al_2O_3

In aqueous hydrazine media green Ni^{2+} ions are reduced to colloidal black Ni^0particles according the equation (1):

$$2Ni^{2+} + N_2H_4 + 4OH^- \rightarrow 2Ni^\circ + N_2 + 4H_2O \qquad (1)$$

The reduction of the SIM supported nickel phase did not occur when the precursors were treated in aqueous hydrazine media at 353 K: the solids became blue and this color was not changed to dark and no nitrogen was detected in the exhaust gas. 1Ni/EDTA/Al_2O_3 catalyst also was not reduced in the hydrazine media. This may be ascribed to the formation of stable nickel-hydrazine surface species. Indeed, it is known that unsupported Ni^{2+} ions form a blue complex $[Ni(N_2H_4)_3]^{2+}$ in basic hydrazine media [27,66]. This complex is formed *via* the substitution of water ligands by hydrazine ligands. When the temperature is increased, the complex decomposes and the reaction media progressively changes to a dark black colloidal solution of metallic nickel and gaseous N_2 evolves according to equation (1). Moreover, for silica supported Ni^{2+} ions, it was shown that the reduction occurs in the same hydrazine media with a rate and conversion depending on the nickel content and reaction conditions [27]. Also for SIM or 1Ni/EDTA/Al_2O_3 catalysts we believe that a stable supported $[Ni(N_2H_4)_n]^{2+}$ complex is intermediately formed. It is not decomposed to metallic nickel and gaseous N_2 as the unsupported complex did.

In case of the 1Ni/EDTA/SiO_2(V) catalyst, the treatment with aqueous hydrazine provided desorption of nickel complex from the support surface. Indeed, after hydrazine injection, the reactant solution became blue while the support changed color from green to white. This phenomenon could be explained by low Ni/EDTA complex compound stability in high pH conditions. When hydrazine was introduced in the liquid media, the Ni-EDTA complex desorption was observed, also a more or less significant part of active phase was out of catalyst. The blue color of the solution is ascribed to the formation of $[Ni(N_2H_4)]^{2+}$ complex stabilized by EDTA [67].

2.2. Characterization of the catalysts.

2.2.1. Isopropanol decomposition

The acidity of the supports used in this work was estimated on the basis of isopropanol dehydration. Intramolecular dehydration towards propene as well as intermolecular reaction producing diisopropyl ether occurred with the participation of acidic centers on the catalyst surface. For all matrices tested, propene was the main reaction product indicating acidity of the materials. However, the conversion of alcohol

(indicating acidity strength or/and concentration) depended on the nature of the support (Fig. III-1). The following order is found: $SiO_2 < Al_2O_3$.

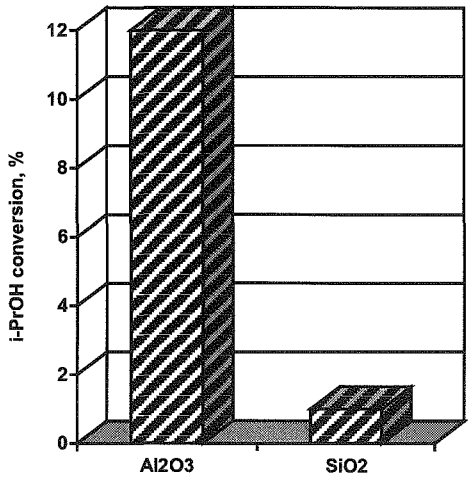

Figure III-1. Isopropanol decomposition at 623 K.

2.2.2. H_2-TPR study

In the H_2-TPR conditions used the SiO_2 and Al_2O_3 supports did not consume hydrogen.

Classical catalysts

The H_2-TPR profile of $1NiSiO_2(V)$ (Fig. III-2) exhibits a broad peak at 892 K as a result of the formation of several nickel species. The profile of the $1Ni/EDTA/SiO_2(V)$ (Fig. III-2) catalyst differs from that of $1NiSiO_2(V)$ one. There is only one sharp peak with the maximum at 1013 K. This let us to suppose that the catalysts containing EDTA have a better nickel dispersion and the nickel active phase is more homogeneous but it is more difficult to reduce. The high temperature reduction peak comes from the reduction of the nickel cationic form.

Alumina supported catalysts are not reduced in TPR experiments. It can be caused by strong interaction between the Ni^{2+} ions and the support. The reducibility of Ni–species depends on the nickel–support interaction, which seems to be very high when Al_2O_3 is used as the matrix [19]. The more intense interaction, the stronger

connection of Ni–oxide with the matrix. This leads to more difficult interaction with hydrogen. At a low nickel loading, a great number of nickel atoms is in close contact with the support so they are more difficultly reduced. At the concentration of the H_2 in the gas flow (1000 ppm) these ions cannot be reduced. In contrast, they are reduced in pure hydrogen at 773 K.

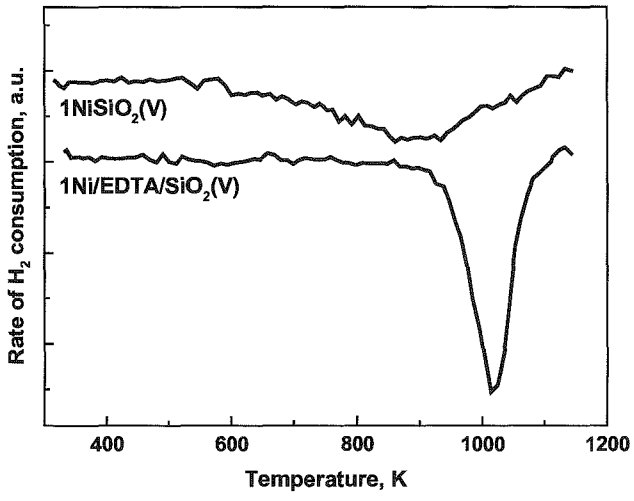

Figure III-2. H_2-TPR profiles for classical SIM and DIM catalysts supported on SiO_2.

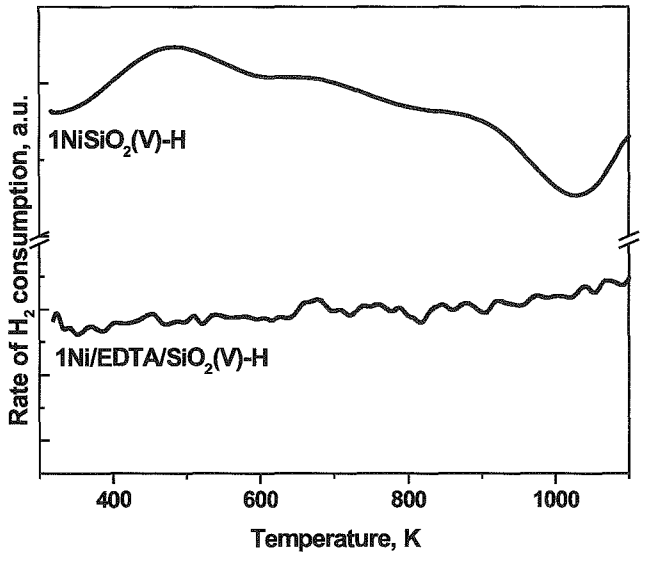

Figure III-3. H_2-TPR profiles for non classical SIM and DIM catalysts supported on SiO_2.

Non classical catalysts

In TPR experiments of non-classical alumina supported catalysts treated by hydrazine no hydrogen consumption was observed as a result of a very strong anchorage of the nickel ions on the support. Contrary to that the non classical SIM catalysts supported on SiO_2 exhibited typical H_2-TPR profiles (Fig. III-3). The peaks observed correspond to the reduction of supported Ni^{2+} ions by the hydrogen since aqueous hydrazine reduction was inefficient, as mentioned above. The reducibility of these species depended on the method of preparation and was different from that of Ni^{2+} ions stemming from classical catalysts. The $1NiSiO_2(V)$-H exhibits a broad H_2-TPR peak (Fig. III-3) at a higher temperature (1024 K) than that of the $1NiSiO_2$ classical catalyst (1013 K) (Fig. III-2). This may be due to a stronger interaction with the support which, in turn, probably results from the formation of smaller particles. In contrast, the double impregnation catalyst $1Ni/EDTA/SiO_2(V)$-H is not reduced at the same conditions (Fig. III-3). This confirms desorption of the active phase from the surface of the catalyst during the preparation in hydrazine media. The non-classical catalysts, strikingly, produced nitrogen around 450 K and hydrogen at higher temperatures (Fig. III-4).

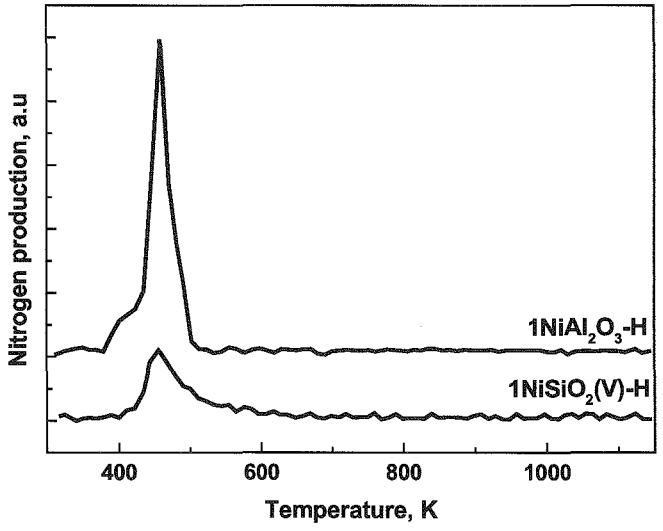

Figure III-4. Nitrogen production during TPR study for non classical catalysts.

These gases are ascribed to the decomposition of surface NH species previously formed during the hydrazine aqueous treatment at 353 K. During the TPR experiments, under the heating in the gas phase, they decomposed at a higher temperature on the catalyst surface.

A detailed examination of the TPR profiles shows that the temperature of hydrazine decomposition changes with the nature of the support and method of preparation (Table III-2). The amounts of nitrogen evolving also changed with the nature of the catalyst and, moreover, were larger than that of nickel loading (Table III-2). This strongly indicates that hydrazine widely adsorbed on the support in the aqueous media at 353 K, in a way which depended on the nature of the support, in very good agreement with the support acidity reported above.

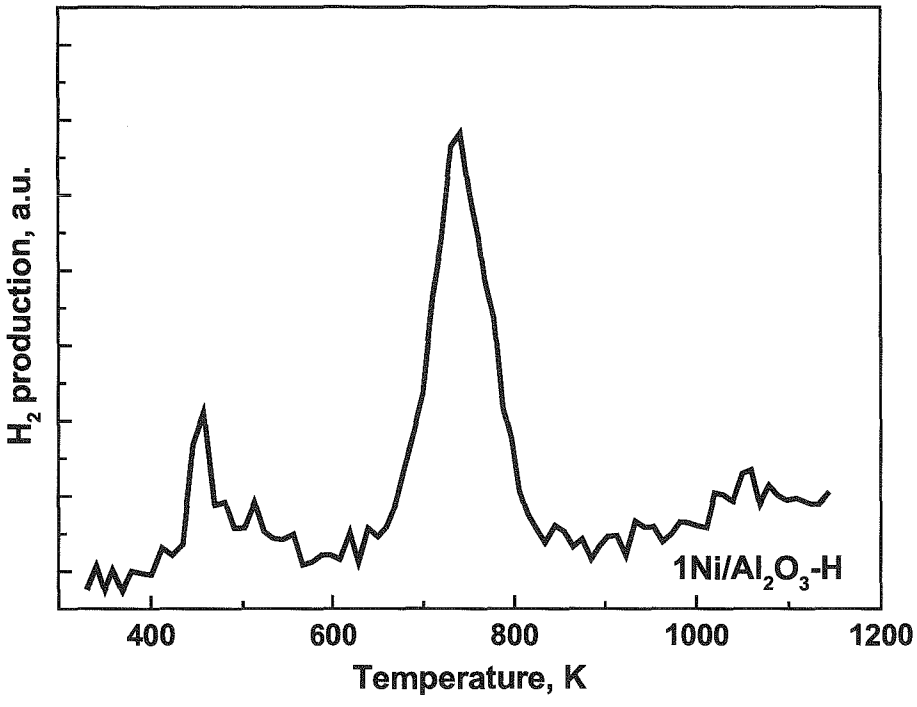

Figure III-5. Hydrogen production during TPR study.

Evolution of nitrogen (Fig. III-4) was observed with both silica SIM and DIM non-classical catalysts. For these catalysts the evolution of nitrogen means that the

adsorbed hydrazine species decomposition occurs at 450 K. The H atoms of hydrazine probably desorbed as gaseous ammonia which was not analyzed during the TPR measurements.

Table III-2. N_2 desorption during H_2-TPR study.

Catalyst	Temperature of N_2 desorption, [K]	N_2 desorbed $*10^{-3}$ [mol$*g_{cat}^{-1}$]
$1NiAl_2O_3$-H	458	2.0
$1Ni/EDTA/Al_2O_3$-H	453	8.6
$1NiSiO_2$(V)-H	439	2.2
$1Ni/EDTA/SiO_2$(V)-H	456	2.0

In contrast, a hydrogen production was observed besides that of nitrogen (Fig. III-5). Two types of hydrogen species are observed. The first one appears at around 450 K, concomitantly with nitrogen desorption and the second one at higher temperatures. The peaks at 450 K are ascribed to the partial decomposition of adsorbed hydrazine as nitrogen and hydrogen [68-69]. As to the high temperature peak of hydrogen, it could be due to the formation and incorporation of H-species in the catalyst at 450 K then desorption at higher temperatures.

Several studies showed that gaseous hydrazine could decompose as mixtures of nitrogen + ammonia or nitrogen + hydrogen [68-69].

2.2.3. XRD study

The XRD study gives the information about the structure and presence of nickel in the metallic state on the support surface. The XRD patterns of the SiO_2 catalysts confirmed the amorphous character of this support (Figure III-6). Moreover the presence of the nickel particles was not detected. This could be ascribed to the relatively low nickel content (1% wt.) and high dispersion on the nickel metal phase.

The XRD study confirmed the structure of the Al_2O_3 (Fig. III-7). This structure is also preserved after hydrazine reduction. No reduction of support occurred during N_2H_4 treatment.

Figure III-8 shows the XRD patterns of the nickel catalysts supported on alumina oxide. There is no reflects originated from the metallic nickel. The reflect at 44.5° of Ni^0 could be hidden by the large reflect of the alumina support observed in the same region or too weak due to the low nickel content or high dispersion. The XRD study confirmed that the modification of alumina with nickel does not change its structure. No aluminates phase was detected in the XRD patterns of the nickel catalysts. Moreover the absence of the reflect due to the reduced nickel could be explained by the relatively low nickel content (~1%) and/or very small nickel particles size and high dispersion.

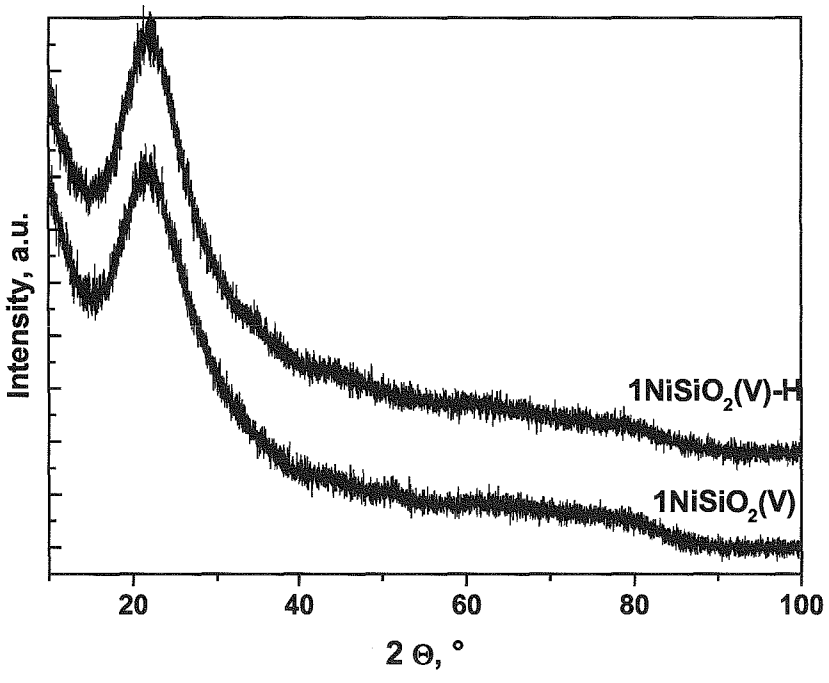

Figure III-6. XRD patterns of the silica supported catalysts.

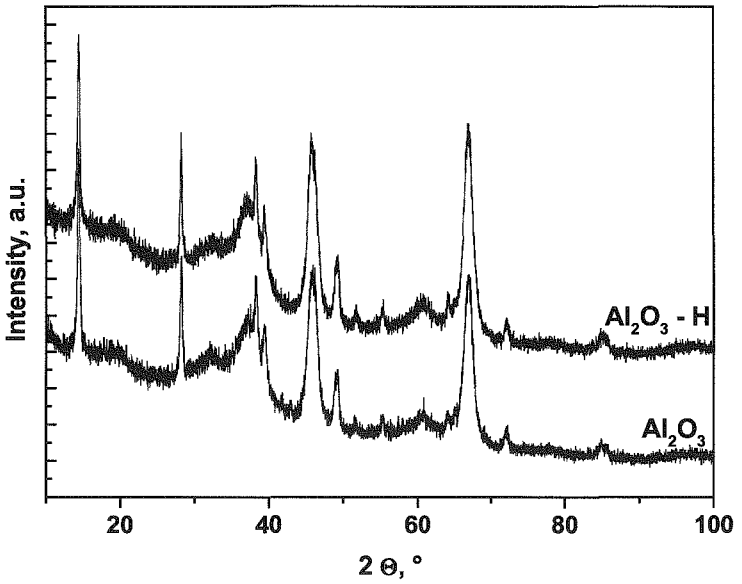

Figure III-7. XRD patterns of the alumina support.

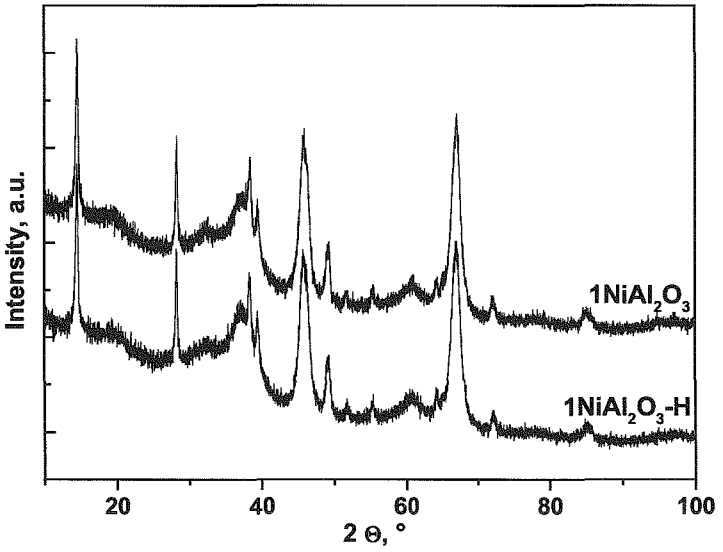

Figure III-8. XRD patterns of the nickel catalysts supported on Al_2O_3.

2.2.4 Degree of reduction

The degree of reduction was determined after a treatment under pure hydrogen for 2 h at 673 K and 773 K for non-classical and classical catalysts respectively. In these conditions, all the catalysts were reduced. The amount of reduced nickel atoms was measured by oxygen adsorption at 723 K and 823 K for non-classical and classical catalysts, respectively. The obtained results show that the method of preparation or nature of the support determined the degree of reduction. These results are reported in Tables III-3 and III-4.

Table III-3. Degree of reduction for classical catalysts.

catalyst	O_2 uptake $x10^{-5}$ [mol $g^{-}_{cat}{}^{-1}$]	degree of reduction %
$1NiAl_2O_3$	**9.31**	**103**
$1Ni/EDTA/Al_2O_3$	**7.32**	**86.1**
$1NiSiO_2(V)$	**5.84**	**68.7**
$1Ni/EDTA/SiO_2(V)$	**2.45**	**27.0**

Classical catalysts

The $1NiAl_2O_3$ catalyst showed the total reduction (103%), whereas the catalyst prepared by double impregnation was only 86.1% reduced (Table III-3). It can be concluded that double impregnation with H_2Na_2EDTA does no facilitate the reduction of the Ni/Al_2O_3 system. The Al_2O_3 catalysts prepared by the hydrazine reduction exhibited lower degree of reduction (Table III-4), in good agreement with the TPR study which showed that they were of lower reducibility. In the hydrazine treated catalysts, the supported nickel acetate precursor was directly reduced under the hydrogen flow, whereas the classical precursor was previously calcined. Earlier studies have shown that, in some cases, a more complete reduction to metallic nickel could be achieved when the supported nickel salt was directly reduced with hydrogen than when a reduction followed a previous calcination in air [70]. This is not the case here; also, as

suggested above, this may be a result of a stronger interaction of nickel ions with the support for the H-catalysts.

Table III-4. Degree of reduction for non classical catalysts.

catalyst	O_2 uptake $x10^{-5}$ [mol $g^{-}_{cat}{}^{-1}$]	degree of reduction %
$1NiAl_2O_3$-H	**3.63**	**42.7**
$1Ni/EDTA/Al_2O_3$-H	**5.86**	**70.6**
$1NiSiO_2$(V)-H	**7.19**	**84.6**
$1Ni/EDTA/SiO_2$(V)-H	**5.76**	**67.7**

Non classical catalysts

The degree of reduction was found lower for the catalysts supported on SiO_2 than that supported on Al_2O_3. On SiO_2, the catalyst prepared with H_2Na_2EDTA presented a very low degree of reduction (27%) whereas the $1NiSiO_2$ catalyst, prepared by simple impregnation, showed a degree of reduction more than two times higher (68.7%). It could be explained by the TPR study. The TPR profile of this catalyst shows one high temperature reduction peak (Fig. III-2). It originates from the reduction of nickel in cationic form. The temperature of the reduction used in this study was not enough high to provide the higher reduction of this catalyst. The SIM catalyst prepared by the chemical treatment with hydrazine showed a higher degree of reduction than the classical one. This is in contrast with the alumina catalysts as a result of the support effect.

2.2.5 H_2-adsorption study

The H_2-adsorption was used for the determination of the dispersion and particle size of the metal active phase after a pretreatment under a hydrogen flow at 673 K or 773 K for the non-classical or classical catalysts, respectively. The results obtained are reported in Tables III-5 and III-6.

SiO_2, and Al_2O_3 as well as EDTA/SiO_2 and EDTA/Al_2O_3 supports did not adsorb hydrogen after the hydrogen thermal pretreatment.

Table III-5. Characteristic of the classical catalysts.

catalyst	H_2 adsorption $x10^{-5}$ [mol g_{cat}^{-1}]	dispersion [%]	particle size [nm]
1NiAl_2O_3	0.35	4.1	24.7
1Ni/EDTA/Al_2O_3	0.38	5.2	19.5
1NiSiO_2(V)	0.59	10.2	9.9
1Ni/EDTA/SiO_2(V)	0.12	5.0	20.0

Table III-6. Characteristic of the non classical catalysts.

catalyst	H_2 adsorption $x10^{-5}$ [mol g_{cat}^{-1}]	dispersion [%]	particle size [nm]
1NiAl_2O_3-H	0.34	9.5	10.6
1Ni/EDTA/Al_2O_3-H	0.17	3.0	33.7
1NiSiO_2(V)-H	0.60	8.4	12.0
1Ni/EDTA/SiO_2(V)-H	0.00	-	-

For the classical catalysts the higher dispersion and smaller nickel particle sizes were found in case of the SiO_2 catalysts. Moreover, the dispersion of the 1NiSiO_2(V) catalyst is two times higher than that of 1Ni/EDTA/SiO_2(V) catalyst. Contrary to that the dispersion of the double impregnated 1Ni/EDTA/Al_2O_3 catalyst is higher than that of the SIM catalyst. It could be concluded that introduction of EDTA allows the reaching a better dispersion for the catalysts supported on Al_2O_3 while for the silica supported catalysts EDTA provides growth of the nickel particles. Moreover, the EDTA addition seems to incorporate the nickel ions at the cationic position into the pores of the catalyst while simple impregnation allows creating the surface nickel species. The

very high temperature reduction peak (1013 K) observed for this catalyst is similar to the H_2-TPR profiles shown in the literature for the catalysts prepared by ion exchange method [71].

Non-classical 1Ni/EDTA/SiO_2(V)-H catalyst did not adsorb the hydrogen at all, which again confirms desorption of the Ni-EDTA complex during the reduction by hydrazine. The more significant part of active phase was out of the catalyst providing absence of the activity for this catalyst. Generally, the classical catalysts prepared by DIM adsorbed more hydrogen than the double impregnated catalysts prepared by the hydrazine reduction. The classical and non-classical catalysts without EDTA adsorb nearly the same quantities of hydrogen.

2.3. Catalytic activity

2.3.1 Testings

After a H_2 thermal treatment, the catalysts became active and selective in the gas phase hydrogenation of benzene to cyclohexane. No activity was observed without this treatment. The bare silica or alumina supports, previously treated or not in aqueous hydrazine, were inactive. The results are reported in Fig. III-9 and III-10.

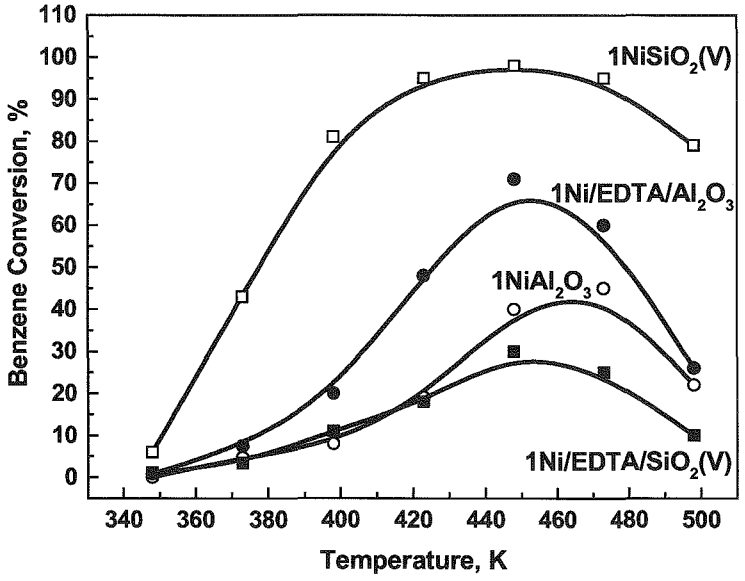

Figure III-9. Catalytic activity for classical catalysts.

The catalysts exhibited a maximum of activity as a function of the reaction temperature. The temperature of this maximum depends on the method of preparation and nature of the support. It is attributed to the competitive adsorption of the benzene and H_2 reactant molecules [26, 60-61]. The activity of the catalysts in the benzene hydrogenation strongly depends on the particle size. It was found that the hydrogenation of benzene reaction is a structure sensitive one [18-20]. In the case of highly dispersed materials, the changes in the catalytic activity were related to the combined effects of particle size, surface coverage with adsorbed species, and active site dimension [21].

Classical catalysts

The best catalytic performances are obtained with the $1NiSiO_2(V)$ catalyst which is active from 348 K (6% of conversion) and totally converts benzene at 448 K (Fig. III-9). The double impregnation method leads to a dramatic decrease of the activity: the maximum of conversion hardly reaches 30% for $1Ni/EDTA/SiO_2(V)$. For the catalysts supported on SiO_2 the activity increases with increasing the dispersion and decreasing the particle size of the nickel. It could be explained by the reducibility of this catalyst. The maximum of the reduction peaks are 892 and 1013 K (Fig. III-2) and the degrees of reduction are 27% and 68%, respectively (Table III-5). The nickel present on the surface is less reduced and the nickel oxide is not an active phase.

The alumina support decreases the maximum of conversion to 45% and at a higher temperature (473 K) (Fig. III-9) as compared to the silica support. In contrast, the double impregnation method enhances the activity since the maximum of conversion increases to 71%, whereas the temperature of this maximum shifts to 448 K. The lower activity of the alumina catalysts, as compared to that of the silica ones, is due to their lower reducibility as shown from the TPR results (see above). In these alumina catalysts the higher degree of reduction was found for the catalyst prepared by double impregnation (Table III-5). Its activity is also higher than that of the catalyst prepared by simple impregnation.

Non classical catalysts

The non-classical $1NiSiO_2(V)$ catalyst exhibits similar activity as classical one for the simple impregnation method (Fig. III-10). In contrast, the non-classical double impregnation catalyst is completely inactive in benzene hydrogenation. It confirms the

desorption of the Ni-EDTA complex when hydrazine was introduced in the liquid media. The more significant part of active phase was out of catalyst, providing the absence of the activity for this catalyst.

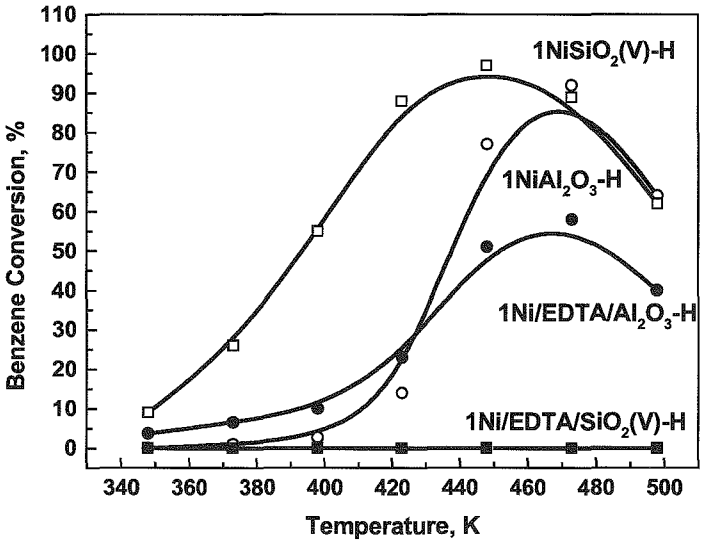

Figure III-10. Catalytic activity for the non classical catalysts.

When alumina is the support, the non-classical catalyst is more active than the classical one for simple impregnation method: the maximum of conversion passed from 45 to 92% at 474 K (Fig. III-9 and III-10). In contrast, the double impregnation decreases the maximum conversion from 71% to 58% and increases the temperature of this maximum from 344 to 474 K. Comparison of the non-classical catalysts shows that the double impregnation decreases the maximum conversion from 71 to 51% at 448 K.

The results of the benzene hydrogenation could be well correlated with the dispersion of nickel active phase. For the non-classical catalysts supported on Al_2O_3 the activity increases with increasing the dispersion and decreasing the particle size of nickel. The $1NiSiO_2(V)$ and $1NiAl_2O_3$ non classical catalysts have a dispersion and catalytic activity comparable at high reaction temperatures. At lower reaction temperatures, the former is much more active due to a better reducibility as showed the H_2-TPR and degree of reduction experiments.

2.3.2 Stability test

The stability test was carried out at 423 K for a set of catalysts. The results are shown in Figures III-11 and III-12.

Figure III-11 shows the conversion of benzene versus time on stream at 423 K for alumina non classical catalysts. The SIM non classical $1NiAl_2O_3$-H catalyst showed high stability with time on stream, although some deactivation was observed. The catalyst is initially activated during the reaction-test from 80% to 90% conversion. This activation is attributable to a deeper reduction during the hydrogenation reaction. It was incompletely reduced by the H_2/623 K pre-treatment. Note that the TPR results showed this catalyst was not reduced under a 100 ppm H_2/Ar flow. Contrary to that, the non classical DIM catalyst was found to be less active and less stable. Deactivation was observed after 20 min of reaction and the activity decreased from 45 % to 22 % after 960 min of test. It could be concluded that the reduction of nickel by hydrazine forms the stable nickel particles which resisted well to the coke formation. EDTA seems to decrease the stability of the nickel supported on alumina catalysts.

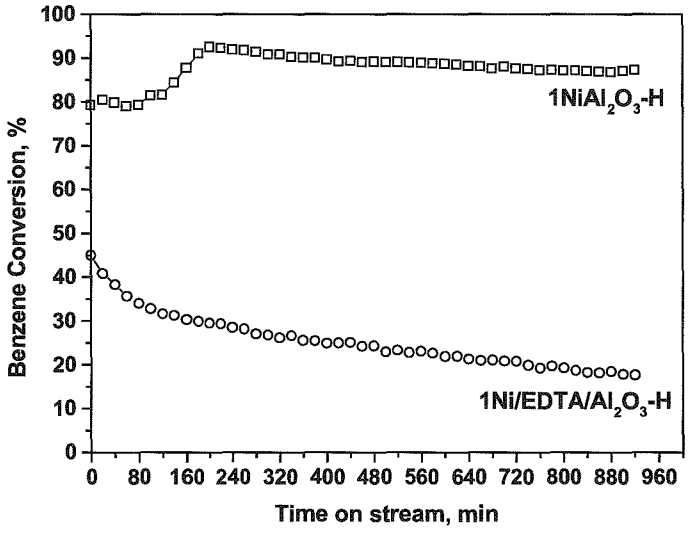

Figure III-11. Benzene conversion versus time on stream for Al_2O_3 SIM and DIM catalysts.

In case of the SIM catalysts supported on the SiO_2 oxide (Figure III-12) the deactivation was lower than for the alumina catalysts. The classical $1NiSiO_2$ showed the highest stability in the conditions used. The non classical $1NiSiO_2(V)$-H catalyst was activated from 90 to almost 100% conversion within 200 min then a little deactivated. The activation process would also be due to a deeper reduction of nickel in the reaction conditions. The catalyst was also found more difficult to reduce in the TPR experiments conditions (Fig. III-2 and III-3).

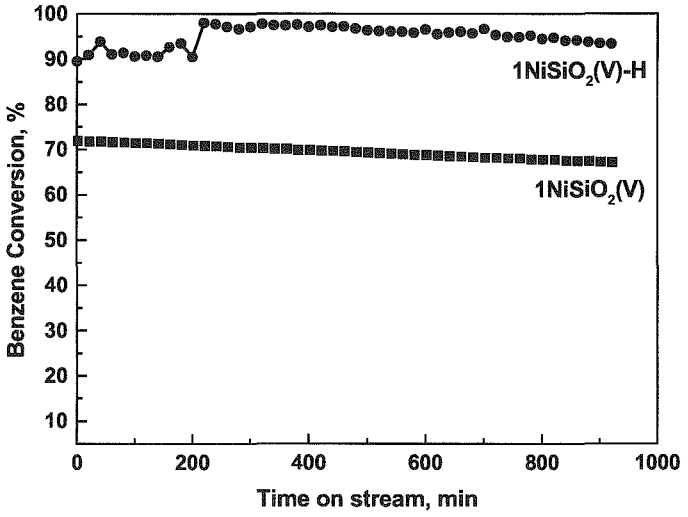

Figure III-12. Benzene conversion versus time on stream for SiO_2 SIM catalysts.

3. CONCLUSIONS

The surface acidity of the supports used changes as manifested by the isopropanol test-reaction: $SiO_2 < Al_2O_3$. The incorporation of Ni^{2+} ions in the oxide matrix by simple or double impregnation method gives rise to metal-support interactions to a more or less extent.

Various nickel surface species were evidenced by the H_2-TPR study. According to the catalyst preparation method used or/and support, the nickel phase exhibited various reducibility, surface or hydrogenating properties. As a general trend, the best performances are obtained with the silica support, which seems to interact less with the

nickel. The metal-support interactions are the highest when Al_2O_3 is used as the matrix for nickel.

The supported precursors were shown to be not reduced in aqueous hydrazine at 353 K, as initially desired, because a stable blue surface complex $[Ni(N_2H_4)_n]^{2+}$ was formed. In the mean time, hydrazine molecules adsorbed on the catalyst support in the aqueous media. Under a heating flow these molecules decomposed to gaseous mixtures $N_2(+NH_3)$ or N_2+H_2 according to the nature of the support with amounts and at a temperature depending on the support acidity, in good agreement with the isopropanol test-reaction.

4. REFERENCES

[1] S.J. Tautster, S.C. Fung, *J. Catal.* 5 (1978) 29

[2] C.H. Bartholomew, D.G. Mustard, *J. Catal.* 67 (1981) 186

[3] W.P. Halperin, *Rev. Mod. Phys.* 58 (1998) 533

[4] G. Schmid, *Chem. Rev.* 92 (1992) 1709

[5] J.S. Bradley, E.W. Will, C. Klein, B. Chaudret, A. Duteil, *Chem. Mater.* 5 (1993) 2540

[6] H. Hirai, Y. Nakao, N. Toshima, *J. Macromol. Sci. Chem. A.* 13 (1979) 727

[7] L.N. Lewis, *Chem. Rev.* 93 (1993) 2693

[8] Y. Volotkin, J. Sinzig, L.J. De Jong, G.Schmid, M.N. Vargaftik, I.I. Moisseev, *Nature* 384 (1996) 621

[9] V.N. Colvin, M.C. Schlamp, A.P. Alivisatos, *Nature* 370 (1994) 354

[10] R.L. Whetten, *Acc. Chem. Res.* 32 (1999) 397

[11] J. Ryczkowski, T. Borowiecki, *React. Kinet. Catal. Lett.* 49(1) (1993) 127

[12] J. Ryczkowski, T. Borowiecki, D. Nazimek, *Adsorp. Sci. And Technol.* 14(2) (1996) 113

[13] B.C. Gates, *Chem. Rev.* 95 (1995) 511

[14] R. Brayner, G. Viau, F. Bozon-Verduraz, , *J. Mol. Catal. A.* 182/183 (2002) 227

[15] W. Yu, H. Liu, X. Ma, Z. Liu, *J. Colloid. Interface Sci.* 208 (1998) 439

[16] T.S. Armadi, Z.L. Wang, T.C. Green, A. Heinglein, M.A. El-Sayed, *Science.* 272 (1996) 1924

[17] J. Zelinski, *J. Catal.* 76 (1982) 157

[18] J.T. Richardson, M. Lei, B. Turk, K. Forster, M.V. Twigg, *Appl. Catal.* 110 (1994) 217

[19] R. Molina, G. Poncelet, *J. Catal.* 173 (1998) 257

[20] A. Miyazaki, I. Balin, K. Aika, Y. Nakano, *J. Catal.* 204 (2001) 364

[21] D. Reinen, P.W. Selwood, *J. Catal.*, 2 (1963) 109

[22] M. Houalla, J. Lemaître, B. Delmon, *J. Chem. Soc. Faraday Trans.* 78 (1982) 1389

[23] G.R. Gavallas, C. Phishitkul, G.E. Voecks, *J. Catal.* 88 (1984) 54

[24] U.A. Paulus, U. Endrushchat, G.J. Feldmeyer, T.J. Schmidt, H. Bonnemann R.J. Behm, *J. Catal.* 195 (2000) 383

[25] E.A. Sales, B. Benhamida, V. Caizergues, J.P. Lagier, F. Fievet, F. Bozon-Verduraz, *Appl. Catal.* **172** (1998) 273

[26] A.G. Boudjahem, S.Monteverdi, M. Mercy, M.M.Bettahar, *J. Catal.*, 221 (2004) 325

[27] A.G. Boudjahem, S. Monteverdi, M. Mercy, M.M. Bettahar, *Langmuir*, 20 (2004) 208

[28] L.K. Kurihara, G.M. Chow, P.E. Shoen, *Nanostruct. Mater.* 5 (1995) 607

[29] T.D. Xiao, S. Torban, P.R. Strut, B.H. Kear, *Nanostruct. Mater.* 7 (1996) 857

[30] J.H. Fendler, F.C. Meldrum, *Adv. Mater.* 7 (1995) 607

[31] F. Fievet, F. Fievet-Vincent, J.P. Lagier, B. Dumont, M. Figlarz, *J. Mater. Chem.* 3 (1993) 627

[32] R.D. Rieke, *Acc. Chem. Res.* 10 (1997) 377

[33] R.D. Rieke, *Science.* 246 (1989) 1260

[34] G.A. Ozin, *Adv. Mater.* 4 (1992) 612

[35] G.N. Glavee, *Inorg. Chem.* 32 (1993) 474

[36] H. Bonnemain, W. Brijoux, T. Joussen, *Angew. Chem. (Int. Ed. Engl.).* 29 (1990) 273

[37] D. Zeng, M.J. Hampten-Smith, *Chem. Mater.* 5 (1993) 68

[38] K. Vijaya Sarathy, G.U. Kulkarny, C.N.R. Rao, *Chem. Commun.* 537 (1997).

[39] P. Gallezot, C. Leclercq, Y. Fort, P. Caubere, *J. Mol. Catal.* 93 (1994) 79

[40] J.J. Brunet, P. Gallois, P. Caubere, *J. Org. Chem.*, 45 (1980) 1937

[41] N. Toshima, Y. Wang, *Adv. Mater.* 6 (1994) 245

[42] A. Heinglein, *J. Phys. Chem.* 97 (1993) 5457

[43] J.S. Bradley, J.M. Millar, E.W. Hill, S. Behal, B. Chaudret, *Faraday Discuss.* 92 (1991) 255

[44] J.C. Poulin, H.B. Kagan, M.N. Vargavtik, I.P. Stolarov, I.I. Moisseev, *J. Mol. Catal.* 95 (1995) 109

[45] C. Amiens, D. de Caro, B. Chaudret, J.S. Bradley, R. Mazel, C. Roucau, *J. Amer. Chem. Soc.* 115 (1993) 11638

[46] N. Toshima, T.Takahashi, *Bull. Chem. Soc. Jpn.* 65 (1992) 400

[47] K. Esumi, K. Matzuhita, K. Torigoe, *Langmuir.* 11 (1995) 3285

[48] D.V. Leff, P.C. Ohara, J.R. Heath, W.M. Gelbart, *J. Phys. Chem.* 99 (1995) 7036

[49] H. Bönnemann, W. Brijoux, R. Brinkmann, E. Dinjus, E. Joussen, B. Korall, *Angew. Chem., Int. Ed. Engl.* 30 (1991) 1312

[50] M.T. Reetz, W. Helbig, *J. Amer. Chem. Soc.* 116 (1994) 7401

[51] N. Toshima, T. Teranishi, H. Asanuma, Y. Saito, *J. Phys. Chem.* 96 (1992) 3796

[52] S.J. Tauster, *Acc. Chem. Res.* 20 (1987) 389

[53] R. Brayner, G. Viau, G.M. da Cruz, F. Fiévet-Vincent, F. Fiévet, F. Bozon-Verduraz, *Catal. Today*. 57 (2000) 187

[54] A. Bensalem, G. Shafeev, F. Bozon-Verduraz, *Catal. Lett.* 18 (1993) 165

[55] Y.D. Li, L.Q. Li, H.W. Liao, H.R. Wang, *J. Mater.Chem.* 9 (1999) 2675

[56] L.M. Bronstein, O.A. Platonova, A.N. Yakunin, I.M. Yanovskaya, P.M. Valetsky, A.T. Dembo, E.S. Obolonkova, E.E. Makhaeva, A.V. Mironov, A.R. Khokhlov, *Colloid Surf.* 147 (1999) 221

[57] J.L. Pellegatta, C. Blandy, V. Collière, R. Choukroun, B. Chaudret, P. Cheng, K. Phillipot, *J. Mol. Catal. A.* 178 (2002) 55

[58] A. Stanislaus, B.H. Cooper, *Catal. Rev. Sci. Eng.* 36 (1994) 75

[59] K. Weissermel, H.J. Arple, in *« Industral Organic Chemistry »,* 3 rd Ed. VCH, New York, 1997.

[60] M.A. Keane, *J. Catal.* 166 (1997) 347

[61] R. Molina, G. Poncelet, *J. Catal.* 199 (2001) 162

[62] B. Coughlan, M.A. Keane, *Zeolites.* 11 (1991) 12

[63] K.J. Yoon, M.A. Vannice, *J. Catal.* 82 (1983) 457

[64] L. Daza, B. Pawelec, J.A. Anderson, J.L.G. Fierro, *Appl. Catal.* 87 (1992) 145

[65] R. Burch, R. Flambard, *J. Catal.* 85 (1984) 16

[66] Y.D. Li, L.Q. Li, H.W. Liao, H.R. Wang *J. Mater.Chem.*, 9 (1999) 2675

[67] K.V.R. Chary, K.S. Lakshmi, P.V. Ramana Rao, K.S. Rama Rao, M. Papadaki, *J. Mol. Catal. A:Chem.*, 223 (2004) 353

[68] X. Chen, T. Zhang, M. Zheng, Z. Wu, W. Wu, C. Li, *J. Catal.* 224 (2004) 473

[69] R. Brayner, G. Djéga-Mariadassou, G. Marques da Cruz, J.A.J. Rodrigues, *Catalysis Today* 57 (2000) 225

[70] C.H. Bartholomew, R.J. Farrauto, *J. Catal.* 45 (1976) 41

[71] R. Wojcieszak, S. Monteverdi, M. Mercy, I. Nowak, M. Ziolek, M.M. Bettahar, *Applied Catalysis A:General*, 268 (2004) 241

CHAPTER IV
NICKEL CATALYSTS SUPPORTED ON REDUCIBLE OXIDES-Nb_2O_5

INTRODUCTION

La fonction du support des catalyseurs métalliques supportés est généralement double : elle fournit et stabilise le métal dans un état fortement dispersé et, en agissant sur le métal, elle peut influencer ses propriétés catalytiques. Les interactions entre le support et le métal peuvent moduler les propriétés catalytiques intrinsèques de la phase supportée. Il est connu généralement que les oxydes réductibles sont de bons candidats pour mettre en évidence ce genre de phénomène. Les oxydes de niobium et de cérium, selon la littérature, peuvent subir une réduction par traitement thermique sous flux de H_2. Les interactions metal-support fortes semblent jouer un rôle crucial dans la réactivité des catalyseurs de nickel supportés sur ces oxydes. Les effets des supports Nb_2O_5 ou CeO_2 sur les propriétés du nickel ont été étudiés. Dans ce chapitre nous présentons les catalyseurs Ni/Nb_2O_5. Les catalyseurs Ni/CeO_2 seront présentés dans le chapitre suivant.

Nb_2O_5 est un support à la fois réductible et acide. Ses propriétés de support ou de promoteur des réactions catalytiques sont remarquables. Il a un comportement différent de ses voisins du Tableau Périodique des Eléments (V, Zr, Mo), d'où l'intérêt croissant de son utilisation en catalyse. Les catalyseurs Ni/Nb_2O_5 préparés ont été étudiés dans la réaction d'hydrogénation de benzène. La préparation a été effectuée par la méthode de l'hydrazine ou par voie classique, à partir de précurseurs obtenus par simple ou double (EDTA) imprégnation.

1. INTRODUCTION

A great variety of catalysts contain active phases in the form of nanometer-sized particles, of metal or oxide, dispersed over the surface of a second carrier or support material. The function of an oxide carrier in supported metal catalysts is generally two-fold: it provides and stabilizes the metal in a highly dispersed state and, by interacting with the metal, it may influence its catalytic properties. The properties of the bulk and surface structure of the metal particles are the key factors that control their performance [1]. The metal support interactions that can be established between the supported phase and the support can further modulate the intrinsic catalytic properties of the supported phase [2]. It is generally acknowledged that reducible oxides are good candidates to exhibit this kind of phenomenon [2].

Ceria and niobium oxides, according to the literature, can undergo reduction processes when treated with H_2 under relatively mild conditions [3-4]. The strong metal-support interaction (SMSI) in this case seems to play a crucial role in the catalytic properties of these oxides used as the support for nickel catalysts.

The activity and selectivity of a supported metal catalyst are strongly influenced by the amount of metal, the size of dispersed metal particles, the preparation method and the support composition [5-6]. Evidence has been found that in many systems the carrier exerts a marked influence on the properties of the metal particles supported on it [5]. The application of H_2Na_2EDTA in the stage of nickel catalysts preparation favored a high dispersion of an active phase [7-9]. Modification of the support using impregnation by H_2Na_2EDTA has influence on the way of metal bonding, which is added in the next stage of preparation. It changes the concentration of metal in catalyst, decreases average nickel crystals size. Presence of the EDTA adsorbed on the support surface assures homogenous distribution of the metal ions. The effect of the presence of EDTA is particularly visible in the low and average concentration of metal ions.

The supported nickel catalysts exhibit various nickel species due to the existence of various metal-support interaction strengths. As a consequence, the reducibility, surface or hydrogenating properties changed as a function of the nature of the support or method of preparation.

In this chapter we present results on the surface and catalytic properties of Ni/Nb_2O_5 catalysts. Next chapter is devoted to Ni/CeO_2 catalysts.

Hydrated niobium pentoxide, $Nb_2O_5*nH_2O$, which is usually called niobic acid, have strong acidic properties on the surfaces and is used as solid acid catalyst. In particular, niobic acid containing large amounts of water exhibits high catalytic performances for acid-catalyzed reactions in which water molecules participate or are liberated [10].

Niobium compounds and materials are now interesting and important catalysts for various reactions. Although there are few differences in electronegativity and ionic radius between Nb and its neighbors (V, Zr, Mo) in the periodic table, it is intriguing that the catalytic behaviors of niobium compounds are quite different from those of the surrounding elements compounds [10]. Thus, the research and development on the catalytic application of niobium compounds have been very active for the last 20 years. The characteristic features of niobium compounds are the promoter effect and the support effect [11]. Niobium oxides remarkably enhance catalytic activity and prolong catalyst life when the small amounts are added to known catalysts. Moreover, niobium oxides exhibit a pronounced effect as supports of metal and metal oxide catalysts [10].

In our study two methods of impregnation were used, namely simple (SIM) and EDTA double (DIM) impregnation method. Two methods of preparation were used. In classical preparation, the impregnated precursor salt (nickel acetate) is calcined in air then reduced under a hydrogen flow. In non classical preparation, the impregnated precursor salt is reduced in aqueous hydrazine media at 353 K then treated under same hydrogen flow. For more details, see Experimental section. Notation of prepared catalysts is listed in Table IV-1.

Table IV-1. Nickel catalysts supported on Nb_2O_5.

catalyst	% wt. of Ni	Ni impregnation
$1Ni/Nb_2O_5$	1	SIM, classical
$5Ni/Nb_2O_5$	5	SIM, classical
$1Ni/EDTA/Nb_2O_5$	1	DIM,classical
$1Ni/Nb_2O_5$-H	1	SIM, non classical
$1Ni/EDTA/Nb_2O_5$-H	1	DIM, non classical
$3Ni/Nb_2O_5$-H	3	SIM, non classical
$5Ni/Nb_2O_5$-H	5	SIM, non classical
$5Ni/Nb_2O_5$-H(b)*	5	3 steps (1%-3%-5%) Non classical
Nb_2O_5	-	-
Nb_2O_5-H	-	Non classical

* (b): stepwise reduction in hydrazine media (see Experimental Section).

2. RESULTS AND DISCUSSION

2.1. Reduction of Ni/Nb_2O_5 catalysts by hydrazine

In the reduction of nickel by the hydrazine, the reaction is expected to proceed according to the following equation [8-9]:

$$2Ni^{2+} + N_2H_4 + 4\,OH^- \rightarrow 2\,Ni^\circ + N_2 + 4\,H_2O \qquad (1)$$

The green color of Ni^{2+} ions first changes to blue, that of the $[Ni(N_2H_4)_n]^{2+}$ complex intermediately formed, then progressively to dark, that of colloidal Ni° particles. In addition, dinitrogen evolves in the exit gas from the reduction flask. The blue complex is formed via the substitution of water ligands by hydrazine ligands and decomposes by heating.

For SIM or DIM Ni/Nb_2O_5 precursors, all these color changes did not occur and no gaseous dinitrogen evolved, whatever the nickel content used: 1, 3, or 5wt.%. The catalyst color became blue and not changed to dark. This is ascribed the formation of a very stable $[Ni(N_2H_4)_n]^{2+}$, firmly attached to the niobia support.

In contrast, we remarkably succeeded in nickel reduction by using a stepwise procedure in case of 5%Ni content catalyst. Indeed, after three successive impregnations (total Ni content: 1% then 3% and finally 5wt.%), the final solid, denoted as $5Ni/Nb_2O_5$-H(b), was prone to the reduction by aqueous hydrazine at 353 K. The green color of the solid was changed to blue then dark and nitrogen was detected in the exit gas.

It is now well established that stepwise impregnation of Ni/SiO_2 catalysts leads to strongly and weakly adsorbed Ni^{2+} [14]. Nickel in strong interaction is obtained by impregnation of the nickel salt followed by water-washing or by ion-exchange then calcination. Nickel in weak interaction is obtained by impregnation to Ni^{2+} ions previously strongly attached to silica. The latter ions serves as a "chemical glue" [15] to the former. Nickel in strong interaction is identified as phillosilicate or grafted nickel depending on the preparation conditions. The anchoring of the metal particles onto the support was found to occur via Ni^+ or Ni^{2+} ions located at the metal-support interface [16]. Basing on these data one can suggest that, for Ni/Nb_2O_5 catalysts, nickel ions are strongly anchored to the support up to 3% content and thus cannot be reduced by the hydrazine. These ions, in turn, make up an interface on which the excess nickel introduced by the third impregnation weakly adsorbs and, consequently, becomes more

reducible and gives rise to metallic nickel phase: the reduction by hydrazine then proceeds via reaction (1) to a certain extent (see below H_2-TPR studies).

2.2. Characterization of catalysts

2.2.1. XRD study

Fresh hydrated Nb_2O_5 is amorphous. This was confirmed by the XRD patterns (Fig. IV-1). The H_2 as well as hydrazine treatment did not change the structure of niobium pentoxide (Fig. IV-1).

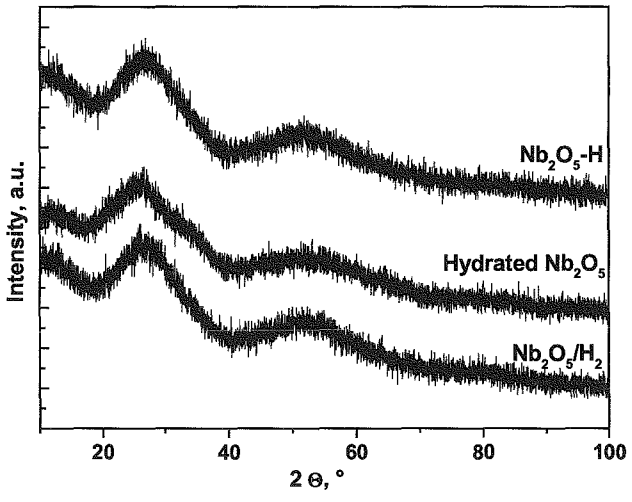

Figure IV-1. XRD patterns of the niobium support.

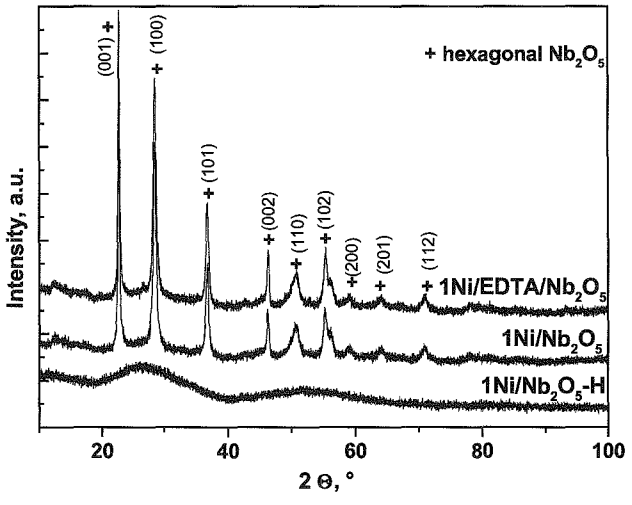

Figure IV-2. XRD patterns of the nickel supported on Nb_2O_5 catalysts.

In contrast, the XRD pattern of the calcined $NiNb_2O_5$ samples showed a crystallized phase of niobium oxide with the hexagonal structure (Fig. IV-2) after a H_2 treatement at 773 K.

Impregnation of the support with 1 wt.% of nickel does not change the hexagonal order of the material. However, at the higher nickel content (5wt.%), the XRD patterns (Fig. IV-3) showed two crystallized phases after the hydrogen treatment at 773 K of classical catalyst. The first phase with the main reflection peaks at 22.686 and 28.585 could be ascribed to hexagonal Nb_2O_5 and the second with the main peaks at 26.132, 35.336 and 51.954 to the rutile structure of the NbO_2 phase [17]. The hydrogen treatment of Nb_2O_5 provided the change of the sample color from white to gray which could confirm the partial reduction of white Nb_2O_5 to black NbO_2. In contrast, the XRD pattern of the non classical $5Ni/Nb_2O_5$-H(b) catalyst differs from that of the classical catalyst. There is no diffraction reflects from the hexagonal NbO_2 phase. The started material stays amorphous after the hydrazine reduction.

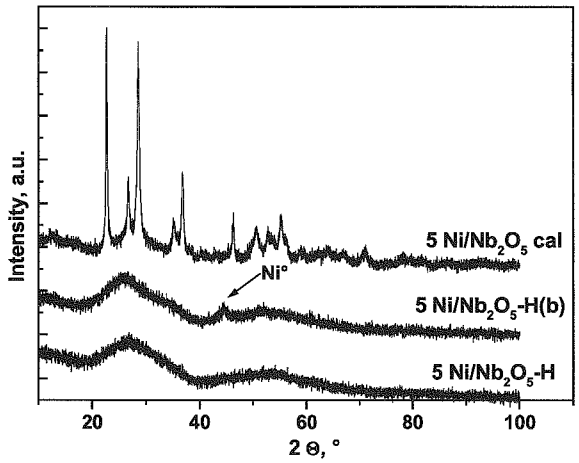

Figure IV-3. XRD patterns of the $5Ni/Nb_2O_5$, $5Ni/Nb_2O_5$-H and $5Ni/Nb_2O_5$-H(b) fresh catalysts.

XRD patterns for both 1 (Fig. IV-2) and 5 (Fig. IV-3) wt.% Ni classical catalysts did not show peaks which could originate from metallic nickel. However, one should remember that XRD technique is not sensitive if the amount of phase is too low (less than 5 wt%). Moreover, if the particle size of nickel is very small, XRD patterns cannot detect them. Nevertheless, the XRD pattern of the $5Ni/Nb_2O_5$-H(b) catalyst prepared by

the 3 steps impregnation, showed one detectable reflect at 44.5 ° which originates from the metallic nickel with *fcc* structure. It confirmed that the reduction on nickel has taken place after stepwise procedure of impregnation.

2.2.2. TEM study

The TEM micrographs of the calcined classical $5NiNb_2O_5$ and non classical $5NiNb_2O_5$-H(b) catalysts are shown in Fig. IV-4 and IV-5, respectively. For the former catalyst, the TEM image showed well dispersed nickel particles with the average particle size of 30 nm (Fig. IV-4). The TEM image of the non classical catalyst differs from that of classical one. Indeed, the nickel particles are not visible (Fig. IV-5). However, the X-ray microanalysis carried out on this sample showed the presence of the reduced nickel species. Very small nickel particles (~1nm) are formed and not detected by the TEM technique used in this study. The method of preparation strongly influences the final metal particle size.

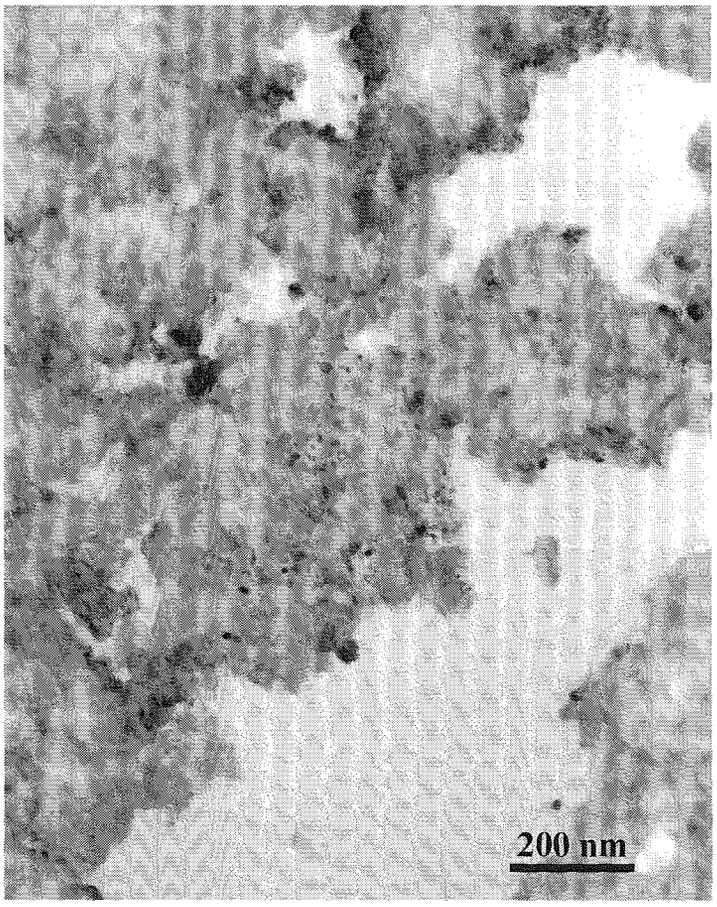

Figure IV-4. TEM image of the $5Ni/Nb_2O_5$ calcined catalysts.

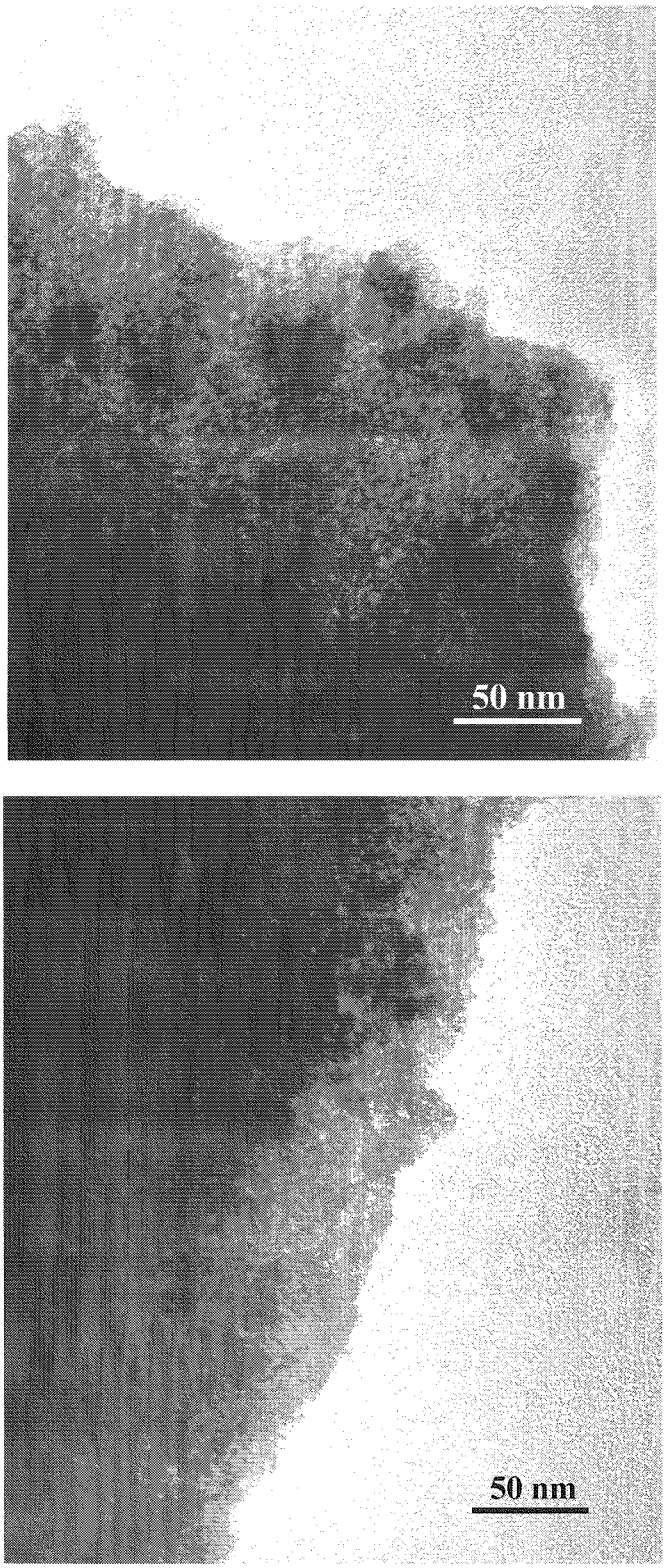

Figure IV-5. TEM images of the $5NiNb_2O_5$-H(b) catalyst.

2.2.3. XPS study

Niobium oxide

The XPS Nb $3d_{5/2}$ spectra of the pure Nb_2O_5 and Nb_2O_5-H(b) samples (Fig. IV-6) show two well defined peaks at 207.1 and 209.5 eV which correspond well to the reported binding energies of Nb_2O_5 [18]. The O 1s (Fig. IV-7) spectra of both samples are also nearly the same. There is one predominant peak at 529.8 eV which originates from the skeleton oxygen from Nb_2O_5. A second peak at 532.7 eV could be attributed to the formation of hydroxyls groups on the catalyst surface.

Interestingly, the spectra of the Nb_2O_5-H(b) sample, exhibit a N 1s peak (Fig. IV-8) at a binding energy B_E = 400 eV due to N_2H_4 adsorbed on the surface [18].

Ni/Nb_2O_5 catalysts

The XPS spectra of classical $5NiNb_2O_5$ and non classical $5NiNb_2O_5$-H(b) catalysts were recorded before and after hydrogen reduction at 773 K.

1. The XPS $Nb3d_{5/2}$ spectra of the calcined classical catalyst and fresh hydrazine treated catalysts (Fig. IV-6) are very similar and show the same peaks from niobium oxide. It means that the reduction with hydrazine does not change the structure of the niobium species.

Contrary to that, the XPS spectra of catalysts reduced by hydrogen show four peaks at 209.5, 208, 207.1, and 205.5 eV. The peaks at 208 and 205.5 originate from NbO_2 oxide [18]. It is known that the high temperature reduction (1073-1573 K) of Nb_2O_5 with hydrogen gives the bluish–black dioxide NbO_2 that has a distorted rutile structure and is diamagnetic. This reduction is reversible [4]. In the case of this work, the temperature of the hydrogen treatment is much lower (773 K) and nevertheless the reduction occurred, although probably for a few superficial oxide layers (gray color instead of dark). This could be ascribed to the presence of nickel in the surface layers which promoted the niobium partial reduction. This reduction is in a good agreement with the XRD study findings.

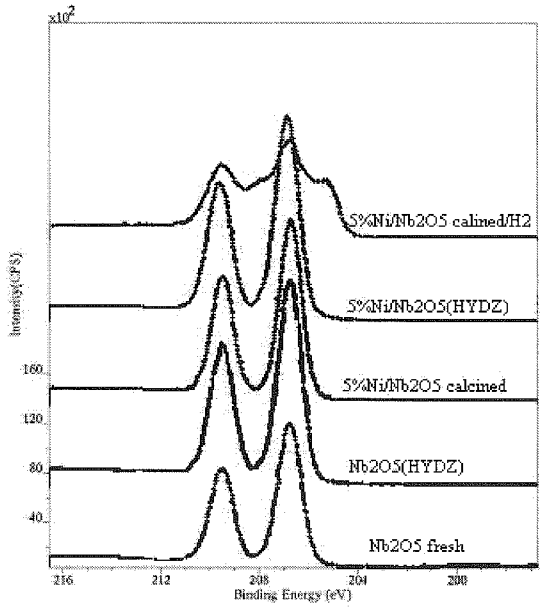

Figure IV-6. XPS spectra of the $Nb3d_{5/2}$ region.

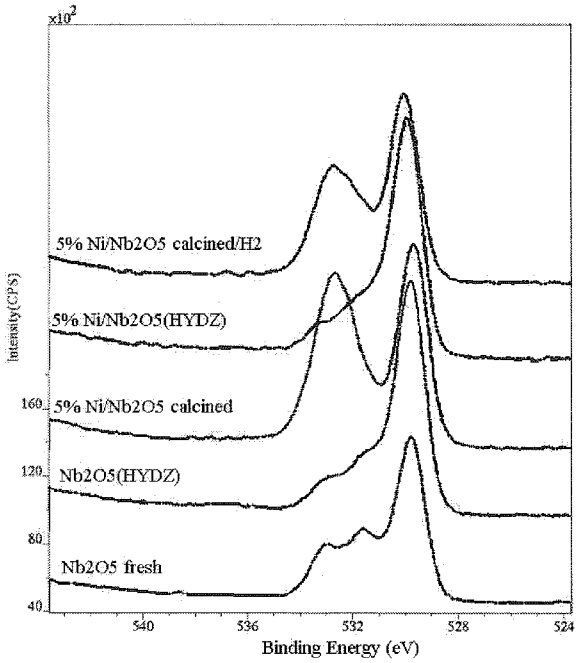

Figure IV-7. XPS spectra of the O 1s region.

2. The O 1s region was also investigated (Fig. IV-7). The analysis of the corresponding spectra showed the presence of two peaks at 529.7 eV and 532.7 eV for classical catalysts calcined or reduced. The main peak at 529.7 eV is related to the oxygen anions, O^{2-} , bound to the metal cations in the lattice [18]. The second peak at 532.7 could be attributed to the formation of hydroxyl groups on the catalyst surface. Non-classical $5NiNb_2O_5$-H(b) catalyst also showed one well defined peak at 529.7 eV which originates from the O^{2-} anions. However, the hydroxyl group peak at 532.7 is less intense.

3. The Ni $2p_{3/2}$ spectrum of the calcined classical catalyst exhibits a peak at 856.1 eV, characteristic of the presence of Ni_2O_3. The spectrum (not shown here) of H_2 reduced classical catalyst shows one very small but detectable peak at 852.5 eV which corresponds to Ni^0 [18]. The spectra of fresh and reduced non classical catalysts show the presence of the Ni_2O_3 only, detectable by the peak at 856.1 eV. The absence of Ni° on the surface of the catalyst can be explained by the reoxidation of the nickel particles by air during the drying. Small nickel particles of the hydrazine treated catalyst are probably more rapidly oxidized than the larger ones for classical catalyst. Moreover, the low concentration of surface nickel species detected by XPS could confirm the passivation of nickel by niobium. The catalysts were not activated in hydrogen flow before the XPS study.

4. The N 1s spectra of the hydrazine catalyst (Fig. IV-8) shows one peak at 400 eV due to the N_2H_4 adsorbed on the surface. The position of the peak, identical to that found for Nb_2O_5-H alone (Fig. IV-8), shows that hydrazine is probably adsorbed only on the niobium oxide support.

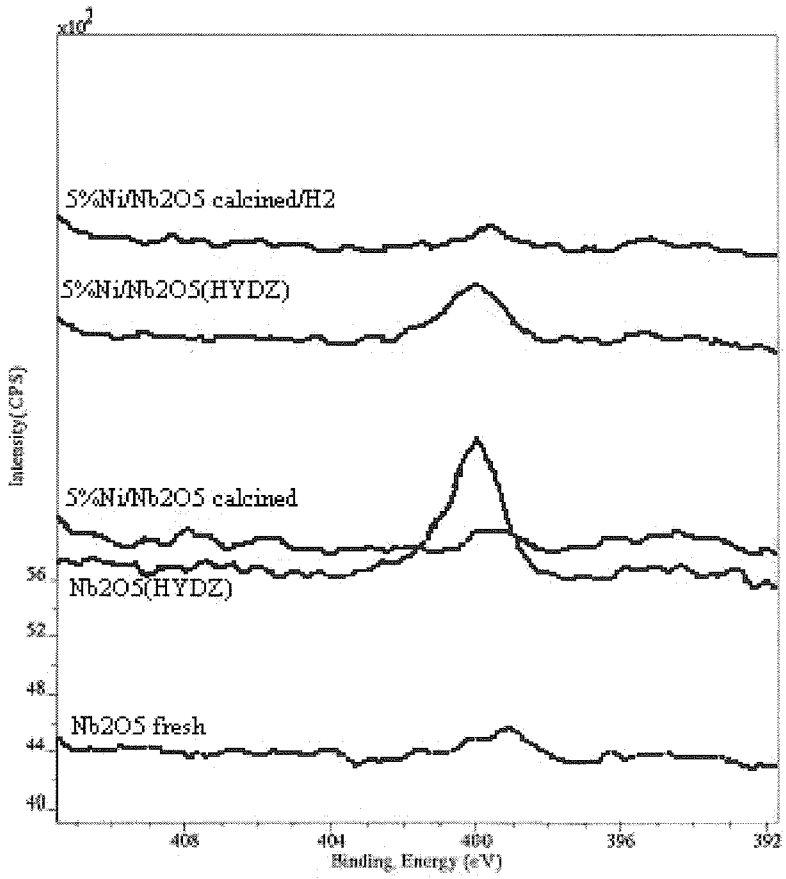

Figure IV-8. XPS spectra of the N 1s region.

2.2.4. FTIR measurements

IR bands in the skeletal region (Figure IV-9) for hydrated Nb_2O_5 and that detected for Ni-impregnated samples were compared. Because of the high acidity of the support one can expect the strong interaction of Nb_2O_5 with the nickel salt. In fact, acidic hydrated niobia oxide reacted chemically with Ni-acetate during the impregnation followed by calcination. IR bands in the skeletal region for hydrated Nb_2O_5 and that detected for Ni-impregnated samples were compared.

In case of both impregnated methods, the final materials exhibit well resolved bands in the 500-1000 cm^{-1} region not characteristic for the initial support. It indicates the chemical reaction between nickel species and niobia support leading to the change in the IR spectra.

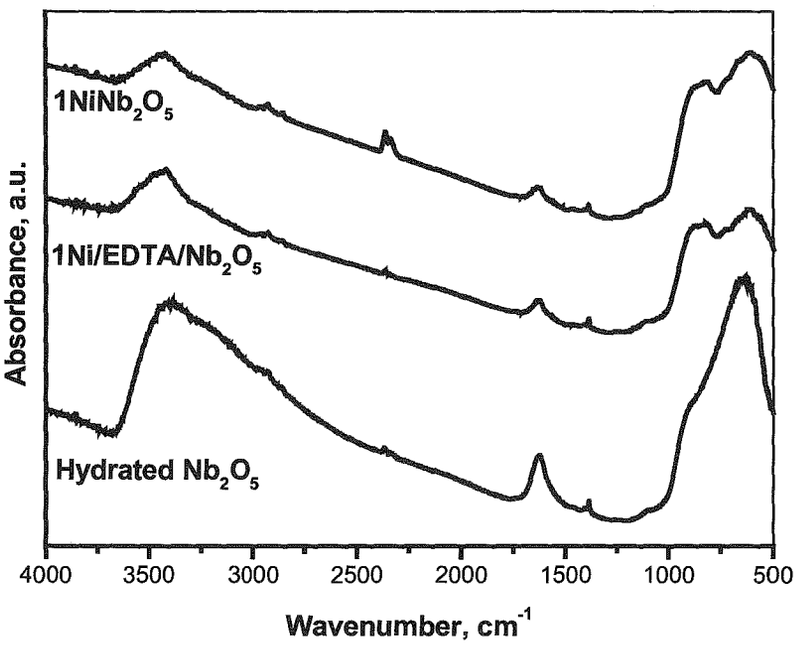

Figure IV-9. FTIR measurements of niobia catalysts.

2.2.5. Isopropanol decomposition

The acidity of the support plays a crucial role in the chemistry of the supported nickel catalysts [19]. The acidity of the hydrated niobia used as the support and the classical catalysts was estimated on the basis of isopropanol dehydration (Fig. IV-10). Dehydration towards propene formation as well as reaction producing diisopropyl ether occurs with the participation of acidic centers on the catalyst surface. For all catalysts tested, propene was the main reaction product, indicating acidity of the materials. Moreover, the high conversion of alcohol (>15%) confirmed the high acidity of the niobia oxide materials. Remarkably, in the presence of nickel, the conversion increased. Moreover, the results showed that the impregnation with EDTA salt decreases the acidity of the final material.

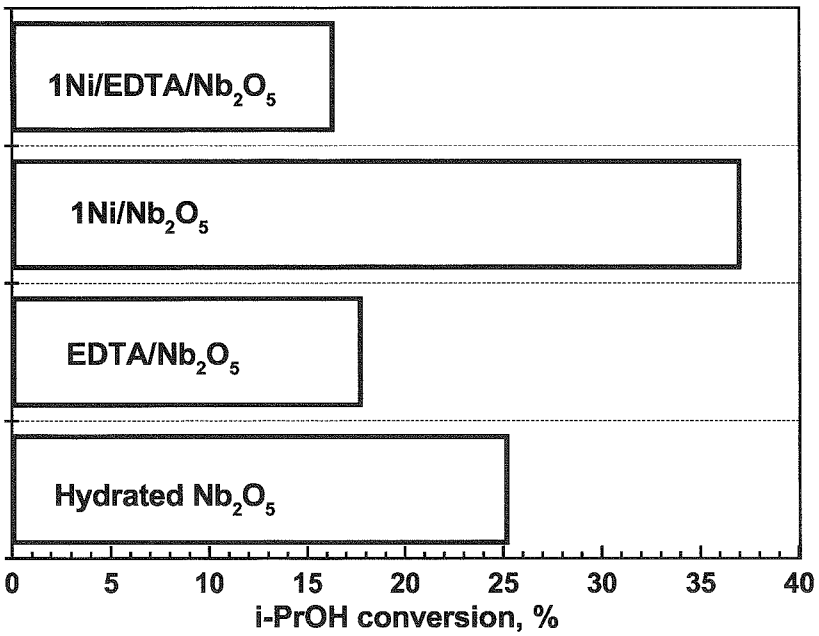

Figure IV-10. Isopropanol decomposition for niobia catalysts.

Because of the high acidity of the support one can expect the strong interaction of Nb_2O_5 with the nickel salt. In fact, acidic hydrated niobia oxide reacted chemically with Ni-acetate during the impregnation step followed by calcination. This was evidenced by IR spectroscopy measurements, as described above.

2.2.6. H_2-TPR study

Support

The pristine Nb_2O_5 support, previously calcined, is reduced under hydrogen flow (100 ppm/Ar) in programmed temperature as shown in Fig. IV-11. The main step of reduction occurs at 1023 K and is ascribed to the reduction of bulk niobium oxide, in a good agreement with the XRD and XPS studies presented above. A second peak is also observed from 523 K. It could be due to the reduction of NbOx superficial species. The reduction of the superficial oxide species could also account for the shoulder arising at

750 K. The partial reduction of the support could be confirmed also by the change of the sample color after TPR test from white to gray.

It is worth noting that the H_2-TPR of pure Nb_2O_5 calcined in air at 773 K for 5 h has been reported [20] and did not show any reduction peaks up to 773 K. This may originate from the oxide precursor which was supplied from another commercial source.

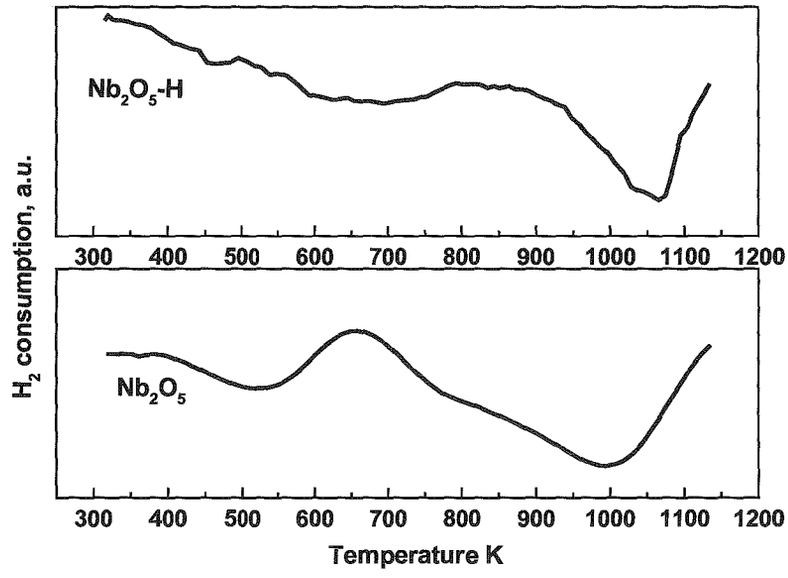

Figure IV-11. H_2-TPR profiles of Nb_2O_5 and Nb_2O_5-H.

The H_2-TPR profile of Nb_2O_5 somewhat changed after a treatment in aqueous hydrazine (Fig. IV-11). Pure Nb_2O_5 support, previously treated in aqueous hydrazine, consumed very small amount of hydrogen which gave rise to a peak at around 1050 K, ascribed to the reduction of bulk niobium oxide. In contrast, the peak at 523 K and a shoulder at 750 K were absent and, in addition, the oxide released gaseous nitrogen at 440 K (Fig. IV-12). In the basic aqueous media, the fresh oxide reacted with hydrazine and formed stable NH-surface species. These species were evidenced by the XPS study. They were decomposed by the heating under hydrogen during the TPR experiments. Superficial reduction of the support by hydrazine may explain the absence of the reduction peak at 523 K and the shoulder at 750 K. Bulk Nb_2O_5 was also partially reduced by the

hydrazine, explaining the low amounts of hydrogen consumed as compared to classical Nb_2O_5 behavior.

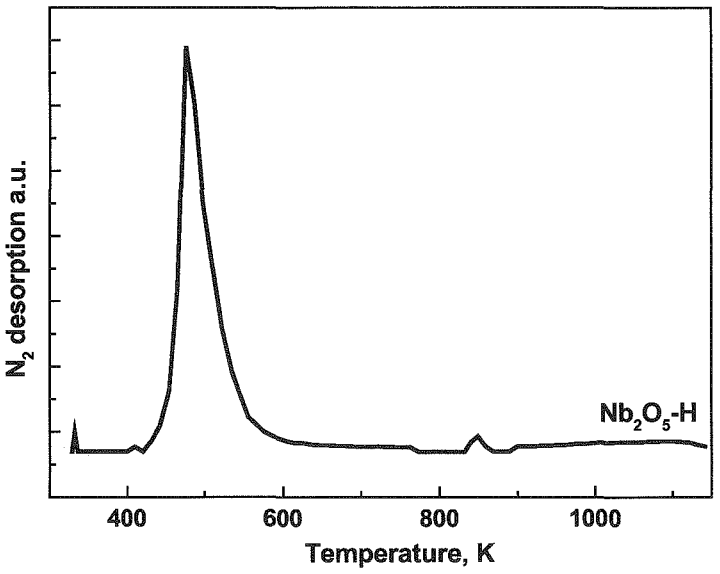

Figure IV-12. production of N_2 during H_2-TPR study on Nb_2O_5-H.

Classical catalysts

The TPR profiles of the calcined classical catalysts comprise two peaks (Fig. IV-13-15). The high temperature peak (900- 1050 K) may be ascribed to niobium reduction whereas the lower temperature peak (700 - 850 K) may be due to the reduction of nickel species strongly interacted with the support [20]. Very strong Ni-niobium oxide interactions are very well known [20-24]. It causes a mutual influence on the reduction of the two components. Recall that bulk NiO reduction under H_2 flow occurs from 500 K [25-26]. Thus for $1Ni/Nb_2O_5$ catalyst the temperature peak of reduction of is decreased to 963 K whereas that of NiO is as high as 790 K. However, this is not a case for the higher Ni content of 5 %: for $5Ni/Nb_2O_5$, the temperature peak of Nb_2O_5 reduction is not changed whereas that of NiO is lowered to 695 K.

These results reflect the various strengths of metal-support interactions in the catalysts. Let us first consider nickel reduction. At a low nickel loading, a great part of nickel atoms is in a close contact with the support, also the high temperature peak prevails for nickel reduction. In contrast, at a higher loading, a part of the Ni precursor

not directly or less attached to the support will probably more easily form NiO species, which are reduced at lower temperatures. If one considers the support, its temperature of reduction is lowered by the strong interaction with nickel in the presence of 1% metal loading. At the higher loading of 5% the weakness of metal-interaction does not change the reduction temperature of Nb_2O_5.

The H_2-TPR study of 2%-15%Ni/Nb_2O_5 catalysts was reported [20]. Examination of the profiles showed that the peak of reduction occurred at temperatures depending on the nickel loading. This was ascribed to the existence of strong-metal support interactions.

Note that the DIM preparation (Fig. IV-13) gives rise to a higher temperature of nickel reduction as compared to the SIM preparation.

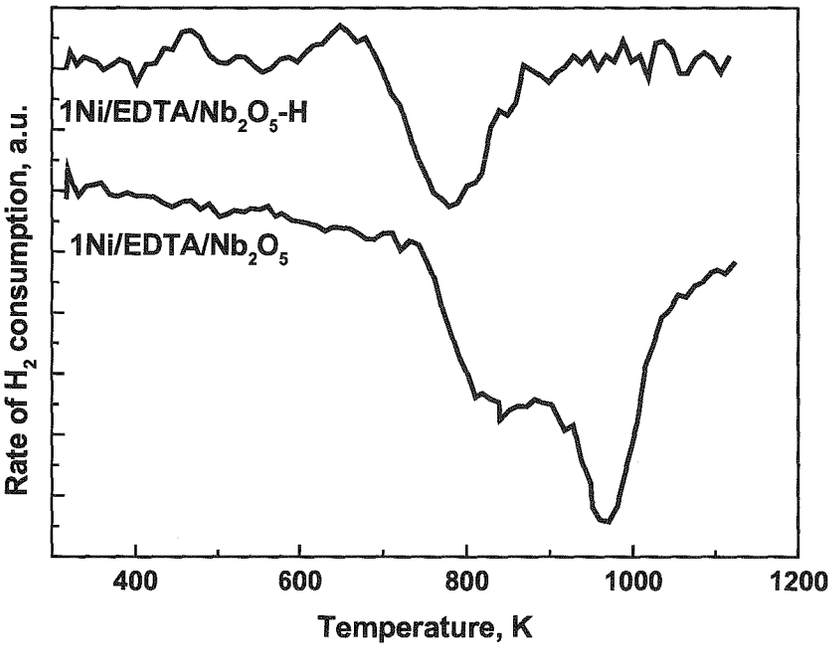

Figure IV-13. H_2-TPR profiles for 1% Ni DIM catalysts.

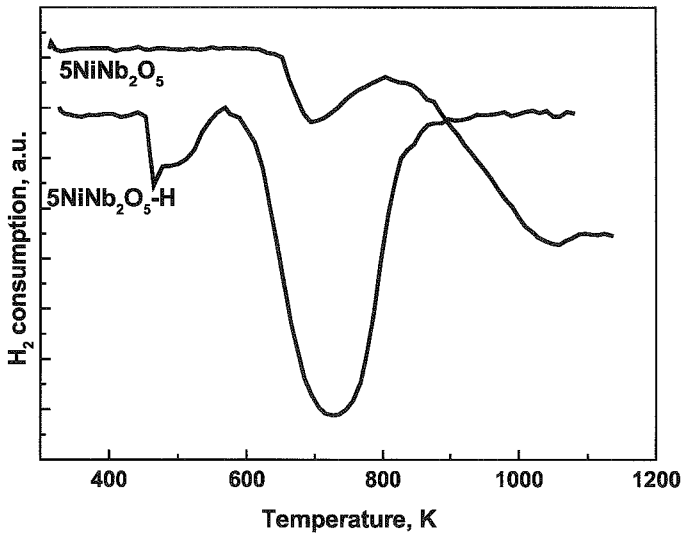

Figure IV-14. H_2-TPR profiles of 5% Ni catalysts.

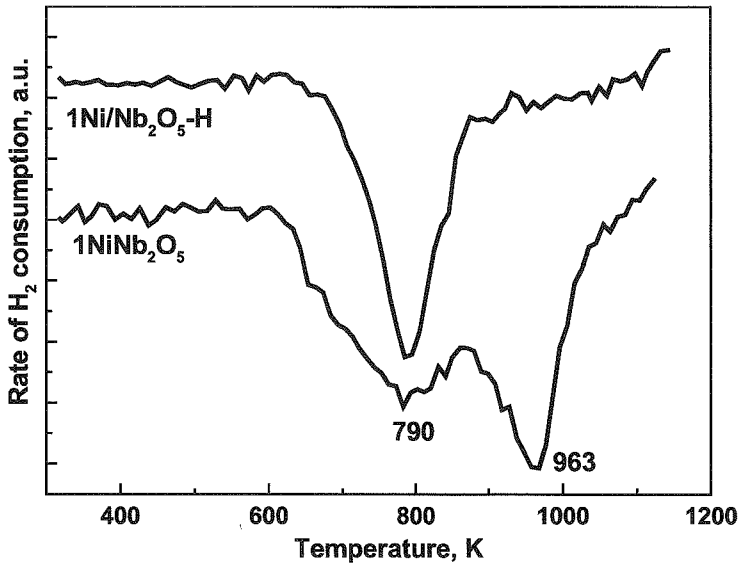

Figure IV-15. H_2-TPR profiles of the 1% Ni catalysts.

Non classical catalysts

The non classical catalysts exhibit H_2-TPR profiles due to presence of unreduced nickel species. These species may arise from an incomplete reduction of the supported Ni^{2+} ions by hydrazine [27] or from reoxidation of Ni° species due to moisture contamination.

The TPR profiles obtained differ from that of classical catalysts (Fig. IV-15). There is only a more or less well-defined peak with the maximum at 780-790 K (1wt.%Ni) or 723 K (5wt.%Ni) which originates from the reduction of nickel species. Stronger interactions are expected to occur in 1wt.%Ni catalyst. The small peak at 450 K in case of 5%Ni content can be attributed to isolated NiO particles more easily reduced. The partial reduction of this catalyst is attested by a change of the color from green to gray. The peak of support reduction is not observed in the temperature range examined. One may speculate it was reduced in the aqueous hydrazine media catalyzed by the nickel.

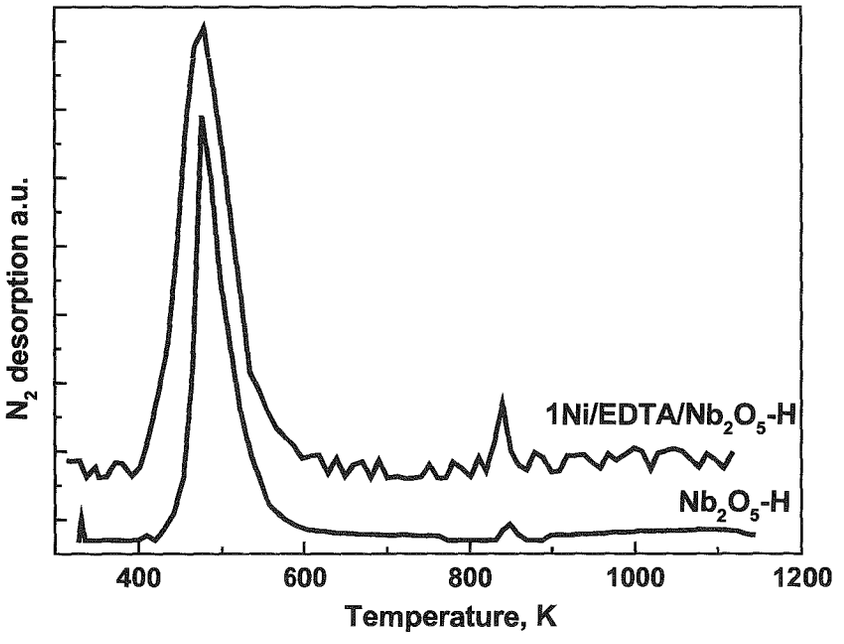

Figure IV-16. N_2 desorption during H_2-TPR.

The N_2 desorption, due to the decomposition of hydrazine species adsorbed on the surface, was observed for the catalyst with 1 wt.% Ni loading. This is shown in Fig. IV-16 for DIM catalysts. A main peak arises at 440 K (with a shoulder) and a smaller one at 830 K. These peaks are ascribed to different adsorption sites of hydrazine on the niobia support. N_2 desorption was not observed for $5Ni/Nb_2O_5$-H(b) catalyst. An excess of nickel ions prevented the reaction of hydrazine with the niobia support.

2.2.7. Degree of reduction

The amount of reduced nickel atoms was measured by oxygen adsorption at 723 K after a treatment under pure hydrogen for 2 h at 673 K. The obtained results are reported in Table IV-3.

It is known that the high temperature reduction of Nb_2O_5 with hydrogen gives the bluish-black dioxide NbO_2 that has a distorted rutile structure [4]. The presence of the NbO_2 phase with a rutile structure was well confirmed by the results of XPS and XRD studies. This reduction is reversible and the NbO_2 reoxidation gives rise to Nb_2O_5. Taking into account this reaction, the degree of reduction after H_2 treatment at 673 K was calculated as 54.4% for calcined Nb_2O_5 and 27% for Nb_2O_5-H treated with aqueous hydrazine (Table IV-3).

This reaction was also taken into account for the calculation of the reduction degree of the nickel-niobia catalysts, supposing the same degree of support reduction. This is an approximation since, in the presence of nickel, the reduction of Nb_2O_5 was facilitated according to the TPR study. The values obtained are in fact maximum degree of reduction. From Table IV-3 it can be seen that the degree of reduction changes with the nickel content and method of preparation.

Table IV-3. Degree of reduction for niobia catalysts.

catalyst	amounts of O_2 consumed $[mol*g_{cat}^{-1}]*10^{-5}$	degree of reduction calculated [%]
$1NiNb_2O_5$	24.28	78
$1Ni/EDTA/Nb_2O_5$	25.22	89
$5NiNb_2O_5$	70.11	123
Nb_2O_5	17.63	56
$1NiNb_2O_5$-H	17.59	87
$1Ni/EDTA/Nb_2O_5$-H	19.26	104
$5NiNb_2O_5$-H	44.02	79
$5NiNb_2O_5$-H(b)	47.29	89
Nb_2O_5-H	10.23	27

The classical $1Ni/EDTA/Nb_2O_5$ catalysts showed a higher degree of reduction than that of the SIM catalyst (89.3% against 78.2%). This is also the case of 1%Ni non classical catalysts (104% against 87%). One can suppose that EDTA ions could facilitate the reduction of nickel species formed on the surface when Nb_2O_5 support is applied. These results also show an improvement in nickel reduction for hydrazine treated catalysts.

Remarkably, $5NiNb_2O_5$ classical catalyst exhibits a degree of reduction (123%) which exceeds the stoichiometric ratio. This high maximum value may reflect excess reduction of niobium oxide (>56%) in the presence of nickel, not taken into account in our calculations. In contrast, for hydrazine treated materials, increasing nickel content to 5wt.% does not increase the degree of reduction, although the metal phase became more reducible according to the TPR study (Fig. IV-14). Recall that $5Ni/Nb_2O_5$-H(b) comes from a stepwise preparation method which included the intermediate formation of nickel species firmly attached to the support. These species were less prone to the reduction. The method of preparation influences on the interaction of the catalyst surface with hydrogen.

2.2.8. H_2 adsorption study

After a H_2 thermal treatment, both SIM and DIM classical as well as non classical catalysts did not adsorb hydrogen at room temperature. This is true for 1 or 5 wt.%Ni contents. It could be attributed to a very strong interaction of nickel particles with the matrix [4, 22]. As evidenced from the IR spectra, the nickel ions reacted with the niobium oxide providing the blockage of the hydrogen adsorption capacity of nickel.

Hydrogen adsorption on Nb_2O_5 supported nickel catalysts has been already reported for higher nickel contents (2%-15%) [20]. Very low surface areas (≤ 1 m^2 g^{-1}) were found after a reduction with hydrogen at the temperature of 673 K, i. e. nickel atoms are not easily accessible for hydrogen. SMSI would be responsible for the suppression of hydrogen adsorption. However, it was suggested that, during the reduction and cooling down the sample in flowing hydrogen, the nickel surface remained covered with hydrogen atoms [20, 22-23].

2.3. Catalytic activity in benzene hydrogenation

After a H_2 thermal treatment, the niobia supported catalysts are not active in the gas phase hydrogenation of benzene to cyclohexane. Only the classical 5%Ni exhibits some activity (1.1% of conversion at 448 K). The absence of activity is ascribed to strong metal-support interactions, which hide the access of nickel to the reactant molecules [25]. Nickel particles on the niobia surface did not present catalytic activity and are randomly distributed at the surface, and then the catalytic activity decay is expected to be of the same order of magnitude as surface coverage. Another reason of inactivity may reside in the mechanism of benzene hydrogenation. It is admitted that the support can furnish the adsorption sites for the aromatic molecule, in the form of carbonium ions, and in the vicinity of the metal particles, the adsorbed molecule can react with the spilt-over hydrogen from the metal [28-30]. In this work, niobium oxide is acidic and probably strongly adsorbs the benzene molecules and also may suppress the catalytic activity. It is worth noting that Ni/Nb_2O_5 catalysts were found active in hydrogenation of carbon monoxide [22-23]. In this case, the adsorption strength of CO on the support is much weaker than that of benzene and also CO could be more easily converted.

3. CONCLUSSIONS

The results obtained in this work confirmed that niobia is a typical SMSI oxide. The SMSI effect is manifested in the preparation of non classical catalysts. Indeed, in this case, it prevents the supported Ni^{2+} ions from the reduction by aqueous hydrazine for 1, 3 or 5wt.% Ni content. The prevention in nickel reduction is also observed when the support is pre-adsorbed with EDTA. Only when stepwise procedure is performed the reduction could proceed: superficial Ni^{2+} ions weakly attached are formed and reduced on a layer of nickel species strongly bonded to the support. In contrast, hydrazine reduced the support and formed stable surface N-H species.

The very strong interaction between niobia surface and metal active phase not always is favorable for the catalytic processes. The interaction of nickel with Nb_2O_5 caused a high suppression of nickel activity in the hydrogenation reaction. Moreover, it was shown that Ni supported on hydrated niobia was not active towards hydrogen.

It could be proposed that preferential deposition on nickel occurred on the niobia monolayer which is more difficult to reduce and which could favor the formation of nickel niobate compounds. The very strong nickel–niobia interaction could play a crucial role in the passivation phenomenon of nickel active sites.

4. REFERENCES

[1] K. Hayek, M. Fuchs, B. Klötzer, W. Reichl, G. Rupprechter, *Topics in Catal.* 13 (2000) 55

[2] S.J. Tauster, S.C. Fung, R.L. Garten, *J. Am. Chem. Soc.* 100 (1978) 170

[3] L. Filotti, A. Bensalem, F. Bozon Verduraz, G.A. Shafeev, V.V. Voronov *Appl. Surf. Sci.* 109/110 (1997) 249

[4] I. Nowak, M. Ziolek, *Chem. Rev.* 99 (1999) 3603

[5] C.H. Bartholomew, D.G. Mustard, *J. Catal.* 67 (1981) 186

[6] W.P. Halperin, *Rev. Mod. Phys.* 58 (1998) 533

[7] V.N. Colvin, M.C. Schlamp, A.P. Alivisatos, *Nature* 370 (1994) 354

[8] R.L. Whetten, *Acc. Chem. Res.* 32 (1999) 397

[9] W. Yu, H. Liu, X. Ma, Z. Liu, *J. Colloid. Interface Sci.* 208 (1998) 439

[10] K. Tanabe, *Catal. Today* 78 (2003) 65

[11] J.C. Védrine, G. Coudurier, A. Ouqour, P.G. Pries de Oliveira, J.C. Volta, *Catal. Today* 28 (1996) 3

[12] A.G. Boudjahem, S. Monteverdi, M. Mercy, M.M. Bettahar, *J. Catal.*, 221 (2004) 325

[13] Y.D. Li, L.Q. Li, H.W. Liao, H.R. Wang, *J. Mater.Chem.* 9 (1999) 2675

[14] M. Che, Z.X. Cheng, C. Louis, *J. Amer. Chem. Soc.* 117 (1995) 2008

[15] J.W. Coenen, *Preparation of catalysts II*; Poncelet G., Grange P., Jacobs P.A., Ed; Elsevier, Amsterdam, 1979; pp. 89-108.

[16] L. Bonneviot, M. Che, D. Olivier, G.A. Martin, E. Freud, *J. Phys. Chem.* 90 (1986) 2112

[17] JCPDS-*International Centre for Diffraction Data*, 1999

[18] La Surface Com-*XPS Data Base*

[19] A. Jasik, R. Wojcieszak, S. Monteverdi, M. Ziolek, M.M. Bettahar, *J. Mol.Catal. A:Chem.*, 242 (2005) 81

[20] K.V.R. Chary, K.S. Lakshmi, P.V. Ramana Rao, K.S. Rama Rao, M. Papadaki, *J. Mol. Catal. A:Chem.*, 223 (2004) 353

[21] A. Lewandowska, S. Monteverdi, M. Bettahar, M. Ziolek, *J.Mol. Catal. A:Chemical* 3713 (2002) 1

[22] E.I. Ko, J.M. Hupp, F.H. Rogan, N.J. Wagner, *J. Catal.* 84 (1983) 85

[23] E.I. Ko, J.M. Hupp, N.J. Wagner, *J. Catal.* 86 (1984) 315

[24] T. Fung, *J. Am. Chem. Soc.* 100 (1978) 170

[25] J. Estellé, P. Salagre, Y. Casteros, M. Serra, F. Medina, J.E. Sueiras, *Solid State Ionics* 156 (2003) 233

[26] R. Wojcieszak, S. Monteverdi, M. Mercy, I. Nowak, M. Ziolek, M.M. Bettahar *Appl. Catal. A : General* 268 (2004) 241

[27] A. Boudjahem, S. Monteverdi, M. Mercy, M.M. Bettahar, *Langmuir*, 20 (2004) 208

[28] F. Benseradj, F. Sadi, M. Chater, *Appl. Catal. A*, 228 (2002) 135

[29] S.D. Lin, M.A. Vannice, *J. Catal.* 143 (1993) 539

[30] S.D. Lin, M.A. Vannice, *J. Catal.* 143 (1993) 554

CHAPTER V
NICKEL CATALYSTS SUPPORTED ON REDUCIBLE OXIDES-CeO_2

INTRODUCTION

L'oxyde réductible CeO_2 est jaune, stable, avec une structure cubique de type fluorine. C'est un non–stoechiométrique qui se transforme réversiblement de Ce^{IV}, en atmosphère oxydante, en Ce^{III} (Ce_2O_3), en atmosphère réductrice. Il est isolant sous forme CeO_2 et conducteur sous forme CeO_{2-x}. La non-stochiométrie apparaît au-delà de 620 K sous flux d'hydrogène. Les lacunes d'oxygène sont responsables de la conductivité ionique. La mobilité superficielle de l'oxygène dans ce matériau en fait un bon réservoir d'oxygène qui catalyse la combustion du carbone et résiste au cokage.

Les catalyseurs métalliques supportés sur oxyde de cérium ont été beaucoup étudiés. Les métaux de transition accroissent les propriétés redox de cet oxyde. L'effet bénéfique mutuel entre CeO_2 et le nickel a été mise en évidence, notamment en catalyse d'hydrogénation. Le phénomène du « spillover » d'hydrogène y a été démontré.

Nous avons étudié une série de catalyseurs Ni/CeO_2, préparés par la méthode de l'hydrazine avec une composition en nickel de 1%, 3% et 5%. La réaction test est l'hydrogénation du benzène.

1. INTRODUCTION

Cerium (IV) oxide is a stable yellow oxide with a cubic fluorite structure. It has been extensively studied because of its interesting redox and high dispersive properties [1]. CeO_2 is able to change reversibly from Ce^{IV}, under oxidizing conditions, to Ce^{III} (giving Ce_2O_3), under reducing conditions. Oxygen atoms in CeO_2 units are very mobile and leave easily the ceria lattice, giving rise to a large variety of non-stoichiometric oxides with two limiting cases, CeO_2 and Ce_2O_3. These non stoichiometric oxides can be produced by reduction at temperatures much higher than ambient ($\geq$ 620 K) in hydrogen [1]. The oxygen vacancies are responsible for the ionic conductivity of the ceria. Ceria has an insulator behavior in the stoichiometric oxidized state CeO_2 and becomes conductor in the reduced state CeO_{2-x}, acquiring a great capacity to store and to carry oxygen.

Cerium oxide is used as a catalyst in a wide variety of reactions involving the total oxidation or partial oxidation of hydrocarbons [2-3]. It is well known that the ceria can act as a local source or sink for oxygen involved in reactions taking place on the ceria surface or on other catalytic materials supported on ceria [2].Ceria is also noted for its ability to resist to carbon deposition and to catalyze the combustion of carbon [4].

Cerium-based catalysts containing transition metals have attracted increasingly attention in recent years due to their high oxygen storage capability [5-12]. Various studies have shown that the redox properties can be considerably enhanced if additional elements are introduced into the CeO_2 lattice [7, 12-20]. Because 4f orbitals give them a surplus of atomic electron valence, rare earth elements can be used to promote the activity and stability of metal catalysts [14]. Some authors concluded that the modification of the cerium oxide with noble metals considerably decreases the reduction temperature and it was postulated that hydrogen atoms formed by dissociative adsorption on the noble metals were spilled over CeO_2 oxide [21-22]. The beneficial association between species based on nickel and cerium both in oxidized and reduced states have been evidenced [13-14]. CeO_2–NiO catalysts have been studied in many hydrogenation reactions [14-17] by taking the advantage of their redox property. The spillover phenomenon was also postulated for the NiO supported ceria catalysts [23-24].

In this study, the nickel supported on CeO_2 oxide catalysts were prepared by the chemical reduction with hydrazine as described in the Experimental section. The catalysts prepared are listed in Table V-1.

Table V-1. Catalysts preparation.

Catalyst	wt.% of Ni
$1NiCeO_2$-H	1.00
$3NiCeO_2$-H	3.00
$5NiCeO_2$-H	5.00
CeO_2	-
CeO_2-H	-

2. RESULTS AND DISCUSSION

2.1. Reduction of Ni^{2+} supported on CeO_2

In contrast with hydrazine reduction of the Nb_2O_5 nickel supported catalysts, that of the catalysts supported on CeO_2 occurred very easily. The base and redox properties of CeO_2 enhance the reducibility of nickel [1]. After hydrazine addition, the impregnated solid changed color from green to blue, indicating the formation of nickel complex $[Ni(N_2H_4)_3]^{2+}$. This complex readily turned next to black, indicating that the reduction of nickel ions occurred.

2.2. Characterization of the catalysts

2.2.1. XRD study

XRD patterns of the cerium oxide are given in Figure V-1. The spectra show well crystallized CeO_2 oxide with the fluorite structure. Moreover the hydrazine reduction does not change the structure of the oxide.

Fig. V-2 shows the XRD patterns of the nickel catalysts supported on CeO_2 after hydrazine reduction. The presence of the reflects originated from the support confirmed that the fluorite structure of the CeO_2 is well preserved. The reduction of cerium oxide was not observed. However, it is known that hydrazine can reduce the cerium [1]. The absence of the additional diffraction signal was explained by the low extent of the reduction of ceria which takes place in a thin surface layer of the sample [1].

XRD study confirmed the reduction of nickel ions. All nickel catalysts showed one large reflect at 44.56° which corresponds well to the metallic nickel with *fcc* structure [25]. Intensity of this reflect increases with increasing the nickel content in the sample. Using the Scherrer formula the average size of nickel particles could be calculated. The results are given in Table V-2.

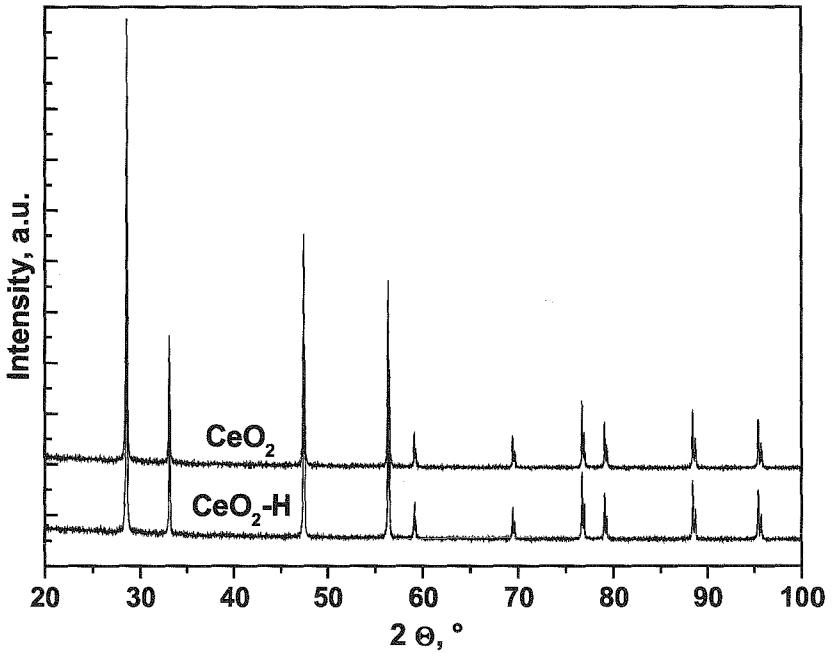

Figure V-1. XRD patterns of the CeO_2 and CeO_2-H oxides.

Table V-2. XRD study.

Catalyst	Diffraction reflect [°]	Particle size [nm]
1NiCeO$_2$-H	44.535	26.3
3NiCeO$_2$-H	44.535	42.1
5NiCeO$_2$-H	44.535	37.2

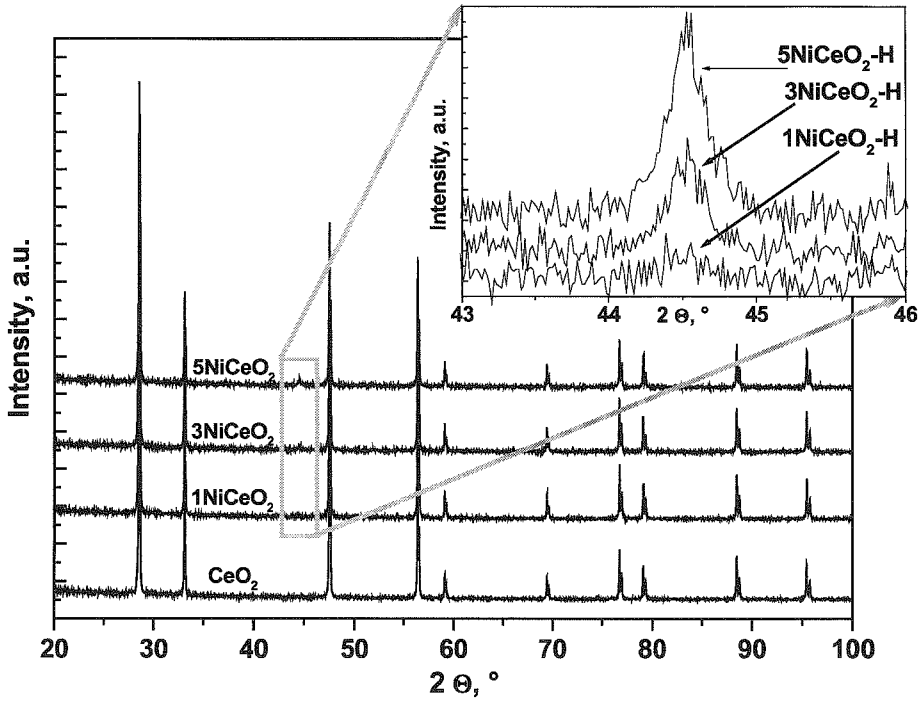

Figure V-2. XRD patterns of the nickel supported catalysts after hydrazine reduction.

The lowest particle size was obtained for $1NiCeO_2$-H material (26 nm) as compared to the $3NiCeO_2$-H (42 nm) and $5NiCeO_2$-H (37 nm) catalysts. This could be explained by the dispersion of nickel particles on the surface. Lower nickel content allows to obtain the higher dispersion of the nickel active phase.

2.2.2. TEM and STEM studies

The TEM study was carried out on the $1NiCeO_2$-H catalyst. TEM and STEM images have been taken. Moreover, the EDS and X-mapping analysis have been done. The results are given in the Fig. V-3–V-9.

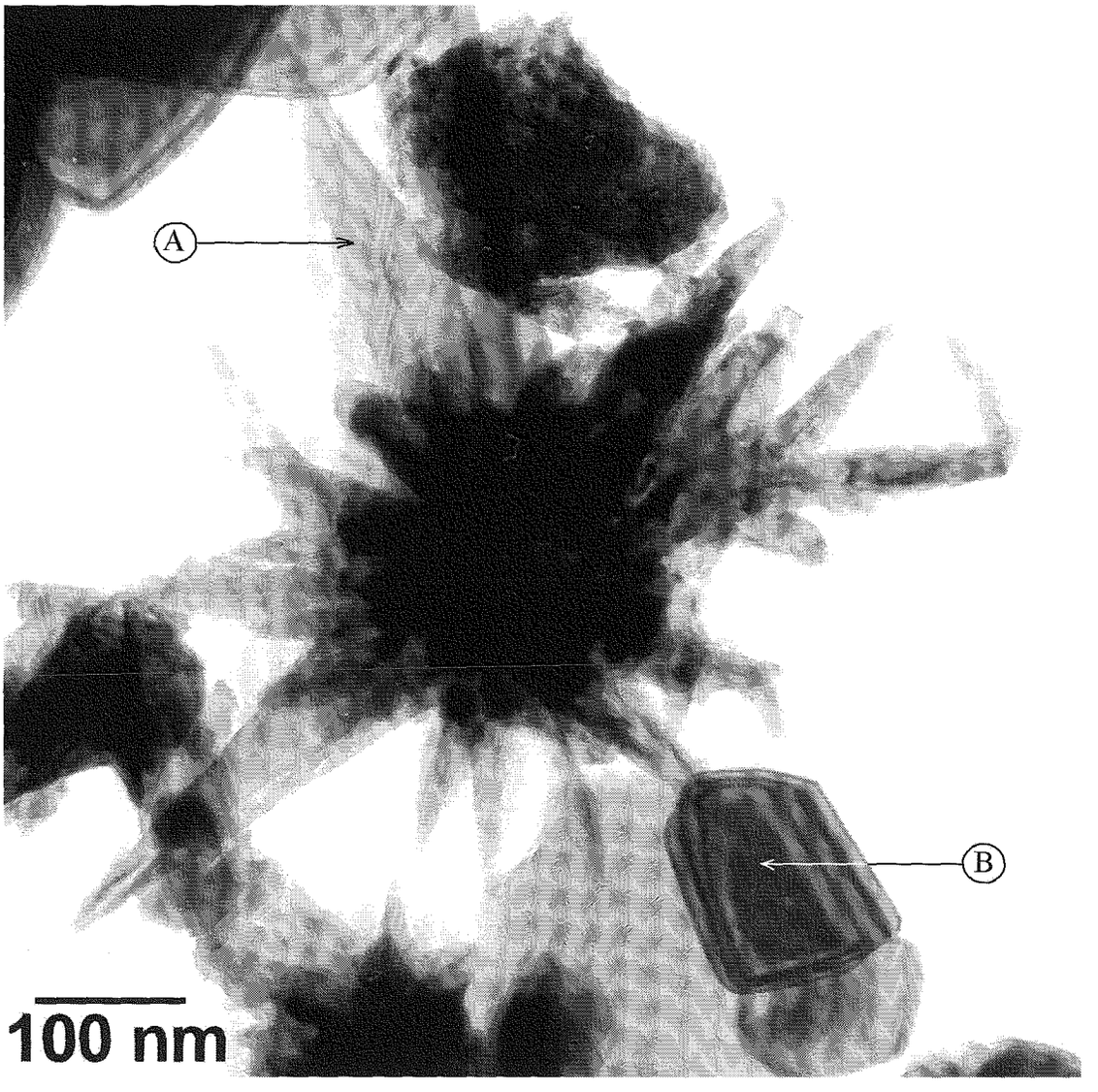

Figure V-3. TEM image of the 1NiCeO$_2$-H catalyst.

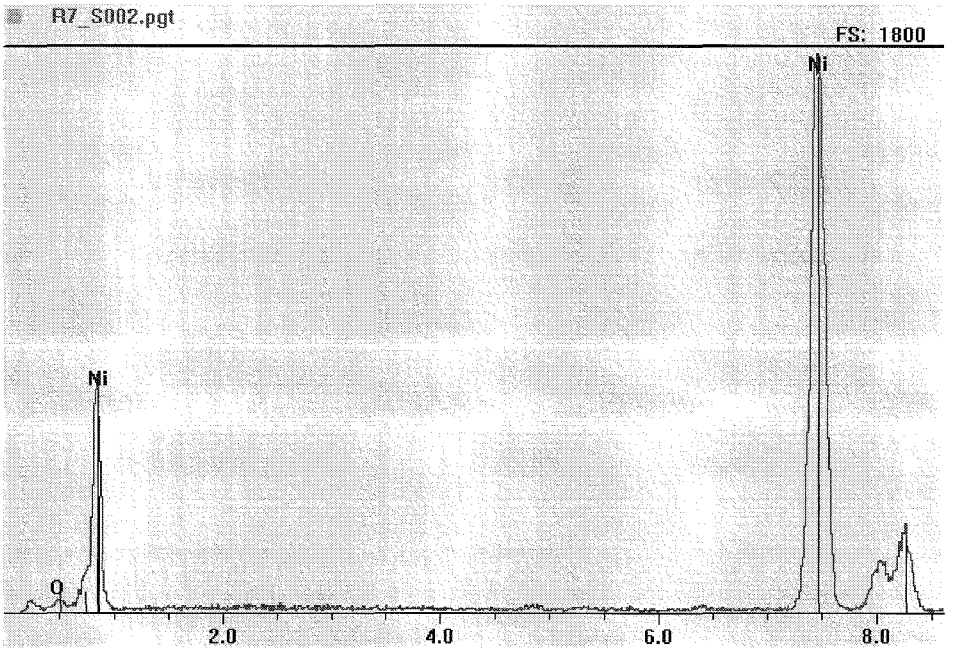

Figure V-4. EDS analysis of the A region.

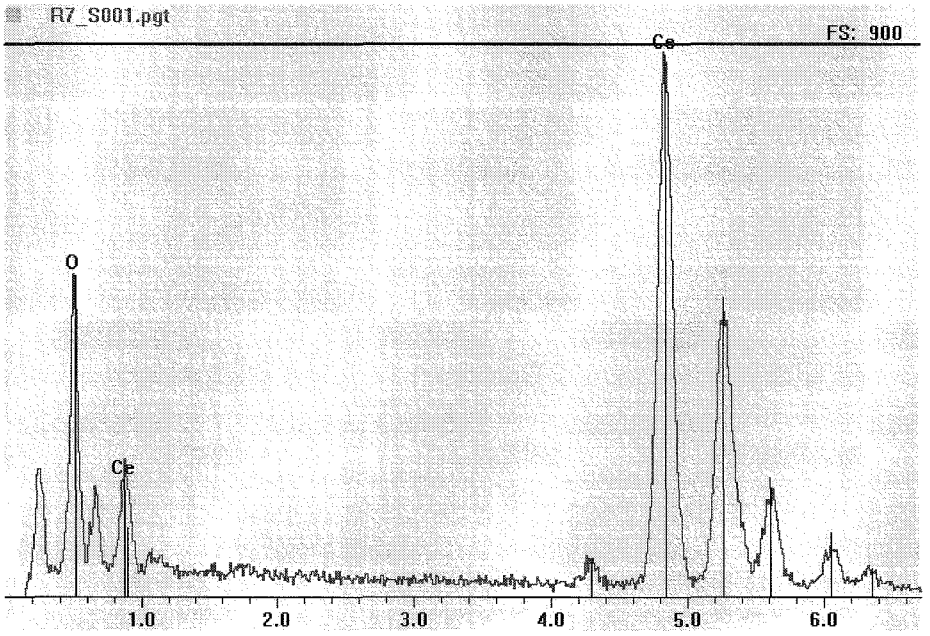

Figure V-5. EDS analysis of the B region.

TEM study showed that nickel on the cerium oxide surface exists in two different forms. The spherical very small particles detected by X mapping analysis (Fig. V-7) and bigger star-like nickel structures as shown on the Figure V-3. The presence of these nickel structures is very interesting and not yet presented in the literature for the nickel supported on CeO_2 support. The EDS analysis confirmed high degree of reduction of these nickel structure (Figure V-4): no NiO species were detected. X mapping analysis also shows that O species (Fig. V-9) come from CeO_2 (Fig. V-8) and not from NiO (Fig. V-7). These images also confirmed that, after reduction by hydrazine then washing and drying, the nickel stay in reduced form.

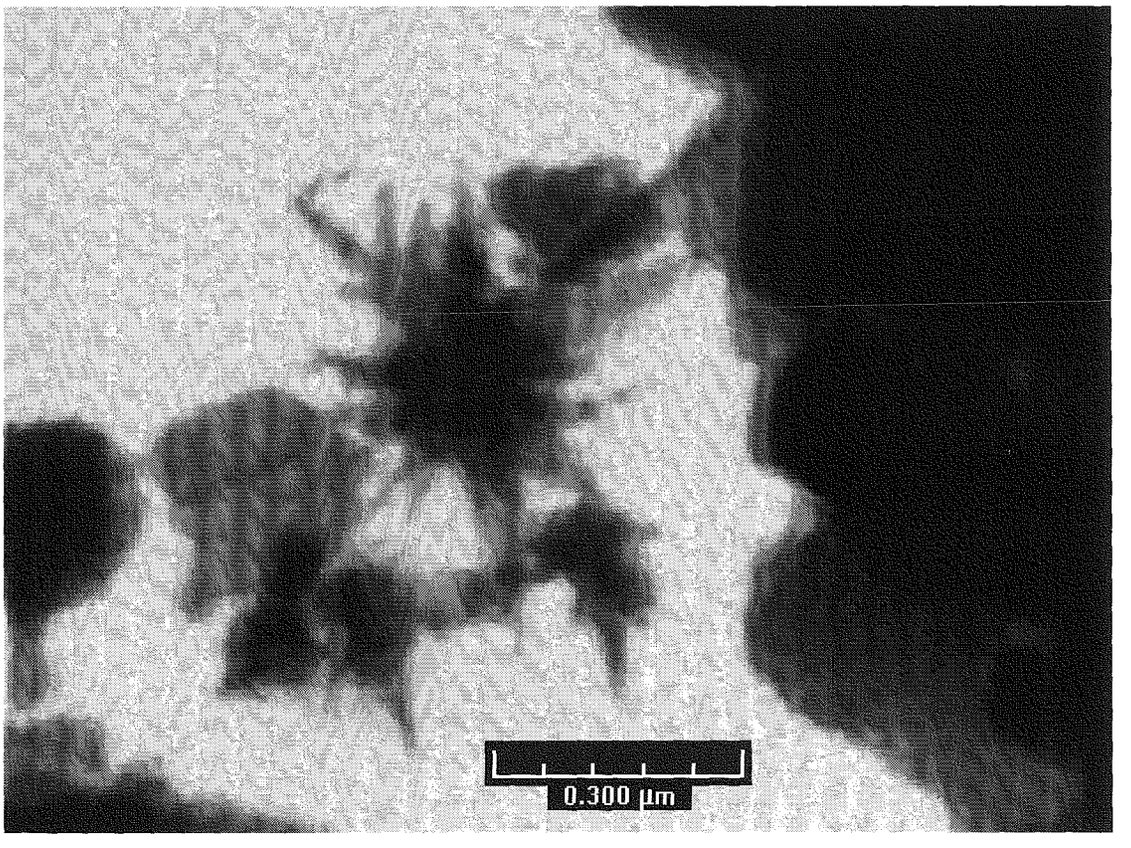

Figure V-6. STEM image of the 1NiCeO$_2$-H catalyst.

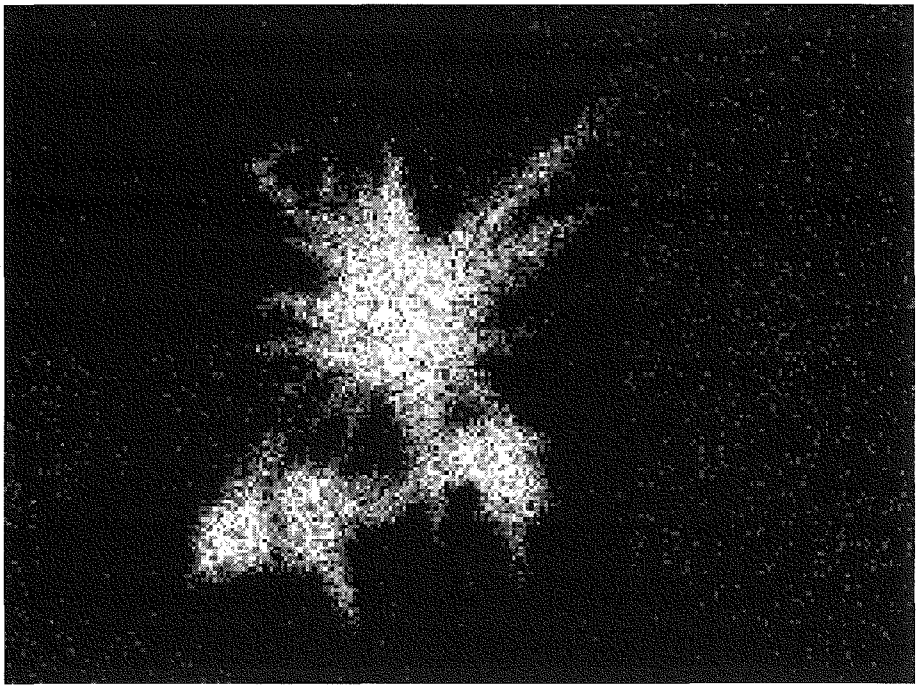

Figure V-7. X – mapping analysis–NiKA.

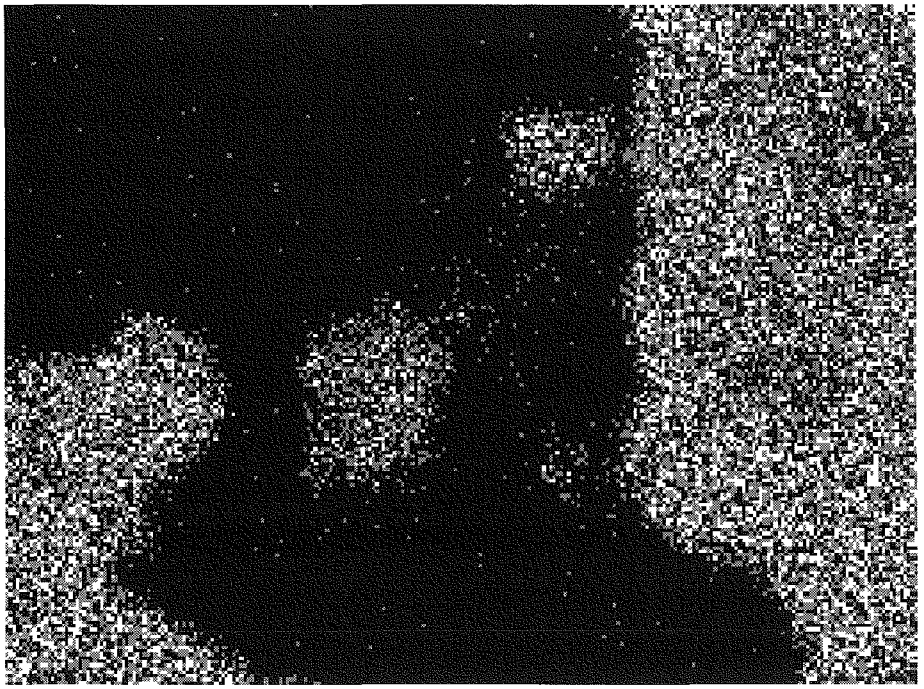

Figure V-8. X – mapping analysis–CeLA.

Figure V-9. X- mapping analysis-OKA

STEM image is shown in Fig. V-6. It also shows the nickel star-like structures with a size of 0.45 μm.

The EDS analysis has permitted to identify the chemical constitution of the cerium oxide. It confirmed the CeO_2 chemical structure of the support. It is in good accordance with the XRD study which showed the rutile structure of the cerium oxide. The reduction of CeO_2 by hydrazine may occur but in the superficial region not detectable by the EDS or XRD techniques.

2.2.3. H_2–TPR study

The H_2-TPR studies on the samples were carried out after hydrazine reduction. The results are given in Fig. V-10 and V-11.

H_2-TPR profile of the CeO_2 oxide (Fig. V-10) showed two high temperature peaks at 832 K and 1019 K. These peaks originated from the reduction of CeO_2 into Ce_2O_3. The reduction occurs first at the surface (oxygen atoms in a tetrahedral coordination site, bonded to one atom of Ce^{4+}) [5-6, 13], then progressively in the bulk. Thus the lower temperature peak is assigned to the easily reducible surface oxygen, while the high temperature peak results from the removal of the bulk oxygen [5-6, 13].

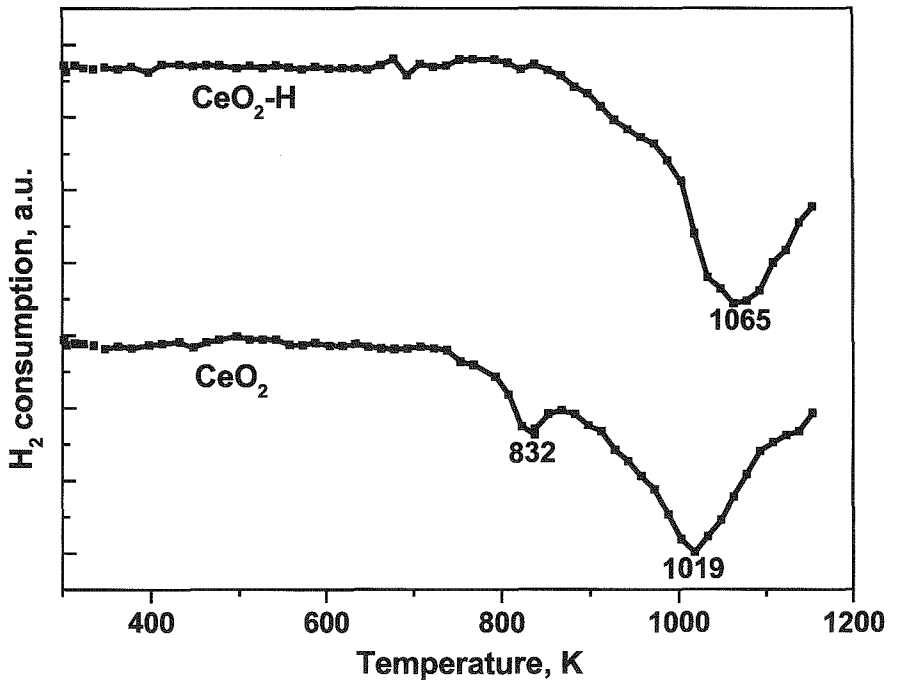

Figure V-10. TPR profiles of the CeO_2 and CeO_2-H.

The TPR profile of the CeO_2-H sample treated with hydrazine differs from that of the CeO_2 material. The profile showed only one high temperature peak at 1065 K whereas the peak at 832 K characteristic for the non-treated oxide is not present. The temperature peak at 1065 K for CeO_2-H sample corresponds well to the high temperature peak at 1019 K observed for the CeO_2 sample. However, it is shifted to higher temperature, which could be explained by the larger fraction of reduction of the bulk by the hydrazine. As to the absence of the low temperature peak around 830 K, it could also be explained by the partial reduction of reducible surface oxygen by the hydrazine during the treatment.

Fig. V-11 shows the TPR profiles of the nickel supported catalyst. The profiles exhibit two peaks, the one at 453 K and the other above 1100 K. These peaks correspond to the presence of unreduced nickel species. These species may arise from an incomplete reduction of the supported Ni^{2+} ions by the hydrazine [27-28] or from

reoxidation of Ni° species due to moisture contamination. This can be set out from other observations.

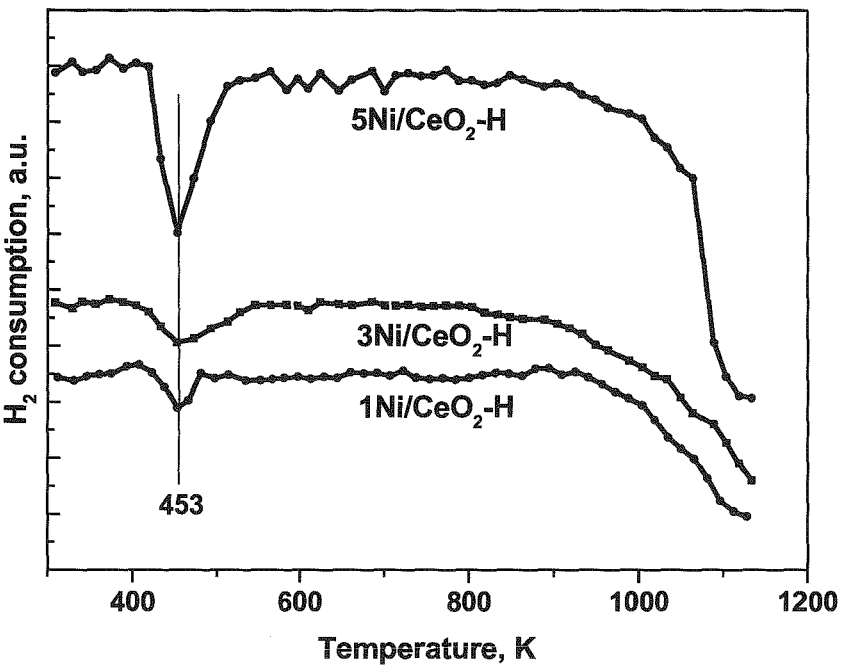

Figure V-11. H_2-TPR profiles of the nickel supported on CeO_2-H catalysts.

The very low temperature peak at 453 K may be due to isolated surface Ni^{2+} ions. The peak observed could be explained by the XRD study. Indeed, this study confirmed that the nickel is reduced after the hydrazine treatment. In addition, the presence of the nickel oxide on the XRD patterns was not detected. It can be supposed that, after hydrazine reduction, nickel particles could be reoxidized by oxygen from air during the filtration and drying (see Experimental section). This oxidation is superficial and reversible. This could explain the very low temperature of the reduction of these particles in TPR. The small quantities of hydrogen consumed (3%- 7%) as shown in Table V-3, confirms superficial oxidation. Moreover, although the intensity of this peak increases with increasing nickel content in the catalyst, strikingly, there is no decrease

in the temperature of reduction with increasing nickel content. Such a decrease in temperature is expected as a result of decreasing metal-support interactions [29]. This settles the assumption of the existence of nickel oxide surface species due to moisture contamination. In addition, the peak of reduction of these species appears at the lower temperature as compared to classically prepared catalysts [26, 30-31].

Table V-3. Hydrogen consumption during H_2-TPR study.

Catalyst	H_2 *10^{-5} consumption [mol*min^{-1}*g_{cat}^{-1}]	% of Ni [%]
1NiCeO$_2$-H	**0.94**	**5.5**
3NiCeO$_2$-H	**1.71**	**3.4**
5NiCeO$_2$-H	**5.72**	**6.7**

The second large peak above 1100 K originates from the reduction of the support. This peak well corresponds to the high temperature peak (1065 K) observed for the CeO_2-H sample. However, it is shifted to higher temperature which could be explained by the larger fraction of reduction of the bulk oxygen as compared to the support alone: the reduction of the least reductible CeO_2 species is promoted. The promoter role of the nickel could play the crucial role in these reduction processes.

2.2.4. Degree of reduction

The cerium support showed some reduction at 573 K. However, the reduction is negligible as compared to the nickel content. The results (shown in Table V-4) are in good accordance with the H_2-TPR study which showed that the reduction of cerium support occurs at high temperatures (Figure V-10). Compared to the fresh sample, the cerium oxide treated with hydrazine at 353 K showed a little higher degree of reduction (2.6 against 3.2%). It could be concluded that the hydrazine treatment provide the some

reduction of the ceria surface. Indeed, it was shown that the hydrazine reduced ceria oxide but reduction occurred only in the thin layers on the oxide surface [1]. Moreover, the TPR study showed absence of the reduction peak at 832 K observed for the fresh oxide.

Table V-4. Degree of reduction of the support and supported catalysts.

Catalyst	O_2 *10^{-5} consumption [mol*min^{-1}*g_{cat}^{-1}]	Degree of Reduction [%]
1NiCeO$_2$-H	7.36	86.8
3NiCeO$_2$-H	23.3	91.3
5NiCeO$_2$-H	39.3	92.5
CeO$_2$	0.78	2.6
CeO$_2$-H	0.97	3.2

The degree of reduction for nickel supported CeO_2 catalysts is high (86.8%-92.5%). It increases a little with increasing the Ni loading from 1% to 3% then almost not changes for 5%.

2.2.5. H_2-adsorption study

The chemisorption behavior of the supports (CeO_2 and CeO_2-H) was studied under the same condition as the nickel supported CeO_2 catalysts.

The chemisorption study at room temperature showed that, whatever the state is (treated or not with hydrazine), support did not adsorb the hydrogen. The quantities of the hydrogen adsorbed by the nickel catalysts (Table V-5) allow to calculate the dispersion and average size of the nickel particles. The results are given in Table V-5.

Table V-5. Characteristics of the catalysts.

Catalyst	H_2 adsorbed [mol*g_{cat}^{-1}]*10^{-5}	H_2 desorbed [mol*g_{cat}^{-1}]*10^{-5}	Dispersion [%]	Particle Size[a] [nm]	Particle Size[b] [nm]
1NiCeO$_2$-H	**0.36**	**0.41**	**4.2**	**23.5**	**26.3**
3NiCeO$_2$-H	**0.63**	**0.58**	**2.4**	**41.0**	**42.1**
5NiCeO$_2$-H	**1.06**	**0.87**	**2.5**	**40.1**	**37.2**
CeO$_2$	-	-	-	-	-
CeO$_2$-H	-	-	-	-	-

[a]from the H_2-adsorption
[b]from the XRD study

The highest dispersion was found for the catalyst with 1% wt. content. It was nearly two times higher than that for the catalysts with higher nickel loading (4.2% against 2.4%). It is very well known that metal loading influences the metal dispersion on the support. More metal ions present during the impregnation gives rise to particle size growth. The impregnation is one of the size determining step in preparation of nickel catalysts supported on oxides.

The particle size calculated from the H_2 adsorption data correspond well to the average particle size calculated from the XRD study using the Scherrer formula (Table V-5). The lowest average size of nickel particle was found for 1NiCeO$_2$-H catalyst (23.5 nm) while nearly the same values of 40 nm were found for catalysts with higher nickel loading.

2.2.6. H_2-TPD study

The H_2-TPD study (Figure V-12) permits to designate different species of nickel active phase. Desorption of hydrogen depends on the interaction between the hydrogen molecule and nickel active phase.

Temperature of desorption could give the information about the hydrogen-nickel strength. The TPD profile of the 3NiCeO$_2$-H catalyst showed two main domains of

desorption in low (658 K) and high (868 K) temperature ranges respectively. The first peak of desorption could be attributed to the hydrogen weakly adsorbed on the nickel surface and the second peak with the maximum of desorption originates from the desorption of hydrogen strongly adsorbed on nickel surface. Remarkably, the desorption starts at a relatively high temperature, around 575 K.

The TPD profile of the catalyst with 1 wt.% of nickel showed only one large domain of desorption at higher temperature range with the maximum of desorption at 868 K. This peak corresponds to the nickel strongly adsorbed on the nickel surface. It is also present on the TPD profile of the $3NiCeO_2$-H catalyst (Figure V-12). The starting desorption temperature is remarkably much lower (450 K) for 1%Ni catalyst.

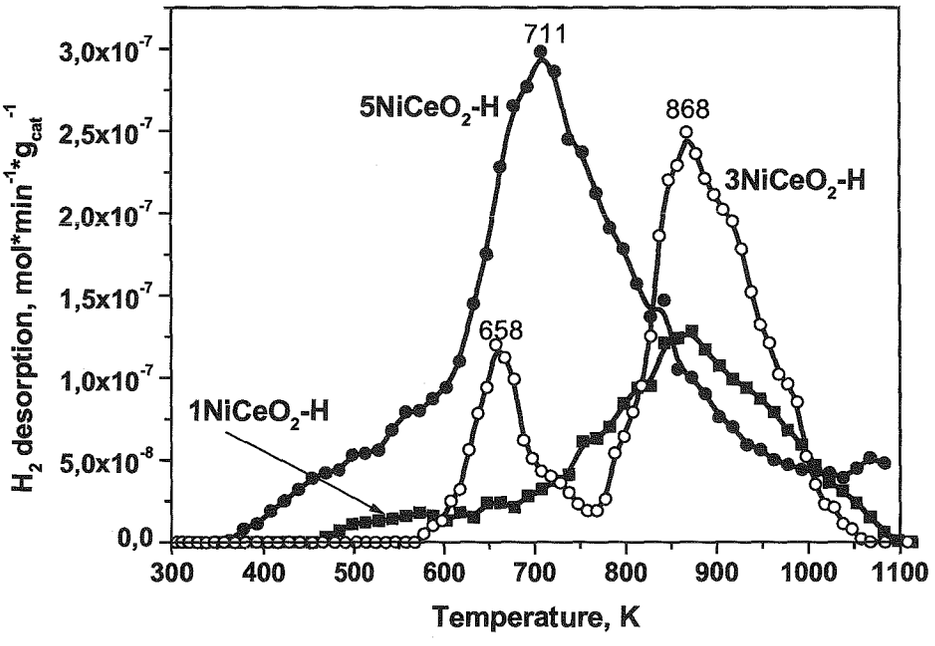

Figure V-12. TPD-H_2 profiles of the supported nickel catalysts.

The TPD profile of the $5NiCeO_2$-H catalyst differs from that of the catalysts with lower nickel loading. There is only one very large desorption peak with the maximum of desorption at 711 K. This peak comprises several shoulders, the one may

correspond to the low temperature peak (658 K) of 3%Ni catalyst. In addition, this peak starts from almost room temperature.

The TPD results also showed that the quantities of the hydrogen desorbed are similar or lower than the quantities of the hydrogen adsorbed at room temperature. It could be supposed that the hydrogen was adsorbed only on the nickel surface.

2.3. Catalytic activity

The nickel catalyst supported on CeO_2 are claimed to be active in the gas phase hydrogenation of benzene. Indeed, all nickel catalysts studied showed catalytic activity in the temperature range 348-498 K. The support was inactive in this reaction. The results are given in Table V-6 and Fig. V-13.

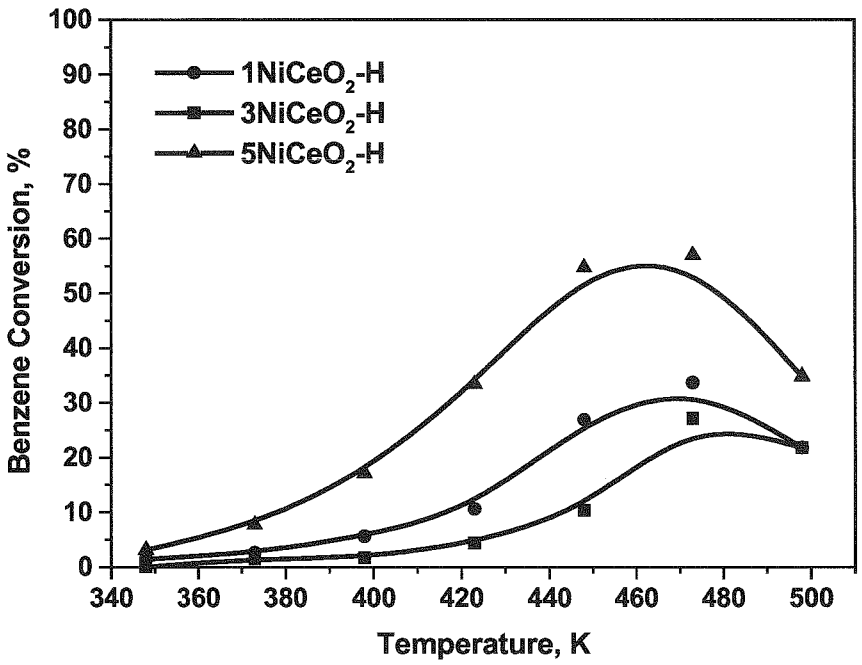

Figure V-13. Catalytic activity for $NiCeO_2$ catalysts.

The maximum activity was reached around 440-480 K. This maximum is always observed in aromatic hydrogenation over group VIII metal catalysts. The existence of a maximum of activity may have several causes. It has been ascribed to a decrease in the surface coverage by the aromatic with increasing temperature which, at some point, results in a decrease in the reaction probability. However, the observed maximum could also be accounted for by the competitive adsorption of the benzene and hydrogen reactant molecules.

The temperature of the maximum activity is almost the same with 1%Ni and 5%Ni catalysts (around 460 K) and higher for 3%Ni catalyst (around 480 K).

Table V-6. TOF's for $NiCeO_2$ catalysts.

Catalyst	Benzene conversion at 373 K [%]	TOF at 373 K [molecBz*s^{-1}*$site^{-1}$]
1$NiCeO_2$-H	**1.9**	**0.010**
3$NiCeO_2$-H	**2.5**	**0.004**
5$NiCeO_2$-H	**7.5**	**0.011**

The highest conversion was obtained for the catalyst with 5% wt. of nickel. Conversion of benzene for this catalyst reached 57% at 473 K (Fig. V-13). However, the catalytic activity passes through a minimum for 3% Ni content (conversion of 27 % at the same temperature). TOF at 373 K is also minimum for 3%Ni (0.004 s^{-1}) whereas that of 1 and 5%Ni are similar (0.010 s^{-1}) (Table V-6). It is worth to note that the results obtained at 373 K (0.004-0.011 s^{-1}) are in fair agreement with that reported values obtained at 353 K over classical nickel catalysts supported on different oxides (0.005-0.025 s^{-1}) [32].

The benzene hydrogenation reaction has been recently used as a tool for estimating the percentage of metal exposed on low loaded ceria supported rhodium catalysts [33], because of the structure insensitive character of this reaction for that

catalysts. Thus the catalytic activity in this reaction will only depend on the number of metal atoms available at the surface of the catalyst [34].

There is not a complete agreement about the origin of the metal ceria interaction produced after high temperature reduction. Two effects of SMSI have been invoked, namely the decoration of the metal particles by cerium suboxides patches and formation of metal–cerium alloys [33]. These effects would not affect the structure intensivity of the benzene hydrogenation reaction. However, they can modify the intrinsic activity of the catalysts.

The particle size (Table V-5) seems to not play a role in the determination of these properties, probably because the dimensions obtained (>20 nm) are too big to observe variations in nickel surface atom topology. In contrast, 3%Ni catalyst reactivity is very low, notably at low temperature: at 373 K the TOF is almost twice lower than that of 1 or 5%Ni catalysts. This may be due to Ni-CeO_2 interactions where the nickel phase is partly decorated by the support component [29-32].

The existence of the spillover hydrogen phenomenon is well evidenced [35-36]. The molecules of hydrogen dissociate on the nickel surface and migrate to the support. Spillover hydrogen under reducing conditions contributes to achieve the reduction of the nickel ions or even produce Ce^{III} sites through an electron transfer from the nickel particles to ceria [22]. These electrons are accepted in the 4f hybrid orbital of cerium. Ramoroson et al. [22] reported the existence of a spill-over effect of hydrogen atoms over Ni/CeO_2 catalysts. The hydrogen dissociates at the nickel surface (Ni^0) and transfers protons to the ceria support, generating new hydroxyl groups. The high activity is explained in this case by the excess of electrons at the metal surface.

The activity order of the prepared catalysts may be related to hydrogen activation process during the hydrogenation reaction. Indeed, it is worth noting that 1 and 5%Ni catalysts desorb hydrogen from a lower temperature (300 K- 450 K) than 3%Ni catalyst (575 K). This means the existence of low energy activation sites for the hydrogen, producing very reactive H-species during the hydrogenation reaction. As a result, minimum activity is observed with 3%Ni catalyst and higher activity with 1 and 5%Ni catalysts. As far as hydrogen spillover effect is concerned, its intensity would be minimum for 3%Ni catalyst and same for 1 and 5%Ni catalysts.

3. CONCLUSIONS

The chemical reduction by hydrazine of nickel catalysts supported on CeO_2 oxide occurred very easily. The partial reduction of the support by hydrazine was observed. Moreover, this soft reduction is especially remarkable since the reduction of ceria with hydrogen starts only at 640 K. The chemical reduction permits to obtain [relatively well dispersed] nickel particles with average particle size $\leq$ 40 nm. The catalysts showed great reducibility.

Prepared catalysts showed activity in the gas phase hydrogenation of benzene and confirmed the hydrogenating properties of the nickel supported ceria catalysts. Metal support interactions seem to be responsible for variations in both dispersion and activity with the nickel content.

The TEM and STEM studies showed the presence of the star-like structures of nickel not observed before for the nickel supported on CeO_2 catalysts.

4. REFERENCES

[1] L. Filotti, A. Bensalem, F. Bozon Verduraz, G.A. Shafeev, V.V. Voronov *Appl. Surf. Sci.* 109(110) (1997) 249

[2] E. Ramirez Cabrera, N. Laosiripojana, A. Atkinson, D. Chadwick *Catal. Today* 78 (2003) 433

[3] M.F. Wilkens, P. Hayden, A.K. Bhattacharya *J. Catal.* 219 (2003) 286

[4] B.C.H. Steele, P.H. Middleton, R.A. Rudkin *Solid State Ionics* 28 (1990) 388

[5] A. Trovarelli, *Catal. Rev. Sci. Eng.* 38 (1996) 439.

[6] P.L.J. Gunter, J.W. Niemantsverdriet, F.H. Riebeiro, G.A. Somorjai, *Catal. Rev. Sci. Eng.* 39 (1997) 77.

[7] R.K. Usmen, G.W. Graham, W.L.H. Watkins, R.M. Mc Cabe, *Catal. Lett.* 30 (1995) 53.

[8] B. Ernst, L. Hilaire, A. Kiennemann, *Catal. Today* 50 (1999) 413

[9] A. Bensalem, F. Bozon-Verduraz, M. Delamar, G. Bugli, *Appl. Catal. A: Gen.* 121 (1995) 81.

[10] G. Avgouropoulos, T. Ioannides, H.K. Matralis, J. Batista, S. Hocevar, *Catal. Lett.* 73 (1) (2001) 33.

[11] M. Daturi, E. Finocchio, C. Binet, J.C. Lavalley, F. Fally, V. Perrichon, H. Vidal, N. Hickey, J. Kaspar, *J. Phys. Chem. B* 104 (2000) 9186

[12] J. Kaspar, P. Fornasiero, M. Grazini, *Catal. Today* 50 (1999) 285.

[13] W. Shan, M. Luo, P. Ying,W. Shen, C. Li, *Appl. Catal. A: Gen.* 246 (2003) 1.

[14] T. Takeshita, W.E. Wallace, R.S. Craig, *J. Catal.* 44 (1976) 236.

[15] V.T.Y. Coon, T. Takeshita, W.E. Wallace, R.S. Craig, *J. Phys. Chem.* 80 (1976) 1878.

[16] J. Barrault, A. Alouche, V. Paul-Boncour, L. Hilaire, A. Percheron-Guegan, *Appl. Catal.* 46 (1989) 269.

[17] G. Wrobel, M.P. Sohier, A. D'Huysser, J.P. Bonnelle, J.P. Marcq, *Appl. Catal. A: Gen.* 101 (1993) 73.

[18] A.M. Diskin, R.H. Cunningham, R.M. Ormerod, *Catal. Today* 46 (1998) 147.

[19] G.A. El-Shobaky, M.M. Doheim, A.M. Ghozza, *Radiat. Phys. Chem.* 69 (2004) 31.

[20] G. Wrobel, C. Lamonier, A. Bennani, A. D'Huysser, A. Aboukais *J. Chem. Soc. Faraday Trans.* 92 (1996) 2001

[21] P. Fornasiero, J. Kaspar, V. Sergo, M. Grazini *J. Catal.* 182 (1999) 56

[22] E. Ramaroson, J.F. Tempere, M. F. Guilleux, F. Vergand, H. Roulet, G. Dufour, *J. Chem. Soc. Faraday Trans.* 88 (1992) 1211

[23] T. Takeguchi, S.N. Furukawa, M. Inoue *J. Catal.* 202 (2001) 14

[24] J.C. Summers, S.A. Ausen *J. Catal.* 58 (1979) 131

[25] *Internation Centre for Diffraction Data* 1999

[26] S. Chettibi, R. Wojcieszak, E.H. Boudjennad, J. Belloni, M.M. Bettahar, N. Keghouche *Catal. Today* (2006)

[27] A.G; Boudjahem, S. Monteverdi, M. Mercy, M.M. Bettahar *J. Catal.* 221 (2004) 325

[28] Y.D. Li, L.Q. Li, H.W. Liao., H.R. Wang, *J. Mater. Chem.* 9 (1999) 2675

[29] S.J. Tauster *J. Am. Chem. Soc.* 100 (1978) 178

[30] S.J. Tauster *Acc. Chem. Res.* 20 (1987) 389

[31] M.A. Ermakova, D.Yu. Ermakov, S.V. Cherepanova, L.M. Plyasova, *J. Phys. Chem. B* 160 (2002) 11922.

[32] J.B. Wang, Y.L. Tai, W.P. Dow, T.J. Huang, *Appl. Catal. A: Gen.* 218 (2001) 69.

[33] F. Fajardie, J.F. Tempére, G. Djèga Mariadassou G. Blanchard, *J. Catal.* 163 (1996) 77

[34] M. Boudart, A. Aldag, J.E. Benson, N.A. Dougharty, C. Girvin Harkins *J. Catal.* 6 (1966) 92

[35] F. Benseradj, F. Sadi, M. Chater, *Appl. Catal. A*, 228 (2002) 135

[36] W.C. Conner, J. L. Falconer , *Chem. Rev.* **95** (1995) 759

CHAPTER VI
BIMETALLIC Ni/Ag NON CLASSICAL CATALYSTS

INTRODUCTION

Les nanoparticles de métaux nobles ou de transition ont attiré beaucoup d'attention en raison de leurs propriétés peu communes comparées à celles des matériaux conventionnels polycristallins. Considérant que dans le solide macromoléculaire, les atomes superficiels contribuent à seulement une fraction relativement petite du nombre d'atomes de métal, les nanoparticles contiennent presque tous les atomes en surface. On peut supposer que tels atomes ont des nombres de coordination inférieurs à ceux des atomes de cœur et, par conséquent, ils montrent une activité considérablement grande.

La synthèse des nanoparticles métalliques a été au centre de nombreuses études dans les dernières décennies. Quelques techniques très réussies ont été développées pour produire l'or, l'argent, le nickel, le platine, le cuivre et d'autres matériaux comme nanoparticles. Récemment, l'intérêt croissant pour la préparation d'alliages métalliques comme Au/Pd, Au/Pt, Fe/Ni, Ni/Cu and Ni/Ag a été montré. On a démontré que les nanoparticules bimétalliques présentent des performances très largement supérieures à celles des particules monométalliques.

Des catalyseurs nickel-argent (1%) supportés, préparés par réduction chimique avec de l'hydrazine, ont été étudiés. Différentes concentrations en Ag et Ni ont été employées. Deux modes de réduction d'hydrazine ont été utilisées : réduction du nickel supporté et réduction-précipitation du nickel. Deux types de silice commerciale ont été employés comme supports pour la phase active de Ni-Ag : la silice Chempur d'aire spécifique de 15 m^2g^{-1} très bien cristallisée et la silice Degussa qui est une silice amorphe d'aire spécifique de 250 m^2g^{-1}.

1. INTRODUCTION

Nanoparticles of transition or noble metals have attracted much attention because of their unusual properties compared with the conventional polycrystalline materials. Whereas in the macromolecular solid, surface atoms contribute only a relatively small fraction of the total number of metal atoms, the nanoparticles contain almost all surface atoms [1]. It follows that such atoms have lower coordination numbers than in the bulk, and as a consequence, are expected to exhibit greatly enhanced activity to all manner of substrates [1]. The synthesis of metal nanoparticles has been focus of numerous studies in the last decade. Some very successful techniques have been developed for producing gold [2-4], silver [5-7], nickel [8-12], platinum [13], copper [14] and other materials as nanoparticles.

Recently, increasing interest has been shown in preparing metal alloys such as Au/Pd [15], Au/Pt [16], Fe/Ni [17], Ni/Cu [18-19] and Ni/Ag [20-23]. It has been demonstrated that, even with small particles, bimetallic clusters are vastly superior to their monometallic counterparts [1,15].

Nickel supported catalysts are widely used in heterogeneous catalysis due to their high hydrogenating properties. Many parameters determine their catalytic activity in hydrogenation processes. The activity strongly depends on the nature of the support which may modify the properties of the active phase. The extent of metal-support interaction and support acidity seems to play a crucial role in complex chemistry of nickel supported catalysts [24-27]. Silver supported catalyst is considered as an excellent catalyst in epoxidation and oxidation reaction [28-29]. However, it is not active in the hydrogenation processes. Nevertheless, incorporation of silver to palladium catalysts improves the hydrogenation properties [30].

The study of 1% nickel-silver supported catalysts prepared by the chemical reduction with hydrazine has been investigated. Different concentrations of Ni and Ag have been used. Two modes of hydrazine reduction were used (see Experimental section): i) the reduction of previously impregnated nickel acetate (I-mode); ii) the precipitation-reduction of dissolved nickel acetate in the presence of a suspension of the support (P-mode). Two types of commercial silica were used as the support for Ni-Ag active phase: amorphous silica from Degussa with high surface area of 250 m^2g^{-1} denoted as SiO_2(D) and well crystallized silica gel from Chempur with the low specific surface area of 15 m^2g^{-1} denoted as SiO_2(C). The catalysts are denoted as follows:

xNi(Ag)I(P)C(D) where x, I(P), C(D) and H represent the nickel content, the impregnation(precipitation) catalyst preparation method, C(D) the crystallized(amorphous) nature of the support and H the hydrazine treatment, respectively. The list of catalysts prepared is given in Tables VI-1 and VI-2.

Table VI-1. Bimetallic $NiAgSiO_2$(C)-H catalysts prepared.

catalyst	wt. % Ag	wt. % Ni	SiO_2 support
1NiP(C)-H	-	1.00	C
90NiAgP(C)-H	0.10	0.90	C
75NiAgP(C)-H	0.25	0.75	C
50NiAgP(C)-H	0.50	0.50	C
1NiI(C)-H	-	1.00	C
90NiAgI(C)-H	0.10	0.90	C
75NiAgI(C)-H	0.25	0.75	C
50NiAgI(C)-H	0.50	0.50	C
1AgI(C)-H	1.00	-	C

Table VI-2. Bimetallic $NiAgSiO_2$(D)-H catalysts prepared.

catalyst	Wt. % Ag	Wt. % Ni	SiO_2 support
90NiAgP(D)-H	0.10	0.90	D
75NiAgP(D)-H	0.25	0.75	D
50NiAgP(D)-H	0.50	0.50	D
90NiAgI(D)-H	0.90	0.10	D
75NiAgI(D)-H	0.25	0.75	D
50NiAgI(D)-H	0.50	0.50	D
1AgI(D)-H	1.00	-	D

2. RESULTS AND DISCUSSION

2.1. Study of the supports

Fig. VI-1 shows the XRD patterns of the SiO_2(C) before and after hydrazine treatment [denoted as SiO_2(C)-H support]. The hydrazine treatment does not change the quartz structure of the support.

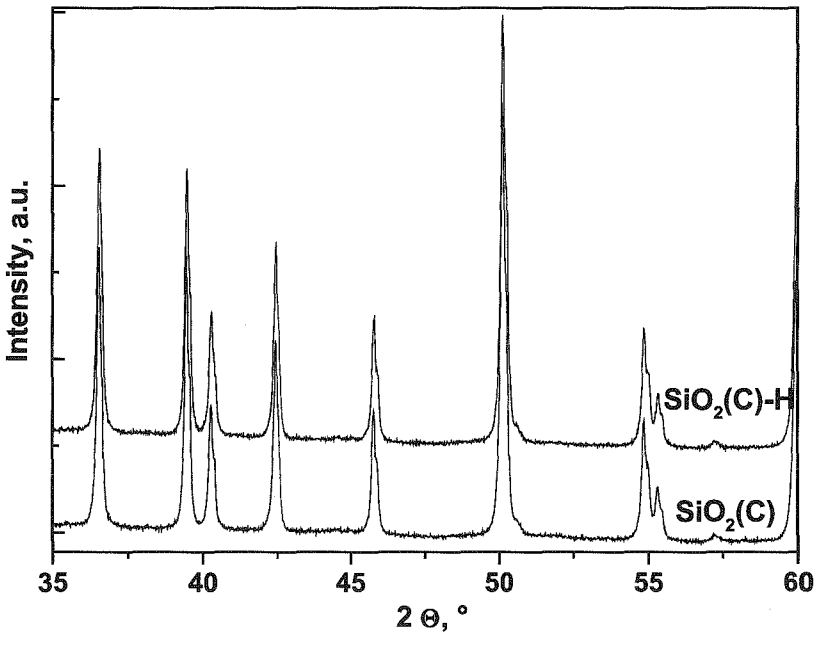

Figure VI-1. XRD patterns of the SiO2(C) and SiO2(C)-H supports.

The amorphous character of SiO_2(D) was well confirmed by the XRD study (Figure VI-2). The hydrazine treatment [see SiO_2(D)-H] did not also change the support.

It can be supposed that textural and structural properties of these supports differ and provide the different interaction with nickel active phase. These interactions are responsible for different catalytic activity of the catalysts

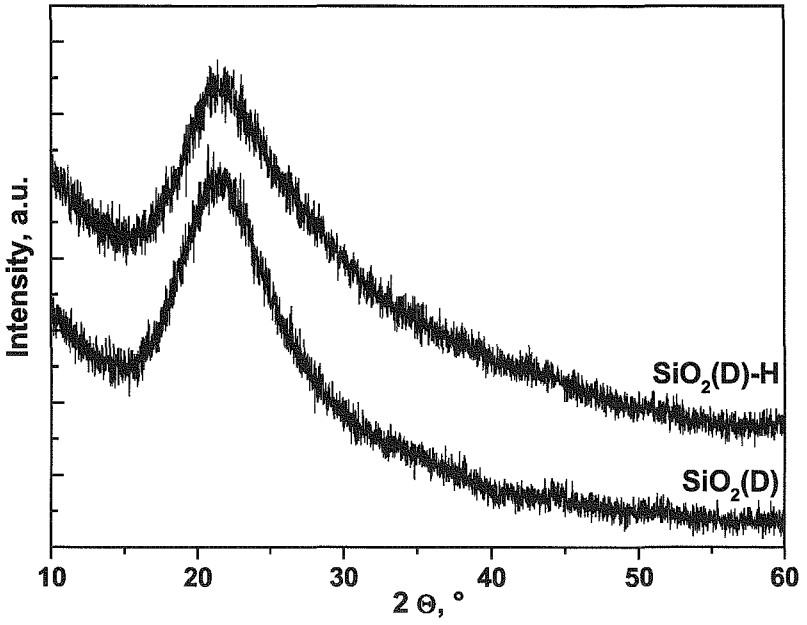

Figure VI-2: XRD patterns of the SiO_2(D) and SiO_2(D)-H supports.

The acidity of the supports was determined by adsorption of pyridine coupled with FTIR measurements which allows a clear distinction between Brønsted and Lewis acid sites. The pyridine molecule reacts with the Lewis acid centers giving the characteristic band, at around 1590 and 1450 cm^{-1} [31-32]. IR band at 1545 cm^{-1} is attributed to pyridine adsorbed on Brønsted acid sites. The results obtained are shown in Fig. VI-3. In case of the SiO_2(D) support, the IR spectra showed two mains sharp bands at 1596 and 1445 cm^{-1}. The bands gradually disappeared after evacuation. After successive evacuations, the initial spectrum of silica is recovered. No irreversibly adsorbed amine was found. It could be concluded that the SiO_2(D) silica comprised Lewis acidity. The 1584 cm^{-1} shoulder peak originates from the weakly adsorbed pyridine and weak band at 1485 cm^{-1} could be ascribed to the overlapping of Lewis acid sites [33]. Contrary to that, the crystallized SiO_2(C) exhibit weak bands at 1590 and 1450 cm^{-1} as a result of very weak Lewis acidity. A shoulder (1580 cm^{-1}) or weak bands (1438 and 1432 cm-1) are also detected. They are ascribed to physisorbed pyridine [32]. Chempur silica appears as less acidic than Degussa

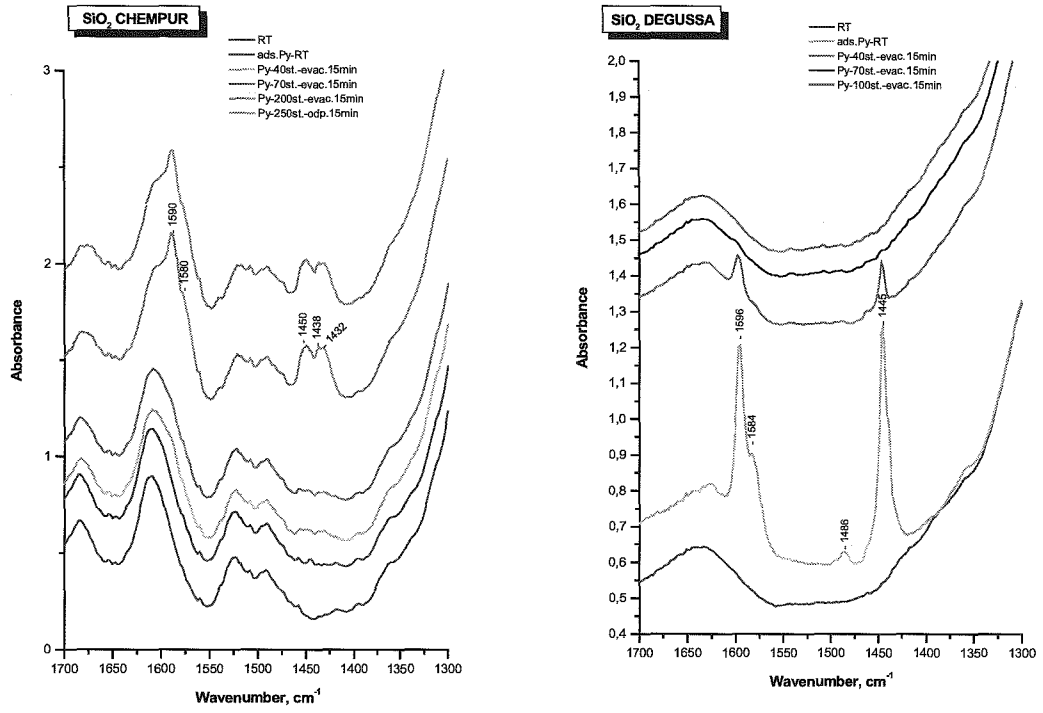

Figure VI-3. FTIR-Pyridine measurements.

2.2. Reduction of the supported Ni^{2+} ions

For metal-supported catalysts, the reducibility of the metal phase depends on the acidity of the support. Basic supports promote the metal reduction. The FTIR study indeed showed differences in the surface acidity of the silica supports used (Fig. VI-3). The less acidic SiO_2(C) support was expected to facilitate the reduction of the Ni^{2+} ions in the hydrazine aqueous media more than the SiO_2(D) support could do.

Impregnated catalysts

The green color of Ni or Ni-Ag catalysts impregnated on SiO_2(C) changed to dark due to Ni^{2+} and Ag^+ ions reduction. Colourless monometallic silver turned to black Ag° for both supports. Contrary to that, the reduction of nickel ions supported on SiO_2(D) occurs only in the presence of Ag^+ ions. In the absence of these ions, SiO_2(D) impregnated nickel became blue in hydrazine solution and did not change to black supported Ni°.

The blue colour observed for monometallic nickel supported on SiO_2(D) is ascribed to supported $[Ni(N_2H_4)_3]^{2+}$ complex which is known to form intermediately in nickel reduction by aqueous hydrazine [34]. We can admit that the interactions between nickel complex and the silica surface on SiO_2(D) are stronger than on the crystallized SiO_2(C) silica. As a result, the reducibility of nickel is weakened. In contrast, in the presence of silver, the added metal is very easily reduced and the Ag° metal particles formed play the role of active centers for nickel reduction. It has been shown that silver ions added to the reactant mixture accelerate the reduction of transition metals ions [35]. This effect was also observed during the reduction of nickel oxide with hydrogen in the presence of Ag_2O [36].

Precipitated catalysts

For the Ni or Ni-AgPC precipitated catalysts, the reduction solution transitorily became blue before it turned to dark, the colour of colloidal Ni°. Same is observed with Ni-AgPD precipitated catalysts. The changes observed are ascribed to formation of $[Ni(N_2H_4)_3]^{2+}$ complex which next is reduced in the solution or in the vicinity of the silica support (with the help of the silver for bimetallic systems), allowing Ni° particles to precipitate on the surface.

In contrast, for monometallic NiPD catalyst, the blue solution readily discolored whereas the white silica grains became blue. No reduction occurred in this case. The overall process is ascribed to $[Ni(N_2H_4)_3]^{2+}$ complex formation then fast precipitation on the support. Strong interactions with the support inhibited its subsequent reduction.

2.3. Characterization of the catalysts

2.3.1. XRD study

XRD patterns of the pure Ni, Ag and Ni-Ag(1/1) particles prepared by the hydrazine reduction at 343 K were recorded (Figures VI-4 and VI-5). Well crystallized metallic particles were obtained.

Fig. VI-4A shows the XRD pattern of the silver particles. The reflects correspond well to silver with the face–centered–cubic (*fcc*) structure.

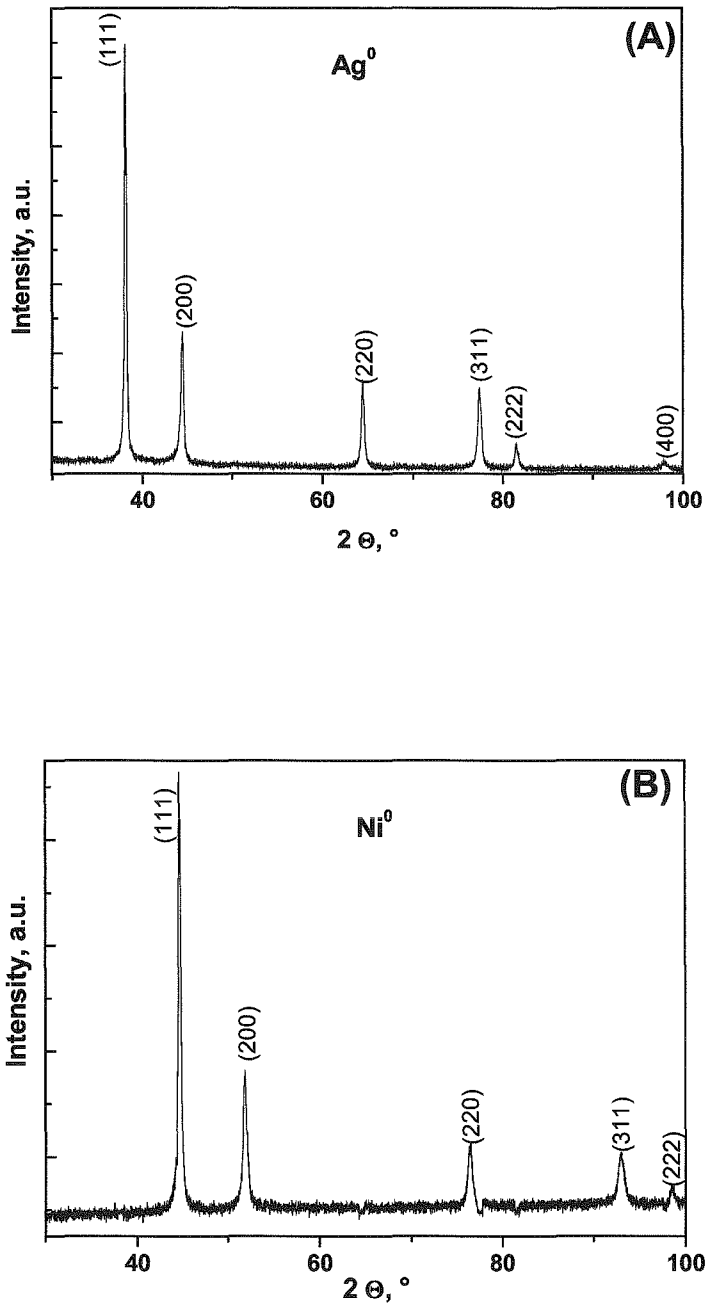

Figure VI-4. XRD patterns of the unsupported silver (A) and nickel (B) particles.

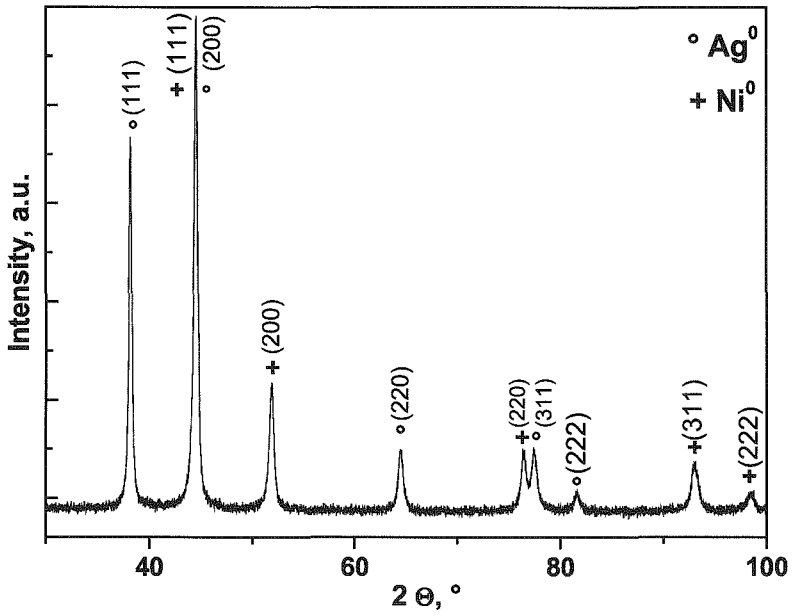

Figure VI-5. XRD pattern of the bimetallic Ni/Ag unsupported particles.

Fig. VI-4B shows the XRD pattern of the nickel particles with the *fcc* structure.

In case of the bimetallic particles the XRD pattern (Figure VI-5) shows well resolved reflects originated from the Ni^0 and Ag^0 particles in *fcc* structure. In addition the characteristic reflect for the (111) plane of Ni at $2\Theta = 44.5$ overlapped with that for the (200) plane of Ag. It could be concluded that both Ni and Ag particles have a fcc structure and most probably they form the core-shell particles with silver atoms as the core [37]. Very easily to reduce silvers ions play a role of the foreign nuclei for growth of Ni particles.

Weaker metallic signals were found with metal supported materials as shown in Figures VI-6 and VI-7.

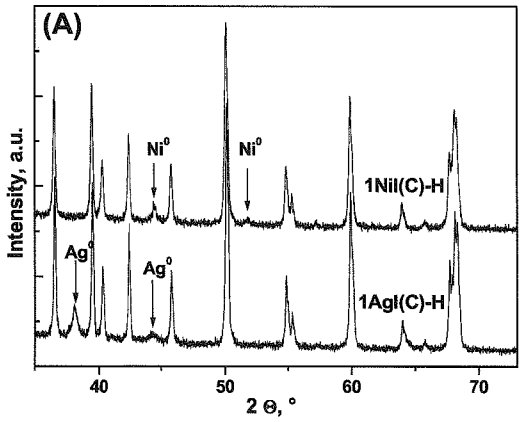

(A) monometallic catalysts

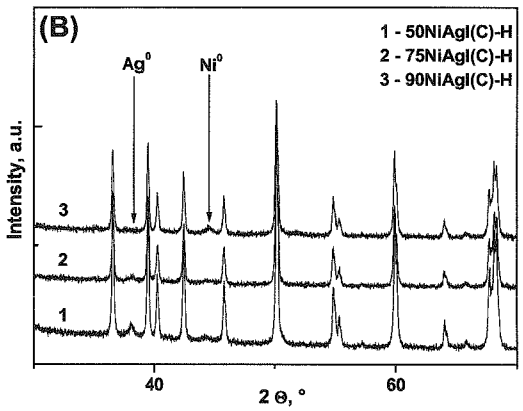

(B) impregnated bimetallic catalysts

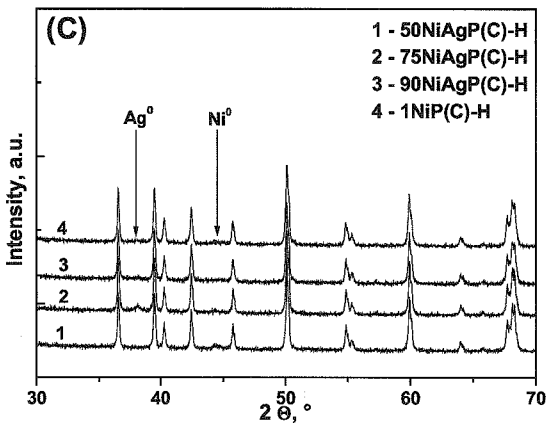

(C) precipitated bimetallic catalysts

Figure VI-6: XRD patterns of the $NiSiO_2$ and $NiAgSiO_2$(C) catalysts.

Fig VI-6A and B show the XRD patterns for the SiO_2(C) impregnated catalysts. The peaks of nickel and silver metallic particles with fcc structure [38] were detected for 1NiI(C)-H and 1AgI(C)-H monometallic catalysts respectively (Fig. VI-6A). Fig. VI-6B reports the XRD patterns of the IC impregnated bimetallic catalysts. The intensity of the (111) silver peak at 38,116 increases as the silver content in the catalyst increases. The (111) characteristic peak at 44.599 for metallic nickel was almost not detected.

In case of the SiO_2(D) catalysts, the peaks of nickel and silver were detectable but their intensity were very small. This is shown in Fig VI-7A and VI-7B for impregnated catalysts. Patterns are similar for precipitated catalysts. For both C or D supports no Ni-Ag alloys were detected.

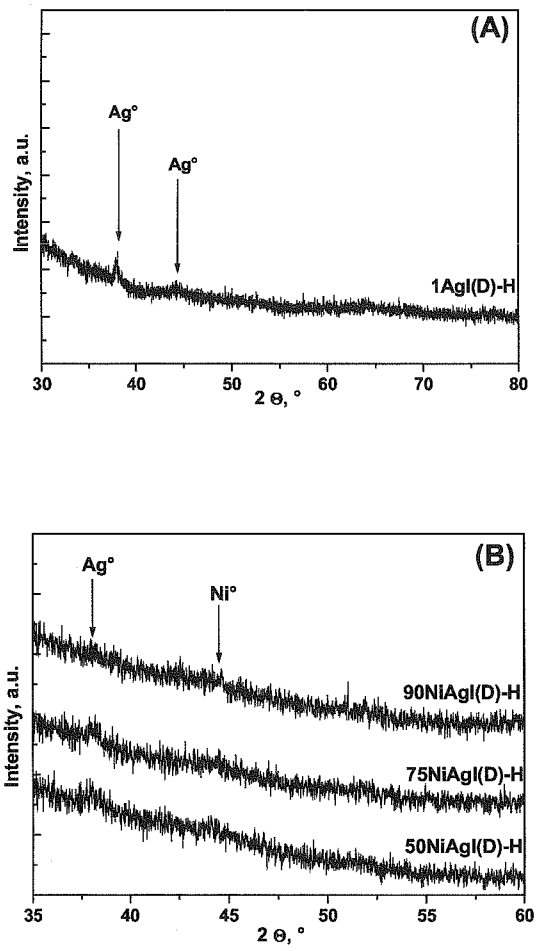

Figure VI-7. XRD patterns of the 1AgI(D)(A) and Ni/Ag(B) precipitated SiO_2(D) catalysts.

The absence of a signal or the existence of a very weak signal could confirm a high dispersion of nickel active phase or express its low content in the catalysts.

2.3.2. TEM and STEM studies

Figure VI-8 shows the TEM images for 50NiAgI(C)-H catalyst. The EDXS analysis confirmed the presence of the nickel and silver on the support. The particles were found as monometallic Ni or Ag crystallites or as bimetallic Ni-Ag crystallites. In the bimetallic crystallites no alloy was detected but segregated metallic Ni and Ag phases with a Ni/Ag ratio of 1. Mean particle size range was 8-30 nm for both monometallic and bimetallic Ni-Ag phases. Bigger agglomerates were also found (Fig. VI-9).

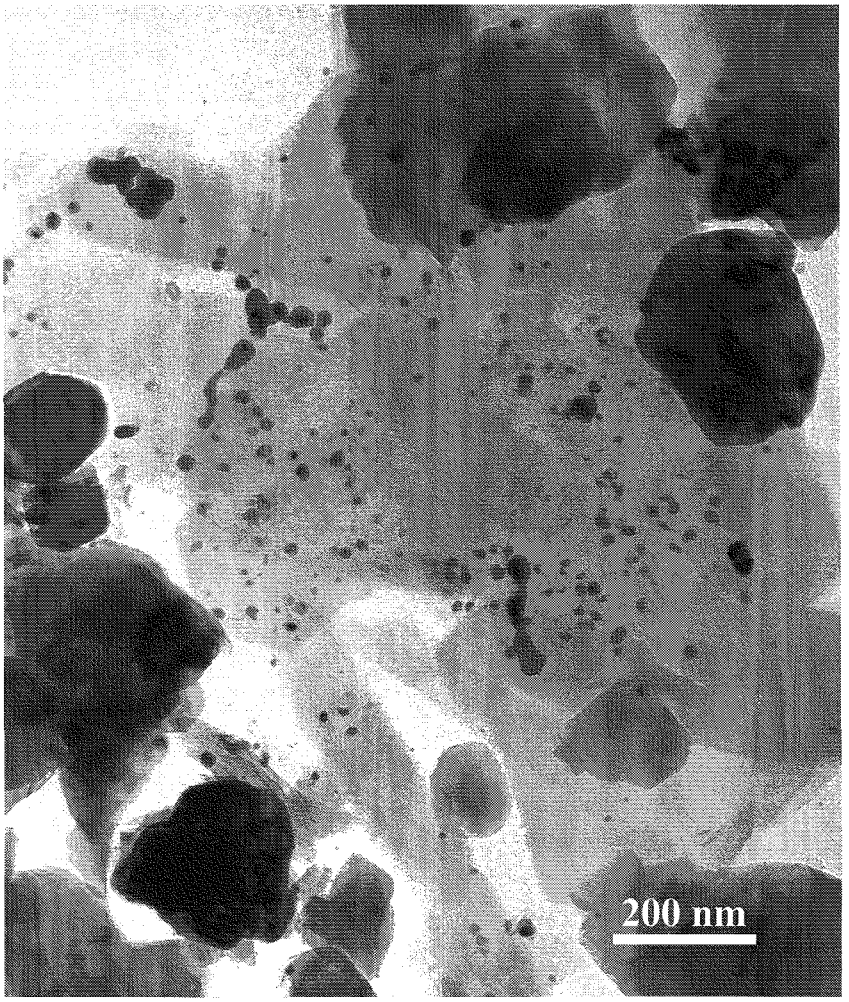

Figure VI-8. TEM image of the 50NiAgI(C)-H catalyst.

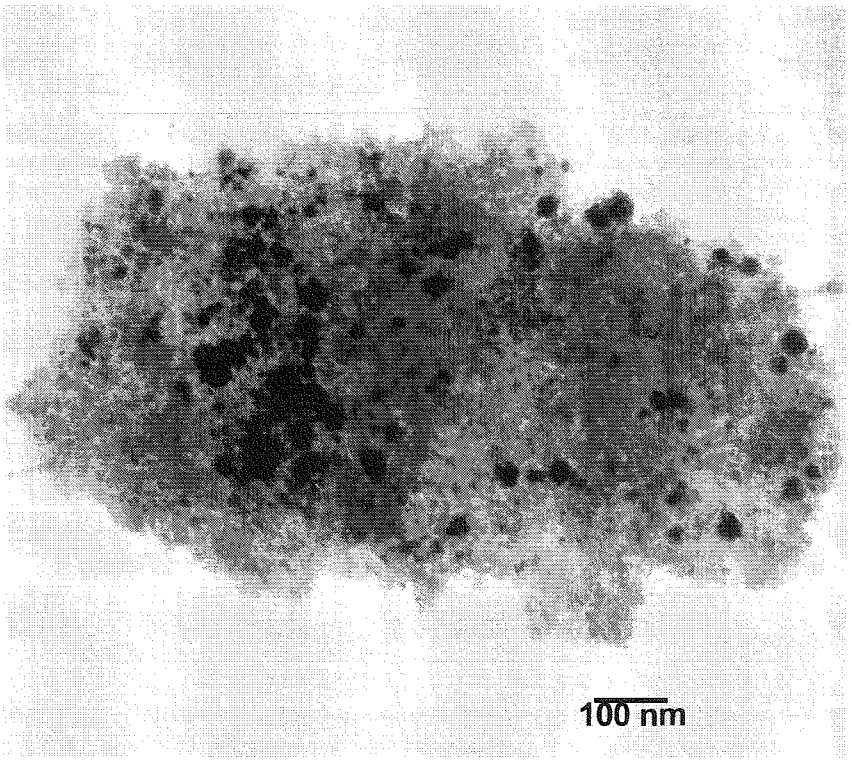

Figure VI-9. TEM image of the 50NiAg(D)-H catalyst.

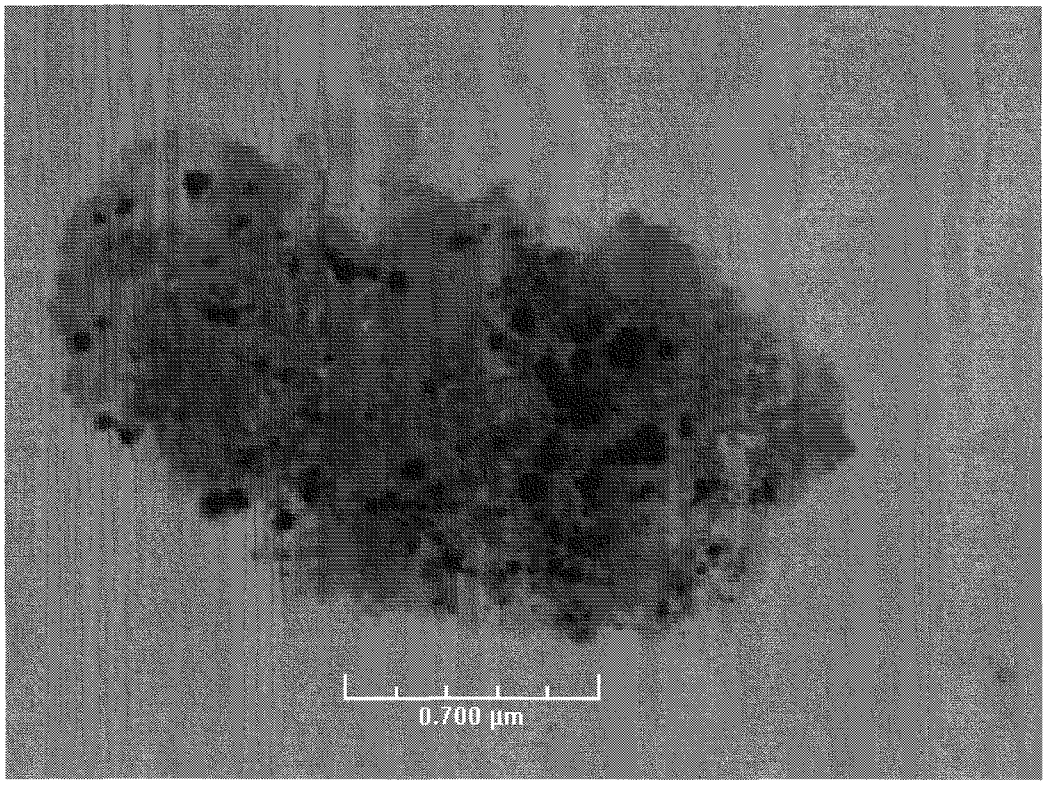

Figure VI-10. STEM image of the 50NiAg(D)-H catalyst.

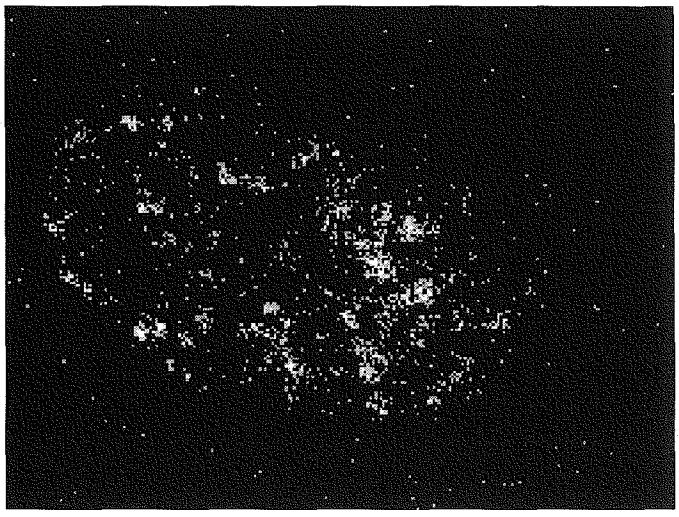

(A) X – mapping – Ag

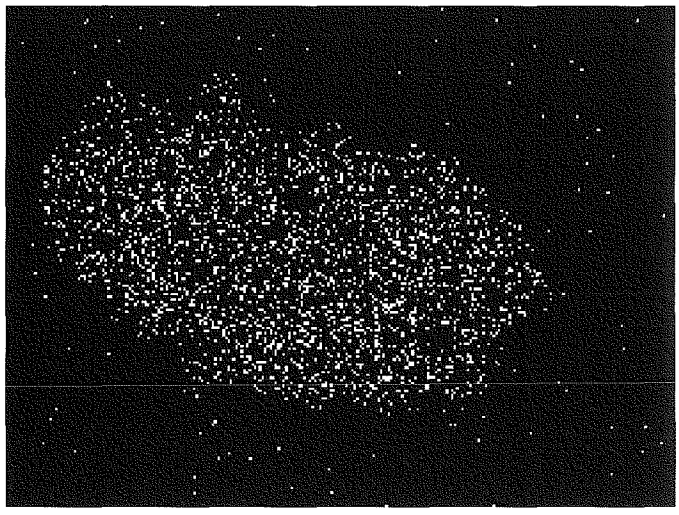

(B) X – mapping- Ni

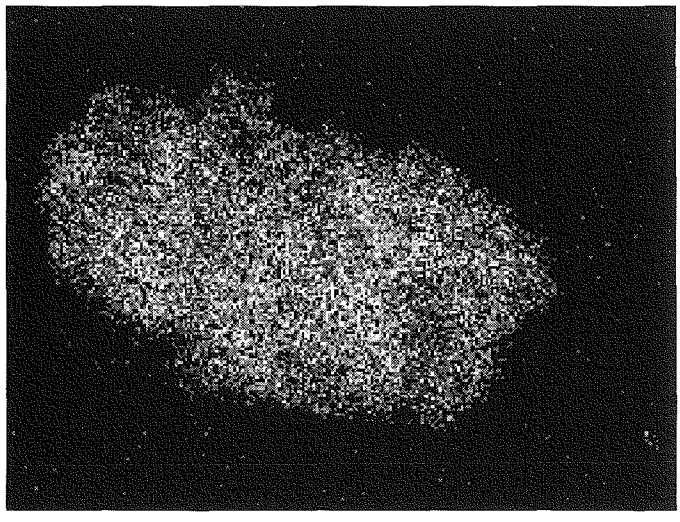

(C) X – mapping- Si

Figure VI-11. X-mapping analysis for 50NiAg(D)-H catalyst.

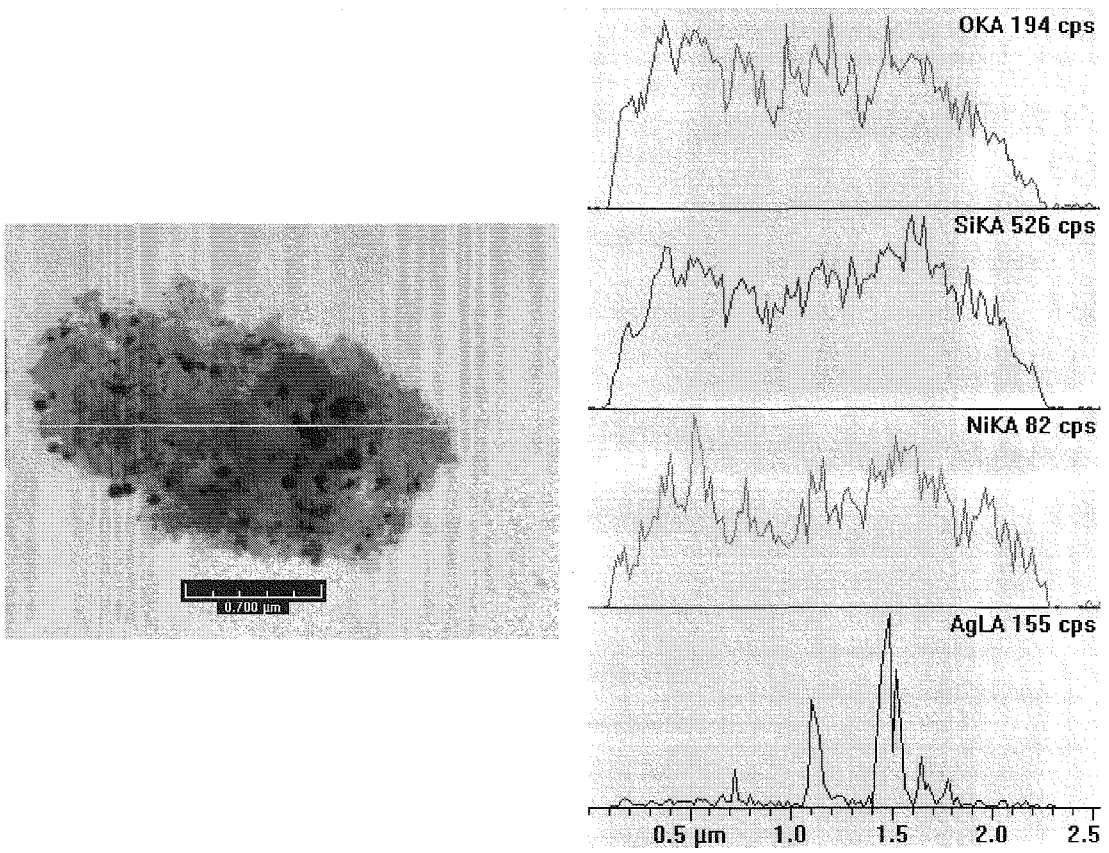

Figure VI-12. EDS analysis for 50NiAg(D)-H catalyst.

Fig. VI-9 shows the TEM image of the 50NiAg(D)-H catalyst. It confirmed the high heterogeneity of the Ni/Ag phase. The same catalyst sample was examined by the EDS and X–mapping analysis. The results are given on Fig VI-11 and VI-12. Fig. VI-10 shows the STEM image of this sample.

The EDS analysis showed very high dispersion of the nickel phase (VI-12B) well confirmed with the X-mapping study shown in Fig. VI-11B. The bimetallic Ni/Ag systems were detected (Fig VI-11A and VI-12), however their distribution on silica surface is not homogeneous. Moreover, the particle size of these bimetallic systems was found bigger than the mono metallic nickel particles.

2.3.3. Degree of reduction

The degree of reduction was determined by oxygen adsorption measurements, after a heat treatment under pure hydrogen (see Experimental Section). The results are reported in Tables VI-3 and VI-4. The values reported comprise total metal (Ni+Ag) reduction.

Silver alone is totally reduced for both silica supports. Nickel alone supported on the SiO_2(C) is almost totally reduced (99.7%). Remarkably, for impregnated bimetallic catalysts, the degree of reduction is higher with SiO_2(D) (91.6%- 99.9%) than with SiO_2(C) support (76.2%- 85.5%). This is ascribed to a greater specific surface area which gives rise to a greater metal dispersion in the supported precursor and then to a deeper reduction of nickel. It is also worth noting that, in precipitated catalysts, the degree of reduction practically does not depend on the nature of the support. Indeed, it is similar for both supports for a given chemical composition. This is because, in the hydrazine media, metal particles mainly formed in the solution or in the vicinity of the support, not on the support.

Surprisingly, higher degree of reduction was found for monometallic nickel SiO_2(C) catalysts as compared to bimetallic catalysts. This could be explained by the different structure of the metal particles formed on silica surface. In case of the Ni catalysts the TEM study showed the presence of the fiber-like nickel particles [34] while for the bimetallic catalysts the only spherical particles were observed. However, the degree of reduction increases with the increasing the silver content. Thus is also the case for SiO_2(D) catalysts. Reduced silver forms metal particles acting as foreign nuclei for subsequent reduction of nickel. More silver was introduced in the reaction mixture, more nuclei formed and nickel was reduced.

Table VI-3. Characteristics of the SiO_2(C)-H catalysts.

catalyst	H_2 ads $*10^{-5}$ [$molH_2g_{cat}^{-1}$]	H_2 des* $*10^{-5}$ [$molH_2g_{cat}^{-1}$]	Degree of reduction [%]	Dispersion [%]	Particle Size [nm]
1NiP(C)-H	0.39	0.88	95.6	4.5	22.3
90NiAgP(C)-H	0.27	0.29	79.4	4.4	22.8
75NiAgP(C)-H	0.63	0.38	85.3	11.4	8.8
50NiAgP(C)-H	0.27	0.20	93.2	6.7	14.8
1NiI(C)-H	0.62	1.61	99.7	7.2	13.9
90NiAgI(C)-H	0.34	1.07	76.2	5.9	17.2
75NiAgI(C)-H	0.28	1.43	82.7	5.3	19.0
50NiAgI(C)-H	0.20	1.10	85.5	4.3	23.5
1AgI(C)-H	0.00	0.00	100	-	-

Table VI-4. Characteristics of the SiO_2(D)-H catalysts.

catalyst	H_2 ads $*10^{-5}$ [$molH_2g_{cat}^{-1}$]	H_2 des* $*10^{-5}$ [$molH_2g_{cat}^{-1}$]	Degree of reduction [%]	Dispersion [%]	Particle Size [nm]
90NiAgP(D)-H	0.52	2.04	85.2	7.6	13.1
75NiAgP(D)-H	0.45	3.03	86.2	8.2	12.4
50NiAgP(D)-H	0.35	3.17	95.6	8.8	11.6
90NiAgI(D)-H	0.35	2.51	91.6	5.1	20.1
75NiAgI(D)-H	0.24	2.39	99.1	3.8	26.4
50NiAgI(D)-H	0.15	2.10	99.9	3.4	29.2
1AgI(D)-H	0.00	0.00	100	-	-

2.3.4. H_2-adsorption

Hydrogen adsorption at room temperature was used for the study of metal surface area. Average metal particle size and dispersion were then calculated. The results are shown in Tables VI-3 and VI-4.

As expected [28-29,39], silver does not adsorb hydrogen at room temperature. Higher dispersion and smaller particle size are obtained with the SiO_2(C) support as compared to the SiO_2(D) support. Higher dispersion is obtained with precipitated catalysts than with impregnated catalysts. The 75NiAgP(C)-H catalyst exhibits the highest dispersion of 11.4% and the lowest particle size of 8.8 nm. In bimetallic systems, the dispersion decreases with increasing silver content for impregnated catalysts but increases or passes through a maximum for precipitated catalysts.

Several factors could explain the metal dispersion observed, notably the mode of reduction by the hydrazine and the degree of reduction. The mechanism of metal particle formation consists in two steps: nucleation and particle growth. The difference in the observed properties arose from the difference in the number of nuclei formed or/and the growth rate. This difference depends on the reduction conditions (metal ion concentration, nature of the support).

For the impregnated IC or ID catalysts, metal dispersion is already determined in the impregnation step and depends on the Ni/Ag ratio. Also, during the hydrazine reduction, nucleation and growth mainly took place on the support. For bimetallic catalysts, Ag° metal particles are readily formed and play the role of active centers for nickel reduction. As to the growth processes of the metal nuclei formed, it is expected to occur through surface diffusion for almost all the nuclei formed. In other words, the final size would be determined by the primary metal particles formed. In contrast, for PC and PD precipitated catalysts, the reduction and particle growth take place in the solution or in the vicinity of the support (with the help of the silver) and metal dispersion may be determined during the $[Ni(N_2H_4)_3]^{2+}$ complex precipitation. The overall process could be controlled by liquid/solid surface equilibriums. Ag° metal particles formed also play the role of active centers during the nickel reduction processes.

To fully explain the metal dispersion observed, remind that reduction processes and degree of reduction are intimately correlated for impregnated catalysts [40-41]. The degree of reduction of nickel may be determined by the number of nuclei formed and,

consequently, would increase with increasing specific surface area of the support or with increasing silver content, as reported above. In turn, the degree of reduction may influence the particle size growth [40-41]. In effect, decreasing the degree of reduction of metal ions induces the smaller particle growth: the unreduced metal species slowdown the rate of migration and agglomeration of the metal atoms with the metal particle formed. This can be shown for the IC or ID impregnated catalysts (Tables VI-3 and VI-4).

The above reasoning does not hold with precipitated catalysts for which metal reduction took place in the solution or in the vicinity of the support.

One can expect that, if the nickel and silver particles exist on the surface as separate entities, the incorporation of silver as a second metal could decrease the metal dispersion of the system. This would be the case of 50NiAgI(C)-H impregnated catalyst for which segregated metallic Ni and Ag phases with a Ni/Ag ratio of 1 were identified. For precipitated catalysts one can speculate the existence of a great number of homogeneously distributed Ag^0 centers in solution on which nickel ions are readily reduced. In order to obtain monodisperse particles a first general condition must be fulfilled: nucleation and growth must be two completely separated steps [35]. In case of the bimetallic catalyst preparation, the heterogeneous nucleation can be achieved by forming in situ seed particles before the nucleation takes place [35]. For precipitated catalysts, the silver ions are more easily reduced than the nickel ions. Reduced silver particles form metallic particles acting as foreign nuclei for subsequent growth of nickel particles. This could explain the increase of metal dispersion with increasing the silver content. More silver ions introduced to the reactant mixture more silver nuclei for nickel particles growth. The level and variation (e. g. maximum) of dispersion depends on the Ni/Ag ratio and support nature. The support could control liquid/solid surface equilibrium. This situation favors a better dispersion as compared to impregnated catalysts. Study of electronic and structural properties of these systems by means of magnetism, XPS, UV-vis, Raman is in hand. Preliminary magnetic experiments suggests the existence of Ag-core Ni-shell structure for 75NiAgP(C)-H catalyst.

2.3.5. H_2-TPD studies

The H_2-TPD experiment results are shown in Fig VI-13 -15 and Tables VI-3-4.

The catalysts exhibit two main domains of desorption in low (<600 K) and high (>600 K) temperature ranges respectively. A third domain appears at temperatures higher than 1000 K for the set of precipitated D catalysts (Fig. VI-15). The first domain at low temperatures corresponds to hydrogen weakly adsorbed on the nickel surface whereas the second at high temperature range could originate from much more strongly adsorbed hydrogen.

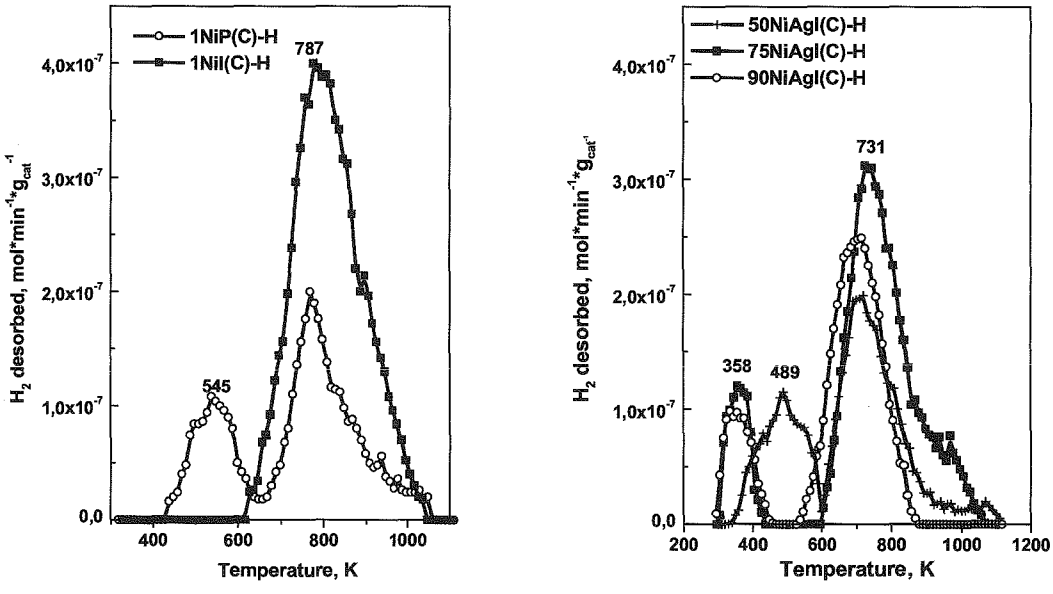

Figure VI-13. H_2-TPD profiles of the SiO_2(C) monometallic (A) and bimetallic (B) impregnated SiO_2(C) catalysts.

The catalysts desorb higher amounts of hydrogen than they adsorb at room temperature, except C precipitated Ni-Ag catalysts (Tables VI-3 and VI-4). In addition, the hydrogen desorption is higher with the SiO_2(D) than with the SiO_2(C) (maximums are 31.7 and 14.3 μmol g_{cat}^{-1} respectively) and follows metal dispersion for almost all catalysts. The H/Ni ratio calculated from the desorption data could reach a value as high as 0.4 [for 50NiAgP(D)-H catalyst].

The excess hydrogen desorbed may be ascribed to the hydrogen molecules retained on the catalyst during the heat pre-treatment at 573 K under flowing hydrogen.

These molecules are strongly adsorbed, probably at the metal-support interface or on the support as spilt-over species [42-43]. Indeed, at room temperature, thermodynamic experiments and calculations showed that only pressures of 50,000 bars the H/Ni ratio will reach values closer to 1, which is where the phase transition of nickel hydride takes place [44-45]. Although these literature data accounted for massive nickel, we conclude that the hydrogen desorbed here from the supported nickel arose, at least partly, from species incorporated in the support and not in the metal. Recall also that the hydrogen spillover phenomenon is favored by surface acid sites, extended area of the support and good metal-support contacts [42]. This could explain that greatest amounts of hydrogen desorbed are observed with catalysts deposited on SiO_2(D), the most acidic support which possesses the largest specific surface area catalysts. This also could explain that evolution of these amounts roughly follows metal dispersion since high metal dispersion involves good metal-support contacts.

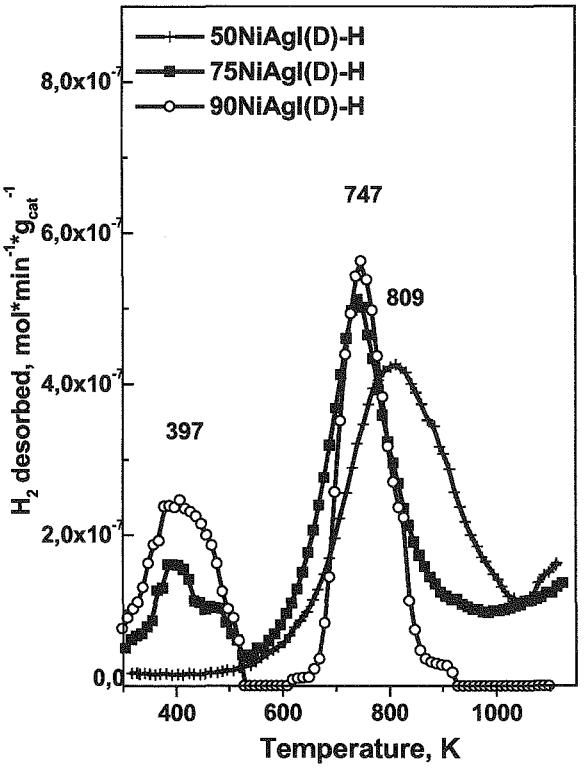

Figure VI-14. H_2-TPD profiles of the SiO_2(D) bimetallic impregnated catalysts.

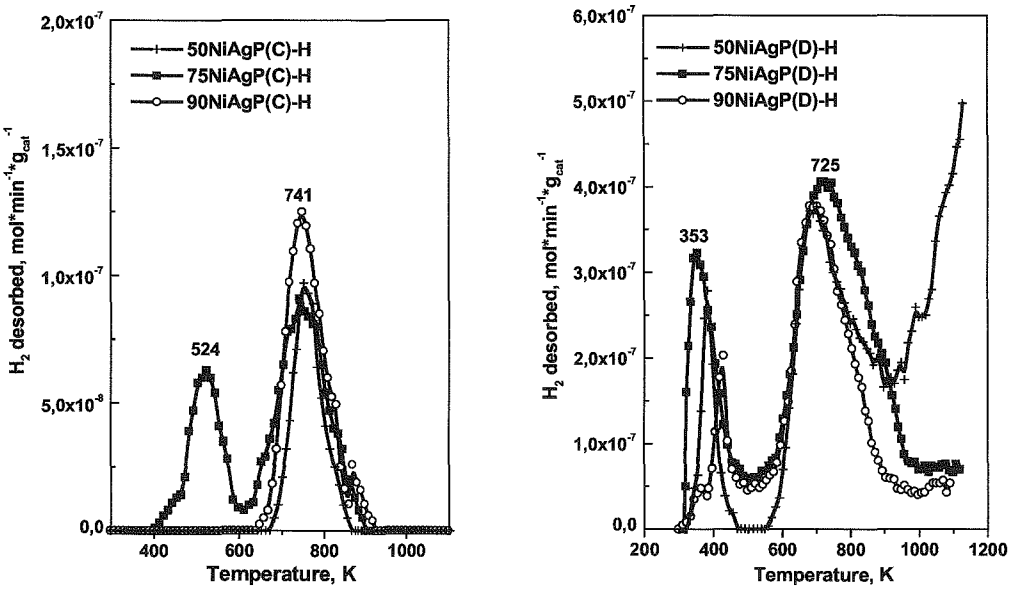

Figure VI-15. H_2-TPD profiles of the precipitated bimetallic catalysts.

In case of precipitated SiO_2(C) catalysts (Fig. VI-15), the high temperature hydrogen uptake is lower than the room temperature hydrogen adsorption, notably for 75NiAgP(C)-H (3.8 against 6.3 μmol g_{cat}^{-1}, Table V-3). The hydrogen lacking originates from hydrogen molecules loosely adsorbed on nickel sites and desorbing during the purging before the TPD experiments started (see Experimental Section). We can conclude that there exist the low energy active sites for hydrogen adsorption.

2.3. Catalytic activity

2.3.1. Testings

The gas phase hydrogenation of benzene was used as a catalytic test for prepared catalysts. All the catalysts showed 100% selectivity to cyclohexane. The bare supports did not exhibit catalytic activity in this reaction. The results obtained are reported in Fig VI-16-17 and Table VI-5.

The catalysts exhibited a maximum of activity as a function of the reaction temperature. The temperature of this maximum depends on the method of preparation of

the catalysts and nature of the support. This maximum is accounted for a positive influence of the reaction kinetics at lower temperatures whereas, at higher temperatures, the thermodynamic effect of the reaction was prevailing and then conversion decreased [46]. The maximum of activity is also attributed to a decrease of the surface coverage by benzene molecules at the higher temperatures [47-48].

The results obtained show that the catalytic activity is determined by the method of preparation, Ni/Ag ratio and nature of the support. For monometallic SiO_2(C) catalysts, impregnation method is better than precipitation method (conversions at 348 K are 16.2 and 2.8% respectively). In contrast, for bimetallic catalysts, precipitated ones are the most active (Fig VI-16 and VI-17): the conversion is total from 373 K for the former and from 413 K for the impregnated catalysts. At 373 K the conversion hardly reaches 30% for the latter. The effect of the support or of the silver content strongly depends on the method of preparation. For example, 75NiAgP(C)-H and 50NiAgP(D)-H are the most active catalysts for the SiO_2(C) and SiO_2(D) supports respectively (Fig VI-16-VI-17). Remarkably, both catalysts showed catalytic activity at room temperature (about 1% of benzene conversion) which is not common for nickel catalysts. This is ascribed to combined effect of method of preparation and presence of a second metal.

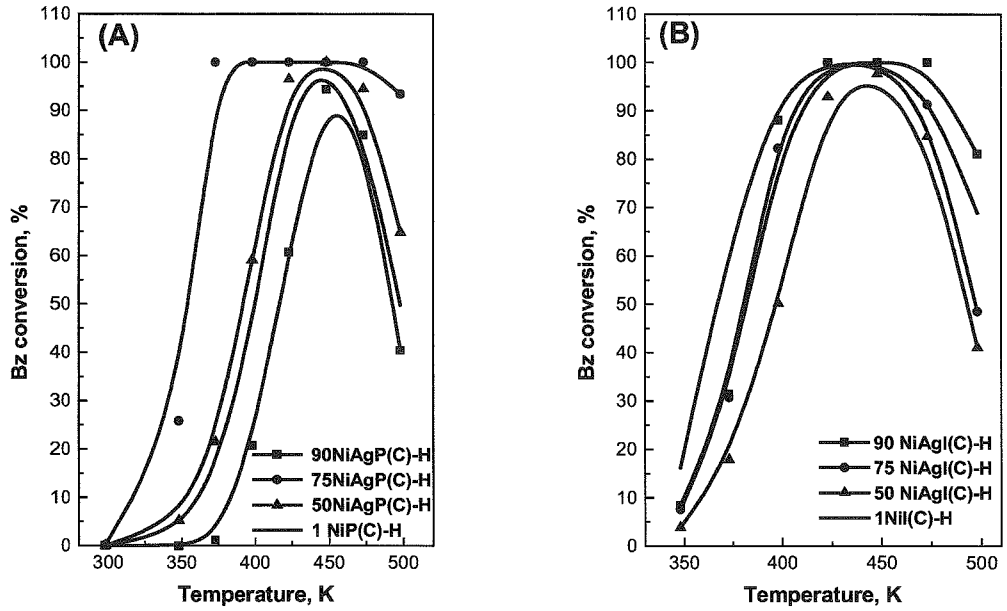

Figure VI-16. Catalytic activity of the catalysts in the benzene hydrogenation of the precipitated SiO_2(C) catalysts (A), Impregnated SiO_2(C) catalysts (B).

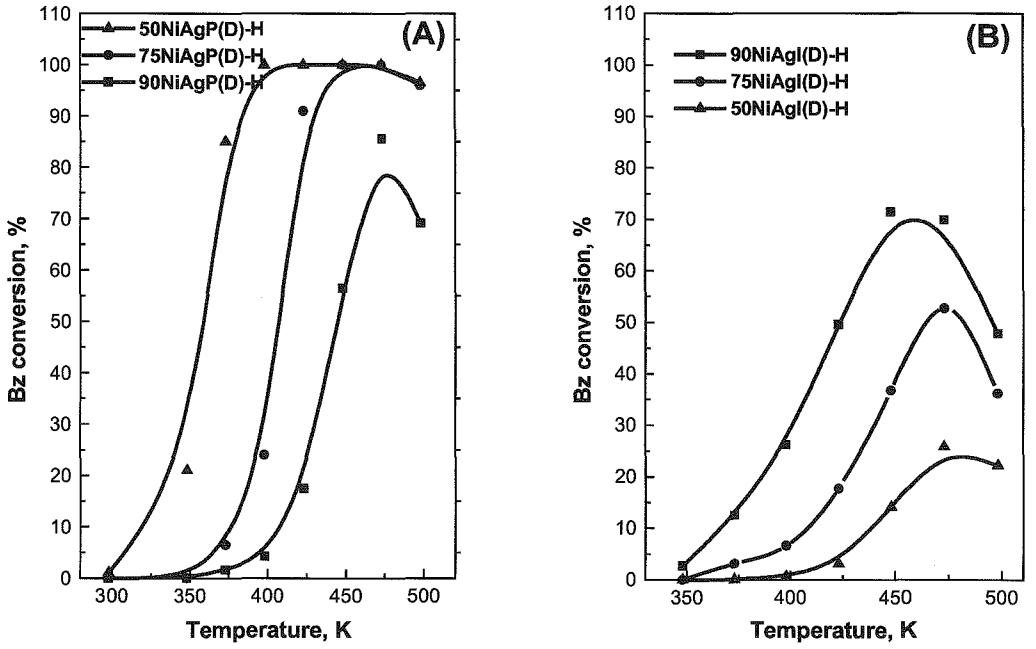

Figure VI-17. Catalytic activity of the catalysts in the benzene hydrogenation of the precipitated SiO_2(D) catalysts (A), impregnated SiO_2(D) catalysts (B).

2.3.2. Stability tests

The stability of the catalysts was tested at 423 K for 16h. Typical results are given in Fig VI-18B and VI-18D for impregnated and in Fig VI-18A and VI-18C for precipitated catalysts tested at 373 K. All tested catalysts showed some deactivation in the presence of silver. Bad stability is observed with 90NiAg(C)-H catalyst. This effect is due to the negatives processes occurring during the hydrogenation reaction, notably the poisoning of active centers by the coke formation.

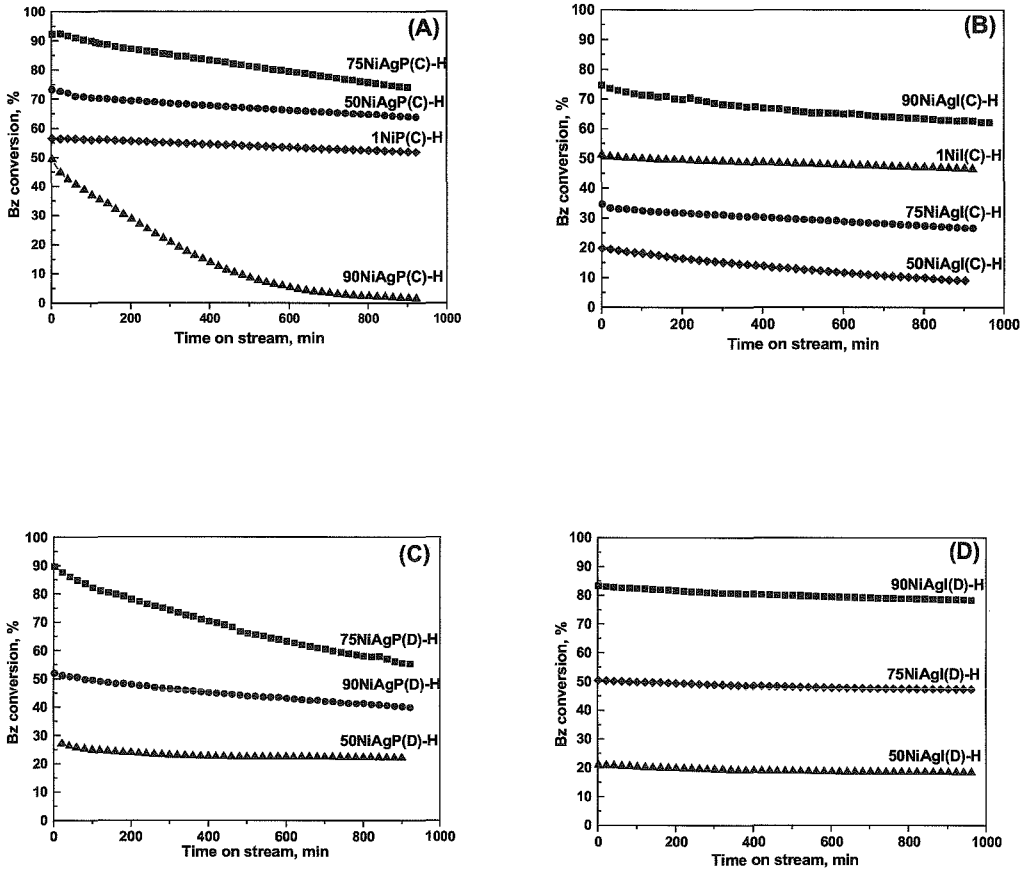

Figure VI-18. Catalytic activity versus time on stream

(A) Precipitated SiO_2(C) catalysts

(B) Impregnated SiO_2(C) catalysts

(C) Precipitated SiO_2(D) catalysts

(D) Impregnated SiO_2(D) catalysts

2.3.3. Nickel reactivity

The use of the turnover frequencies (TOF's) allows one to make a valuable comparison of the intrinsic activity of the nickel surface atoms. The results obtained at 348 and 373 K are reported in Table VI-5. Generally speaking, the TOF's follow the metal dispersion variations which are higher with SiO_2(C) than with SiO_2(D) and for precipitated than for impregnated catalysts. However, important gaps of activity are observed which could not be accounted for metal dispersion effect only. Indeed, very high TOF's are obtained for 75NiAgP(C)-H (0.061 s^{-1}- 0.233 s^{-1}) and 50NiAgP(D)-H (0.084 s^{-1}- 0.341 s^{-1}) catalysts as compared to that of their homologues. For the latter catalyst, the homologues are almost inactive. Moreover, at 348 K, the values observed are higher than the standard values reported for nickel catalysts (0.005-0.033 s^{-1}) [34, 49] and close to that obtained for platinum catalysts at 333 K (0.033-0.078 s^{-1}) [24].

Table VI-5. Benzene conversion, TOF's and activation energy.

Catalyst	Benzene conversion [%]		TOF*10^{-3} [molecule Bz *s^{-1}*$site^{-1}$]		Activation Energy [kJ*mol^{-1}]
	348 K	373 K	348 K	373 K	
1NiP(C)-H	2.8	15.2	11	59	44.6
90NiAgP(C)-H	0	1.2	0	7	41.8
75NiAgP(C)-H	25.8	100	61	233	39.6
50NiAgP(C)-H	5.2	21.5	28	115	39.6
1NiI(C)-H	16.2	61.7	39	149	38.2
90NiAgI(C)-H	8.4	31.4	36	136	44.4
75NiAgI(C)-H	7.5	30.7	39	163	43.3
50NiAgI(C)-H	3.8	17.9	28	132	40.6
90NiAgP(D)-H	0	1.6	0	4	48.3
75NiAgP(D)-H	0.2	6.5	0.5	22	45.6
50NiAgP(D)-H	21.1	85.3	84	341	43.8
90NiAgI(D)-H	2.7	12.5	11	52	47.7
75NiAgI(D)-H	0	3.1	0	19	44.3
50NiAgI(D)-H	0	0	0	0	41.3

The apparent energy of activation was determined at 248 K-423 K (Fig. VI-19) at conversions < 15%. The results obtained are reported in Table VI- 4. The values obtained are in the lower range of published results for SiO_2 supported catalysts (> 50 kJ mol^{-1}) [50]. They change with the method of preparation, silver content and nature of the support. For example, they are in the ranges 38.2 kJ mol^{-1}- 44.6 kJ mol^{-1} and 41.3 kJ mol^{-1}- 48.27 kJ mol^{-1} for SiO_2(C) and SiO_2(D) catalysts respectively.

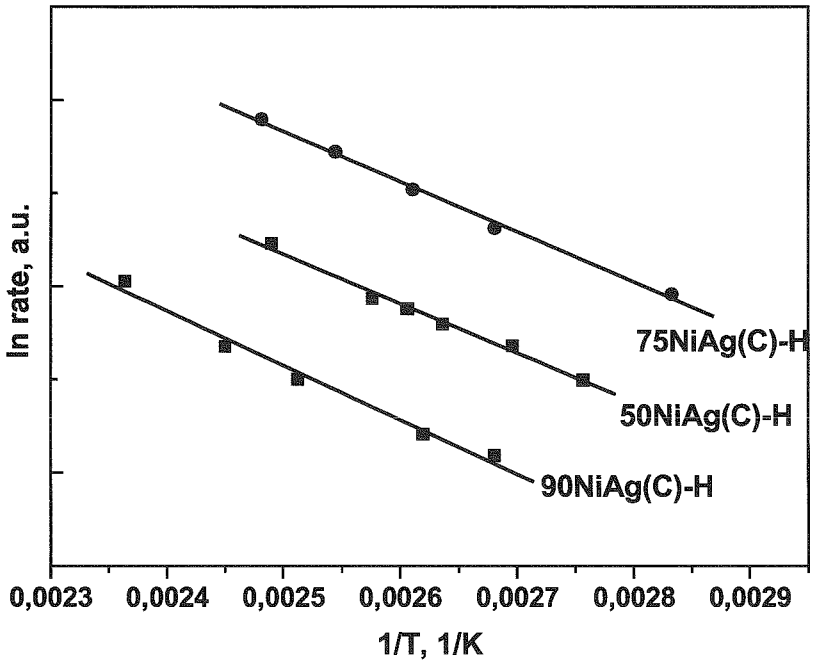

Figure VI-19. Arrhenius plots for precipitated bimetallic SiO_2(C) catalysts.

2.3.4. Discussion

Benzene hydrogenation is frequently used as a model reaction for hydrogenation of aromatic hydrocarbons. Catalytic studies on supported bimetallic Ni-Ag systems have not received attention. However, in considering such systems, one may pose the question: will the individual components exist as separate entities on the surface, or will there be mixing of atoms of the individual metals in form of the heteroatomic groupings on the carrier surface [51]. If the first situation applies, there would be no direct

interaction between atoms of the different metals, and one would expect to find a simple type of additive catalytic behavior of the individual metallic entities. However, if the second situation applies, one might expect to find a different behavior, especially if the individual metals have very different catalytic activities for the reaction of interest [51]. Both situations seem to exist with the prepared catalysts.

In benzene hydrogenation, most kinetic studies show that the rate determining step would be the reaction between adsorbed benzene molecule and an adsorbed H atom [52]. This means that the apparent energy of activation comprised the energy of activation of the rate determining plus that of adsorption pre-equilibriums of the benzene and hydrogen molecules. These steps are controlled by the metallic and acidic character of the catalyst, respectively. Benzene adsorption is determined by the support acidity. Interestingly, from Table VI-5 it can be seen that, the apparent energy of activation of bimetallic catalysts is higher (41.3 kJ mol^{-1} -48.3 kJ mol^{1}) for the more acidic SiO_2(D) support as than for the less acidic SiO_2(C) support (39.6 kJ mol^{-1}- 44.4 kJ mol^{-1}). This could be ascribed to a relative adsorption energy stronger for the benzene on the SiO_2(D) support which retards the overall chemical processes. In contrast, the TPD study (Table VI-3) evidenced the existence of weak H_2-adsorption on metal sites for Ni-Ag precipitated C catalysts but not for the impregnated homologues. On low energy sites, adsorbed hydrogen species are more reactive and this could explain a lower overall apparent energy of activation (39.6 kJ mol^{-1}- 41.7 kJ mol^{-1}) observed for precipitated C catalysts as compared with the impregnated homologues (40.6 kJ mol^{-1}- 44.4 kJ mol^{-1}). Obviously, energy of activation alone cannot fully explain all the catalytic activity results because of the existence of the entropic factor. Moreover, the reaction paths have to be known in more details. This needs a further kinetic work.

In case of the present bimetallic Ni-Ag systems, only nickel is active in the hydrogenation reaction. In addition, segregated metallic Ni and Ag phases with a Ni/Ag ratio of 1 were identified for 50NiAgI(C)-H catalyst. One can expect that if the nickel and silver particles exist on the surface as separate entities the incorporation of silver as a second metal could decrease the activity of the systems.

This seems to be practically verified for impregnated catalysts where metal dispersion and TOF's both decrease with increasing silver content. For impregnated catalysts, it is also worth noting the correlation between the metal dispersion, the degree of reduction and the catalytic activity. This correlation has also been reported in the

literature data for classical monometallic supported nickel catalysts [50]; it is believed that the presence of unreduced metal at the support surface diminishes the metal particle size required for the adsorption of benzene in a planar mode; also the TOF's increased with increasing metal dispersion and decreasing degree of reduction.

In contrast, for precipitated catalysts, increased silver content led to increased metal dispersion and activity [with maximums for SiO_2(C) support]. This could be accounted for Ni-Ag groupings, generated in hydrazine solution during precipitation of metal particles on the support, and active in benzene hydrogenation. Structural properties of these groupings may be responsible for the high activity of 75NiAgP(C)-H and 50NiAgP(D)-H catalysts. As reported above, preliminary magnetic experiments suggests the existence of Ag-core Ni-shell structure for 75NiAgP(C)-H catalyst.

For a more refined analysis of the activity results, one has to get in mind that the overall reactivity of a catalyst is determined not only by structural properties of metal particles but also by surface chemical processes. In benzene hydrogenation over metal supported catalysts, it is believed that the reaction occurs both on the metal and on the support [24, 53-55]. The contribution of the support may be important because it can furnish adsorption sites for the aromatic molecule, and in the vicinity of the metal particles, the adsorbed molecule can react with the spilt-over hydrogen from the metal, thus contributing to the overall activity. In this way, the acidity of the support (strength and concentration of acidic sites) plays an important role [53-56]. Remarkably, the highest TOF is obtained with 50NiAgP(D)-H (0.341 s^{-1}) with the more acidic SiO_2(D) support. Moreover, it is worth noting that this catalyst also exhibits the highest amount of hydrogen desorbed at high temperature (31.7 μmol g_{cat}^{-1}), i.e. hydrogen species incorporated at high temperature and identified as spilt-over species. Generally speaking, the absence of correlation between TOF's and dispersion observed could be due to the existence of the spillover effect which brings an additional activity on the support. In other words, eventual TOF's calculation does not take into account active sites from the support.

3. CONCLUSIONS

The present study shows that the surface properties and reducibility of the supported catalysts prepared strongly depend on the mode of reduction by the hydrazine, the Ni/Ag ratio and the nature of the support. For example, incorporation of silver decreases nickel reducibility, notably at 0.1%Ag. In the mean time, metal dispersion decreases for impregnated catalysts whereas, for precipitated catalysts it increased for SiO_2(D) support or passed by a maximum for SiO_2(C) support. These results could be explained by the mechanism of metal reduction in the hydrazine media. For the supported IC or ID systems, nucleation and growth probably mainly took place on the support whereas for the precipitated C or D catalysts, the metal reduction mostly occurred in the liquid phase or in the vicinity of the support. In the presence of silver, Ag° clusters first formed and served as active centers for nickel subsequent reduction. As a result, various Ni-Ag species formed where Ni and Ag phases were separated clusters or interacted as heteroatomic groupings on the carrier surface.

In case of the bimetallic Ni-Ag systems, only nickel is active in benzene hydrogenation reaction. For impregnated catalysts, the incorporation of silver as a second metal decreases the catalytic activity in parallel with the metal dispersion due to the existence of separate Ni and Ag phases. In case of precipitated catalysts, the metal dispersion increases and so did the catalytic activity as probably a result of the presence of heteroatomic Ni-Ag species more active than monometallic nickel particles. Close inspection of the results show that sharp catalytic activity could be obtained which cannot be accounted for by the metal dispersion level only but to structural properties of these groupings. Surface chemical processes could also explain the catalytic results obtained. Adsorption properties of the reactant molecules or contribution of hydrogen spillover effect particularly could affect the reaction rate.

Finally, from the practical point of view, TOF's values observed in this study could be higher than the standard values reported for nickel catalysts and close to that obtained for platinum catalysts.

4. REFERENCES

[1] B.F.G. Johnson, *Topics in Catalysis* 24 (2003) 147

[2] S. Panigrahi, S. Kundu, S.K. Ghosh, S. Nath, T. Pal, *J. Nanoparticles Research* 6 (2004) 411

[3] S.I. Dolgaev, A.V. Simakin, V.V. Voronov, G.A. Shafeev, F. Bozon-Verduraz, *Appl. Surf. Sci.* 186 (2002) 546

[4] A. Pal, K. Esumi, T. Pal, *J. Coll. Interf. Sci.* 288(2) (2005) 396

[5] D. Wang, C. Song, Z. Hu, X. Zhou, *Mater. Letters* 59 (2005) 1760

[6] Y.H. Kim, D.K. Lee, Y.S. Kang, *Colloids and Surfaces A:* 257-258 (2005) 273

[7] H. Wang, X. Qiao, J. Chen, S. Ding, *Colloids and Surfaces A:* 256 (2005) 111

[8] K.H. Kim, H.C. Park, S.D. Lee, W.J. Hwa, S.S. Hong, G.D. Lee, S.S. Park, *Mater. Chem. Phys.* 92 (2005) 234

[9] Y. Duan, J. Li, *Mater. Chem. Phys.* 87 (2004) 452

[10] D.H. Chen, C.H. Hsieh, *J. Mater. Chem.* 12 (2002) 2412

[11] Y. Hou, H. Kondoh, T. Ohta, S. Gao, *Appl. Surf. Sci.* 241 (2005) 218

[12] K.N. Kim, S.G. Kim, *Powder Technol.* 145 (2004) 155

[13] M. Seipenbusch, A.P. Weber, A. Schiel, G. Kasper, *Aerosol Sci.* 34 (2003) 1699

[14] Y.V. Bokshits, G.P. Shevchenko, A.N. Ponyavina, S.K. Rakhmanov, *Colloid Journal* 66(5) (2004) 517

[15] Y. Kobayashi, S. Kiao, M. Seto, H. Takatani, M. Nakanishi, R. Oshima, *Hyperfine Interactions* 156/157 (2004) 75

[16] A. Henglein, *J. Phys. Chem. B*: 104 (2000) 2201

[17] X. Su, H. Zheng, Z. Yang, Y. Zhu, A. Pan, *J. Mater. Sci.* 28 (2003) 4581

[18] Y.D. Li, L.Q. Li, H.W. Liao, H.R. Wang, *J. Mater. Chem.* 9 (1999) 2675

[19] C.H. Jung, H.G. Lee, C.J. Kim, S.B. Bhaduri, *J. Nanoparticle Research* 5 (2003) 383

[20] S.Y. Yang, S.G. Kim, *Powder Technol.* 146 (2004) 185

[21] A. Kumar, Ch. Damle, M. Sastry, *Appl. Phys. Lett.* 79(20) (2001) 3314

[22] D. Poondi, J. Singh, *J. Mater. Sci.* 35 (2000) 2467

[23] T. Bala, A. Swami, B.L.V. Prasad, M. Sastry, *J. Coll. Interf. Sci.* 283 (2005) 422

[24] S.D. Lin, M.A. Vannice, *J. Catal.* 143 (1993) 539

[25] M. Houalla, B. Delmon, *J. Phys. Chem.* 84 (1980) 2194

[26] S.P. Noskova, M.S. Borisova, V.A. Dzisko, *Kinetika i Kataliz* 16(2) (1975) 497

[27] C.H. Bartholomew, R.J. Farrauto, *J. Catal.* 45 (1976) 41

[28] J.J.F. Scholten, J.A. Konvalinka, F.W. Beekman, *J. Catal.* 28 (1973) 209

[29] S.R. Seyedmonir, D.E. Strohmayer, G.L. Geoffroy, M.A. Vannice, H.W. Young, J.W. Linowski, *J. Catal.* 87 (1984) 424

[30] J. Rynkowski, D. Rajski, I. Szyszka, J.R. Grzechowiak, *Catal. Today* 90 (2004) 159

[31] X. Ma, J. Gong, S. Wang, N. Gao, D. Wang, X. Yang, F. He, *Catal. Comm.* 5 (2004) 101

[32] M.I. Zaki, M.A. Hasan, F.A. Al-Sagheer, L. Pasupulety, *Colloid. and Surf. A.* 190 (2001) 261

[33] C.A. Emeis, *J. Catal.* 141 (1993) 347

[34] A.G. Boudjahem, S. Monteverdi, M.Mercy, M.M. Bettahar, *J. Catal.* 221 (2004) 325

[35] G. Viau, F. Fievet-Vicent, F. Fievet, *Solid State Ionics* 84 (1996) 259

[36] J.T. Richardson, B. Turk, M. Lei, K. Forster, M.V. Twigg, *Appl. Catal. A: General* 83 (1992) 87

[37] D.W. Chen, S.R. Wang *Mater. Chem. and Physics* (2006) in press

[38] 1999 JCPDS *Inter. Centre For Diff. Data*

[39] S.R. Seyedmonir D.E., Strohmayer, G.J. Guskey, G.L. Geoffroy, M.A. Vannice, *J. Catal.* 93 (1985) 288

[40] M. Che, Z.X. Cheng, C. Louis, *J. Amer. Chem. Soc.* 117 (1995) 2008

[41] C. Louis, Z.X. Cheng, M. Che, *J. Phys. Chem.* 97 (1993) 5703

[42] W.C. Conner, J.L. Falconer, *Chem. Rev.* 95 (1995) 759

[43] U. Roland, T. Braunschweig, F. Roessner, *J. Mol. Catal., A: Chem.* 127 (1997) 61

[44] M. Tkacz *J. Chem., Thermodyn.* 33 (2001) 891

[45] A. Driessen, P. Sanger, H. Hemmes, R. Griessen, *J. Phys.: Condens. Mat.* 2 (1990) 9797

[46] P. Antonucci, N. Van Truong, N. Giordano, R. Maggiore, *J. Catal.* 75 (1982) 140

[47] I. Ionnanides, X.E. Verykios, *J. Catal.* 143 (1993) 175

[48] S.D. Lin, M.A. Vannice, *J. Catal.* 143 (1993) 563

[49] M. Houalla, F. Delannay, B. Delmon, *J. Chem. Soc. Faraday Trans.* 76 (1980) 2128

[50] R. Molina, G. Poncelet, *J. Catal.* 199 (2001) 162

[51] J.H. Sinfelt, *J. Catal.* 29 (1973) 308

[52] R.Z.C. van Meerten, J.W.E. Coenen, *J. Catal.* 46 (1977) 13

[53] S.D. Lin, M.A. Vannice, *J. Catal.* 143 (1993) 554

[54] F. Benseradj, F. Sadi, M. Chater, *Appl. Catal. A*, 228 (2002) 135

[55] S.T. Srinivas, P. Kanta Rao, *J. Catal.* 148 (1994) 470

[56] J. Wang, L. Huang, Q. Li, *Appl. Catal. A* 175 (1998) 191

CHAPTER VII
NICKEL CATALYSTS SUPPORTED ON ACTIVATED CARBON

INTRODUCTION

Les fonctions chimiques existant sur la surface de support interagissent, plus ou moins, avec les particules de métal qui y sont déposées. L'interaction de type métal-support est habituellement plus forte quand les particules de métal sont petites. Pour les supports utilisés dans la catalyse industrielle, l'intensité de cette interaction diminue de l'alumine à la silice au charbon actif. La superficie élevée et la stabilité thermique relativement élevée font du charbon un très bon support pour les catalyseurs métalliques. Matériau bon marché et relativement inerte, le charbon actif montre aussi une grande stabilité dans les milieux acides ou basiques.

Dans des systèmes métal-carbone, les interactions fortes peuvent être favorisées et jouer un rôle important, déterminant les propriétés du catalyseur, notamment la réactivité et la texture. Ces interactions ont attiré beaucoup d'attention. Ainsi, il a été montré que la nature des pré-traitements thermiques (neutre/reducteur/oxidant) peut changer la superficie ou la porosité aussi bien que l'activité ou la sélectivité du catalyseur. La dissolution des atomes de carbone dans le métal peut causer la diminution de l'activité catalytique par le blocage des sites actifs. Le carbone peut aussi réduire le précurseur métallique pendant la préparation de catalyseur.

Dans la présente étude, nous rapportons des résultats sur la préparation, la caractérisation, les propriétés de surface et d'hydrogénation des catalyseurs non classiques supportés sur le charbon actif commercial. Le but de ce travail est d'examiner l'effet de la méthode de préparation, de la teneur en nickel et de la nature du précurseur sur leurs propriétés de surface et catalytiques. Ces propriétés sont comparées à celles de catalyseurs classiques.

1. INTRODUCTION

The chemical species present on the carrier surface interact, more or less, with the metal particles deposited thereon. The metal-support interaction (MSI) is usually stronger when the metal particles are smaller [1]. For the carriers employed in industrial catalysis the intensity of MSI decreases from alumina to silica to active carbon [1].

The chemical nature of amorphous carbon, combined with a high surface area and porosity, makes it an ideal medium for the adsorption and absorption of organic chemicals. Activated charcoal is a very mature technology that is designed to remove taste, smell and odor from gases and liquids through adsorption of the compounds that cause problems. Activated carbon is used primarily for purifying gases by adsorption, solvent recovery, or deodorization and as an antidote to certain poisons. The high surface area and relatively high thermal stability makes activated carbon very good support for metal catalysts.

The use of activated carbon (AC) as a catalyst support is increasing due to the advantages it offers as compared to traditional oxides [2]. Cheap and relatively inert material, activated carbon exhibits stability in acidic or basic media, a high surface area and oxygen-containing functional groups. In metal-carbon systems, intense interactions can be promoted and play an important role conditioning both textural properties and reactivity of the catalyst [3]. Metal-carbon interactions attracted much attention [2-6]. In this way, the thermal pre-treatment nature (neutral/reductive/oxidative) may change the surface area or porosity as well the activity or selectivity of the catalyst [3-4]. Dissolution of carbon atom in the metal may cause the decrease of the catalytic activity through site blockage [3-4]. Carbon is able to reduce the metal precursor introduced during the catalyst preparation [3, 6].

In the present study we report results on the preparation, the characterization and the surface and hydrogenating properties of non classical catalysts supported on activated carbon. The aim of this work is to examine the effect of the method of preparation, the nickel content and the nature of metal precursor on the surface and catalytic properties of Ni catalysts supported on a commercial activated carbon.

Two modes of hydrazine reduction were used (see Experimental section): i) the reduction of supported nickel acetate (H-method); ii) the reduction-precipitation of dissolved nickel acetate in the presence of a suspension of activated carbon (PH-method). The catalysts were denoted as xNi/AC-A(N)H(PH) where x, AC and A(N)

refer to nickel content (in % wt.), activated carbon support, acetate (or nitrate) precursor and impregnation-reduction (reduction-precipitation) in aqueous hydrazine media respectively. The classical (non hydrazine-treated) catalysts were also prepared for comparison and were denoted as xNi/AC-A(N) with symbols same as above. The obtained catalysts are listed in Table VII-1.

Table VII-1. Catalyst preparation.

Material	Ni precursor	wt.% of Ni	Method of preparation
1 Ni/AC-N	**$Ni(NO_3)_2$**	**1.0**	**Classical**
5 Ni/AC-N	**$Ni(NO_3)_2$**	**5.0**	**Classical**
10 Ni/AC-N	**$Ni(NO_3)_2$**	**10.0**	**Classical**
1 Ni/AC-A	**$Ni(CH_3COO)_2$**	**1.0**	**Classical**
5 Ni/AC-A	**$Ni(CH_3COO)_2$**	**5.0**	**Classical**
10 Ni/AC-A	**$Ni(CH_3COO)_2$**	**10.0**	**Classical**
1 Ni/AC-AH	**$Ni(CH_3COO)_2$**	**1.0**	**Non classical**
5 Ni/AC-AH	**$Ni(CH_3COO)_2$**	**5.0**	**Non classical**
10 Ni/AC-AH	**$Ni(CH_3COO)_2$**	**10.0**	**Non classical**
1 Ni/AC-APH	**$Ni(CH_3COO)_2$**	**1.0**	**Non classical**
5 Ni/AC-APH	**$Ni(CH_3COO)_2$**	**5.0**	**Non classical**
10 Ni/AC-APH	**$Ni(CH_3COO)_2$**	**10.0**	**Non classical**
AC	-	-	**Classical**
ACH	-	-	**Non classical**

2. RESULTS AND DISCUSSION

2.1. Reduction processes in the hydrazine media

2.1.1. Study of the support

The activated carbon used has a specific surface area of 1073 $m^2\ g^{-1}$ (Table VII-2) and a total pore volume of 0.596 $cm^3\ g^{-1}$ comprising 66.4% of micropores. When the activated carbon was treated in hydrazine media at 353 K, the surface is not changed (1116 $m^2\ g^{-1}$). However, during this treatment gaseous nitrogen (Fig. VII-1) and ammonia evolved. It is known that activated carbon decomposes hydrazine to N_2 and NH_3 [7-8]. It can be supposed that this reaction changes the surface of the carbon. The change of the activity in isopropanol decomposition (Fig. VII-3) confirmed the decrease of quantity of acid sites on the carbon surface.

2.2.2. Nickel ion reduction

For nickel acetate precursor, hydrazine provoked gaseous nitrogen and hydrogen evolution (Fig. VII-2) and the solid obtained can be removed with a magnet from the reduction flask. Simultaneous production of N_2 and H_2 is attributed to hydrazine decomposition by the Ni° particles formed according to equation (1):

$$Ni^{2+} + N_2H_4 + 2OH^- \rightarrow Ni° + N_2 + 2H_2O + H_2 \qquad (1)$$

Nitrogen peak arising within 20 min is ascribed to hydrazine decomposition by the carbon support. This makes impossible to determinate the degree of nickel reduction from the quantities of nitrogen produced during the reaction.

In contrast, nickel nitrate precursor did not react with hydrazine in the used conditions and, strikingly, the hydrazine is not decomposed by the activated carbon support for this precursor. Absence of nickel reduction is ascribed to reaction between the nitrate precursor and the support forming stable surface compounds, not reducible by the hydrazine. In addition, this reaction neutralized the acidic sites of the support which then were not available for isopropanol decomposition.

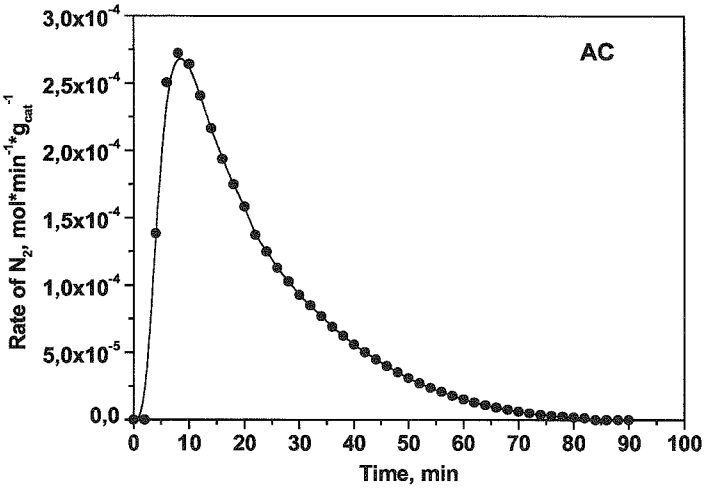

Figure VII-1. N_2 production during N_2H_4 treatment of AC.

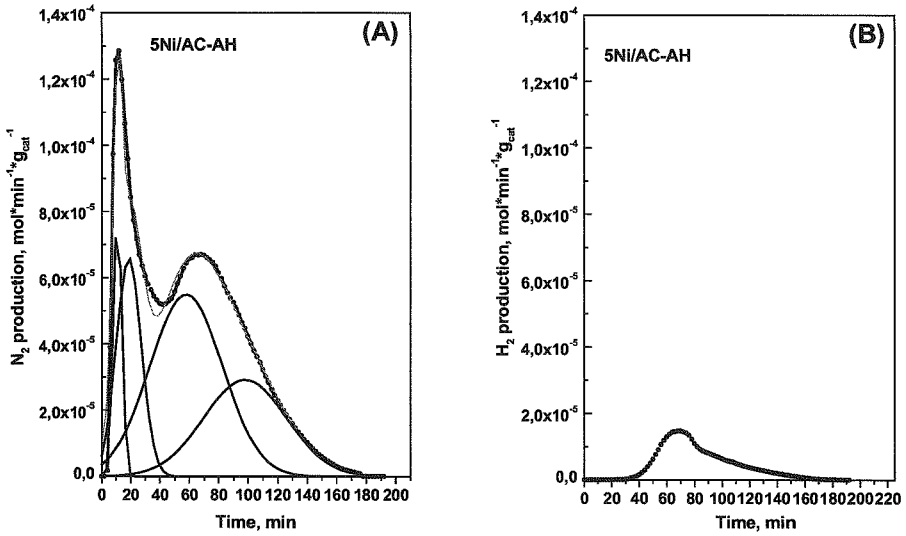

Figure VII-2. N_2 (A) and H_2 (B) emission during N_2H_4 reduction of 5Ni/AC-AH catalyst.

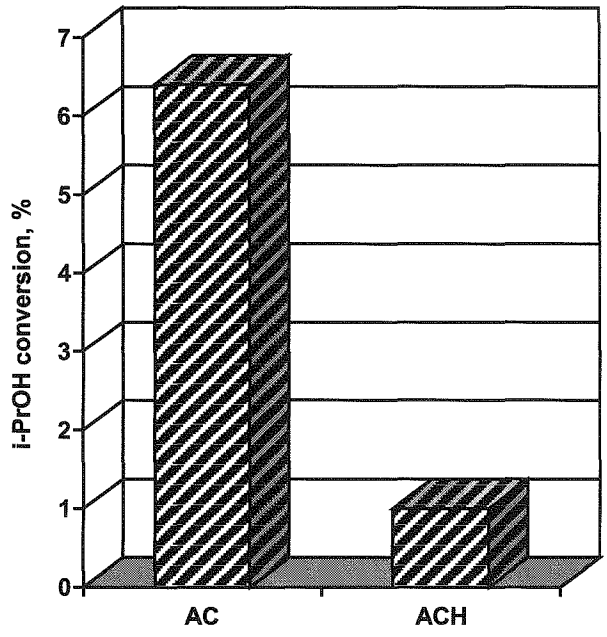

Figure VII-3. Isopropanol decomposition.

2.3. Characterization of the catalysts

2.3.1. Textural and structural properties

The wet impregnation method causes the changes in the texture of the final materials depending on the method of preparation and nickel content (Table VII-2).

The chemical reduction with hydrazine causes a significantly increasing of specific surface area, total pore volume and microporosity which grows to 1694 $m^2 g^{-1}$, 0.743 $cm^3 g^{-1}$ and 80.8% respectively for 1%Ni loading. The benefit is lesser with the Ni/AC-APH non classical catalysts: the specific area of 10Ni/AC-APH is only 971 $m^2 g^{-1}$ against 1056 for 10Ni/AC-AH $m^2 g^{-1}$. For classical preparation, low nickel loading (1wt.%) almost does not change the specific surface area or pore volume. In contrast, greater Ni loadings (5 or 10 wt.%) causes a significantly reduction of the specific surface area which decreases to 487 $m^2 g^{-1}$.

Table VII-2. BET study.

Catalyst	BET surface area [$m^2 g_{cat}^{-1}$]	% μpores [%]	Total pore volume [$cm^3 g_{cat}^{-1}$]
1 Ni/AC-N	**1071**	**65.6**	**0.595**
5 Ni/AC-N	**856**	**66.8**	**0.455**
10 Ni/AC-N	**524**	**63.9**	**0.291**
1 Ni/AC-A	**1107**	**66.0**	**0.595**
5 Ni/AC-A	**705**	**62.3**	**0.402**
10 Ni/AC-A	**487**	**65.5**	**0.264**
1 Ni/AC-AH	**1694**	**80.8**	**0.743**
5 Ni/AC-AH	**1325**	**72.5**	**0.678**
10 Ni/AC-AH	**1056**	**65.5**	**0.572**
1 Ni/AC-APH	**890**	**65.2**	**0.632**
5 Ni/AC-APH	**911**	**65.3**	**0.561**
10 Ni/AC-APH	**971**	**65.7**	**0.525**
AC	**1073**	**66.4**	**0.596**
ACH	**1116**	**66.5**	**0.596**

Several studies have shown that the specific area of carbons is strongly decreased after impregnation with nickel in classical supported catalysts [3, 9]. The greater the nickel content the greater the decrease of surface area [9]. For charcoal as a support, the decrease in the specific surface area is attributed to pore blockage by nickel compounds in the supported precursor obtained [3]. This is probably the case of the Ni/AC-N or Ni/AC-A classical catalysts (Table VII-2). Contrary to that, there is a striking increase or almost stability of the specific area for hydrazine catalysts (Table VII-2). The decrease of the specific area observed with the PH-method of preparation is small (10%) as compared to classical materials. Thus, in hydrazine aqueous media, the surface area of the nickel precursors is enhanced or practically restored. Such an effect has not been reported in the literature. Gasification of carbon may have occurred during catalyst preparation in the hydrazine media and induced an increase of specific surface area. Further work is needed for a better understanding of the effect observed.

2.3.2. XRD study

XRD study was undertaken for the estimation of phases present in the modified materials. XRD patterns for the N-classical and 5 wt% Ni A and AH catalysts did not show peaks which could origin from nickel in metallic form (Fig. VII-4). This suggests the existence of small metal clusters.

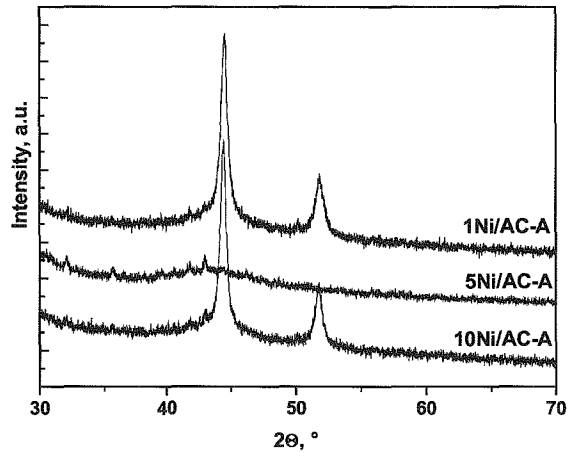

Figure VII-4. XRD patterns of the Ni/AC-A catalysts.

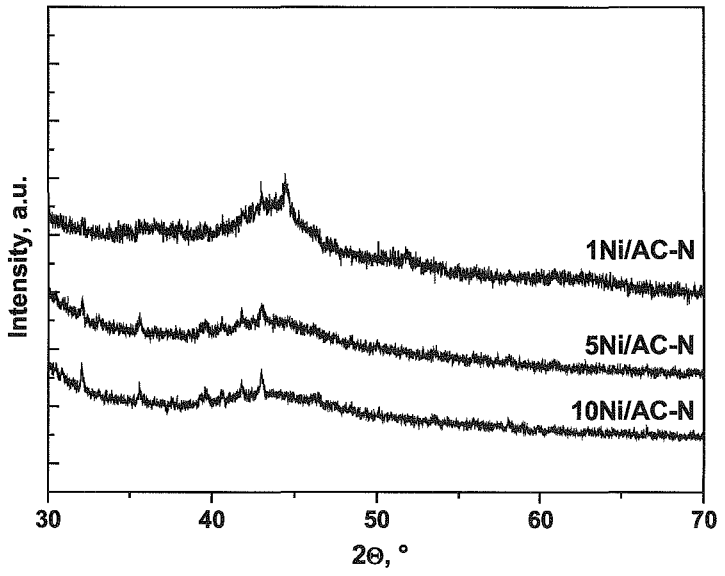

Figure VII-5. XRD patterns of the Ni/AC-N catalysts.

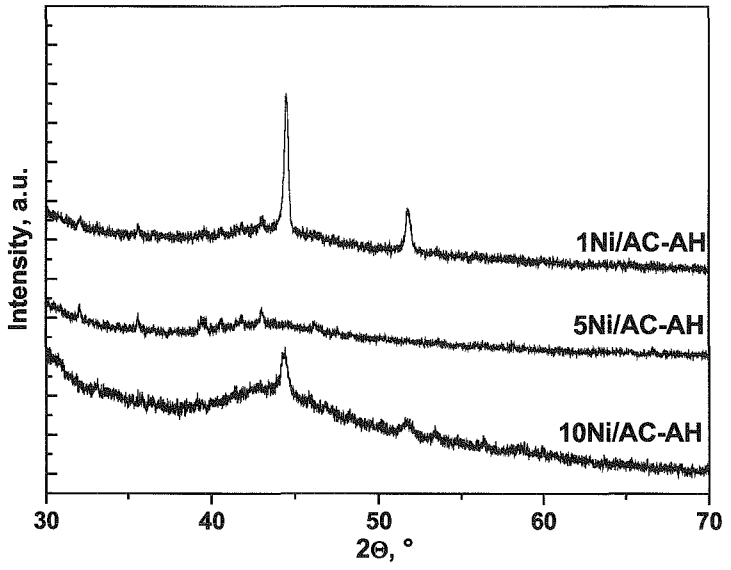

Figure VII-6. XRD patterns of the Ni/AC-AH catalysts.

However, one should remember that XRD technique is not sensitive if the amount of phase is too low. Moreover, if the particle size of nickel is very small, XRD patterns cannot detect them. The XRD pattern of the 10%Ni classical or non classical catalysts showed two large reflection signals (as illustrated in Fig. VII-4 and VII-6) at 44.59 (111) and 51.90° (200) 2Θ characteristic of metallic nickel with a *fcc* structure [10]. However, the hydrazine prepared catalyst signals are less intense, suggesting the existence of smaller particles (Fig. VII-6).

2.3.3. TEM study

The TEM experiments also did not allow the observation of nickel nanoparticles with the lowest nickel contents. Metal nanoparticles were evidenced for 10% Ni content only. In case of classical preparation, the nickel was found homogeneously dispersed on the support surface (Fig VII-7A). The shape of the nickel particles is predominantly spherical. The particles possess a mean size of 10-40 nm. In case of the 10%Ni catalyst prepared by the hydrazine chemical reduction, the TEM image differs from that of the classical catalyst (Fig. VII-7B). very small (<5 nm).

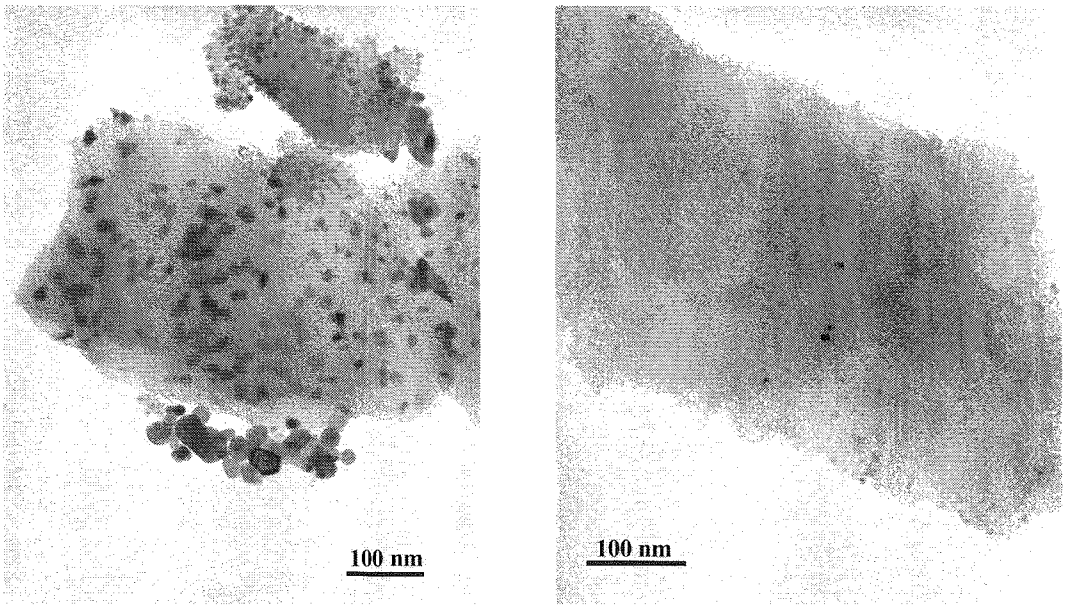

(A) 10Ni/AC-A ***(B) 10Ni/AC-AH***

Figure VII-7. TEM images of the catalysts.

The nickel nanoparticles are practically not visible on this image (Fig. VII-7B), although the surface analysis confirmed the presence of nickel on the surface. Isolated aggregates are also detected which gave rise to the XRD signal (Fig. VII-6). It could be supposed that after the reduction with hydrazine the nickel particles formed are very small (<5 nm).

2.3.4. H_2-TPR profiles

Support gasification

The experiments with both the fresh and hydrazine treated carbon support in programmed temperature under a H_2 flow, does not give rise to hydrogen consumption but to gasification, as expected, according to the literature data [11-12]. Indeed, the temperature profiles (Fig VII-8 and VII-9) indicated the signals of hydrogen and methane emission from 950 K and 600 K respectively. In the same conditions, gasification of the support as methane also occurs for the acetate catalysts but it starts at lower temperature (50 K) and with a larger yield. The presence of nickel gives rise to the formation of methane. In contrast, for the nickel nitrate precursor, the carbon support is gasified to carbon dioxide (large peak starting from 700 K) (Fig. VII-11). Carbon dioxide would be due to the reaction between the support carbon atoms and the water molecules produced by the reduction of the nickel nitrate precursor [13].

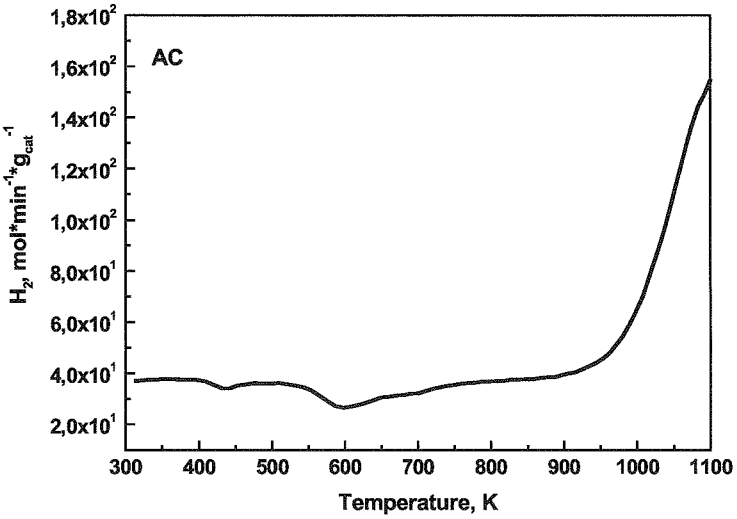

Figure VII-8. H_2 emission during TPR study of AC.

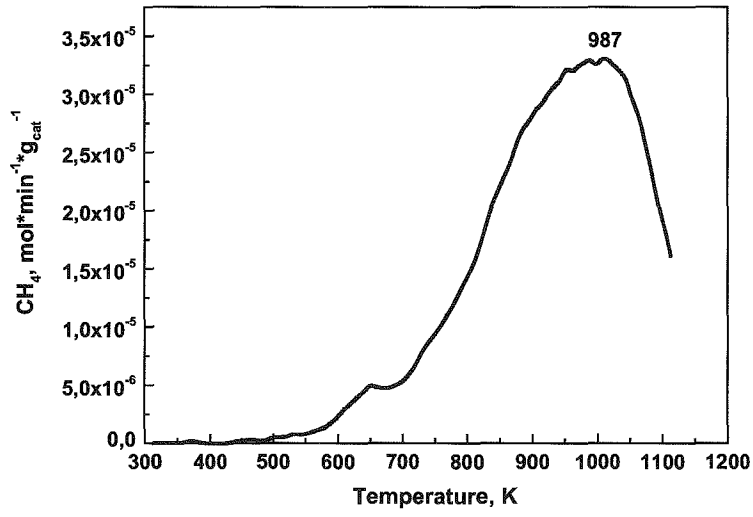

Figure VII-9. CH_4 emission during TPR study of AC.

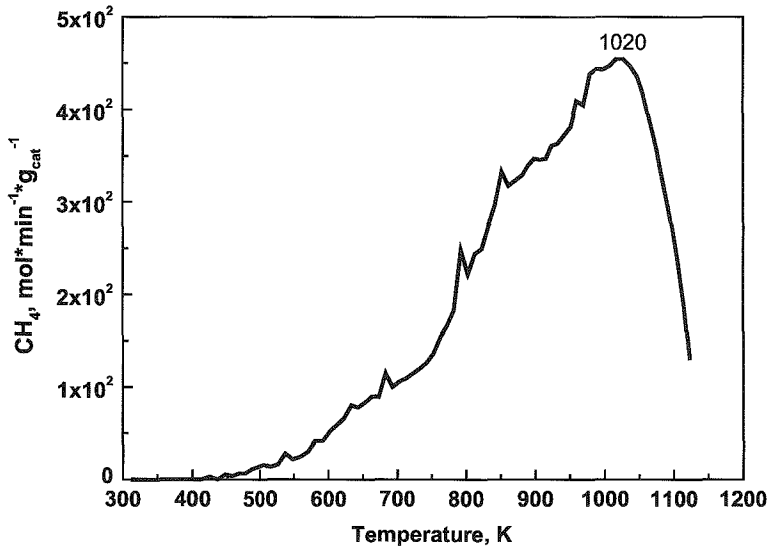

Figure VII-10. CH_4 emission during TPR study of 10Ni/AC-A.

Hydrogen consumption

In parallel to gasification, the catalysts consumed hydrogen. The H_2-TPR profiles obtained for this consumption are reported in Fig VII-12-15. Comparison with Fig VII-10 and VII-11 show that this consumption is not correlated to methane or carbon dioxide production. It is ascribed to the nickel reduction and incorporation of hydrogen into catalyst.

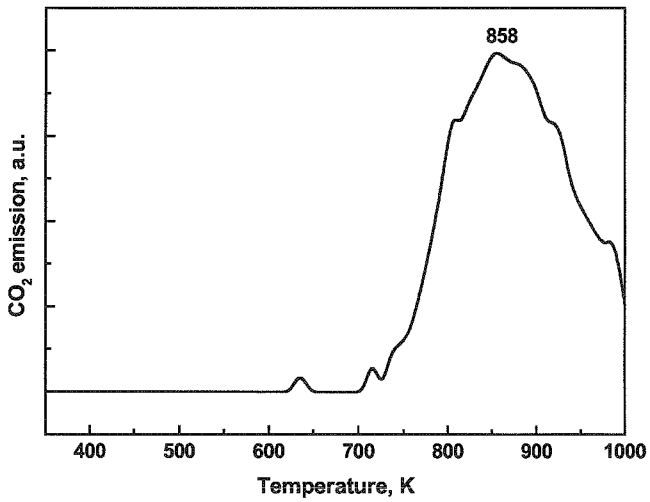

Figure VII-11. CO_2 emission during TPR study of 1Ni/AC-N catalyst.

The profiles of the catalysts obtained from nickel nitrate (Fig. VII-12) show two peaks of hydrogen consumption at ~450 K and ~700 K. The peak at 450 K is absent for 1% of nickel content. The low temperature reduction peak is due to the reduction of NiO nickel oxide form, loosely attached to the support. The high temperature reduction peak originates from the reduction of nickel species much more bonded to the active carbon support or/and the from the hydrogen spillover (see below). At a low nickel loading, a great proportion of nickel atoms are in close contact with the support, also the high temperature peak prevails. In contrast, at greater loadings, part of the precursor not directly or less attached to the support will probably more easily form NiO species which are reduced at lower temperatures. This explains the increasing intensity of the peak at 450 K at the expense of that of the peak at ~700 K with increasing nickel content. In parallel, the temperature of the peaks decreases with increasing nickel

loading for the same reason. These reducibility properties are observed for classical supported nickel catalysts [14-19].

The profiles of the classical catalysts obtained from the nickel acetate (Fig. VII-13.) differ from that of nickel nitrate catalysts. The peaks are shifted to higher temperatures and the amounts of hydrogen consumed are different. This is due to the different nature of the nickel species involved. Indeed, for the nitrate precursor, NiO species are intermediately formed by the heating during the reduction process [3] whereas, for the acetate precursor, Ni^{2+} ion clusters are anchored at the support surface. The reducibility of these species is consequently different.

The H_2-TPR profiles of hydrazine prepared catalysts are more complex. This is exemplified in Fig. VII-14 for the AH catalysts and in Fig. VII-15 for APH catalyst. The peaks correspond to the presence of unreduced nickel species. These species may arise from an incomplete reduction of the supported Ni^{2+} ions by hydrazine [20] or from reoxidation of Ni° species due to air contamination. As a result, it was observed the presence of three forms of nickel species. The very low temperature peak in the range 380-480K may be due to isolated surface Ni^{2+} ions. It would be due to Ni species reoxidized by moisture. This peak does not appear for classical catalysts. The two following peaks at higher temperatures (in the ranges 520-630 K and 650-800K respectively) are ascribed to reduction of nickel species more and more strongly bonded to the support. The temperature of these peaks decreases with increasing nickel content as a result of decreasing metal-support interactions. The profiles are quite similar for the H and PH-acetate catalysts.

The amounts of hydrogen consumed (Table VII-3) were determined from the surface area of the temperature peaks. These amounts could be due to metal reduction. However, remarkably, these amounts are greater (5-7 times) than the stoichiometric amount of nickel in case of 1%Ni loaded catalyst. This means that part of the hydrogen molecules are incorporated in the carbon support through the spillover mechanism (see below) [21-22]. Spilt-over species are probably also produced in case of 5% or 10% nickel catalysts although the H/Ni ratio is lower than 1 (0.7-0.8). Indeed, thermodynamic calculations and experiments showed that a H/Ni ratio of 0.2 at 298 K needs a pressure of hydrogen of 0.6 GPa.

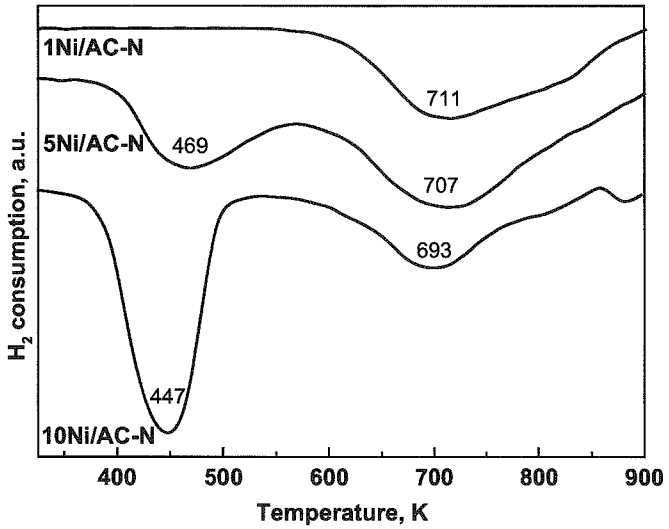

Figure VII-12. TPR profiles of Ni/AC-A catalysts.

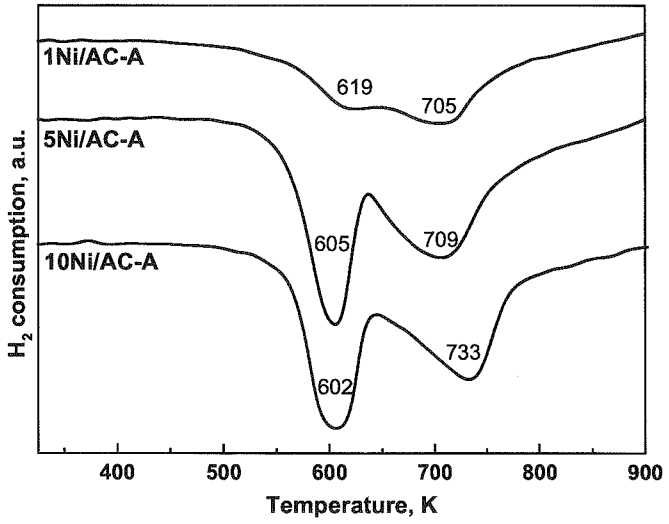

Figure VII-13. TPR profiles of Ni/AC-N catalysts.

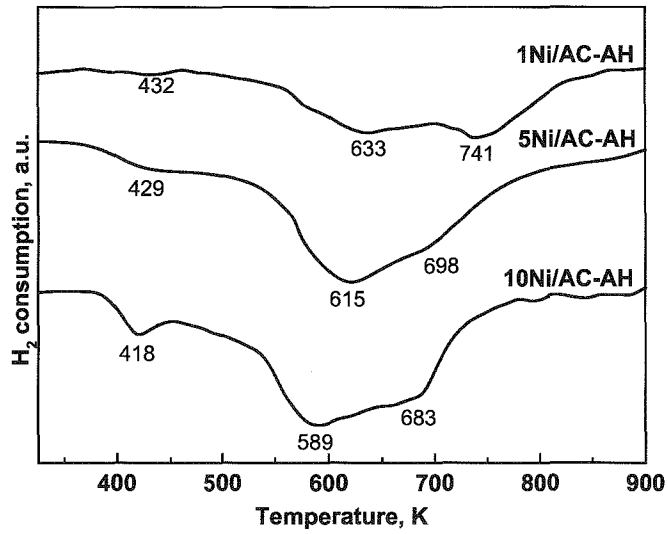

Figure VII-14. TPR profiles of Ni/AC-AH catalysts.

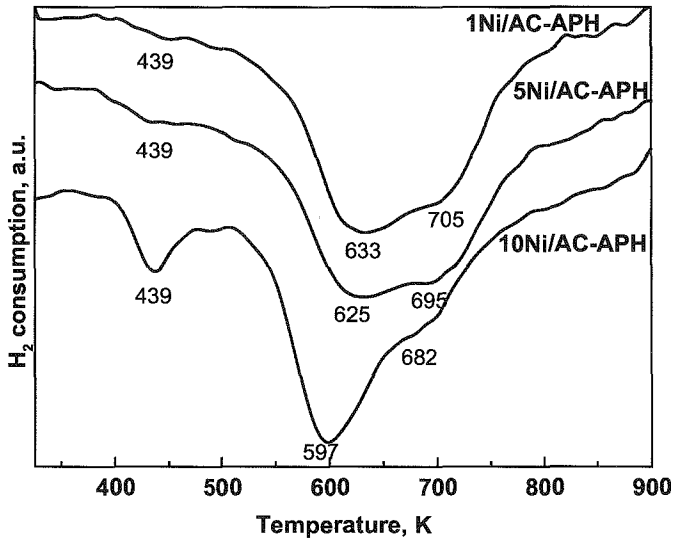

Figure VII-15. TPR profiles of Ni/AC-APH catalysts.

2.3.5. H_2-adsorption study

The accessible metal surface atoms of the catalysts was determined by H_2-adsorption at room temperature after a hydrogen treatment at 623 K for 3 h. Blank experiments showed that the carbon support, treated or not with aqueous hydrazine, did not adsorb hydrogen. Assuming the stoechiometric adsorption of hydrogen, i. e. one molecule of hydrogen occupies two nickel atoms on surface, the total metal surface area (per gram of catalyst) was calculated. The results obtained are reported in Table VII-3.

Table VII-3. Characteristics of the catalysts.

Catalyst	H_2 ads at RT*10^{-5} [mol*g_{cat}^{-1}]	H_2 des* *10^{-5} [mol*g_{cat}^{-1}]	H_2 consumed *10^{-5} [mol*g_{cat}^{-1}]	Metal surface area [m^2*g_{cat}^{-1}]
1 Ni/AC-N	0.17	32.6	69.4	0.13
5 Ni/AC-N	1.09	27.8	113.0	0.85
10 Ni/AC-N	1.98	28.4	87.2	1.55
1 Ni/AC-A	0.09	26.8	65.4	0.07
5 Ni/AC-A	0.17	17.8	69.2	0.13
10 Ni/AC-A	0.34	21.4	122.3	0.27
1 Ni/AC-AH	0.18	37.6	73.1	0.14
5 Ni/AC-AH	0.21	49.2	65.4	0.16
10 Ni/AC-AH	0.31	40.2	39.2	0.24
1 Ni/AC-APH	0.02	48.4	47.6	0.02
5 Ni/AC-APH	0.15	46.6	46.2	0.12
10 Ni/AC-APH	0.26	49.4	61.1	0.20
AC	0	8.71	-	-
ACH	0	3.32	-	-

* from H_2-TPD study

The total metal surface area increases with increasing nickel content and is the highest with the N classical catalysts. In case of the non classical catalysts the H catalysts gave better metal surface area than the PH-catalysts. 1Ni/AC-APH catalyst almost does not adsorb hydrogen. For the H-method the metal dispersion is determined in the impregnation and drying steps and this gives rise to smaller particles than the PH-method for which reduction rather takes place in the solution and not on the carbon surface. For classical catalysts, nitrate precursor exhibits greater metal areas than acetate precursor. This is due to a better reducibility of the former as showed the H_2-TPR study.

Calculations of metal particle size failed. For example, in case of classical catalysts, metal surface area found by hydrogen chemisorption was not compatible with that obtained from TEM experiments: for 10Ni/AC-A, a metal surface area of 0.27 $m^2g_{cat}^{-1}$ was found from the H-adsorption study whereas 3.50 $m^2g_{cat}^{-1}$ was determined from TEM experiments. One cause of these discrepancies would be nickel embedding by the carbon support during the hydrogen pre-treatment at 623 K. In effect, it was shown that the H_2 adsorption on nickel catalysts deposited on charcoal was decreased after a pretreatment under hydrogen at 773 K [3]. The authors attributed this to a poisoning effect of the charcoal support. This action would be accomplished by the carbon itself or/and additionally by mineral impurities present in the support [3]. In the other hand, the occurrence of the hydrogen spillover (see below) would result in the incorporation of hydrogen species in the carbon frame; also the amounts of hydrogen adsorbed are partly fixed on the carbon support and not on the metal phase only. As a result the metal surface area is undetermined by the H_2-adsorption method.

2.3.6. H_2-TPD study

The activated carbon alone or the catalyst was gradually heated under argon after a hydrogen treatment at 623 K for 3 h then hydrogen chemisorption at room temperature (as described in the Experimental Section). Only hydrogen evolved at the outlet of the reactor. Hydrogen exhibits a main peak of desorption starting from 1000 K for all the materials and a minor one at lower temperatures (around 760 K-800 K) in the presence of the metal phase only (Fig VII-16 – VII-19).

The temperature of the minor peak as well as the amounts of hydrogen desorbed varied with the method of preparation, nature of the precursor or nickel content. This peak appears at almost the same temperature (~760 K) for the N (Fig. VII-16)- or A (Fig. VII-17)-classical catalysts and at a roughly higher temperature for the H-catalysts (e. g. 803 and 760 K for 1Ni/AC-AH and 1Ni/AC-A respectively) (Fig. VII-18). The PH-method gave similar profiles (Fig. VII-19) as the H-method, but at higher temperatures. Remarkably, the non classical catalysts desorbed greater amounts of hydrogen than the classical ones (37.6 to 49.4 mol*g_{cat}^{-1} against 17.2 to 32.6 mol*g_{cat}^{-1}). Moreover, the amounts desorbed decrease with increasing nickel content. All these results may be attributed to the formation of different hydrogen adsorption species, the structure of which depends on the kind of the nickel precursor, the nickel content or the method of preparation.

The high temperature peak is due to the heat decomposition of carbon functionalities without the help of the supported metal. In case of Pt/active carbon catalysts reported in ref. [23], a peak starting at about 1125 K, with a maximum desorption rate at 1325 K, was observed and also ascribed to the heat decomposition of carbon functionalities.

The minor peak at 760 K-800 K is ascribed to hydrogen molecules from the previous reduction treatment at 623 K retained at the metal-support interface [17, 24] or incorporated in the support. Indeed, the amounts desorbed are larger than that adsorbed at room temperature (Table VII-3). Moreover, a close examination of the amounts of hydrogen desorbed shows that the H/Ni ratio may exceed 1 (e. g. 3.8-4.7 for 1Ni% content).

This excess hydrogen suggests that a part the reactant molecules, if not all, is strongly retained on the active carbon support. In other words, hydrogen molecules from the reductive atmosphere probably dissociated on the metal phase then spilled over the carbon support. This is in good correlation with the H_2-TPR study which showed that hydrogen was incorporated in the carbon support during the reduction step for 1%Ni catalysts. In case of Pt/active carbon catalysts, a peak desorbing at 750 K after a heat treatment under hydrogen atmosphere was ascribed to hydrogen species strongly adsorbed on the carbon support [23]. Hydrogen spillover on activated carbons has been evidenced by several authors [21-22].

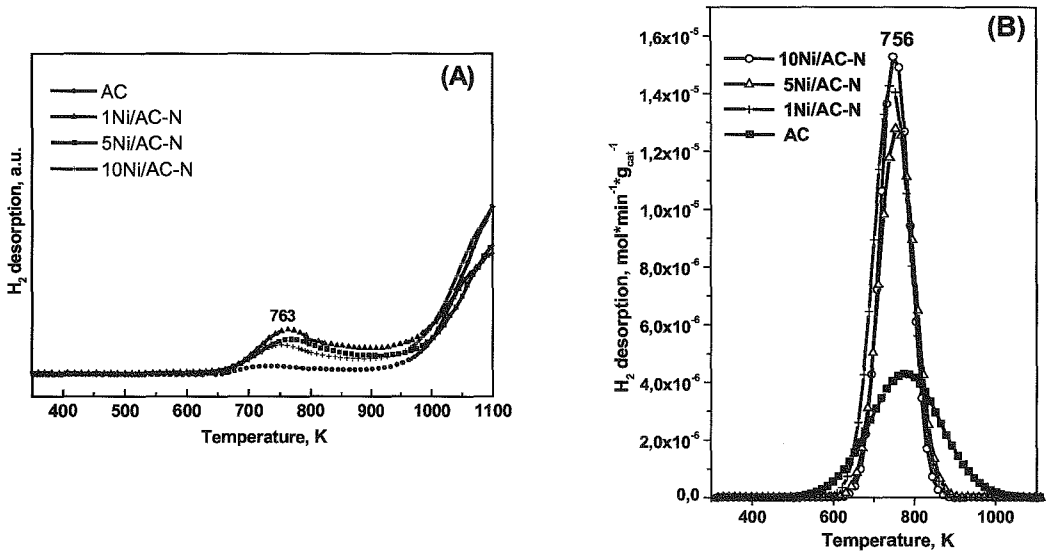

Figure VII-16. (A) H_2-TPD profiles of Ni/AC-N catalysts, (B) deconvolution of the desorption peak.

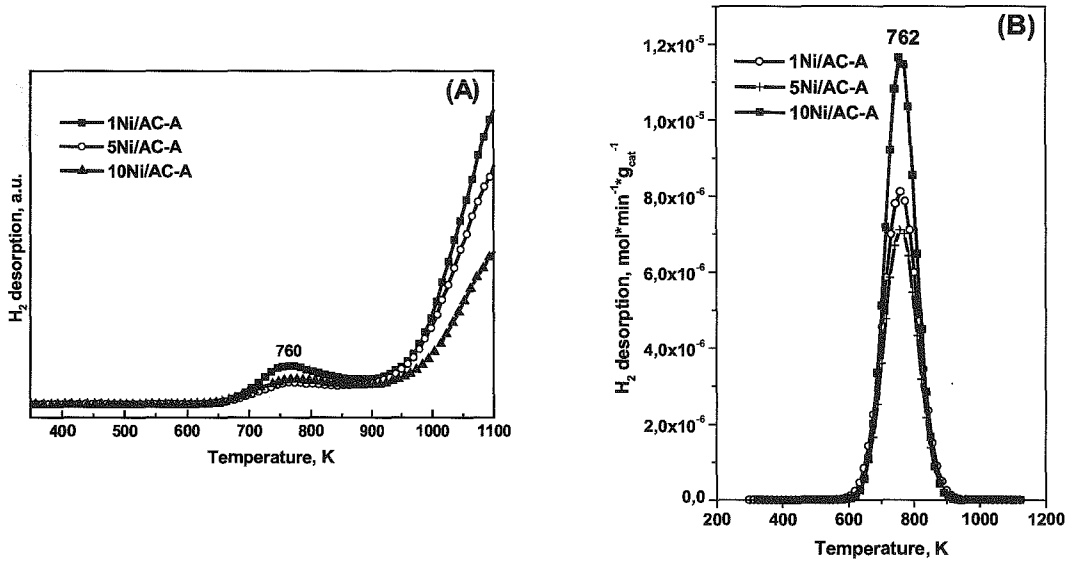

Figure VII-17. (A) H_2-TPD profiles of Ni/AC-A catalysts, (B) deconvolution of the desorption peak.

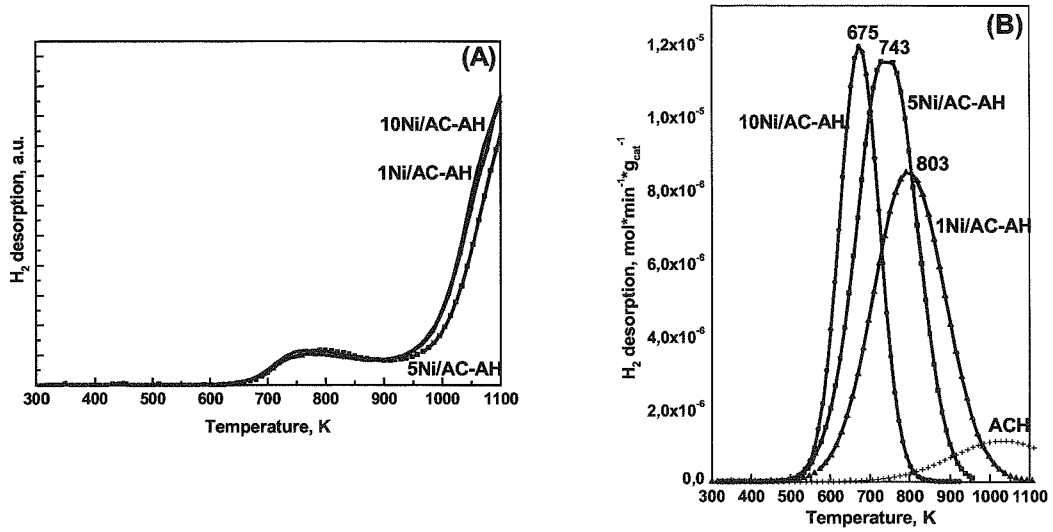

Figure VII-18. (A) H_2-TPD profiles of Ni/AC-AH catalysts, (B) deconvolution of the desorption peak.

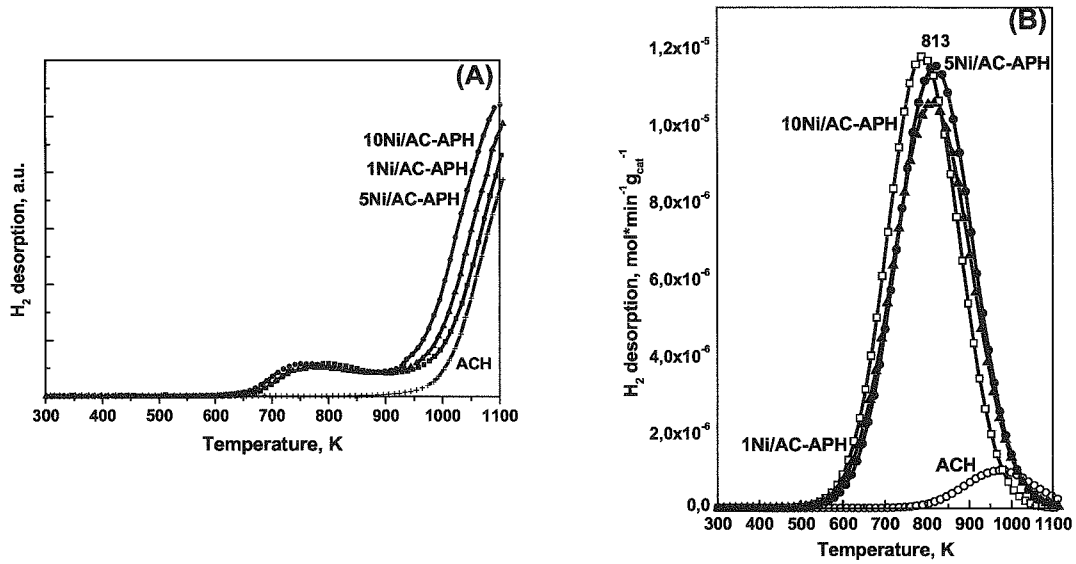

Figure VII-19. (A) H_2-TPD profiles of Ni/AC-APH catalysts, (B) deconvolution of the desorption peak.

2.4. Catalytic activity

After a H_2 thermal treatment, the classical or non classical catalysts became active and selective in the gas phase hydrogenation of benzene to cyclohexane. No activity was observed without this treatment. This is in good agreement with previous studies in our group on Ni/SiO_2 catalysts [20, 25-27, see also Experimental Section]. For non classical catalysts, the effect of the heat pre-treatment was to remove the acetate fragment embedding the nickel phase during the hydrazine reduction: it liberated the access to active sites for the reactant molecules [20, 25-27]. The activated carbon alone, previously treated or not in aqueous hydrazine media, was inactive. The results are reported in Fig. VII-20 – VII-23 and Table VII-4.

The catalysts exhibited a maximum of activity as a function of the reaction temperature. In addition, each maximum could be traversed from either the high or low temperature side without any loss of activity. Maximum of activity with temperature in benzene hydrogenation has been frequently reported [20, 22, 28-29]. This is accounted for a positive influence of the reaction kinetics at lower temperatures whereas, at higher temperatures, the thermodynamic effect of the reaction was prevailing and then conversion decreased [30]. Based on benzene chemisorption studies, the maximum of activity is also attributed to a decrease of the surface coverage by benzene molecules at the higher temperatures [31-32].

Temperature of this maximum depends on the nickel loading, the nature of the metal precursor and the method of preparation. The non classical H-catalysts (Fig. VII-22) exhibit a high activity with a maximum at a lower temperature (420 K, whatever the nickel content is) than the classical ones (460 K) (Fig. VII-21). However, maximum activity shifts to a higher temperature (460 K) also for the PH-non classical catalysts (Fig. VII-23). In case of classical catalysts, maximum temperature is lower (420 K) for the nitrate precursor (Fig. VII-20) than for the acetate precursor (460 K) when the nickel content is 10%. It shifts to higher temperatures (460 K) at lower loadings.

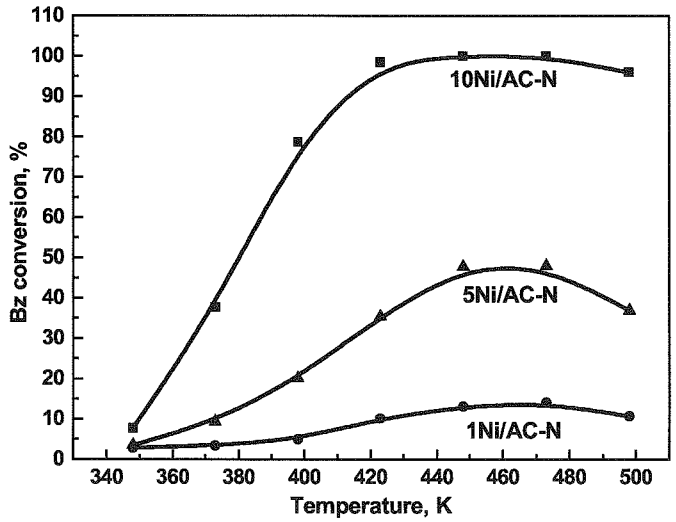

Figure VII-20. Conversion of benzene for Ni/AC-N catalysts.

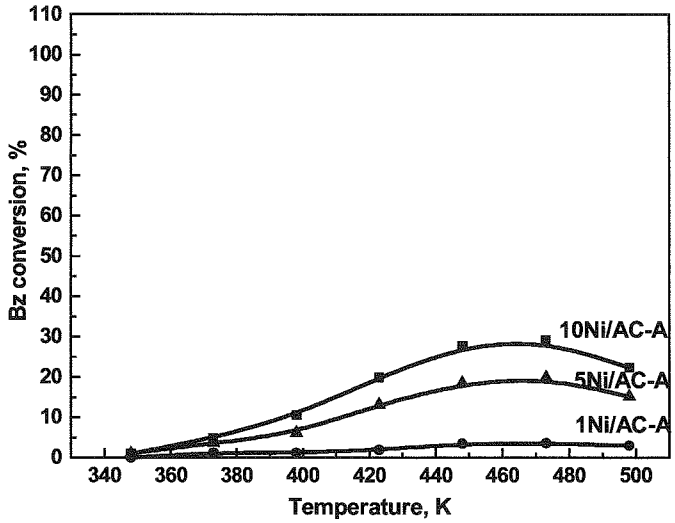

Figure VII-21. Conversion of benzene for the Ni/AC-A catalysts.

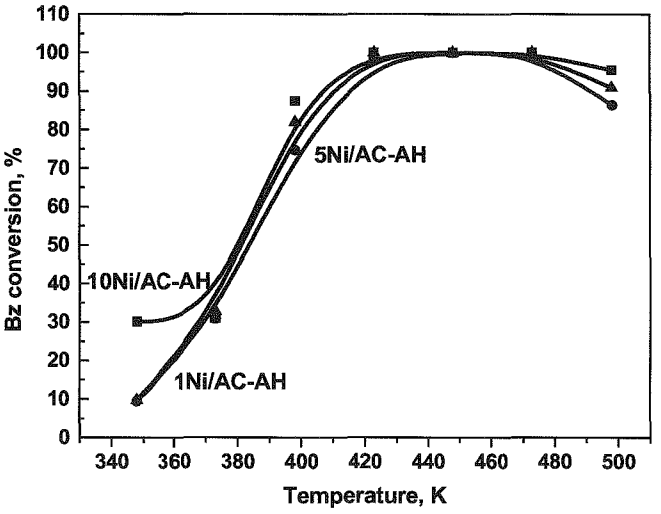

Figure VII-22. Conversion of benzene for the Ni/AC-AH catalysts.

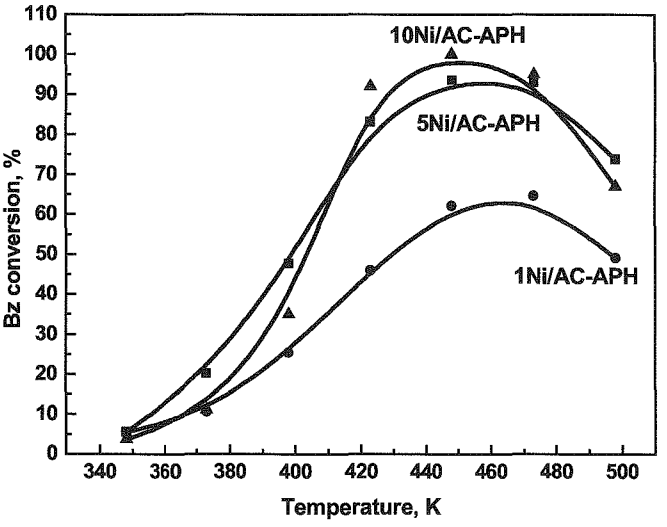

Figure VII-23. Conversion of benzene for the Ni/AC-APH catalysts.

The conversion increases with increasing catalyst nickel content (Fig. VII-20 – VII-23). The hydrazine-prepared catalysts exhibit better conversion than classical catalysts. This is notably the case for 1%Ni content: the conversion is 30% from 373 K with 1Ni/AC-AH (Fig. VII-22) and only 1.2% with 1Ni/AC-A (Fig. VII-21). Medium conversions are obtained with the APH-catalysts: 10% for 1Ni/AC-APH at the same temperature (Fig. VI-23). As to conventional catalysts, they were more active (~100% benzene conversion from 440 K) for the nickel nitrate precursor (Fig. VI-20) than that for nickel acetate precursor (maximum benzene conversion of 30% at 440 K).

Table VII-4. Specific rate and TOF's at 373 K.

Catalyst	Benzene conversion [%]	Specific rate $*10^{-3}$ [mol*min*g_{Ni}^{-1}]	TOF [molecBz*$site^{-1}$*s^{-1}]
1 Ni/AC-N	**3.3**	**0.610**	**0.0301**
5 Ni/AC-N	**9.4**	**0.332**	**0.0127**
10 Ni/AC-N	**37.7**	**0.659**	**0.0277**
1 Ni/AC-A	**1.2**	**0.229**	**0.0217**
5 Ni/AC-A	**4.8**	**0.173**	**0.0424**
10 Ni/AC-A	**3.6**	**0.064**	**0.0157**
1 Ni/AC-AH	**30.9**	**5.485**	**0.2539**
5 Ni/AC-AH	**32.7**	**1.115**	**0.2212**
10 Ni/AC-AH	**42.2**	**0.516**	**0.2001**
1 Ni/AC-APH	**10.6**	**1.885**	-
5 Ni/AC-APH	**20.2**	**0.688**	**0.1911**
10 Ni/AC-APH	**11.0**	**0.188**	**0.0618**
AC	**0**	-	-
ACH	**0**	-	-

The intrinsic rate (mol per min per gram of nickel) is a good indication of the influence of the nickel content on the reaction kinetics. The results obtained at 373 K show (Table VII-4) a much higher rate for the hydrazine than the classical acetate catalysts (up to 25 times for 1%Ni content). The H-method of preparation is better than the PH-method. For classical catalysts the best activity is obtained with the nitrate than the acetate precursor, up to 10 times greater. On the other hand, for the acetate catalysts, the intrinsic rate increases with decreasing nickel content, most probably as a result of decreasing metal particle size (see above). However, this is not the case for nitrate catalysts which activity passes through a minimum. Other factors acted so as to determine the catalytic activity.

The use of the turnover frequencies (TOF's) allows one to make a valuable comparison of the intrinsic activity of the nickel surface atoms. The results obtained at 373 K are reported in Table VII-4. Remarkably, the highest TOF's are obtained with the hydrazine-prepared catalysts. It is worth noting that the TOF of benzene hydrogenation at 373 K on 5%Pt/AC is 0.494 s^{-1}, a value quite comparable to that observed for 5Ni/AC-AH which is 0.2212 s^{-1}. Also one may conclude that the hydrazine preparation allows obtaining performing nickel catalysts e for benzene hydrogenation.

The discussion on the chemisorption study showed that the surface nickel atoms reactivity towards hydrogen is strongly affected by the nickel-carbon interactions, the degree of reduction of nickel or the hydrogen spillover effect. These parameters also may influence the hydrogenation chemical processes. The acetone hydrogenation activity of nickel catalysts, impregnated on charcoal, was found to sharply decrease after activation under a hydrogen flow [3]. For benzene hydrogenation on nickel-silica catalysts, it was reported that the activity of the surface nickel atoms might be modified when hydrogen spillover is involved [24, 33]. In such a case, an additional activity is observed due to benzene hydrogenation on support by H atoms produced from spillover hydrogen. This was shown for same reaction over Pt/activated carbon catalyst [21]. It would also be the case here, as discussed below.

2.5. Spillover hydrogen study

The surface diffusion of active species plays an important role in reactions on metal catalysts. Especially, migration of hydrogen atoms from a metal, which is active

in the dissociative adsorption of hydrogen, to an oxide or carbon surface, which itself has no activity for dissociative hydrogen adsorption, is very important [34-35]. It has been claimed that the hydrogen spillover plays a very important role in aromatic hydrogenation on metal supported catalysts. For example, Teichner et al. [36] found that alumina itself is active for benzene hydrogenation due to the spillover hydrogen introduced by the platinum catalyst supported on alumina. Actually, there is a lot of experimental evidence that hydrogen, which has been activated on metallic sites, is able to spillover onto another phase which plays a role of hydrogen acceptor. Various materials can act as this hydrogen acceptor, for example: SiO_2, Al_2O_3 or activated carbon. To our best knowledge, hydrogen spillover effect for activated carbon supported nickel catalysts has not been investigated for benzene hydrogenation. This prompted us to study this effect over the catalysts we prepared.

A spillover phenomenon is postulated when the dilution of catalyst increases its activity [37-45]. We have investigated the hydrogen spillover in benzene hydrogenation using the mechanical mixtures of 10Ni/AC-N and 10Ni/AC-A catalysts with activated carbon. The results of the dilution ratio (weight of catalyst/ weight of catalyst+activated carbon) effect on the activity are given in Fig. VII-24 and Table VII-5.

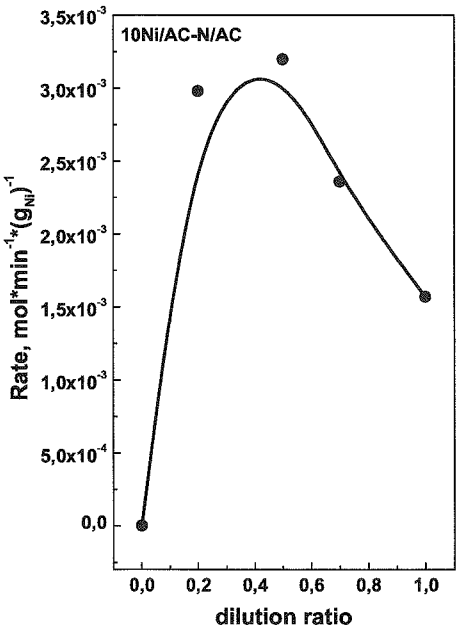

Figure VII-24. Spillover study at 448 K.

The activity of 10Ni/AC-N catalyst increases with the dilution ratio, in good accordance with the hydrogen spillover effect. The maximum of benzene conversion is observed for the mixture with 0.5 dilution ratio at 448 K (Fig. VII-24). The activity of the hybrid catalyst is 2 times higher than that of undiluted catalyst could be ascribed to the hydrogen migration process which is controlled by a distance factor [35]. Dilution is believed to increase the number of H species stabilized by the active carbon by increasing the available surface area and, in the mean time, lowers the recombination of these species in molecular hydrogen. At a certain point, the additional surface area of the dilutent brings no further benefit to the hydrogen uptake. At higher dilution ratio, the number of H spilt-over acceptor sites stabilized by the support increases but the generation of the H spillover decreases as the number of Ni decreases [34].

The effect of the reaction temperature on the 10Ni/AC-N catalyst dilution was also investigated. The results obtained (Table VII-5) show that the spillover effect decreases with increasing reaction temperature. The undiluted/diluted catalyst activity ratio decreases from 5.0 to 2.0 when the reaction temperature is increased from 348 K to 448 K. This may be due to surface coverage dependence [35] which is the highest at the maximum activity at 448 K. Aromatic hydrocarbon hydrogenation on metal supported catalysts is believed to rather occur on the support than on the metal, at least partly [21, 31-32, 35]. This suggests that the involved processes rather occur on the metal phase when the reaction temperature is increased. This is consistent with published chemisorption studies showing that aromatic hydrocarbons are only weakly adsorbed on the support but much more strongly on the metal atoms [31-32].

Table VII-5. Specific rate for spillover study.

catalyst	specific rate $*10^{-3}$ [mol*min*g_{Ni}^{-1}]				
	348 K	373 K	398 K	423 K	448 K
10Ni/AC-N	**0.135**	**0.659**	**1.377**	**1.722**	**1.772**
AC/10Ni/AC-N (1:1)	**0.674**	**2.535**	**3.280**	**3.358**	**3.358**
10 Ni/AC-A	**0.018**	**0.064**	**0.173**	**0.339**	**0.356**
AC/10 Ni/AC-A (1:1)	**0.093**	**0.140**	**0.209**	**0.232**	**0.550**

The support dilution effect was also verified with the least active 10Ni/AC-A catalyst (Table VII-5): the rate of benzene conversion is multiplied by 5.2 at 348 K. This effect also decreases with increasing reaction temperature. It sharply diminishes to 0.68 at 423 K after a maximum at 398 K.

These results are in good accordance with the H_2-TPR and H_2-TPD experiments reported above which clearly showed the existence of H spilt-over species incorporated in the carbon frame for both classical and non classical catalysts. We infer that hydrogen spillover effect also holds for the hydrazine catalysts. The highest reactivity towards hydrogen was obtained with these catalysts.

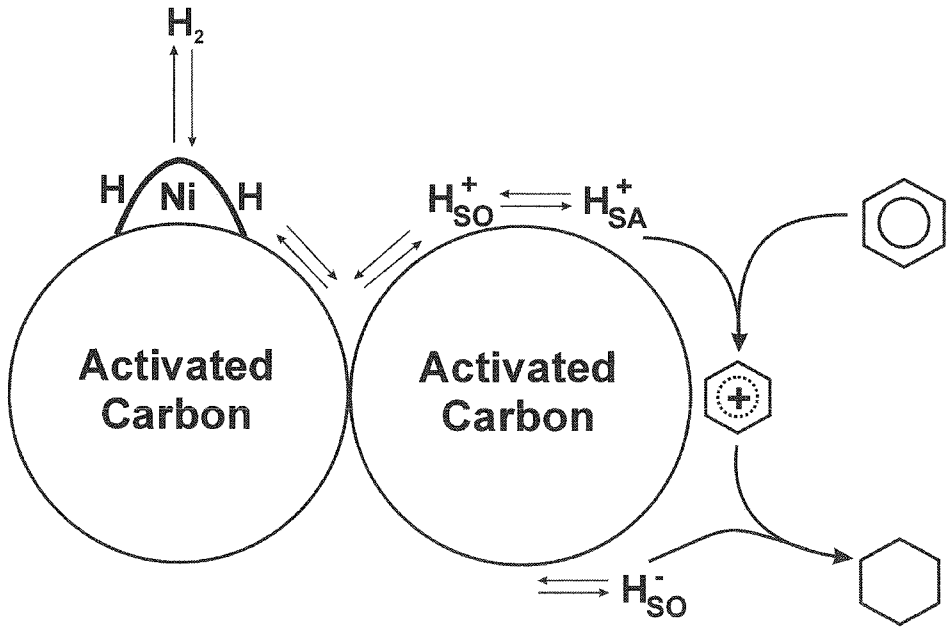

Figure VII-25. Mechanism of spillover phenomenon [40].
(H^+_{SA}: H^+ from acid site, H^+_{SO} and H^-_{SA}: ionic form of hydrogen spillover)

Recall that the hydrogen spillover consists in three steps: the dissociation of hydrogen on metal atoms, then the migration of the H atoms formed onto the support and finally their spreading over the support. Figure VII-25 shows the mechanism of benzene hydrogenation. The benzene molecule is adsorbed on the carbon surface and then hydrogenated by the spilt-over hydrogen. One may conclude that the intensity of this effect is certainly a function of the reactivity of metal atoms, the carbon-metal contact and the support specific surface area [22]. These factors depend on the method of preparation, the nature of the metal phase precursor and the metal content. The latter

parameters, in turn, influence on the catalytic activity which would be determined by both the metal and the support. 1Ni/AC-AH exhibited the smallest metal particles (attested by the XRD and TEM studies) which strongly interacted with the support (attested by the H_2-TPR experiments) and the highest specific surface area (Table VII-2). This could explain the highest performances observed with this catalyst. The necessary combination of the parameters invoked may also be one of the causes of the absence of correlation between catalytic activity and metal surface area we reported above: metal-carbon interactions and extent of specific area have also to be accounted for to explain catalytic activity.

3. CONCLUSIONS

The results obtained confirm the importance of the method of preparation, the nature of metal precursor and the metal content on the surface and hydrogenating properties in case of nickel catalysts supported on activated carbon.

Hydrazine non classical catalysts were found much more dispersed and more active in benzene hydrogenation than classically prepared catalysts. Better performances are obtained by hydrazine reduction of supported Ni^{2+} ions than by hydrazine precipitation-reduction method. Strikingly the reactivity of the metal surface atoms of the non conventional catalysts is comparable to that of Pt classical catalysts supported on activated carbon. This is the case of 5Ni/AC-AH which exhibited a turnover frequency of 0.2212 s^{-1} at 393 K, a value quite comparable to that of 5%Pt/AC (0.4694 s^{-1}). High dispersion and catalytic performances are favored by a low nickel content and by nickel nitrate rather than by nickel acetate precursor. Diluting the catalyst by the support led to increased activity in benzene hydrogenation as a result of the existence the hydrogen spillover effect. This was not reported before in the literature for nickel catalysts supported on activated carbon. Hydrogen spilt-over species were also found to be incorporated in the carbon frame during the pre-treatment of the catalyst at H_2/623 K. The discussion of the results obtained confirmed that hydrogen spillover effect is the driving force in the surface reactivity of nickel catalysts supported on activated carbon in hydrogenation reactions. Its intensity is the optimum combination of metal atoms reactivity, metal-support interaction strength and specific surface area extent.

Finally, it has to be underlined that hydrazine catalysts exhibit a specific surface area 1.5-2.0 times larger than that of classical catalysts. Gasification of carbon may have occurred during catalyst preparation in the hydrazine media and induced an increase of specific surface area.

The results obtained are an original contribution to the literature corpus data on nickel-carbon catalysts and benzene hydrogenation. The method of preparation used is original (hydrazine reduction of Ni^{2+} ions in aqueous media at 353 K) and leads to materials with much better surface and catalytic performances than classical preparation. Moreover, to our best knowledge, the hydrogenation of benzene on nickel catalysts supported on activated carbon has not been reported. The results obtained also give evidence for the hydrogen spillover occurrence in this reaction for the first time for a Ni-activated carbon system.

4. REFERENCES

[1] N. Pernicone, *Cattech* 7(6) (2003) 196

[2] L.R. Radovic, F. Rodriguez-Reinoso, in: P.A. Thrower (Ed.), *Chemistry and Physics of Carbon*, Vol. 25, Marcel Dekker, New-York, 1997, p.243

[3] L.M. Gandia, M. Montes, *J. Catal.* 145 (1994) 276

[4] C. Prado-Burguette, A. Linares-Solano, F. Rodriguez-Reinoso, C. Salinas-Martinez de Lecc, *J. Catal.* 128 (1991) 397

[5] L.C. Isett, J.M. Blakeley, *Surf. Sci.* 58 (1976) 397

[6] I.F. Silva, F.M.B. Fernandes, L.S. Lobo, in " *Actas del XIII Simposio Iberoamericano de Catalisis*,, Segovia, 1992, Vol. 2, p. 841.

[7] J.W. Larsen, J. Jandzinski, M. Sidovar, J.L. Stuart *Carbon* 39 (2001) 473

[8] F.A. Medina, J.W. Larsen, H. H. Schobert, J. Stuart *Fuel* 84 (2005) 1

[9] D. Mehandjiev, E. Bekyarova, M. Khristova, *J. Colloid. Interface. Sci.* 192 (1997) 440

[10] 1999 JCPDS 01-1260

[11] V. Siva Kumar, B.M. Nagaraja, V. Shashikala, A.H. Padmasri, S. Shakuntala Madhavendra, B. David Raju, K.S. Rama Rao, *Journal of Molecular Catalysis A*, 223 (2004) 313

[12] J. Krishna Murthy, S. Chandra Shekar, V. Siva Kumar, K.S. Rama Rao, *Catalysis Communications* 3 (2002) 145

[13] A. Bagreev, J. Lahaye, V. Strelko, , *PICS* 119, *Materiaux carbones adsorbants*, Zakopane, 195 (1994) in D. Mordenti, D. Brodzki, and G. Djega-Mariadassou, *J. Solid State Chemistry* 141 (1998) 114

[14] C.H. Bartholomew, R.B. Pannell, R.W. Fowler, *J. Catal.*, 79 (1983) 34

[15] J.T. Richardson, M. Lei, B. Turk, K. Forster, M.V. Twigg *Appl. Catal.*, 110 (1994)

[16] R. Molina, G. Poncelet *J. Catal.*, 173 (1998) 257

[17] J.J. Sholten, A.P. Pijpers, A.M.L. Husting, *Catal. Rev. Sci. Eng.*, 27 (1985) 151

[18] C. Li, Y-W. Chen, *Thermochimica Acta*, 256 (1995) 457

[19] J. Zieliński, *J. Catal.*, 76 (1982) 157

[20] A.G. Boudjahem, S. Monteverdi, M. Mercy, M.M. Bettahar *J. Catal.* 221 (2004) 325

[21] S.T. Srinivas, P.K. Rao, *J. Catal.* 148 (1994) 470

[22] A.D. Lueking, R.T. Yang, *Appl. Catal. A:General* 265 (2004) 259

[23] F. Coloma, A. Sepuvelda-Escribano, J.L.G. Fierro, F. Rodriguez-Reinoso, *Appl. Catal.* 150 (1997) 165

[24] A. Aguinaga, J.C. De la Cal, J.M. Asua, M. Montes, *Appl. Catal.* 51(1) (1989) 1

[25] A.G. Boudjahem, S. Monteverdi, M. Mercy, J. Ghanbaja, M.M. Bettahar, *Catal. Lett.* 97(3-4) (2004) 177

[26] A.G. Boudjahem, S. Monteverdi, M. Mercy, M.M. Bettahar, *Langmuir* 20 (2004) 208

[27] A.G. Boudjahem, S. Monteverdi, M. Mercy, M.M. Bettahar, *Appl. Catal. A.* 250 (2003) 49

[28] Keane M.A., *J. Catal.* 166 (1997) 347

[29] Molina R., Poncelet G., *J. Catal.* 199 (2001) 162

[30] P. Antonucci, N. Van Truong, N. Giordano, R. Maggiore, *J. Catal.* 75 (1982) 140

[31] S.D. Lin, M.A. Vannice, *J. Catal.* 143 (1993) 563

[32] I. Ionnanides, X. E. Verykios, *J. Catal.* 143 (1993) 175

[33] J.A. Anderson, L. Daza, J.L. Fierro, T. Rodrigo, *J. Chem. Soc. Faraday Trans.* 89 (1993) 3651

[34] F. Benseradj, F. Sadi, Chater M., *Appl. Catal. A*, 228 (2002) 135

[35] W.C. Conner, J.L. Falconer, *Chem. Rev.* 95 (1995) 759

[36] S.T. Teichner, A.R. Mazabrard, G. Pajonk, G.E.E. Gardes, C. Hoang-Van, *J. Colloid Interface Sci.*, 58 (1977) 71

[37] A.M. Sica, E.M. Valles, C.E. Giola, *J. Catal.* 51 (1978) 115

[38] V. Rahaman, M.A. Vannice, *J. Catal.* 143 (1991) 554

[39] S. Ceckiewicz, B. Delmon, *J. Catal.* 108 (1987) 294

[40] J. Wang, L. Huang, Q. Li, *Appl. Catal. A* 175 (1998) 191

[41] R. Wojcieszak, S. Monteverdi, M. Mercy, I. Nowak, M. Ziolek, M.M. Bettahar, *Appl. Catal. A* 268 (2004) 241

[42] M.G. Yang, I. Nakanamura, K. Fujimoto, *Appl. Catal. A* 127 (1995) 115

[43] B. Sen, J.L. Falconner, *J. Catal.* 117 (1984) 404

[44] S.D. Lin, M.A. Vannice, *J. Catal.* 143 (1993) 539

[45] S.D. Lin, M.A. Vannice, *J. Catal.* 143 (1993) 554

CHAPTER VIII
HYDROGEN STORAGE

INTRODUCTION

Un système efficace et bon marché de stockage est crucial pour la future utilisation de l'hydrogène comme porteur d'énergie dans les systèmes non polluants. Outre les systèmes à base de carbone, trois méthodes de stockage d'hydrogène ont été considérées en tant qu'alternatives pour le stockage. Ce sont la compression de l'hydrogène, la liquéfaction de l'hydrogène et les hydrures métalliques. Cependant, ces méthodes sont sans attrait pour l'application automobile du à beaucoup de difficultés technologiques telles que la température cryogénique et la haute pression pour la compression et la liquéfaction de l'hydrogène. Le système des hydrures métalliques fonctionne dans des conditions raisonnables mais il est susceptible de l'empoisonnement d'alliage et il a un inconvénient majeur : un rapport massique hydrogène/métal H/M souvent petit. Par contre, l'adsorption d'hydrogène sur matériaux poreux carbonés semble être une résolution idéale. Ces matériaux offrent beaucoup d'avantages tels que la basse densité massique et une capacité de stockage élevée.

La nature des facteurs qui influencent le niveau du stockage d'hydrogène est encore contestée pour les matériaux carbonés nanostructurés. Dans le cas des nanofibres de carbone, il est suggéré que la présence des défauts superficiels peut dissocier l'hydrogène, qui s'intercale alors dans les plans de graphène. Plus généralement, l'effet des métaux résiduels, issus de la synthèse des nanomatériaux carbonés, dans la prise d'hydrogène, a été en grande partie non étudiée et non caractérisée. Ceci nous a incités à étudier des catalyseurs de nickel supportés sur un charbon actif commercial amorphe comme matériaux pour le stockage d'hydrogène. Le charbon actif est un matériau bon marché par rapport aux matériaux nanostructurés synthétiques du carbone. Le nickel est un métal largement répandu dans l'industrie.

Nous avons exploré plusieurs facteurs déterminant le niveau du stockage: méthode de préparation des catalyseur, nature du précurseur métallique, pourcentage de nickel et dilution de catalyseur par support. Les catalyseurs examinés sont ceux qui ont été étudiés dans l'hydrogénation du benzène dans le chapitre précédent.

1. INTRODUCTION

Interest in hydrogen, which contains more chemical energy per weight than any hydrocarbon fuel [1], as an energy source has grown dramatically since last two decades, and many advances in hydrogen production and utilization technologies have been made [2]. However, hydrogen storage technologies must be significantly advanced if a hydrogen based energy system is to be established [2].

An effective and cheap storage system is crucial for the future utilization of hydrogen as a pollution-free energy carrier [3]. However, the most important condition required for these systems is the safety for transportation or utility use. In addition to carbon adsorption, three other hydrogen storage methods were analyzed as on-board storage alternatives; these are: compression, liquid, and metal hybrids [3]. However, these methods are unattractive for vehicular application due to many technological difficulties such as high pressure and cryogenic temperature. The metal hydride system operates under reasonable conditions but is susceptible to alloy poisoning and has a weight drawback [4]. The first possibility, hydrogen adsorption in porous solids such as activated carbons, seems to be an ideal resolution. Moreover, the carbon-based material offers a lot of advantages such as low mass density and high storage capacity.

Condensation of hydrogen in high surface area carbon materials at liquid nitrogen temperatures has been demonstrated and verified as a viable hydrogen storage option [5]. The need for high pressure and need to maintain very low temperatures are major disadvantages. In recent years there has been considerable experimental and theoretical interest in the use of nano-structured carbon materials, especially in the form of tubes [6-8] fibers [9-10] and mechanically milled graphite [11] as potential hydrogen sorbents. However, claims of hydrogen storage capacity higher than the US Department of Energy of 6.5% by weight have not been reproducible by other groups [8,12]. On the other hand, an important feature of the hydrogen storage is that these materials contain metals (Fe, Co, Ni, Cu), the contents of which are rarely reported because of practical difficulties. The metals are used in the synthesis of the carbonaceous materials and cannot be completely removed during the purification process [13]. Therefore, well characterized material such as activated carbon is more appropriate for studying the influence of metals on their hydrogen adsorption property.

The nature of the factors that influence the level of hydrogen storage is still disputed. In the case of carbon nanofibers, it has been suggested that the presence of

defects in the surface structure may dissociate hydrogen, which then intercalates in the graphene planes [13]. The pre-treatment in neutral, oxidative or reductive atmosphere may modify the structural properties of the carbon material in many ways: purification by removal of the adsorbed species [14], opening of the carbon structure [15], increased graphitization [16], activation of the solid [13]. Changes were also observed in the carbon material structure after exposure to high-pressure hydrogen [17]. As a result, the structural modifications induce important changes in the hydrogen storage of the materials treated [13-16]. Metals used as catalysts for the preparation of carbonaceous materials for hydrogen storage may play a role in the hydrogen uptake [18-22].

The real effect of monometallic nickel on the level of hydrogen storage has not still received much attention, although, it has been recently reported implications of hydrogen spillover from NiMgO oxide onto carbon nanotubes for hydrogen storage [13]. More generally, the effect of residual metals in hydrogen uptake has been largely unstudied and uncharacterized. This prompted us to study nickel catalysts supported on an amorphous commercial activated carbon as materials for hydrogen storage. Activated carbon is a cheap material as compared to nano-structured synthetic carbon materials. Nickel is a metal widely used in the industry. We explored several factors determining the level of storage: method of catalyst preparation, nature of the metal precursor, metal loading and support catalyst dilution.

The catalysts examined were that studied in the hydrogenation of benzene in the precedent section.

2. RESULTS AND DISCUSSION

2.1. Characterization of the catalysts

The structural and surface properties of the nickel supported catalysts studied in the high pressure hydrogen storage were discussed in details in Chapter VII. The brief recall of these results is described below.

The activated carbon used has a BET surface area of 1073 m^2 g_{cat}^{-1} and a total pore volume of 0.596 cm^3 g_{cat}^{-1} comprising 64% of micropores. The wet impregnation method causes the changes in the texture of the final materials as shown in Table VIII-1.

Combined XRD and TEM studies of the 1%Ni hydrazine catalyst indicated the presence of very small particles (<5 nm) accompanied by bigger clusters. Classical 1%Ni nitrate catalyst was also found well dispersed. The dispersion decreased for greater nickel contents. However, these results are at variance with the hydrogen adsorption study. The discrepancies would be due to nickel embedding by the carbon support or formation of H-spiltover species during the hydrogen pre-treatment at 623 K which over/underestimate the real metal dispersion. The H_2-TPD study confirmed the existence of H-spiltover species (H/Ni >1 were found).

It is worth to note that calculations show that the maximum hydrogen uptake is at most of 0.007 wt% and is observed for 10Ni/AC–N. This amount is negligible as compared to the hydrogen uptake at high pressures as shown below.

The H_2-TPD study showed the hydrogen desorption at high temperature with the main peak of desorption starting from 1000 K for all the materials and a minor one at lower temperatures (around 760–780 K) in the presence of the metal phase only. For the low temperature peak, the amounts are maximum $32.6*10^{-5}$ mol g_{cat}^{-1} (Table VIII-1) for 1Ni/AC-N classical catalyst. This is less than 0.1 wt%. If one expresses the corresponding H/Ni (mol/mol) ratios, it could be seen that the hydrogen desorption process is influenced by the nature of the precursor and, to a greater extent, by the nickel content. The highest (4.7–3.8) and lowest (0.2–0.6) H/Ni ratios are obtained with the low (0.5-1%) and high (5-10%) Ni content, respectively. This strikingly follows the decrease of the surface area or pore volume.

Table VIII-1. Characterization of catalysts.

Catalyst	BET Surface Area [$m^2\ g^{-1}_{cat}$]	Pore volume [$cm^3\ g^{-1}_{cat}$]	% of micropore volume	H_2 des[a] $*10^{-5}$ [$mol*g_{cat}^{-1}$]	Surface[b] metal area [$m^2\ g^{-1}_{cat}$]
0.5Ni/AC-A	1035	0.595	66.1	19.9 (4.7)[c]	0.10
1Ni/AC-A	1107	0.595	66.0	26.8 (3.1)[c]	0.13
3Ni/AC-A	945	0.586	65.2	32.1 (1.3)[c]	0.16
5Ni/AC-A	705	0.402	62.3	17.8 (0.4)[c]	0.85
7Ni/AC-A	654	0.385	64.3	22.0 (0.3)[c]	1.05
10Ni/AC-A	487	0.264	65.5	21.4 (0.2)[c]	1.55
1Ni/AC-AH	1694	0.743	80.8	37.6 (4.4)[c]	0.14
5 Ni/AC-AH	1348	0.678	72.3	49.2 (1.1)[c]	0.16
10 Ni/AC-AH	1056	0.572	65.5	40.2 (0.5)[c]	0.25
1 Ni/AC-N	1071	0.595	65.6	32.6 (3.8)[c]	0.01
5 Ni/AC-N	856	0.455	66.8	27.8 (0.6)[c]	0.03
10 Ni/AC-N	524	0.291	63.9	28.4 (0.3)[c]	0.27
AC	1073	0.596	66.4	8.71	-
ACH	1116	0.596	66.5	3.32	-

[a] from H_2-TPD study

[b] from H_2-adorption study.

[c] nH/nNi ratio

2.2. High-pressure hydrogen uptake studies at room temperature

2.2.1. Effect of the nickel content and method of preparation on hydrogen storage

In the absence of metal, the AC active carbon adsorbs small quantities of hydrogen: 0.12% wt. at 20 bars (Fig. VIII-2). This amount is 0.15%wt. when the hydrogen pressure was increased to 30 bars. Physisorption of hydrogen on activated carbons at room temperature and high pressures has been recently reported [23]. The uptake is at most 1.2%wt. at 700 bars. Extrapolation at 25 bars gives 0.16%wt for the ACFC sample which possesses a specific surface area of 1079 m^2 g^{-1}, similar to that of AC support. These characteristics are quite similar to that of the AC support. We also concluded that hydrogen is physisorbed on this support.

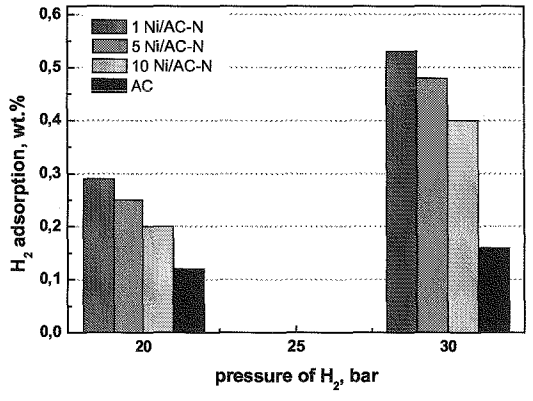

Figure VIII-2. Hydrogen storage for Ni/AC-N catalysts.

In contrast, in the presence of nickel, the amount of hydrogen stored sharply increases. For example, at 20 bars, the hydrogen uptake is 0.29wt.% for 1Ni/AC-N (Fig. VIII-2), that is 3 times higher than that of the pure active carbon. The uptake increases to 0.53% at 30 bars and is also 3 times higher than for carbon alone. Extrapolating the results reported in ref. 44, we calculated that physisorption on the carbon support for such amounts would need a pressure as high as 100 bars at room temperature. Moreover, at room temperature, thermodynamic experiments and calculations showed

that only at pressures of 50,000 bars, the H/Ni ratios will reach values closer to 1, which is where the phase transition of nickel hydride takes place [24-25]. This means that, under the most favorable experimental conditions we used, equilibrium H/M ratios in Ni will still be a quite small value (<<0.01). The obtained results (see Table VIII-2) let us concluded that the hydrogen was chemisorbed on the Ni/AC catalysts at 20 or 30 bars.

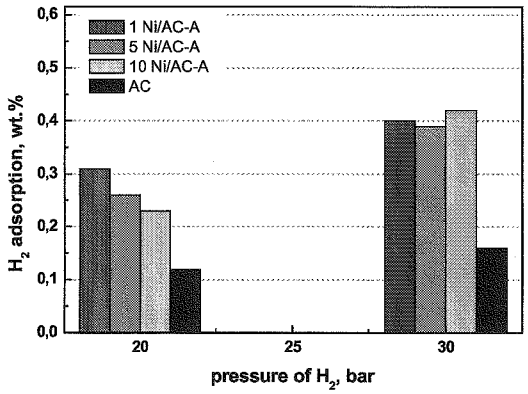

Figure VIII-3. Hydrogen storage for Ni/AC-A catalysts.

Another feature of the study is the decrease of the hydrogen uptake with the increase of the nickel content for all set of catalysts: for example, at 30 bars, it decreases from 0.53 to 0.48 or 0.40 wt. % when the nickel content increases from 1 to 5 or 10% in the case of the Ni/AC-N catalysts. The variation of the hydrogen uptake is clearer when it is expressed as the H/Ni ratio (Table VIII-2).

The Ni/AC-A catalysts are as active as the Ni/AC-N catalysts in the hydrogen storage at 20 bars (Table VIII-2, Fig. VIII-3). However, in contrast, their capability decreases when the pressure of hydrogen increases to 30 bars. At this pressure and for the nickel content of 1%, the H/Ni ratio is 23.4 (hydrogen uptake of 0.40% wt.) against 31.0 (hydrogen uptake of 0.50% wt.) for the nitrate precursor catalyst. The kind of precursor influences the hydrogen uptake.

Table VIII-2. High pressure hydrogen storage at 293 K.

Catalyst	Hydrogen storage [wt.%]		Hydrogen storage [molH/molNi]	
	20 bars	30 bars	20 bars	30 bars
0.5Ni/AC-A	0.30	-	35.29	-
1Ni/AC-A	0.31	0.40	18.19	23.38
3Ni/AC-A	0.29	-	5.68	-
5Ni/AC-A	0.26	0.39	2.89	4.29
7Ni/AC-A	0.24	-	2.01	-
10Ni/AC-A	0.23	0.42	1.22	2.21
1Ni/AC-AH	0.51	-	29.93	-
5Ni/AC-AH	0.40	-	4.45	-
10Ni/AC-AH	0.30	-	1.85	-
1Ni/AC-N	0.29	0.53	17.02	30.96
5Ni/AC-N	0.25	0.48	2.78	5.36
10Ni/AC-N	0.20	0.40	1.06	2.12
AC	0.12	0.16	-	-
ACH	0.17	-	-	-

The hydrogen uptake also depends on the method of preparation of the catalysts. The hydrazine non-classical catalysts showed higher storage capacity than the classical catalysts (Table VIII-2). For example, at 20 bars, the H/Ni ratio is 29.9 (hydrogen storage of 0.51% wt.) for 1Ni/AC-AH against 18.2 (hydrogen storage of 0.31% wt.) for 1Ni/AC-A.

2.2.2. Effect of the thermal treatment on the hydrogen storage

The hydrogen uptake is also influenced by the temperature of the pre-treatment as shown for the 1%Ni content catalysts at 30 bars in Table VIII-3. The results obtained show that the effect is significant at 30 bars for the nitrate catalyst. For 1Ni/AC–N the H/Ni ratio decreases from 31.0 to 26.3 or 19.7 when the pre-treatment temperature under a hydrogen flow is increased from 623 to 773 or 873 K. The total decrease is of 30%. The effect is not significant for 1Ni/AC-A catalyst.

Table VIII-3. Effect of the pre-treatment on the hydrogen storage at 293 K and 30 bars for the 1% Ni/AC catalysts (hydrogen storage in [nH/nNi]).

Catalyst	Pretreatment by H_2 (3h)		
	623K	773K	873K
1Ni/AC-A	23.38	21.4	21.2
1Ni/AC-N	30.96	26.3	19.7

2.2.3. Effect of the mechanical mixture on hydrogen storage

The effect of mechanical mixture of the catalyst and support was studied with various AC/(AC+catalyst) percentages (wt.%). The results for 1Ni/(AC-A+AC) mixtures are presented in Fig. VIII-4. The dilution of the catalyst by the support increases the H/Ni ratio for the prepared mixtures up to a maximum. This maximum (H/Ni=21) was found for the 1:4 mixture. For all the mixtures tested, the H/Ni ratio is >>1. This strongly confirms the intervention of the support in the hydrogen uptake. This is typically the behavior of the spilt over hydrogen species formed [26].

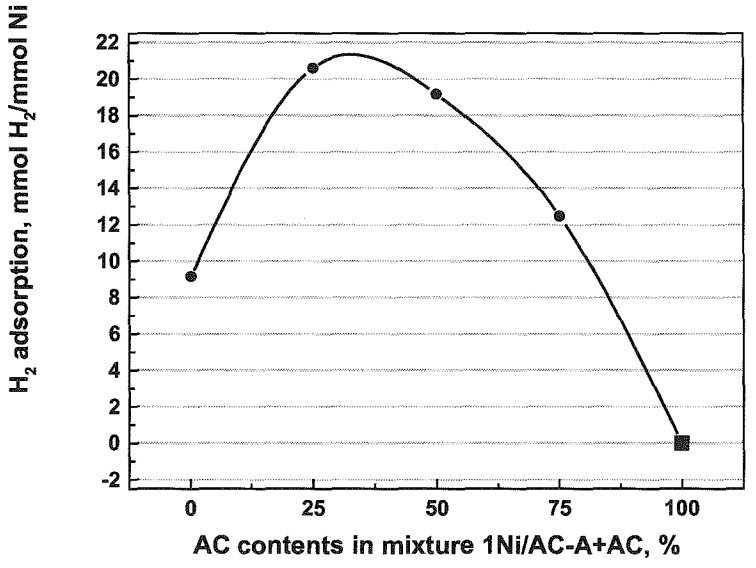

Figure VIII-4. Hydrogen storage at room temperature and 20 bars for mechanical mixtures 1Ni/AC-A+AC(●) and AC(■).

The hydrogen migration process is controlled by a distance factor. Dilution is believed to increase the number of H species stabilized by the active carbon by increasing the available surface area and, in the mean time, lowering the recombination rate of these species in molecular hydrogen. At a certain point, the additional surface area of the dilutent brings no further benefit to the hydrogen uptake. The H atoms formed would be stabilized on the graphite lattice [27].

3. DISCUSSION

The present results clearly show that nickel catalysts supported on active carbon could store significant amounts of hydrogen at room temperature, provided the pressure used is high enough to observe the phenomena. This hydrogen is desorbable under moderate conditions, namely room temperature and pressure.

The role of the metal in the hydrogen uptake is central for the metal-doped activated carbon prepared. Indeed, the uptake is much higher in the presence of the metal and also depends on the metal content, the nature of the metal precursor and the method of catalyst preparation. All these factors are known as determining in the metal

dispersion in case of metal supported catalysts [28-35]. However, close examination of the results obtained shows that there is no correlation between the metal surface area and the hydrogen storage capability of the catalyst. Indeed, increasing nickel content led to increasing metal surface area but decreasing hydrogen uptake (Tables VIII-1 and VIII-2). In contrast, the correlation is between the hydrogen uptake and the specific surface area which both decreased with increasing nickel content (Tables VIII-1 and VIII-2): the uptake level is restricted by the specific surface. The various effects of the metal are summarized on Fig VIII-5 – VIII-8 in case of Ni/AC-AH catalysts tested at 20 bars.

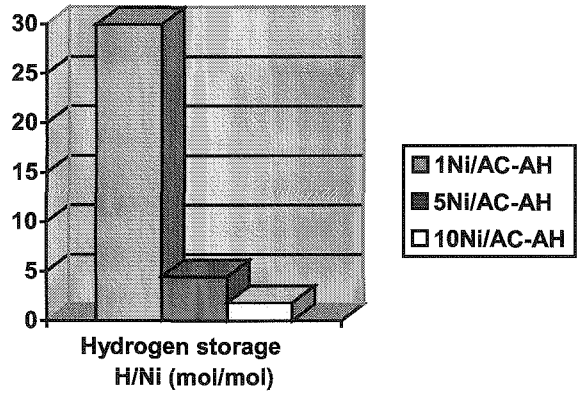

Figure VIII-5. Effect of Ni content on hydrogen storage.

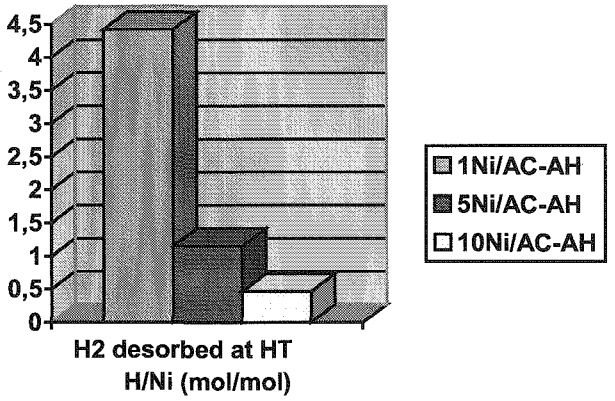

Figure VIII-6. Effect of Ni content on H_2 desorbed at high temperature.

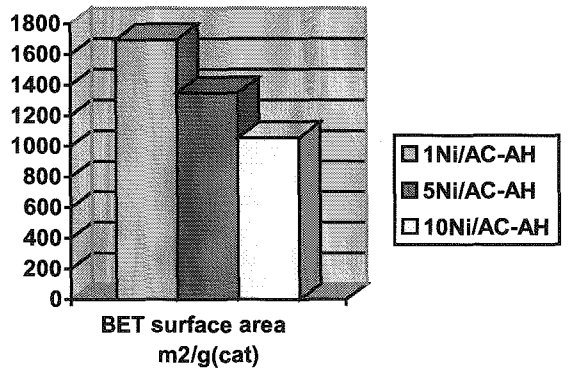

Figure VIII-7. Effect of Ni content on BET specific surface area.

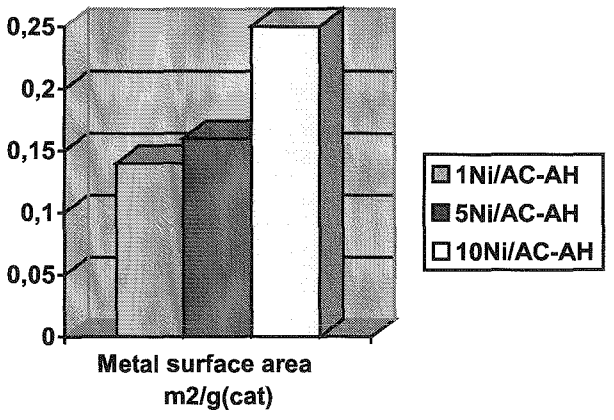

Figure VIII-8. Effect of Ni content on metal surface area.

These apparent contradictions could be explained by the mechanism of the hydrogen uptake, namely the hydrogen spillover effect, as confirmed by the study of the catalyst+active carbon mixtures (Fig. VIII-4). Indeed, the spillover effect may be influenced by textural factors in the carbon skeleton: the migration of the H atoms is probably inhibited in case of the 5 or 10%Ni catalysts because of decreasing specific area, as compared to 1%Ni catalyst. Moreover, the migration of the H atoms needs metal-carbon contacts to occur. The number and quality of these bridges depend on the structural and textural properties of the catalysts and also influence the hydrogen uptake level. These qualities may be encountered in the 1%Ni catalyst which is well dispersed.

The H_2-TPD study showed that hydrogen molecules were incorporated in the carbon support during the hydrogen pre-treatment at 623 K and desorbed at high temperatures only (750 K-780 K) through the direct and reverse spillover effects [35-37]. One may conclude that the hydrogen desorbing at room temperature in the high pressure experiments more likely results from the direct recombination on the active carbon surface then desorption. The loose bonding between the spilt-over species and the carbon surface allows a facile recombination in molecular hydrogen. Accordingly, a possible mechanism of hydrogen storage and desorption would be written as follows:

$$H_2(g) + 2\,M \Leftrightarrow 2\,H_M$$
$$2\,H_M + AC \Leftrightarrow 2\,H_C + 2M$$
$$2\,H_C \Leftrightarrow H_2(g) + AC$$

where M and AC denote metal and active carbon sites respectively and H_M and H_C metal hydrogen atoms adsorbed on a metal or carbon site respectively. It can be schematically presented as (Fig. VIII-9):

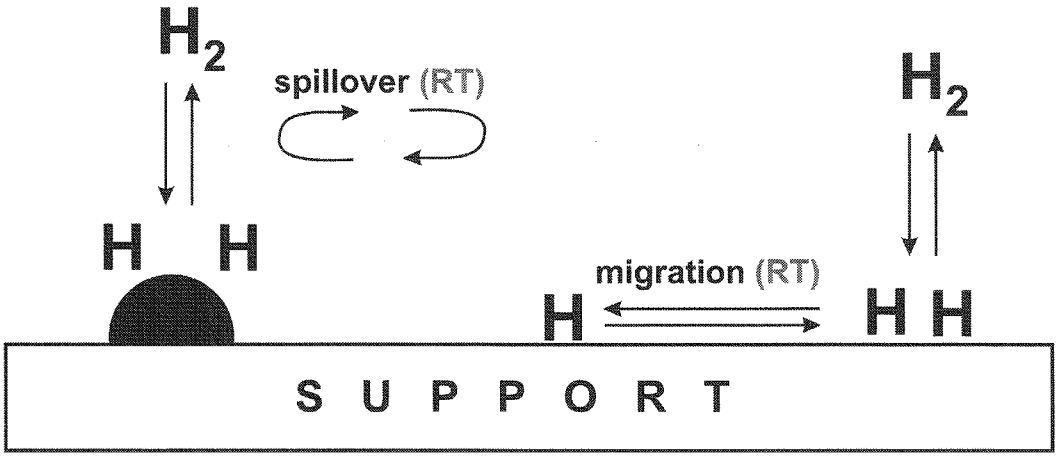

Figure VIII-9. Mechanism of hydrogen spillover at room temperature.

More striking, further examination of the results showed a remarkable correlation between the hydrogen stored at low temperature/high pressure and the hydrogen incorporated at high temperature during the hydrogen treatment at 623 K (Table VIII-1, Figure VIII-11), namely a correlation between low and high temperature spilt-over species. The latter species could play a role in the hydrogen storage through the following mechanism:

$$H_2(g) + 2M \Leftrightarrow 2\ H_M$$

$$2\ H_M + AC \Leftrightarrow 2\ S_C + 2M$$

$$2\ S_C \Leftrightarrow H_2(g) + AC$$

where S_C are carbon sites created by the high temperature hydrogen spilt-over species. The other symbols are similar to that described above. It can be schematically presented as (Figure VIII-10):

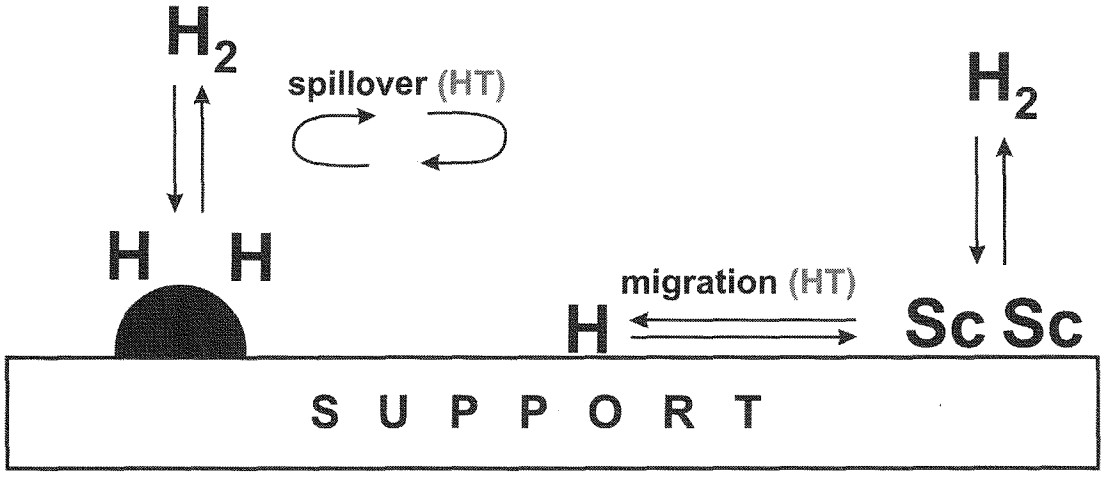

Figure VIII-10. Mechanism of hydrogen spillover at high temperature.

It has been suggested that spilt-over species may modify the electronic properties of a support and create new sites for the adsorption of hydrogen molecules from the gas phase [37-38]. It is also worth noting that spilt-over hydrogen species

linked to a carbon type support were found very active in catalytic hydrogenation reactions. This was demonstrated in the precedent section with the present catalysts. It has also been demonstrated, in case of Pt/active carbon, that benzene would be substantially and directly hydrogenated to cyclohexane on the carbon support [22].

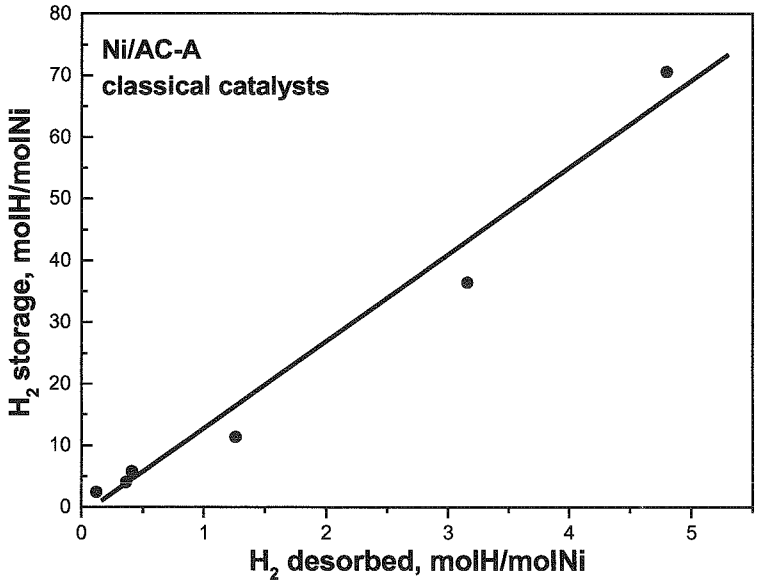

Figure VIII-11. Dependence of the hydrogen storage on hydrogen desorbed at high temperature.

The comparison of the performances of the Ni/AC materials studied with that published in the literature is not obvious. In effect, the various materials and conditions of observation of the hydrogen uptake are a serious obstacle for this comparison. Nevertheless, selected literature data show that these performances are in fairly good accordance with previous studies in similar conditions (Table VIII-4). These performances (H_2 uptake of 0.53%wt at 30 bars) may also be of a practical interest since 1% of hydrogen storage at room temperature and 100 bars is considered as a value close to the target from an application point of view [23]. The conditions of hydrogen uptake have not still been optimized. Calculations showed that the amounts of hydrogen

adsorbed at most represent 1% of monolayer (Table VIII-4). Improvements in metal dispersion or use of higher pressure may improve the hydrogen storage for commercial metal-doped active carbons. The support porosity may also be a crucial factor in hydrogen storage in active carbons, as showed several studies [23]. It needs further work for metal doped active carbons. It would also be of importance to study the effect of the nature of the metal on the hydrogen uptake.

High values in hydrogen storage have recently been claimed with carbon nanostructured materials: 1.9% at 50 bars [39], 3.7% at 69 bars [13], 4% at 100 bars [40], 6.3% at 148 bars [41] as compared to activated carbon materials (Table VIII-4). The graphene entities in carbon nanostructured materials would possess the required geometrical and electronical properties for the absorption of hydrogen and explains the reported performances [27]. In addition, it has to be stressed that these good performances were obtained by using not only high pressures but, also, metals as catalysts for the synthesis of the carbon nanostructures. In case of carbon nanotubes, the metal is directly incorporated in the material during the synthesis. As a result, the metal is intimately mixed with the carbon frame and stabilized in the final solid. This leads to increased metal-carbon contact which enhances the hydrogen spillover effect.

Table VIII-4. Literature data on hydrogen storage for various carbon supports.

material	wt.% H_2	m_{H2}/m_C [mg g_{cat}^{-1}]	H_2 monolayer [%]	volumeH_2/g_{cat} [L_{H2} g_{cat}^{-1}]	Ref.
1 Ni/AC-N 1071 m^2 g^{-1}	0.53	5.2	0.96	0.023 L g^{-1}	this work
AC 1062m^2 g^{-1}	0.15	1.5	0.28	0.016 L g^{-1}	
AC 3000 m^2 g^{-1}	0.3	3.0	0.20	0.036 L g^{-1}	[42]
AC* 1470m^2 g^{-1}	0.17	1.7	0.12	0.019 L g^{-1}	[43]
single-walled carbon nanotube 320m^2 g^{-1}	0.13	1.5	0.4	0.015 L g^{-1}	[44]
carbon nanofibre 70 m^2 g^{-1}	0.1	1.0	27.7	0.02 L g^{-1}	[42]

Unfortunately, as said before, because of practical difficulties, the metal content in nanotubes is rarely reported. This information would be useful for a better analysis of the performances published. We think that the H/metal ratio is a practical criterion in the definition of the performances of carbon materials used in the storage of hydrogen.

4. CONCLUSIONS

The present results clearly show that nickel catalysts supported on active carbon could store significant amounts of hydrogen at room temperature and high pressure (up to 0,53% at 30 bars against 0.1% for the activated carbon). These performances are in fairly good accordance with published results and may be improved in the near future.

The study shows that the hydrogen storage depends on the hydrogen pressure, the metal content, the metal precursor nature and the catalyst preparation method. Three main features arise from the results obtained. First, the hydrogen stored is loosely linked to the catalyst surface: the desorption is operated at room temperature and pressure. Second, the hydrogen spillover is mainly responsible of the formation of the hydrogen reservoir: e. g., the amounts of hydrogen stored increases by physically diluting the catalyst by the activated carbon. Third, the pore volume modulates the level of the hydrogen reservoir: the hydrogen reservoir volume decreases with decreasing pore volume. The best performance at 20 bars (%wt.) is obtained with the 1%Ni non classical hydrazine catalyst which exhibited the greatest specific surface area (1694 $m^2 g_{cat}^{-1}$) and micropore proportions (80.8%).

The discussion of the results shows that, at room temperature and high pressure, the hydrogen spiltover species are most probably stored on the activated carbon. The weak adsorption strength of these species allows an easy recombination and a direct desorption from the support at room pressure and temperature. Moreover, a close examination of the amounts of the hydrogen spilt-over species incorporated in the catalyst during the heat pre-treatment under hydrogen at 623 K, strongly suggests that these species may have created new acceptor sites on the carbon support. On these carbon sites, at room temperature and high pressure, the hydrogen would directly adsorbs from the gas phase. To summarize, the hydrogen reservoir may originate from two sources: i) hydrogen spiltover species adsorbed on the carbon support *via* the nickel

phase; ii) hydrogen species directly adsorbed from the gas phase onto carbon active sites generated by the H_2 pre-treatment at 623 K.

5. REFERENCES

[1] J. Petterson, O. Hjortsberg *KFB-Meddelande* 27 (1999) 1

[2] A.C. Dillon, M.J. Heben *Appl Phys A: Materials Science & Processing* 72(2) (2001) 133

[3] M. Rzepka, P. Lamp, M.A. de la Casa-Lillo *J Phys Chem B* 102(52) (1998) 10894

[4] S. Hirano, K.S. Young, K.A.G. Amankwah, J.A. Schwarz, in: *New Energy Systems and Conversions*, 1993, Universal Academy Press, Inc. p.67

[5] L.O. Valøen *Global Watch Electrochemistry* 2001, NTNU p. 1-20

[6] Q. Wang, J.K. Johnson *J Phys Chem B* 103 (1999) 4809

[7] F.L. Darkrim, P. Malbrunot, G.P. Tartaglia *Int J Hydrogen Energy* 27(2) (2002) 193

[8] R.T. Yang *Carbon* 38(4) (2000) 623

[9] Y.Y. Fan, B. Liao, M. Liu, Y.L. Wei, M.Q. Lu, H.M. Cheng *Carbon* 37 (1999) 1649

[10] A. Chambers, C. Park, R.T.K. Baker, N.M. Rodriguez *J. Phys.Chem. B* 102 (1998) 4253

[11] S. Orimo, G. Meyer, T. Fukunaga, A. Züttel, L. Schlapbach, H. *Fujii Appl Phys Lett* 75(20) (1999) 3093

[12] R. Ströbel, L. Jörissen, T. Schliermann, V. Trapp, W. Schütz, K. Bohmhammel, et al. *J Power Sources* 84 (1999) 221

[13] A. Lueking, R.T. Yang Hydrogen *AIChE Journal* 49(6) (2003) 1556

[14] A. Kuznetsova, J.T. Yates Jr, J. Liu, R.E. Smalley *J Chem Phys* 112(21) (2000) 9590

[15] P.M. Ajayan, S. Iijima *Nature* (London, United Kingdom) 361(6410) (1993) 333

[16] H. Zhu, X. Li, C. Lijie, C. Xu, D. Wu, Z. Mao *Mater Chem Phys* 78 (2003) 670

[17] B. Gupta, O.N. Srivastava *Int J Hydrogen Energy* 25 (2000) 825

[18] M.M. Shaijumon, N. Bejoy, S. Ramaprabhu *Appl Surf Sci* 242 (2005) 192

[19] H. Zhang, X. Fu, Y. Chen, S. Yi, S. Li, Y. Zhu, L. Wang *Physica B* 352 (2004) 66

[20] X. Chen, Y. Zhang, X.P. Gao, G.L. Pan, X.Y. Jiang, J.Q. Qu et al *Int. J. Hydr. Energy* 29 (2004) 743

[21] A. Lueking, R.T. Yang *J Catal* 206 (2002) 165

[22] A. Lueking, R.T. Yang *Appl Catal* 265 (2004) 259

[23] M.A. de la Casa-Lillo, F. Lamari-Darkrim, D. Cazorla-Amorós, A. Lineres-Solano *J Phys Chem B* 106 (2002) 10930

[24] M. Tkacz J *Chem Thermodynamics* 33 (2001) 891

[25] A. Driessen, P. Sänger, H. Hemmes, R. Griessen *J Phys Condens Matter* 2 (1990) 9797

[26] S.T. Srinivas, P.K. Rao *J Catal* 148 (1994) 470

[27] F.H. Yang, R.T. Yang *Carbon* 40 (2000) 437

[28] C.H. Bartholomew, R.B. Pannell, R.W. Fowler *J Catal* 79 (1983) 34

[29] J.T. Richardson, M. Lei, B. Turk, K. Forster, M.V. Twigg *Appl Catal* 110 (1994) 217

[30] R. Molina, G. Poncelet *J Catal* 173 (1998) 257

[31] J.J. Sholten, A.P. Pijpers, A.M.L. Hustings *Catal Rev Sci Eng* 27 (1985) 151

[32] C. Li, Y-W. Chen *Thermochimica Acta* 256 (1995) 457

[33] J. Zieliński *J Catal* 76 (1982) 157

[34] M. Houalla, B. Delmon *J Phys Chem* 84 (1980) 2194

[35] R. Wojcieszak, S. Monteverdi, M. Mercy, I. Nowak, M. Ziolek, M.M. Bettahar *Appl Catal A* 268 (2004) 241

[36] W.C. Conner, J.L. Falconer *Chem Rev* 95 (1995) 759

[37] U. Roland, T. Braunschweig, F. Roessner *J. Mol. Catal. A: Chemical*127 (1997) 61

[38] C. Park, P.E. Anderson, A. Chambers, C.D. Tan, R. Hidalgo, N.M. Rodriguez. *J Phys Chem B* 103 (1999) 10572

[39] H. Lee, Y-S. Kang, S.H. Kim, J.Y. Lee *Appl Phys Lett* 80 (2002) 577

[40] X. Li, H. Zhu, L. Ci, C. Xu, Z. Mao, B. Wei, et al. *Carbon* 39 (2002) 2077

[41] P-X. Hou, Q-H. Yang, S. Bai, S-T. Xu, M. Liu H.M. Cheng *J Phys Chem B* 106 (2002) 963

[42] E. Poirier, R. Chahine, T.K. Bose *J Hydrogen Energy* 26 (2001) 831

[43] K. Shindo, T. Kondo, Y. Sakurai *J of Alloys and Compounds* 379 (2004) 252

[44] H. Takagi, H. Hatori, Y. Soneda, N. Yoshizawa, Y. *Yamada Mater Sci and Engin B* 108 (2004) 143

CHAPTER IX
GENERAL DISCUSSION AND CONCLUSIONS

1. INTRODUCTION

Metallic nanoparticles exhibit unusual chemical and physical properties that are due to the combination of large proportion of high energy surface atoms as compared to the bulk metal. Generally the metal particles are obtained by the reduction of metal salt in hydrogen flow. However, the control of the size and structure of these particles is difficult. In the past two decades the chemical methods of reduction have been developed and largely studied. Different wet chemical methods for well dispersed metal nanoparticles preparation have been established. One of them is the chemical reduction with hydrazine in aqueous media. This relatively soft chemical method seems to be very useful for preparation of nickel nanoparticles with the small average particle size. However, it depends on the various parameters such as kind of the nickel precursor, kind of the support and the foreign ions addition. These parameters mutually influence on each other. This is discussed below.

For a useful discussion nickel catalysts supported on oxides and on activated carbon are presented separately.

2. OXIDES AS NICKEL CATALYSTS SUPPORTS

2.1. Reduction of the supported Ni^{2+} ions

Supported nickel catalysts are widely used in heterogeneous catalysis. The carrier on which the nickel is supported may be visualized as a porous material with a huge amount of surface contained in pores. The metal exists on the surface as small aggregates. It could be supposed that the nature of the support influences the reduction of nickel by hydrazine. In our study six different oxide supports were used. The supports were divided as follows:

- non reducible oxides such as alumina and silica
- reducible oxides such as CeO_2 and Nb_2O_5

The chemical and physical properties may influence the reduction of nickel ions. Its acidity, reducibility and extent of the interaction with nickel play important role in the complex chemistry of this reduction. These parameters are described below.

Recall that in the reduction of nickel with hydrazine, the metal phase is expected to proceed according to the following reaction [1]:

$$2Ni^{2+} + N_2H_4 + 4OH^- \rightarrow 2Ni^\circ + N_2 + 4H_2O \qquad (1)$$

After hydrazine injection at 353 K the solution became blue indicating the $[Ni(N_2H_4)_3]^{2+}$ complex formation. This complex is formed via the substitution of water ligands by hydrazine ligands. When the temperature is increased, the complex decomposes and the reaction media progressively changes to a dark black colloidal solution of metallic nickel and gaseous N_2 evolves according to equation (1). Moreover, it was shown that the reduction occurs in the same hydrazine media with a rate and conversion depending on the nickel content and reaction conditions [1]. In presence of a support, a supported $[Ni(N_2H_4)_n]^{2+}$ complex, more or less stable, is intermediately formed. It could more or less rapidly decompose to metallic nickel and gaseous N_2.

2.1.1. Support effects

The acidity of the supports used in this work was estimated on the basis of isopropanol dehydration. Intramolecular dehydration towards propene as well as intermolecular reaction producing diisopropyl ether occurs with the participation of acidic centers on the catalyst surface. For all matrices tested, propene was the main reaction product, indicating acidity of the materials. However, the conversion of alcohol (indicating acidity) depended on the nature of the support (Fig.IX-1) in the following order:

$$\mathbf{Nb_2O_5 >> Al_2O_3 >> SiO_2(V) \sim SiO_2(D) >> SiO_2(C) \sim CeO_2 \sim 0}$$

The hydrated niobium oxide (niobic acid) was found the most acidic. The lowest acidity was found for the CeO_2 and crystallized $SiO_2(C)$. Amorphous $SiO_2(V)$ and $SiO_2(D)$ showed medium acidity.

It is worth to note that the difference in the acidity of the $SiO_2(C)$ and $SiO_2(D)$ supports was evidenced by the FTIR-Pyridine measurements (see Figure VI-3, Chapter VI). The absence of Brønsted and very low Lewis acidity was found for crystallized $SiO_2(C)$ support. Contrary to that, the surface of the $SiO_2(D)$ support contains the Lewis acidity.

The acidity of the support was found to influence the reduction of nickel ions.

The reduction was inhibited in case of the Nb_2O_5 and γ-Al_2O_3–the most acidic supports. It is also the case for amorphous acidic $SiO_2(V)$ and $SiO_2(D)$ oxides. This is ascribed to superficial nickel mixed oxides, stable in the hydrazine media. Strikingly, the matrix exhibiting the highest acidity (hydrated Nb_2O_5) thoroughly reacted with Ni-acetate during the impregnation as evidenced from IR spectra (see Figure IV-9, Chapter IV). The Ni/Nb_2O_5 system is known to give rise to strong metal-support interaction [2-6]. Moreover, both Al_2O_3 and Nb_2O_5 supports adsorbed the hydrazine as evidenced by the H_2-TPR (Chapter III) and XPS (Chapter IV) studies. Hydrazine adsorbed species decomposed into gaseous hydrogen and nitrogen during the thermal treatment in hydrogen flow.

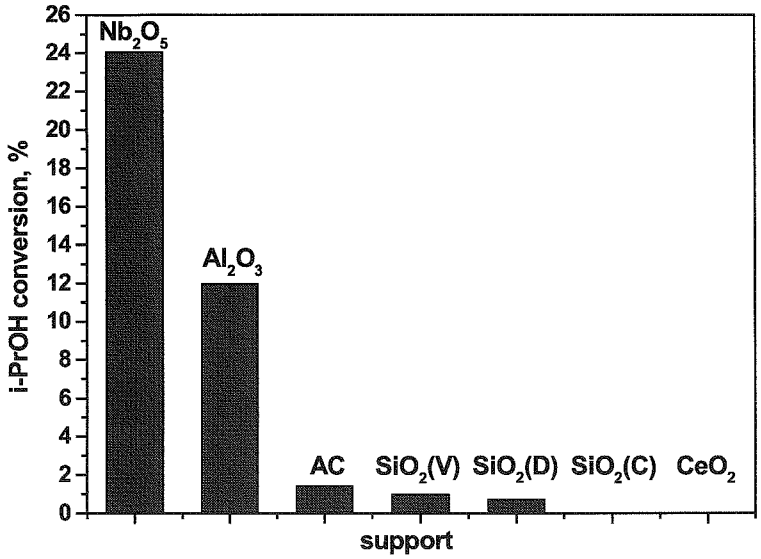

Figure IX-1. Isopropanol conversion for studied supports.

For Nb_2O_5 support, we remarkably succeeded in nickel reduction by using a stepwise procedure with 5%Ni content catalyst. Indeed, after three successive impregnations (1, 3 and 5wt.%Ni), the final $5NiNb_2O_5$-H solid was prone to the reduction by aqueous hydrazine at 353 K. The green color of the solid was changed to blue then dark and nitrogen was detected in the exit gas [see equation (1)].

It is now well established that stepwise impregnation of Ni/SiO_2 catalysts leads to strongly and weakly adsorbed Ni^{2+} [7]. Nickel in strong interaction is obtained by impregnation of the nickel salt followed by water-washing or by ion-exchange then calcination. Nickel in weak interaction is obtained by impregnation to Ni^{2+} ions previously strongly attached to silica. The latter ions serves as a "chemical glue" to the former [8]. Nickel in strong interaction is identified as phillosilicates or grafted nickel, depending on the preparation conditions. The anchoring of the metal particles onto the support was found to occur via Ni^{+} or Ni^{2+} ions located at the metal-support interface [9]. Basing on these data one can suggest that, for Ni/Nb_2O_5 catalysts, nickel ions are strongly anchored to the support up to 3% content and thus cannot be reduced by the hydrazine. These ions, in turn, make up an interface on which the excess nickel

introduced by the third impregnation weakly adsorbs and, consequently, becomes more reducible and gives rise to metallic nickel phase: the reduction by hydrazine then proceeds via reaction (1).

The less acidic supports, $SiO_2(C)$ and CeO_2, were found to accelerate the reduction of nickel ions. The transformation of $[Ni(N_2H_4)_n]^{2+}$ blue complex to dark colloid corresponds to nickel particles in reduced state occurs very easily. For CeO_2, redox properties have also to be considered. For $SiO_2(C)$ surface defects or impurities may play the role of active sites for the reduction.

2.1.2. Method of preparation

Two different methods of hydrazine preparation were used in this study: i) impregnated catalyst-reduction method (denoted as I method); ii) precipitation-reduction method (denoted as P method). Two supports were used for comparison: $SiO_2(C)$ and $SiO_2(D)$.

For the less acidic $SiO_2(C)$ support, the nickel ions were readily reduced whatever the method used: the green colour of the catalyst grain surface (I method) or of the solution (P method) turned to blue then to dark. In contrast, for the more acidic $SiO_2(D)$support, no reduction occurred whatever the method used. For the I catalyst, the $[Ni(N_2H_4)_3]^{2+}$ blue complex formed but did not transform to Ni° species: we can admit that the interactions between nickel complex and the silica surface on $SiO_2(D)$ are stronger than on the crystallized $SiO_2(C)$ silica. As a result, the reducibility of nickel is weakened. For the P catalyst, the blue solution readily discolored whereas the white silica surface grains became blue. No reduction occurred in this case also. The overall process is ascribed to $[Ni(N_2H_4)_3]^{2+}$ blue complex formation then fast precipitation on the support. Strong interactions with the support inhibited its subsequent reduction.

2.1.3. Silver ions addition

Similarly to the unsupported nickel nanoparticles [10], the addition of silver ions to the supported nickel catalysts accelerates the nickel ions reduction. This effect was remarkable for nickel catalyst supported on $SiO_2(D)$ support: the presence of Ag^+ ions induced a rapid reduction of Ni^{2+} ions whereas this reduction does not occur in their absence. In the presence of silver, the added metal is very easily reduced because the

Ag° particles formed played the role of active centers for nickel reduction. It has been shown that silver ions added to the reactant mixture accelerate the reduction of transition metals ions [10]. This effect was also observed during the reduction of nickel oxide with hydrogen in the presence of Ag_2O [11]. For SiO_2(C) supported nickel the reduction occurs in the presence or absence of silver.

2.2. Degree of reduction of nickel

2.2.1. Support effects

The degree of reduction was determined by oxygen adsorption, after a heat treatment under pure hydrogen (see Experimental Section). The obtained results show that the method of preparation, nature of the support or presence of silver as a metal additive determined the degree of reduction.

Let us illustrate these results first for the alumina and amorphous silica supported nickel catalysts (Table IX-1). Recall that the nickel precursor in these catalysts was not reduced in aqueous hydrazine but in the hydrogen atmosphere during the heat pretreatment.

Table IX-1. Characteristics of catalysts supported on SiO_2 and Al_2O_3.

catalyst	H_2 *10^{-5} adsorbed at RT [mol*g_{cat}^{-1}]	Dispersion [%]	Metal Surface are [m^2*g_{Ni}^{-1}]	Degree of Reduction [%]	TOF [molecBz*s^{-1}site^{-1}]		Conversion [%]	
					373 K	448 K	373 K	448 K
1 Ni/Al_2O_3	0.35	4.1	27.3	103	0,019	0.162	4.7	40
1Ni/EDTA/Al_2O_3	0.38	5.2	34.6	86.1	0,029	0.264	7.5	71
1 Ni/Al_2O_3-H	0.34	9.5	62.4	42.7	0,004	0.320	0.98	77
1Ni/EDTA/Al_2O_3-H	0.17	3.0	18.8	70.6	0,009	0.425	6.5	51
1 Ni/SiO_2(V)	0.59	10.2	9.9	68.7	0,103	0.235	43	98
1Ni/EDTA/SiO_2(V)	0.12	5.0	20.0	27.0	0,040	0.354	3.4	30
1 Ni/SiO_2(V)-H	0.60	8.4	12.0	84.6	0,062	0.229	26	98
1Ni/EDTA/Si(V)-H	0.00	-	-	67.7	-		0	0

Strikingly, the degree of reduction of hydrazine catalysts differ from that of classical catalysts. It may be concluded that the hydrazine treatment, whether it really reduces nickel or not, influences on its reducibility in the hydrogen atmosphere. This influence, in turn, depends on the nature of the support and method of preparation (SIM versus DIM).

For the acidic Nb_2O_5 support, hydrazine and classical catalysts gave rise to various degrees of reduction (Table IX-2). The amorphous hydrated Nb_2O_5 support is reduced with hydrogen into the bluish-black dioxide NbO_2 that has a distorted rutile structure [12]. This reduction is reversible so the NbO_2 reoxidized gives the Nb_2O_5. Taking into account this reaction the degree of reduction after H_2 treatment at 773 K was 54.4% for calcined Nb_2O_5. Note that after a previous aqueous hydrazine treatment, hydrated Nb_2O_5 is reduced, with a yield of 27% only, to probably NbO_2 also. The reduction extent of the support was taken into account for calculation of the degree of reduction of the nickel-niobia catalysts, supposing the same degree of support reduction. This is obviously an approximation since, in the presence of nickel, the reduction of Nb_2O_5 was facilitated according to the TPR study (see Chapter IV). The values obtained are in fact maximum degree of reduction. From Table IX-2 it can be seen that the degree of reduction changes with the nickel content and method of preparation.

Table IX- 2. Characteristic of the nickel catalysts supported on CeO_2 and Nb_2O_5.

catalyst	H_2 *10^{-5} adsorbed at RT [mol*g_{cat}^{-1}]	Dispersion [%]	Metal Surface are [m^2*g_{Ni}^{-1}]	Degree of Reduction [%]
1NiNb$_2$O$_5$	-	-	-	**78.2**
1Ni/EDTA/Nb$_2$O$_5$	-	-	-	**89.3**
1NiNb$_2$O$_5$-H	-	-	-	**86.6**
1Ni/EDTA/Nb$_2$O$_5$-H	-	-	-	**104**
5NiNb$_2$O$_5$	-	-	-	**123.4**
5NiNb$_2$O$_5$-H	-	-	-	**89.2**
1NiCeO2-H	**0.36**	**4.2**	**28.7**	**86.8**
3NiCeO2-H	**0.63**	**2.4**	**16.5**	**91.3**
5NiCeO2-H	**1.06**	**2.5**	**16.8**	**92.5**

Remarkably, excess reduction (123%) is obtained with classical $5NiNb_2O_5$ catalyst, probably as a result of excess reduction of niobium oxide in the presence of nickel, not taken into account in our calculations. In contrast, for hydrazine treated materials, increasing nickel content from 1 to 5wt.% does not increase the degree of reduction, although the metal phase became more reducible according to the TPR study (Figure IV-11 – IV-16, Chapter IV). Recall that $5NiNb_2O_5$-H comes from a stepwise preparation method which included the intermediate formation of nickel species firmly attached to the support. These species were less prone to reduction.

$NiCeO_2$-H catalysts are highly reduced (86%- 93%) in the hydrazine media. Redox properties of ceria are probably involved in the mechanism of reduction [13].

2.2.2. Silver additive effect

Silver alone is totally reduced for both SiO_2(C) and SiO_2(D) silica supports as did nickel alone (99.7%) on the former support only. The silver additive has an influence on the degree of reduction as reported in Table IX-3.

i) for impregnated bimetallic catalysts, the reduction is deeper with SiO_2(D) (91.6%- 99.9%) than with SiO_2(C) support (76.2%- 85.5%) due to greater specific surface area which gives rise to a greater metal dispersion in the supported precursor and then to a deeper reduction of nickel.

ii) for precipitated catalysts, the degree of reduction practically does not depend on the nature of the support. This is because, in the hydrazine media, metal particles mainly formed in the solution or in the vicinity of the support, not on the support.

iii) in bimetallic systems, the higher the silver content the deeper the reduction is. As reported above, reduced silver particles form tiny metallic particles acting as foreign nuclei for subsequent growth of nickel particles. More silver ions introduced to the reactant mixture more silver nuclei for nickel particles growth and deeper the reduction is.

iv) the higher degree of reduction found for the monometallic nickel catalyst as compared to the bimetallic catalysts could be explained by the different structure of the metal particles formed on silica surface. In case of the Ni catalysts the TEM study

showed the presence of the whisker like nickel particles while for the bimetallic catalysts the only spherical particles were observed.

2.3. Dispersion of the nickel active phase

2.3.1. Effect of the nature of the support

We have shown that, in case of acidic non reducible oxide supports, hydrazine–treated nickel catalysts, although not reduced in this media, are reduced to different extents as compared to classical catalysts under a hydrogen heating flow. Changes were also found for metal dispersion. Metal dispersion varied with the nature of the support and method of impregnation (SIM versus DIM) (Table IX-1). For example, nickel alone is better dispersed on SiO_2(V) (10.2%) than on alumina (4.1%) for SIM classical catalyst. This is not the case of DIM or hydrazine catalysts.

In case of the acidic reducible oxides the results obtained confirmed that niobia is a typical SMSI oxide whatever the method of impregnation (SIM versus DIM) or preparation (classical versus non classical) or nickel content. No surface nickel atoms were detected in hydrogen adsorption experiments (Table IX-2). It could be proposed that preferential deposition on nickel occurred on the niobia monolayer which is more difficult to reduce and which could favor the formation of nickel niobate compounds. The very strong nickel-niobia interaction could play a crucial role in the passivation phenomenon of nickel active sites towards the hydrogen.

Contrary to the niobia catalysts the results showed that the chemical reduction by hydrazine of nickel supported on CeO_2 oxide catalysts occurred very easily. Dispersion passed through a minimum with increased nickel content (Table IX-2). It is very well known that metal loading influences the metal dispersion on the support. More metal ions present during the impregnation gives rise to particle size growth. It is worth noting that dispersion increased with decreasing degree of reduction. Influence of the degree of reduction on particle size growth is well known [14-15]. It is admitted that decreasing the degree of reduction of metal ions induces the smaller particle growth: the unreduced metal species slowdown the rate of migration and agglomeration of the metal atoms with the metal particle formed.

2.3.2 Influence of the silver additive

The dispersion of the nickel active phase on the surface was found to depend on the silver concentration (Table IX-3).

For impregnated catalysts, dispersion decreases with increased silver content. Dispersion decrease could be explained by the fact that the metal dispersion is already determined in the impregnation step and depends on the Ni/Ag ratio. It is known that silver does not adsorb the hydrogen and this was verified here. It means that more silver atoms exposed on the surface lower hydrogen adsorption will occur. TEM images showed the existence of bimetallic aggregates with a Ni/Ag of 1 and comprising Ni and Ag clusters separated during the hydrazine reduction. For bimetallic catalysts, Ag° metal particles are readily formed and play the role of active centers for nickel reduction. As to the growth processes of the metal nuclei formed, it is expected to occur through surface diffusion for almost all the nuclei formed. In other words, the final size would be determined by the primary metal particles formed.

It is noticeable that the support nature of impregnated catalysts plays some role. Indeed, it has to be noted that the less acidic and very low surface area support led to better dispersion (4.3%- 5.9% against 3.4%- 5.1%) (Table IX-3).

Interestingly also, for impregnated catalysts, metal dispersion increased with decreasing degree of reduction (Table IX-3). Indeed, as reported above, decreasing the degree of reduction of metal ions induces the smaller particle growth: the unreduced metal species slowdown the rate of migration and agglomeration of the metal atoms with the metal particle formed.

Table IX-3. Characteristic of the bimetallic Ni/Ag catalysts.

catalyst	H_2 *10^{-5} adsorbed at RT [mol*g_{cat}^{-1}]	Dispersion [%]	Degree of Reduction [%]	Conversion [%] 373 K	TOF [molecBz*$s^{-1}$$site^{-1}$] 373 K
1NiPC	0.39	4.5	95.6	15.2	0.059
90NiAgPC	0.27	5.2	72.2	1.2	0.007
75NiAgPC	0.63	11.4	85.3	100	0.233
50NiAgPC	0.27	6.7	93.2	21.5	0.115
1NiIC	0.62	7.2	99.7	61.7	0.149
90NiAgIC	0.34	5.9	76.2	31.4	0.136
75NiAgIC	0.28	5.3	82.7	30.7	0.163
50NiAgIC	0.20	4.3	85.5	17.9	0.132
90NiAgPD	0.52	7.6	85.2	1.6	0.004
75NiAgPD	0.45	8.2	86.2	6.5	0.022
50NiAgPD	0.35	8.8	95.6	85.3	0.341
90NiAgID	0.35	5.1	91.6	12.5	0.052
75NiAgID	0.24	3.8	99.1	3.1	0.019
50NiAgID	0.15	3.4	99.9	0	0.000

In contrast to impregnated catalysts, for precipitated catalysts, dispersion increases with silver content. In thos case the reduction and particle growth take place in solution or in the vicinity of the support (with the help of the silver) and metal dispersion may be determined during the $[Ni(N_2H_4)_3]^{2+}$ complex precipitation. Ag° metal particles formed also play the role of active centers during the nickel reduction processes. For precipitated catalysts one can speculate the existence of a great number of homogeneously distributed Ag° centers in solution on which nickel ions are readily reduced and subsequently grow. This could explain the increase of metal dispersion with increasing the silver content (Table IX-3). More silver ions introduced to the

reactant mixture more silver nuclei for nickel particles growth. Study of electronic and structural properties of these systems by means of magnetism, XPS, UV-vis, Raman is in hand. Preliminary magnetic experiments suggests the existence of Ag-core Ni-shell structure for 75NiAgPC catalyst.

Interestingly, the effect of silver on dispersion is relatively weak on the highest surface specific area SiO_2(D) support (7.6%- 8.8%) and more intense (up to 11.4%) on the lowest surface specific area SiO_2(C) support. This could mean that, although the reduction probably takes place mostly in solution, the overall process could be controlled by liquid/solid surface equilibriums. The effect of the support adds to that of the silver additive.

2.4. Activity of the nickel catalysts towards hydrogen

Metallic nickel adsorbs very limited amounts of hydrogen under ordinary conditions but is known to form a nearly stoichiometric hybride NiH at high hydrogen pressure [16]. However, not always the nH/nNi ratio near 1 (or more) confirms the nickel hybride formation. It is very well known that reduction of nickel supported catalysts at high temperature in hydrogen flow may result in strongly chemisorbed hydrogen, give rise to hydrogen spillover effect or affect reduction of the support resulting in the alloy formation with atoms from the support [17]. Especially, hydrogen spillover phenomenon seems to be very important in heterogeneous catalysis because most of the catalysts consist in small metal particles supported on high surface area oxides or carbon, and many catalytic reactions involve hydrogen [18]. Hydrogen spillover takes place during surface measurements, then nH/nNi ratios much greater then one can be obtained [18]. In this case the H_2 chemisorption is not always a viable method for metallic surface area measurements.

Hydrogen spillover effect can also be observed by the H_2-TPD desorption study. It could be considered that the hydrogen desorbed at high temperatures is due to the strongly chemisorbed hydrogen or reverse spillover. Moreover, the desorption nH/nNi ratios near or higher than 1 can testify the spillover effect. It was postulated that hydroxyls groups on the support stabilize spiltover hydrogen. Also the amount of hydrogen spiltover strongly depends on the acidity of the support [18]. During the high temperature reduction with H_2 the spiltover hydrogen can react with the hydroxyl groups present on the support surface giving rise to water production and active sites

creation. These sites are very active in the catalytic processes. The number of these active sites can be estimated assuming that one water molecule is produced for each hydroxyl that reacts with spiltover hydrogen [18]. The concentration of active sites created on silica surface was estimated to be in order to 10^{12} sites per cm^2 of the surface [19]. This concentration is dramatically higher in case of the carbon supports where 10^{13}-10^{15} sites per cm^2 have been estimated [20].

The H_2-TPD study permits to designate different species of nickel active phase. The desorption of hydrogen depends on the interaction between hydrogen molecule and nickel active phase. Temperature of desorption could give the information about the hydrogen-nickel strength. Generally, for all catalysts we studied, the TPD profiles showed two main domains of desorption in low and high temperature. The first peak of desorption at low temperature could be attributed to the hydrogen weakly adsorbed on the nickel surface and the second peak with the maximum of desorption at high temperature originates from the desorption of hydrogen strongly adsorbed on nickel surface or/and from the reverse spillover effect.

The amount of hydrogen spiltover strongly depends on the acidity of the support [3], the hydroxyls groups being responsible for the migration of hydrogen spiltover onto the support. One could be supposed that the quantities of desorbed hydrogen would be depend on the support acidity. Indeed, as shown in Figure IX-3, the amounts of hydrogen desorbed during the H_2-TPD study for nickel catalysts supported on SiO_2, CeO_2 or Nb_2O_5 oxides increase with increasing the support acidity.

It can be seen also from Tables IX-4 and IX-5 that the most acidic SiO_2 (D) silica desorbs more hydrogen than the less acidic SiO_2 (C) silica in case of supported Ni-Ag systems. However, this order also comprises the influence of the specific surface area, which is bigger for SiO_2 (D) support. Indeed, the intensity of the spillover effect depends on the specific area extent. Distances as long as 12 cm were found to be crossed by H spiltover species on metal supported catalysts [18]. Note that this order also takes into account, the strength of the metal-support interactions which are much more important with SiO_2 (D) (recall that Ni^{2+} ion reduction started only in the presence of the silver additive) than with SiO_2 (C).

Further, hydrogen spillover also depends on metal-support contacts or bridges (number and structure). The higher the metal dispersion the larger the metal-support interface (or greater the number of metal-support contacts) the more intense the spillover is. This is observed with the higher the case SiO_2 (D) support which interacted

much more with the metal phase: the amounts of hydrogen desorbed increases with increasing dispersion (Table IX-5). No such a correlation is observed with SiO_2 (C) where metal-support are rather bad (Table IX-4). These bad interactions are more striking for SiO_2 (C) precipitated catalysts which, although they adsorbed hydrogen at room temperature, desorbed almost no hydrogen. In this case, the hydrogen interacted loosely with the catalyst and, most probably, rather interacted with the nickel component than with the support.

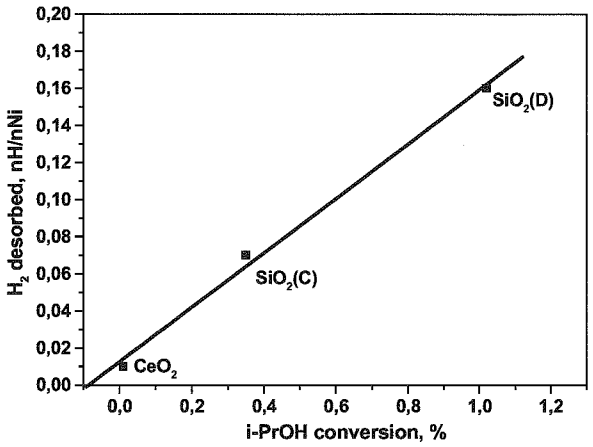

Figure IX-2. Hydrogen desorption versus isopropanol decomposition.

Table IX-4. Desorption data for Ni/SiO_2(C) catalysts.

catalyst	Dispersion [%]	Ni %	H_2 des. [nH/nNi]	catalyst	Dispersion [%]	Ni %	H_2 des. [nH/nNi]
90NiAgPC	**5.2**	**0.90**	**0.02**	**90NiAgIC**	**5.9**	**0.90**	**0.07**
75NiAgPC	**11.4**	**0.75**	**0.03**	**75NiAgIC**	**5.3**	**0.75**	**0.12**
50NiAgPC	**6.7**	**0.50**	**0.02**	**50NiAgIC**	**4.3**	**0.50**	**0.13**

Table IX-5. Desorption data for $Ni/SiO_2(D)$ catalysts.

catalyst	Dispersion [%]	Ni %	H_2 des. [nH/nNi]	catalyst	Dispersion [%]	Ni %	H_2 des. [nH/nNi]
90NiAgPD	**7.6**	**0.90**	**0.13**	**90NiAgID**	**5.1**	**0.90**	**0.16**
75NiAgPD	**8.2**	**0.75**	**0.24**	**75NiAgID**	**3.8**	**0.75**	**0.19**
50NiAgPD	**8.8**	**0.50**	**0.37**	**50NiAgID**	**3.4**	**0.50**	**0.25**

2.5. Activity of the nickel catalysts in benzene hydrogenation

Catalytic activity is known to be determined by the metal particle size (or dispersion) and shape which, in turn, depend on the method of preparation, the metal content, the nature of the support and the presence of a second metal additive. The nature of the chemical processes involved could also be rate determining. All these factors are acting in the hydrogenation of benzene on the prepared catalysts. Recall that this reaction is favored on acidic supports on which the benzene molecule is activated and reacts with H atoms through the hydrogen spillover effect [21-22].

2.5.1. Effect of the support

Catalytic activity of non reducible oxide catalysts is typically a combination of the several factors involved. For $1NiSiO_2(V)$ catalysts, TOF is almost proportional to the metal dispersion which seems to be rate determining (Table IX-1). In contrast, classical $1NiSiO_2(V)$ is twice more dispersed as compared to classical $1NiAl_2O_3$ whereas its TOF (at 373 K) is five fold greater. Maximum activity of the silica catalyst was found to occur at a lower temperature (448 K) than for the alumina catalyst (473 K). In the same way, for non classical $1NiAl_2O_3$-H, the dispersion is twice that of classical $1NiAl_2O_3$ whereas its TOF is five fold lower.

Very high acidity of the niobia supports give rise to the very strong metal support interaction. The catalysts supported on Nb_2O_5 were found to be completely inactive in the benzene hydrogenation.

The MSI have been claimed for classical nickel catalysts supported on CeO_2 [23]. Our results well confirmed this effect (Table IX-6). 1 and 5%Ni catalysts exhibit similar reactivity (same TOF and same temperature for maximum activity) with different dispersions. Reactivity and dispersion is minimum for the 3%Ni catalyst. According to the literature data, two effects of SMSI could be invoked, namely the decoration of the metal particles by cerium suboxides patches and formation of metal–cerium alloys [24]. These effects would not affect the structure insensivity of the benzene hydrogenation reaction. However, they can modify the intrinsic activity of the catalysts.

Table IX-6. Activity of the nickel supported on CeO_2 catalysts.

catalyst	TOF [molecBz*s^{-1}site^{-1}]		Conversion [%]	
	373 K	448 K	373 K	448 K
1NiCeO$_2$-H	0,010	0.111	2.6	26.9
3NiCeO$_2$-H	0,004	0.025	1.5	10.3
5NiCeO$_2$-H	0,011	0.079	7.7	54.7

Note that the H_2-TPD study evidenced surface H-species desorbing at a much lower temperature for 1 and 5%Ni catalysts (300 K- 450 K) than 3%Ni catalyst (from 675 K only). This suggests the existence of low energy activation sites for the hydrogen, producing very reactive H-species during the hydrogenation reaction.

Despite the base character of the support, the existence of the spillover hydrogen phenomenon could also operate in the hydrogenation reaction over the Ni/CeO_2-H catalysts [25-26]. H-Spilt-over species under reducing conditions contributes to achieve the reduction of the nickel ions or even produce Ce^{III} sites through an electron transfer from the nickel particles to ceria [26]. The hydrogen dissociates at the nickel (Ni^0) surface and transfers protons to the ceria support, generating new hydroxyl groups. The high activity is explained in this case by the excess of electrons at the metal surface.

2.5.2. Effect of the silver ion addition

The results obtained on the effect of silver additive on the catalytic activity at 373 K are reported in Tables IX-3. Silver is inactive in the reaction. The TOF's are higher with SiO_2(C) than with SiO_2(D) and for precipitated than for impregnated catalysts. In addition, important gaps of activity are observed for 75NiAgPC (0.007 s^{-1}→0.233 s^{-1}) and 50NiAgPD (0.004 s^{-1}→0.341 s^{-1}) catalysts as compared to that of their homologues. Moreover, at 348 K, the values observed (0.061-0.084 s^{-1}) are higher than the standard values reported for nickel catalysts (0.005-0.033 s^{-1}) [27-28] and close to that obtained for platinum catalysts at 333 K (0.033-0.078 s^{-1}) [29].

For impregnated catalysts, incorporation of silver as a second metal decreases the catalytic activity in parallel with the metal dispersion due to the existence of separate Ni and Ag phases. For these catalysts it is worth noting the correlation between metal dispersion, degree of reduction and catalytic activity: increased silver content led to increased metal dispersion and activity [with maximums for SiO_2(C) support] (Table IX-3). It is believed [30] that the presence of unreduced metal at the support surface diminishes the metal particle size required for the adsorption of benzene in a planar mode; also the TOF's increased with increasing metal dispersion and decreasing degree of reduction.

In contrast, with the precipitated catalysts the metal dispersion and activity increased the silver content. Thus could be accounted for Ni-Ag groupings, generated in hydrazine solution during precipitation of metal particles on the support, and active in benzene hydrogenation. Structural properties of these groupings may be responsible for the high activity of 75NiAgPC and 50NiAgPD catalysts. As reported above, preliminary magnetic experiments suggests the existence of Ag-core Ni-shell structure for 75NiAgPC catalyst.

For a more refined analysis of the activity results, one has to get in mind that the overall reactivity of a catalyst is determined not only by structural properties of metal particles but also by surface chemical processes. In benzene hydrogenation over metal supported catalysts, it is believed that the reaction occurs both on the metal and on the support through the hydrogen spillover [29, 31-33]. In this way, the acidity of the support (strength and concentration of acidic sites) plays an important role [32-34]. Remarkably, the highest TOF is obtained with 50NiAgPD (0.341 s^{-1}) with the more acidic SiO_2(D) support. Moreover, it is worth noting that this catalyst also exhibits the

highest amount of hydrogen desorbed at high temperature, i. e. hydrogen species incorporated in the support and identified as spilt-over species.

Interestingly, from Table VI-5, (Chapter VI) it can be seen that the apparent energy of activation of bimetallic catalysts is higher (41.3 kJ mol^{-1} -48.3 kJ mol^{-1}) for the more acidic SiO_2(D) support as compared to that of the less acidic SiO_2(C) support (39.6 kJ mol^{-1}- 44.4 kJ mol^{-1}). This could be ascribed to a relative adsorption energy stronger for the benzene on the SiO_2(D) support which retards the overall chemical processes. Interesting also is the lower apparent energy of activation of C precipitated catalysts (39.6 kJ mol^{-1}- 41.7 kJ mol^{-1}) as compared to that of C impregnated catalysts (40.6 kJ mol^{-1}- 44.4 kJ mol^{-1}). This may be due to the existence of very reactive surface H-species in the former case as suggested the H_2-TPD study (Chapter VI).

3. ACTIVATED CARBON AS NICKEL CATALYST SUPPORT

3.1. Support properties

Activated carbon is a relatively weak support as showed isopropanol decomposition experiments (Figure IX-1). This acidity is strongly decreased in aqueous hydrazine media at 353 K: dry hydrazine-treated support decomposes isopropanol to 1% only (against 6% for dry fresh support, see Figure VII-3, Chapter VII). During the aqueous hydrazine treatment of activated carbon gaseous, nitrogen and ammonia evolved. One can be supposed that aqueous hydrazine reacts with acidic surface groups of the carbon material. Note that the treatment does not affect the textural properties of the carbon since both specific surface area and pore volume are not changed.

3.2. Reduction of the supported Ni^{2+} ions

For nickel acetate precursor, hydrazine provoked gaseous nitrogen and hydrogen evolution and the solid obtained can be removed with a magnet from the reduction flask. This is ascribed to Ni° particle formation according to equation (1). Absence of nickel reduction is found with the nickel nitrate and this is ascribed to reaction between the metal precursor and the support forming stable surface compounds, not reducible by the hydrazine.

Strikingly, specific area of the carbon increased in presence of the nickel acetate during the hydrazine reduction. This is particularly the case of 1Ni/AC-AH where the specific surface increased from 1107 to 1694 m^2*g^{-1} and pore volume from to. This increase could be explained by the gasification of the carbon surface by the hydrazine.

3.3. Interaction of hydrogen with the nickel catalysts

In metal-carbon systems, intense interactions can be promoted and play an important role conditioning both textural properties and reactivity of the catalyst [35]. Metal-carbon interactions attracted much attention [36-37]. In this way, the thermal pre-treatment nature (neutral/reductive/oxidative) may change the surface area or porosity as well the activity or selectivity of the catalyst [35-36]. Dissolution of carbon atom in

the metal [35-36] may cause the decrease of the catalytic activity through site blockage [35].

The results of the hydrogen chemisorption at room temperature showed very low hydrogen uptakes. The catalysts exhibited poor dispersion (Table IX-7). Dispersion decreased with increasing nickel content (A and AH catalysts) or passed by a maximum (N and APH catalysts). It is the highest with the N classical catalysts. On the other hand, discrepancies appeared between TEM experiments and H-adsorption study: for 10Ni/AC-A, metal surface area was 3.50 $m^2g_{cat}^{-1}$ or 0.27 $m^2g_{cat}^{-1}$ respectively. This could be caused by nickel embedding by the carbon support [35-36] during the hydrogen pre-treatment at 623 K which limits the access to the surface nickel atoms. It was shown that the H_2-adsorption on nickel catalysts deposited on charcoal was decreased after a pretreatment under hydrogen at 773 K [35]. The authors attributed this to a poisoning effect of the charcoal support. This action would be accomplished by the carbon itself or/and additionally by mineral impurities present in the support [35].

Strikingly, the amounts of hydrogen desorbed during TPD study are larger than that adsorbed at room temperature (Table IX-7). Moreover, a close examination of these amounts showed that the H/Ni ratio may exceed 1 (e. g. 3.8-4.7 for 1Ni% content). This excess hydrogen suggests that a part the reactant molecules, if not all, is strongly retained on the active carbon support. In other words, hydrogen molecules from the reductive atmosphere probably dissociated on the metal phase then spilled over the carbon support. This is in good correlation with the H_2-TPR study which showed that hydrogen was incorporated in the carbon support during the reduction step, particularly for 1%Ni catalysts (H/Ni >1) (see Chapter VII). Hydrogen spillover on activated carbons has been evidenced by several authors [38-39].

Table IX-7. Characteristic of activated carbon supported nickel.

catalyst	Dispersion [%]	Metal Surface area [$m^2*g_{Ni}^{-1}$]	TOF [molecBz*$s^{-1}site^{-1}$] 373 K	Conversion [%] 373 K
1Ni/AC-A	1.13	7.1	0.022	1.20
5Ni/AC-A	0.41	2.7	0.042	4.84
10Ni/AC-A	0.39	2.7	0.016	3.62
1Ni/AC-AH	2.11	14.1	0.254	30.88
5Ni/AC-AH	0.51	3.3	0.221	32.74
10Ni/AC-AH	0.30	2.4	0.200	31.02
1Ni/AC-APH	0.26	1.6	0.783	10.56
5Ni/AC-APH	0.35	2.4	0.191	20.23
10Ni/AC-APH	0.30	2.0	0.062	11.01
1Ni/AC-N	1.96	13.3	0.030	3.35
5Ni/AC-N	2.52	17.1	0.013	9.38
10Ni/AC-N	2.27	15.5	0.028	37.7

3.4. Catalytic activity

The activated carbon supported catalysts also exhibited a maximum of activity as a function of the reaction temperature. Temperature of this maximum depends on the nickel loading, the nature of the metal precursor and the method of preparation. Typical results are reported in Fig IX-3 and IX-4 and Table IX-7. Remarkably, best performances are obtained with the hydrazine-prepared catalysts. It is worth noting that the TOF of benzene hydrogenation at 373 K on 5%Pt/AC is 0.494 s^{-1}, a value quite comparable to that observed for 5Ni/AC-AH which is 0.2212 s^{-1}. Also one may

conclude that the hydrazine preparation allows obtaining nickel catalyst very performing for benzene hydrogenation

Discussion on the chemisorption study showed that the surface nickel atoms reactivity towards hydrogen is strongly affected by the nickel-carbon interactions or the hydrogen spillover effect. These parameters also may influence the hydrogenation chemical processes. The spillover phenomenon was evidenced in benzene hydrogenation using the mechanical mixtures of 10Ni/AC-N and 10Ni/AC-A catalysts with activated carbon. The activity of 10Ni/AC-N catalyst increases with dilution ratio which is in good accordance with the hydrogen spillover effect.

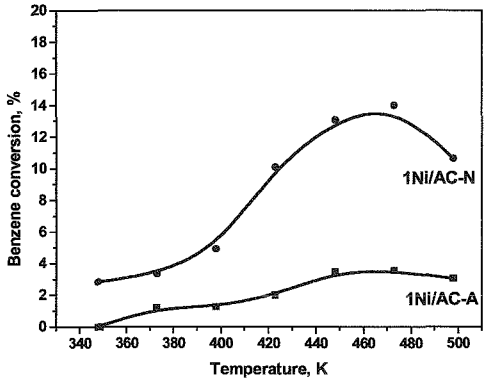

Figure IX-3. Benzene conversion for 1% Ni A and N classical catalysts.

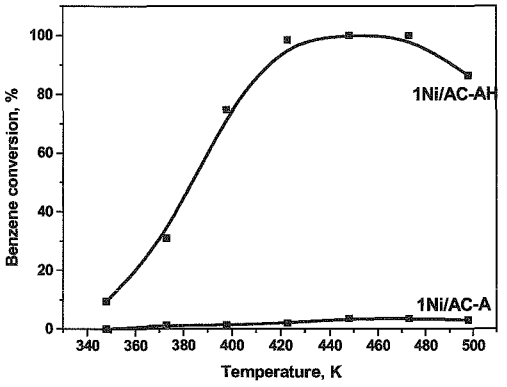

Figure IX-4. Benzene conversion for 1% Ni A and AH catalysts.

The maximum of benzene conversion is observed for the mixture with 0.5 dilution ratio at 448 K (Fig. IX-6). The activity of the hybrid catalyst, which is 2 times higher than that of undiluted catalyst, could be ascribed to the hydrogen migration process which is controlled by a distance factor [38]. Dilution is believed to increase the number of H species stabilized by the active carbon by increasing the available surface area and, in the mean time, lowers the recombination of these species in molecular hydrogen. At a certain point, the additional surface area of the dilutent brings no further benefit to the hydrogen uptake. At higher dilution ratio, the number of H spilt-over

acceptor sites stabilized by the support increases but the generation of the H spillover decreases as the number of Ni decreases [39].

4. Hydrogen storage

The real effect of monometallic nickel on the level of hydrogen storage has not still received much attention, although it has been recently reported implications of hydrogen spillover from NiMgO oxide onto carbon nanotubes for hydrogen storage [40]. More generally, the effect of residual metals in hydrogen uptake has been largely unstudied and uncharacterized. This prompted us to study nickel catalysts supported on an amorphous commercial activated carbon as materials for hydrogen storage.

The role of the metal in the hydrogen uptake is shown to be central for the metal-doped activated carbon prepared. Indeed, the uptake is much higher in the presence of the metal and also depends on the metal content, the nature of the metal precursor and the method of catalyst preparation. Typical results are reported in Table IX-8.

Table IX-8. Hydrogen storage.

Catalyst	H_2 uptake at 20 bars and RT [%]	Specific surface area $[m^2*g_{cat}^{-1}]$	Metal surface area $[m^2*g_{Ni}^{-1}]$
1Ni/AC-A	**0.31**	**1107**	**7.1**
1Ni/AC-N	**0.29**	**1071**	**13.1**
1Ni/AC-AH	**0.51**	**1671**	**14.1**

All these factors are known as determining in the metal dispersion in case of metal supported catalysts [41-42]. However, close examination of the results obtained shows that there is no correlation between the metal surface area and the hydrogen storage capability of the catalyst. In contrast, the correlation is between the hydrogen uptake and the specific surface area which both decreased with increasing nickel content: the uptake level is restricted by the specific surface (see Tables VIII-1 and VIII-2 for more details).

These apparent contradictions could be explained by the mechanism of the hydrogen uptake, namely the hydrogen spillover effect, as confirmed by the study of the catalyst+active carbon mixtures (Fig. IX-5). Indeed, the spillover effect may be influenced by textural factors in the carbon skeleton: the migration of the H atoms is probably inhibited in case of the 5 or 10%Ni catalysts because of decreasing specific area. Moreover, the migration of the H atoms needs metal-carbon contacts to occur. The number and quality of these bridges depend on the structural and textural properties of the catalysts and also influence on the hydrogen uptake level.

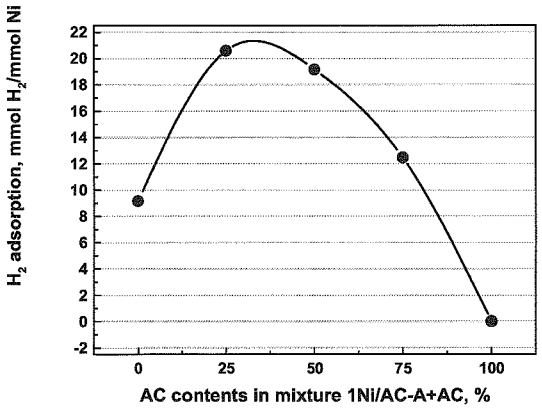

Figure IX-5. Spillover study for hydrogen storage.

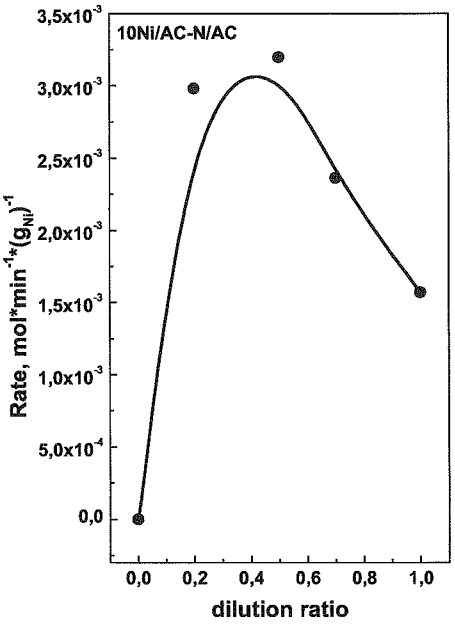

Figure IX-6. Spillover study for benzene hydrogenation.

The dilution of nickel catalysts with the carbon gives rise to higher hydrogen storage (Fig. IX-5) and higher activity in the gas phase benzene hydrogenation reaction (Fig. IX-6). It could be concluded that the spilt over sites responsible for the increase of catalytic activity may also responsible for the increase of hydrogen storage at room temperature.

5. CONCLUSIONS AND PERSPECTIVES

In conclusions, the objective of this study, which was to modify the electronic structure of nickel by exploring certain factors (method of preparation, nature of the support, metal addition), was achieved. From a practical point of view, it is important to stress that, realizing certain operating conditions and for certain chemical compositions (Ni or Ag) or for certain support (activated carbon), we can prepare nickel based catalysts with performances close to that to that of platinum (a noble metal) catalysts. From a fundamental point of view, a good correlation was established between the performances observed for these catalysts and the reduction mechanisms of the supported Ni^{2+} ions. The metal-support interactions which, mainly, govern the surface and hydrogenating properties of final material, were evidenced by various methods: H_2-TPR, H_2-TPD, FTIR. The mechanisms of the hydrogenation reaction, as well as the solid-molecule (benzene or hydrogen) interactions or the hydrogen spillover phenomenon were also found to strongly influence the catalytic performances of the catalysts. In a specific study of the hydrogen-catalyst interaction, we showed that the activated carbon, doped by nickel, is a good candidate as a material for hydrogen storage. The driving force of this storage would be also the hydrogen spillover.

This work raises some questions and opens prospects for later research. We shall evoke three of them.

We allotted the very good reducibility of nickel, when the crystallized silica was used as a support, to the existence of rather weak metal-support interactions. However, the presence of surface defects or impurities could also facilitate the reduction of the supported Ni^{2+} ions. A FTIR and UV-visible study of the adsorption of these ions on crystallized silica, as well as a fine chemical analysis of the silica, could bring answers to this question.

High dispersion and activity were observed for the supported Ni-Ag catalysts obtained by precipitation-reduction method. That was allotted to the existence of

bimetallic crystallites in which nickel would wet the silver. A more complete physico-chemical study (XRD, STEM, magnetism, XPS, UV-visible, Raman) should inform us on the structure of these metal particles. Further, a FTIR and UV-visible study of the competitive adsorption of Ni^{2+} and Ag^{+} ions on the silica would give useful information on the mechanism of formation of the bimetallic Ni-Ag aggregates.

The results of the hydrogen storage study on the catalysts supported on activated carbon are very interesting because they showed the possibility of carrying out the storage with inexpensive materials compared to the synthetic carbon nanotubes or nanofibres. Let us note, however, that this study was led to relatively low pressures (10 bars 30 bars) compared with that reported in the literature (>100 bars). Our study will have thus to be extended to the highest pressures for confirmation of the results and phenomena highlighted. It will also be necessary to explore the influence of parameters such as the porosity or the metal nature which were not examined here.

CONCLUSIONS GENERALES ET PERSPECTIVES

En conclusions, l'objectif de cette étude qui était de modifier la structure électronique du nickel en jouant sur certains facteurs (méthode de préparation, nature du support, ajout métallique) a été atteint et démontré. D'un point de vue pratique, il est important de souligner que, moyennant certaines conditions opératoires et pour certaines compositions chimiques (Ni-Ag) ou pour certain support (charbon actif), nous pouvons préparer des catalyseurs au nickel (métal commun) avec des performances voisines de celles des catalyseurs au platine (métal noble). D'un point de vue fondamental, une bonne corrélation a été établie entre les performances observées pour ces catalyseurs et les mécanismes de réduction des ions Ni^{2+} supportés. Les interactions métal-support qui, pour l'essentiel, gouvernent les propriétés de surface et hydrogénantes du matériau final, ont été mises en évidence par diverses méthodes : H_2-TPR, H_2-TPD, FTIR. Les mécanismes réactionnels d'hydrogénation, les interactions molécule (benzène ou hydrogène)-solide ou l'effet « spillover » de l'hydrogène influent fortement sur les performances catalytiques. L'étude particulière de l'interaction hydrogène-catalyseur montre que le charbon actif, dopé par le nickel, est un bon candidat comme matériau de stockage de l'hydrogène. Le moteur de ce stockage serait aussi le « spillover » de l'hydrogène.

Ce travail soulève quelques questions et ouvre des perspectives de recherches ultérieures. Nous en évoquerons trois.

Nous avons attribué la très grande réductibilité du nickel lorsque le support est la silice cristallisée à l'absence d'interactions fortes métal-support. Toutefois, la présence de défauts superficiels ou d'impuretés pourrait aussi faciliter la réduction des ions Ni^{2+} supportés. Une étude FTIR et UV-visible de l'adsorption de ces ions sur la silice considérée, de même qu'une analyse chimique fine pourraient apporter des réponses à la question posée.

Dispersion et activité sont fortes pour les catalyseurs Ni-Ag supportés obtenus par précipitation-réduction. Cela a été attribué à l'existence de cristallites bimétalliques dans lesquelles le nickel mouillerait l'argent. Une étude plus complète (DRX, STEM, magnétisme, XPS, UV-visible, Raman) devrait nous éclairer sur la structure de ces particules métalliques. Une étude FTIR et UV-visible de l'adsorption compétitive des ions Ni^{2+} et Ag^{+} sur la silice nous donnerait des indications sur le mécanisme de formation des agrégats bimétalliques Ni-Ag.

Les résultats de l'étude du stockage de l'hydrogène sur catalyseurs supportés sur charbon actif sont des plus intéressants car ils montrent la possibilité de réaliser l'opération avec des matériaux peu coûteux par rapport aux nanotubes ou nanofibres synthétiques. Notons, toutefois, que cette étude a été conduite à des pressions relativement faibles (10 bars- 30 bars) comparées à celles rapportées dans la littérature (> 100 bars). Notre étude devra donc être étendue aux plus hautes pressions pour confirmation des résultats et phénomènes mis en évidence. Il faudra aussi explorer les paramètres porosité et nature du métal qui n'ont pas été examinés ici.

6. REFERENCES:

[1] A.G; Boudjahem, S. Monteverdi, M. Mercy, M.M. Bettahar *J. Catal.* 221 (2004) 325

[2] A. Lewandowska, S. Monteverdi, M.M. Bettahar, M. Ziolek, *J.Mol. Catal. A:Chemical*, 3713 (2002) 1

[3] E.I. Ko, J.M. Hupp, F.H. Rogan, N.J. Wagner, *J. Catal.* 84 (1983) 85

[4] E.I. Ko, J.M. Hupp, N.J. Wagner, *J. Catal.* 86 (1984) 315

[5] T. Fung, *J. Am. Chem. Soc.* 100 (1978) 170

[6] K.V.R. Chary, K.S. Lakshmi, P.V. Ramana Rao, K.S. Rama Rao, M. Papadaki, *J. Mol. Catal. A:Chem.*, 223 (2004) 353

[7] M. Che, Z.X. Cheng, C. Louis, *J. Amer. Chem. Soc.* 117 (1995) 2008

[8] J.W. Coenen, *Preparation of catalysts II*; G. Poncelet, P.Grange, P.A. Jacobs, Eds; Elsevier, Amsterdam, 1979; pp. 89-108.

[9] L. Bonneviot, M. Che, D. Olivier, G.A. Martin, E. Freud, *J. Phys. Chem.* 90 (1986) 2112

[10] G. Viau, F. Fievet-Vicent, F. Fievet *Solid State Ionics* 84 (1996) 259

[11] J.T. Richardson, B. Turk, M. Lei, K. Forster, M.V. Twigg, *Appl. Catal. A: General* 83 (1992) 87

[12] I. Nowak, M. Ziolek, *Chem. Rev.* 99 (1999) 3603

[13] C. Louis, Z.X. Cheng, M. Che, *J. Phys. Chem.* 97 (1993) 5703

[14] C.H. Bartholomew, R.J. Farrauto, *J. Catal.* 45 (1976) 41

[15] K.H. Tonge, *Thermochim. Acta* 74 (1984) 151

[16] Y. Shizuka, S. Yamamoto, Y. Fukai *J. All. Comp.* 336 (2002) 159

[17] J.T. Miller, B.L. Meyers, F.S. Modica, G.S. Lane, M. Vaarkamp, D.C. Koningsberger *J. Catal.* 143 (1993) 395

[18] W.C. Conner, J.L. Falconer *Chem. Rev.* 95 (1995) 759

[19] J.F. Cevallos-Candau, W.C. Conner *J. Catal.* 106 (1987) 378

[20] A.J. Robell, E.V. Ballow, M. Boudart *J. Phys. Chem.* 68 (1964) 2748

[21] F. Benseradj, F. Sadi, M. Chater, *Appl. Catal. A*, 228 (2002) 135

[22] J. Wang, L. Huang, Q. Li, *Appl. Catal. A*, 175 (1998) 191

[23] J.B. Wang, Y.L. Tai, W.P. Dow, T.J. Huang, *Appl. Catal. A: Gen.* 218 (2001) 69

[24] S.J. Tauster *J. Am. Chem. Soc.* 100 (1978) 178

[25] S.J. Tauster, S.C. Fung, R.T.K. Baker, J.A. Horsely, *Science* 211 (1981) 1121

[26] E. Ramaroson, J.F. Tempere, M.F. Guilleux, F. Vergand, H. Roulet, G. Dufour, *J. Chem. Soc. Faraday Trans.* 88 (1992) 1211.

[27] S. Smets, T. Salmi, D. Murzin, *Appl. Catal. A* 145 (1996) 253

[28] M. Houalla, F. Delannay, B. Delmon, *J. Chem. Soc. Faraday Trans.* 76 (1980) 2128

[29] S.D. Lin, M.A. Vannice, *J. Catal.* 143 (1993) 539

[30] R. Molina, G. Poncelet, *J. Catal.* 199 (2001) 162

[31] S.T. Srinivas, P. Kanta Rao, *J. Catal.* 148 (1994) 470

[32] S. Ceckiewicz, B. Delmon, *J. Catal.* 108 (1987) 294

[33] P. Antonucci, N.V. Truong, N. Giordano, R. Maggiore, *J. Catal.* 75 (1982) 140

[34] B. Sen, J.L. Falconner, *J. Catal.* 117 (1984) 404

[35] P. Marecot, E. Paraiso, J.M. Dumas, J. Barbier, *Appl. Catal.* 74 (1991) 261

[36] L.R. Radovic, F. Rodriguez-Reinoso, in: P.A. Thrower (Ed.), *Chemistry and Physics of Carbon*, Vol. 25, Marcel Dekker, New-York, 1997, p.243

[37] L.M. Gandia, M. Montes, *J. Catal.* 145 (1994) 276

[38] A. Aguinaga, J.C. De la Cal, J.M. Asua, M. Montes, *Appl. Catal.* 51(1) (1989) 1

[39] J.A. Anderson, L. Daza, J.L. Fierro, T. Rodrigo, *J. Chem. Soc. Faraday Trans.* 89 (1993) 3651

[40] A. Lueking, R.T. Yang *AIChE Journal* 49(6) (2003) 1556

[41] M. Houalla, B. Delmon *J Phys Chem* 84 (1980) 2194

[42] R. Wojcieszak, S. Monteverdi, M. Mercy, I. Nowak, M. Ziolek, M.M. Bettahar, *Appl Catal A* 268 (2004) 241

ANNEX

Available online at www.sciencedirect.com
SCIENCE DIRECT
ELSEVIER
Catalysis Today xxx (2006) xxx–xxx
CATALYSIS TODAY
www.elsevier.com/locate/cattod

Ni–Ce intermetallic phases in CeO_2-supported nickel catalysts synthesized by γ-radiolysis

S. Chettibi [a], R. Wojcieszak [b], E.H. Boudjennad [a], J. Belloni [c], M.M. Bettahar [b], N. Keghouche [a,*]

[a] *Laboratoire Microstructures et Défauts, Université Mentouri Constantine, Route de Ain El Bey, 25 110 Constantine, Algeria*
[b] *Laboratoire de Catalyse Hétérogène, UMR 7565, Université Henri Poincaré, Nancy 1, 54506 Vandoeuvre-les-Nancy, France*
[c] *Laboratoire de Chimie Physique, UMR CNRS/UPS 8000, ELYSE, Université Paris-Sud, Bât. 349, 91405 Orsay, France*

Abstract

This work concerns the study of nickel clusters synthesized by radiation-induced reduction of Ni^{2+} ions previously adsorbed on ceria by ionic exchange in the aim to test their performance in catalytic hydrogenation. The nickel catalyst and CeO_2 support were characterized by SEM coupled to X analysis, XRD, H_2-adsorption and H-TPD. The catalyst prepared by irradiation presents high reducibility, dispersion and homogeneity of the metal phase. It is shown that the CeO_2 support stores hydrogen during the radiolytic reduction of Ni ions and that the adsorbed hydrogen amounts strongly increase in the presence of nickel. The catalyst displays high catalytic performance in the benzene hydrogenation reaction (total conversion in a large and low temperature range). These properties are assigned to the high dispersion of nickel and to the promoter role of the support: actually, after the catalytic test, intermetallic nickel–cerium compounds (CeNi and $CeNi_3$) are detected in the sample in addition to the Ni^0 phase.

Keywords: Ni/CeO_2; Ni–Ce intermetallic phases; Catalyst; Clusters; Radiolysis; Benzene hydrogenation

1. Introduction

Nanosized particles are extensively studied because of their large potential applications. Matter in ultra-divided state has indeed specific properties due to its quasi-atomic state [1,2]. The aggregates of a few atoms are much more easily oxidized than the bulk metal and can be corroded as soon as they are formed. This specific property improves the activity of small metal particles but also makes their stabilization more difficult. Non-noble metals such as nickel, cooper and iron are still more difficult than noble metals to be synthesized at the atomic or oligomeric states [3,4]. Nevertheless, nickel nanoparticles were produced using different methods such as: chemical reduction with hydrazine or alcohol in water solution [4–6], electrochemical reduction [7], sonochemical method [8], microemulsion technique [9] or sol–gel method [10]. As an alternative way, the radiolysis has been proven to be a powerful tool to produce dispersed and monosized metal clusters [1]. Using irradiation, nickel particles have been synthesized in the colloidal state [3] or supported on α-alumina [11]. The radiation-induced reduction of metal ions is achieved by solvated electrons and reducing radicals generated from the solvent and by electrons generated from the support, both having a strong reducing power [11].

The support ceria, a stable fluorite-type oxide, has been extensively studied because of its interesting redox and high dispersive properties [12–14]. Ceria is able to change reversibly from Ce^{IV} under oxidizing conditions to Ce^{III} under reducing conditions. Oxygen atoms in CeO_2 units are very mobile and leave easily the ceria lattice, giving rise to a large variety of non-stoichiometric oxides with the two limiting cases CeO_2 and Ce_2O_3 [13]. Ceria has an insulator behavior in the stoichiometric oxidized state CeO_2 and becomes conductor in the reduced state CeO_{2-x}, acquiring a great capacity to store and to carry oxygen. It was studied in particular in the aim to be used in the automobile emission control system [14,15].

Cerium-based catalysts containing transition metals have attracted increasingly attention in recent years due to their

* Corresponding author. Tel.: +213 31 61 46 14; fax: +213 31 61 46 14.
E-mail address: nassira.keghouche@caramail.com (N. Keghouche).

0920-5861/$ – see front matter © 2005 Elsevier B.V. All rights reserved.
doi:10.1016/j.cattod.2005.11.058

Available online at www.sciencedirect.com
SCIENCE DIRECT
Journal of Colloid and Interface Science ••• (••••) •••–•••
JOURNAL OF Colloid and Interface Science
www.elsevier.com/locate/jcis

Study of nickel nanoparticles supported on activated carbon prepared by aqueous hydrazine reduction

R. Wojcieszak, M. Zieliński, S. Monteverdi, M.M. Bettahar*

Catalyse Hétérogène, UMR 7565, Faculté des Sciences, Université Henri Poincaré, Nancy-I, BP 239, 54506 Vandoeuvre-les-Nancy Cedex, France

Received 22 June 2005; accepted 31 January 2006

Abstract

Nickel nanoparticles were obtained by the reduction in hydrazine aqueous media of nickel acetate as a precursor supported on activated carbon of high surface area. Classical catalysts using nickel acetate or nitrate were prepared for comparison. The catalysts were characterized by N_2 physisorption, H_2-TPR, H_2-adsorption, TPD, TEM, and XRD, and tested in the gas phase hydrogenation of benzene. Hydrazine catalysts were found much more active in benzene hydrogenation than corresponding classically prepared catalysts. Remarkably, their reactivity is comparable (turn-over frequency of 0.2001–0.2539 s^{-1} at 393 K) to that of Pt classical catalysts supported on activated carbon in the same conditions. Evidence is given for the existence of the hydrogen spillover effect in benzene hydrogenation, not reported before in the literature. As a result of the hydrogen spillover effect, catalysts performances can be explained by a combination of surface metal atom reactivity, metal-support interaction strength, and specific surface area extent. Maximum effect is observed with hydrazine preparation method, for 1% Ni content and nickel acetate as a precursor. Unexpectedly, it was also found that hydrazine preparation increases the specific area of the catalysts.

Keywords: Nickel; Hydrazine; Catalysts; Activated carbon; Hydrogen chemisorption; Benzene hydrogenation

1. Introduction

The activity and selectivity of supported metal catalysts are strongly influenced by the amount of metal, the size of dispersed metal particles, the preparation method, and the support composition [1,2]. To improve the catalyst activity and its durability, it is necessary to obtain a well-dispersed active phase in the catalyst [3,4]. The chemical species present on the carrier surface interact, more or less, with the metal particles deposited thereon. The metal-support interaction (MSI) is usually stronger when the metal particles are smaller [5]. For the carriers employed in industrial catalysis the intensity of MSI decreases from alumina to silica to active carbon [5]. In the case of highly dispersed materials, the changes in the catalytic activity were related to the combined effects of particle size, surface coverage with adsorbed species, and active site dimension [6].

Conventional supported metal catalysts are prepared by in situ reduction of metal salt. However, it is often difficult to control the morphology of the final material. The control of metal particle nanosize is of the utmost importance for the performance of any industrial catalyst based on supported metals. The synthesis of the metal nanoparticles of uniform shape and high purity has received considerable attention in the past two decades due to their unusual properties compared to bulk metal [7].

The metal nanoparticles are generally produced by the reduction of metal compounds. The number of procedures is fairly large, for example photolytic reduction [8], radiolytic reduction [9], solvent extraction reduction [10], microemulsion technique [11], alcohol reduction [12], chemical reduction in aqueous [13] and nonaqueous [14] media by hydrazine. Hydrazine is a powerful strong reductant widely used in various chemical operations. A series of striking results have been obtained where hydrazine is used as a reducing agent for the production of finely divided metals [15,16]. Degan and Macek [17] used hydrazine as a reducing agent to prepare nickel powders in the submicrometer size range from nonaqueous solutions of

* Corresponding author.
E-mail address: mohammed.bettahar@leah.uhp-nancy.fr (M.M. Bettahar).

0021-9797/$ – see front matter
doi:10.1016/j.jcis.2006.01.067

Available online at www.sciencedirect.com
SCIENCE DIRECT
Catalysis Communications 6 (2005) 777–783
CATALYSIS COMMUNICATIONS
www.elsevier.com/locate/catcom

Hydrogen storage on nickel catalysts supported on amorphous activated carbon

M. Zieliński, R. Wojcieszak, S. Monteverdi, M. Mercy, M.M. Bettahar *

UMR CNRS 7565, Laboratoire de Catalyse Hétérogène, Faculté des Sciences, Université Henri Poincaré, Nancy-I, BP 239, 54506 Vandoeuvre-lès-Nancy Cedex, France

Received 24 March 2005; received in revised form 1 July 2005; accepted 1 July 2005
Available online 19 September 2005

Abstract

We have studied the hydrogen storage at room temperature and high pressure on nickel catalysts impregnated on an amorphous commercial activated carbon. The catalysts were studied by means of the BET method, XRD, metal surface area and temperature programmed desorption. It was shown that the catalysts could store significant amounts of hydrogen at room temperature and high pressure (up to 0.53% at 30 bars against 0.1% for the activated carbon). Various factors influencing the level of hydrogen uptake were examined and discussed. The hydrogen spillover would be the driving force for the hydrogen storage. Two mechanisms of hydrogen uptake are proposed.

Keywords: Hydrogen; Storage; Metal; Catalysts; Activated carbon

1. Introduction

Hydrogen storage has attracted considerable attention because of its potential application in high energy-density rechargeable batteries and hydrogen-powered vehicles [1–3]. In recent years, there has been considerable experimental and theoretical interest in the use of nano-structured carbon materials, especially in the form of tubes [4–7] fibers [8,9] and mechanically milled graphite [10] as potential hydrogen sorbents. The results of these studies show that high storage concentrations of hydrogen can be achieved. However, claims of hydrogen storage capacity higher than the US Department of Energy of 6.5% by weight have not been reproducible by other groups [7,11]. On the other hand, an important feature of the hydrogen storage is the use of transition metals (Fe, Co, Ni, Cu) in the synthesis of the carbonaceous materials which, in addition, cannot be completely removed during the purification process [12].

The nature of the factors that influence the level of hydrogen storage is still disputed. In the case of carbon nanofibers, it has been suggested that the presence of defects in the surface structure may dissociate hydrogen, which then intercalates in the graphene planes [12–14]. The pre-treatment in neutral, oxidative or reductive atmosphere may modify the structural properties of the carbon material in many ways: purification by removal of the adsorbed species [15], opening of the carbon structure [16], increased graphitization [17], activation of the solid [12]. Changes were also observed in the carbon material structure after exposure to high-pressure hydrogen [18]. As a result, the structural modifications induce important changes in the hydrogen storage of the materials treated [12,15–17]. Metals used as catalysts for the preparation of carbonaceous materials for hydrogen storage may play a role in the hydrogen

* Corresponding author. Tel.: +33 3 83 68 49 48; fax: +33 3 83 68 49 48/55.
E-mail address: Mohammed.Bettahar@lcah.uhp-nancy.fr (M.M. Bettahar).

1566-7367/$ - see front matter
doi:10.1016/j.catcom.2005.07.001

Monsieur **WOJCIESZAK Robert**

DOCTORAT DE L'UNIVERSITE HENRI POINCARE, NANCY 1

en CHIMIE & PHYSICO-CHIMIE MOLECULAIRES

VU, APPROUVÉ ET PERMIS D'IMPRIMER N° 1200

Nancy, le 3 juillet 2006

Le Président de l'Université

UNIVERSITÉ HENRI POINCARÉ, NANCY 1 ★ LE PRÉSIDENT

J.P. FINANCE

Université Henri Poincaré, Nancy I
24-30 rue Lionnois - B.P. 3069 - 54013 NANCY Cédex
Tél : 03 83 68 20 00 - Fax : 03 83 68 21 00

ABSTRACT

Nous avons étudié des nanoparticles de Ni ou de NiAg obtenus par la réduction de sels de nickel (acétate ou nitrate) par l'hydrazine et déposés par imprégnation simple ou EDTA-double sur de divers supports (γ-Al_2O_3, SiO_2 amorphe ou cristallisé, Nb_2O_5, CeO_2 et carbone). Des catalyseurs préparés ont été caractérisés par différentes méthodes (DRX, XPS, adsorption et désorption de N_2 à basse température, FTIR, TEM, STEM, EDS, H_2-TPR, H_2-adsorption, H_2-TPD, décomposition de isopropanol) et examinés dans l'hydrogénation du benzène en phase gazeuse ou comme matériaux de carbone dans le stockage d'hydrogène à la température ambiante/haute pression.

Les catalyseurs préparés ont montrés une meilleure dispersion et activité que les catalyseurs classiques. Les TOF des catalyseurs de NiAg/SiO_2 ou de Ni/carbon étaient semblables aux catalyseurs de platine dans l'hydrogénation de benzène. Différences dans l'acidité de support ou la méthode de préparation et présence d'Ag comme métal additif jeu un rôle crucial dans la réduction chimique de Ni par l'hydrazine et dans les propriétés finales des matériaux. Les catalyseurs de Ni/carbon pourraient stocker des quantités significatives d'hydrogène à la température ambiante et à haute pression (0.53%/30 barre), probablement par l'effet de spillover d'hydrogène.

ABSTRACT

We have studied Ni or NiAg nanoparticles obtained by the reduction of nickel salts (acetate or nitrate) by hydrazine and deposited by simple or EDTA-double impregnation on various supports (γ-Al_2O_3, amorphous or crystallized SiO_2, Nb_2O_5, CeO_2 and carbon). Prepared catalysts were characterized by different methods (XRD, XPS, low temperature adsorption and desorption of N_2, FTIR, TEM, STEM, EDS, H_2-TPR, H_2-adsorption, H_2-TPD, isopropanol decomposition) and tested in the gas phase hydrogenation of benzene or as carbon materials in the hydrogen storage at room temperature/high pressure.

The catalysts prepared exhibited better dispersion and activity than classical catalysts. TOF's of NiAg/SiO_2 or Ni/carbon catalysts were similar to Pt catalysts in benzene hydrogenation. Differences in support acidity or preparation method and presence of Ag as metal additive play a crucial role in the chemical reduction of Ni by hydrazine and in the final properties of the materials. Ni/carbon catalysts could store significant amounts of hydrogen at room temperature and high pressure (0.53%/30 bars), probably through the hydrogen spillover effect.